

DEVELOPMENT OF AN INTRAOPERATIVE TOOL TO DETECT
PARATHYROID GLAND AUTOFLUORESCENCE

By

Melanie Ann McWade

Dissertation

Submitted to the Faculty of the
Graduate School of Vanderbilt University
in partial fulfillment of the requirements
for the degree of

DOCTOR OF PHILOSOPHY

in

Biomedical Engineering

May 2016

Nashville, Tennessee

Approved:

Anita Mahadevan-Jansen, Ph.D.

E. Duco Jansen, Ph.D.

Robert L. Galloway, Jr., Ph.D.

W. Hayes McDonald, Ph.D.

James T. Broome, M.D.

ABSTRACT

The inability to identify the parathyroid glands is a significant challenge during endocrine procedures. Successful parathyroid and thyroid surgeries require careful resection of diseased tissue and preservation of normal tissues, but this is not always the reality. Inaccurate localization of parathyroid glands during these procedures may permanently prevent patients from achieving normal calcium levels after surgery. Current parathyroid detection methods cannot convey real-time information and are limited to localization of only diseased glands. There is, therefore, a large unmet need in endocrine surgery for a technique to find diseased *and normal* parathyroid glands *during* surgery. Previous studies have observed an intrinsic near-infrared (NIR) fluorescence signal in the parathyroid gland that is higher than the fluorescence of surrounding neck tissues. The goal of this dissertation is to develop NIR fluorescence spectroscopy and imaging into a reliable, real-time tool for parathyroid detection regardless of disease state. The clinical utility of NIR fluorescence spectroscopy was established over a diverse patient population. Studies show 97% accuracy in NIR fluorescence detection of the parathyroid glands with minimal effects from patient factors. Parathyroid imaging was achieved to replace point measurements acquired from spectroscopy with spatial images to show gland location. A novel Overlay Tissue Imaging System (OTIS) was developed to project fluorescence information directly on the patient in the surgeon's line of sight. This imaging approach could replace traditional display monitors and reduce errors in image perception. Finally, the mechanism of the NIR fluorescence signal in the parathyroid was investigated. The endogenous NIR fluorophore in the parathyroid gland has an emission peak at a wavelength that has been thought to be devoid of autofluorescence. Studies revealed the biochemical behavior and location of the fluorophore. Ultimately this combination of studies lowers the barrier for clinical translation of the technology. Widespread adoption of NIR fluorescence detection of the parathyroid glands will greatly improve patient care by reducing harmful surgical complications.

To my family

*For their love, support, and
unwavering belief in me*

ACKNOWLEDGEMENTS

I would first like to thank my advisor, Dr. Anita Mahadevan-Jansen. She gave me the freedom to become an independent researcher but also offering important feedback and guidance when I needed it. I feel grateful for her example of a strong female leader in the sciences who has balanced family and other life passions. Dr. Duco Jansen has given me many years of support beginning early on in my undergraduate years. Thank you for your good sense of humor and always bringing thought-provoking questions to the table to remind me why we do this research in the first place. I want to thank Dr. James Broome and Dr. Carmen Solórzano who welcomed me into their operating rooms with patience and hospitality while I tested new devices and asked for their feedback. They reminded me of the impact this work could someday have. I want to thank Dr. Bob Galloway for engaging me in thoughtful conversations about graduate school, which were highly influential me deciding to start a PhD and later deciding to stick it out when doubts creeped in. Thank you to Dr. Hayes McDonald who provided invaluable guidance in biochemistry experiments. Your help in designing many of these experiments was absolutely critical. In addition to these faculty advisors, I want to thank the members of the biophotonics lab who helped me navigate the nitty gritty details in lab and provided much needed comradery about graduate school life.

I would like to thank my church small group for your support as we all navigated the transitions in our lives these past four years. Finding community, getting married, and figuring out career aspirations would have been much more confusing and less fun without all of you. To Bess and Ciara, without wine night therapy I could not have completed this work. Thank you for adopting me as a covert humanities person, and inviting me into your poetry discussions. I know your inquiries to teach you “a fact about science” were your best attempts at engaging my engineering side.

Thank you to my older sister, Christy, for paving the way to a Ph.D. You influenced me to go this route more than I realized when I started. Your encouragement and related experiences were crucial. I want to thank my loving parents, Jane and Doug, for your time, emotional, and financial investment in my education over the years. I used to believe your confidence in me was blindly given because you are my parents and the role requires it. However, through graduate

school I have seen how genuine you are in that, which has increased my own self-confidence as a result. I will one day aspire to be as wonderful of a parent as the two of you have been to me.

Most of all, I am thankful for my husband, Conor. Teaming up with you is the best choice I've made. I am so grateful for your companionship, thoughtful advice, and sense of humor. You have listened well and challenged me often to think differently as I've asked the question "what do I do with a PhD?" Thank you for fielding countless medical questions; I am lucky to have my own personal textbook. If I could, I would go back and re-write you as a second author on all of my papers, just like you always asked.

This work was made possible by the financial support of a National Science Foundation Graduate Fellowship, and grants from the National Institute of Health and the Vanderbilt Institute for Clinical and Translational Research (VICTR). This funding was instrumental in the completion of this dissertation.

TABLE OF CONTENTS

	Page
ABSTRACT.....	ii
ACKNOWLEDGEMENTS.....	iv
LIST OF FIGURES	x
LIST OF TABLES.....	xii
 Chapter	
1. INTRODUCTION	1
1.1 Goal.....	2
1.2 Motivation.....	2
1.3 Specific Aims.....	3
1.4 Summary of chapters	5
1.5 References.....	6
 2: BACKGROUND	 7
2.1 Anatomy and physiology of parathyroid and thyroid glands.....	8
2.1.1 Parathyroid gland anatomy and physiology.....	8
2.1.2 Thyroid Gland Anatomy and Physiology	9
2.2 Parathyroid and Thyroid Disease.....	10
2.3 Challenge: Parathyroid Detection during Endocrine Surgery	12
2.4 Current Parathyroid Detection Techniques.....	13
2.5 Optical Imaging and Spectroscopy	14
2.5.1 Optical Coherence Tomography for Parathyroid Detection	14
2.5.2 Optical Spectroscopy for Parathyroid Detection	15
2.5.3 Fluorescence Spectroscopy and Imaging.....	16
2.5.3.1 NIR Fluorophores: Extrinsic and Intrinsic.....	17
2.5.3.2 Current Near-infrared Fluorescence Imaging Systems.....	19
2.5.4 Previous work on NIR fluorescence detection of the parathyroid.....	19
2.6 Significance and Impact.	21
2.6.1 Novel intraoperative method for parathyroid gland identification	21
2.6.2 Novel endogenous near-infrared fluorophore.....	22
2.6.3 A Unique Approach to Surgical Imaging	22
2.7 References.....	23
 3: A NOVEL OPTICAL APPROACH TO INTRAOPERATIVE DETECTION OF PARATHYROID GLANDS.....	 29
3.1 Abstract.....	30
3.2 Introduction.....	31
3.3 Patients and Methods	32
3.3.1 Fluorescence Measurement.....	33
3.3.2 Data Processing and Statistical Analysis	34
3.4 Results.....	36
3.5 Discussion.....	40
3.6 Conclusions.....	42

3.7 Acknowledgements.....	43
3.8 References.....	43
4: ESTABLISHING THE CLINICAL UTILITY OF AUTOFLUORESCENCE SPECTROSCOPY FOR PARATHYROID DETECTION	45
4.1 Abstract.....	46
4.2 Introduction.....	47
4.3 Materials and Methods.....	48
4.3.1 Patient Selection.....	48
4.3.2 Fluorescence Measurement.....	48
4.3.3 Data Analysis.....	49
4.3.4 Alternative sources of variability.....	50
4.4 Results.....	50
4.4.1 Accuracy of Parathyroid Detection.....	52
4.4.2 Analysis of Variability in Parathyroid Fluorescence.....	54
4.4.3 Low Fluorescence in Secondary Hyperparathyroidism Patients.....	56
4.4.4 Alternative sources of variability.....	57
4.5 Discussion.....	59
4.6 Acknowledgements.....	62
4.7 References.....	63
5 CHARACTERIZATION OF AN ENDOGENOUS NEAR-INFRARED FLUOROPHORE IN PARATHYROID AND OTHER ENDOCRINE TISSUES.....	65
5.1 Abstract.....	66
5.2 Introduction.....	67
5.3 Materials and Methods.....	68
5.3.1 Fluorescence microscopy.....	68
5.3.1.1 Histopathology.....	69
5.3.1.2 Image Analysis.....	69
5.3.2 Fluorescence over time.....	69
5.3.3 Fluorescence response to proteases.....	70
5.3.4 Fluorescence response to heat.....	70
5.3.5 Differential centrifugation.....	70
5.3.6 SDS-PAGE.....	71
5.3.7 Autofluorescence measurement of additional endocrine tissues.....	71
5.3.8 Parathyroid and Adrenal tissue fractionation.....	72
5.3.9 Transmission Electron Microscopy of Isolated Fluorescent Tissue.....	72
5.3.10 Chromogranin A (CgA) Immunohistochemistry.....	73
5.4 Results.....	73
5.4.1 Fluorescence Microscopy Reveals Cytoplasmic Autofluorescence.....	73
5.4.2 NIR Fluorophore Heat-Stable with Mild Proteinase-Sensitivity.....	76
5.4.3 Differential Centrifugation Suggests NIR Fluorophore Housed In Organellar-Sized Subcellular Structure.....	76
5.4.4 SDS-PAGE reveals Molecular Weight of NIR Fluorophore.....	79
5.4.5 Multiple Endocrine Tissues Emit NIR Autofluorescence.....	79
5.4.6 Fluorophore Localized in Electron-Dense Granular Structure.....	81

5.5 Discussion.....	83
5.6 Conclusion.....	88
5.7 Acknowledgements.....	88
5.8 References.....	88
6: IMAGING SYSTEM DESIGN FOR SURGICAL GUIDANCE WITH NEAR-INFRARED AUTOFLUORESCENCE.....	92
6.1 Abstract.....	93
6.2 Introduction.....	94
6.3 Materials and Methods.....	96
6.3.1 System Description.....	96
6.3.2 System Performance Tests.....	98
6.3.3 Signal Validation Tests.....	99
6.4 Results.....	100
6.4.1 System Performance Tests.....	100
6.4.2 Signal Validation Tests.....	103
6.5 Discussion.....	107
6.6 Acknowledgements.....	110
6.7 References.....	110
7: LABEL-FREE INTRAOPERATIVE PARATHYROID LOCALIZATION WITH NEAR-INFRARED AUTOFLUORESCENCE IMAGING.....	113
7.1 Abstract.....	114
7.2 Introduction.....	115
7.3 Materials and Methods.....	116
7.3.1 Patient Recruitment.....	116
7.3.2 Clinical Fluorescence Spectroscopy.....	116
7.3.3 Intraoperative Fluorescence Imaging.....	117
7.3.4 Ex vivo tissue measurements.....	118
7.3.5 Statistical Analysis.....	118
7.4 Results.....	119
7.4.1 Validation of parathyroid autofluorescence in large patient population.....	119
7.4.2 Patient characteristics.....	121
7.4.3 Intraoperative imaging of the parathyroid.....	122
7.4.4 Ex vivo fluorescence imaging of healthy canine parathyroid tissue.....	124
7.5 Discussion.....	125
7.6 References.....	128
8: FLUORESCENCE-GUIDED SURGERY WITH OVERLAY TISSUE IMAGING SYSTEM: FIRST IN-HUMAN RESULTS FOR LABEL-FREE PARATHYROID LOCALIZATION.....	131
8.1 Abstract.....	132
8.2 Introduction.....	133
8.3 Materials and Methods.....	135
8.3.1 Study Design.....	135
8.3.2 Overlay Tissue Imaging System.....	135

8.3.3 Intraoperative Overlay Imaging.....	136
8.3.4 Dye Imaging.....	137
8.3.5 Statistical Analysis.....	137
8.4 Results.....	137
8.4.1 Design of overlay tissue imaging system (OTIS)	137
8.4.2 OTIS Deployment in Operating Room	138
8.4.3 Patient Characteristics.....	139
8.4.4 Intraoperative OTIS imaging in Endocrine Surgery	139
8.4.5 Enhancing dye contrast with OTIS imaging.....	143
8.5 Discussion.....	144
8.6 References.....	148
9: CONCLUSIONS AND FUTURE DIRECTIONS	152
9.1 Summary and Integration.....	153
9.2 Major Conclusions	156
9.3 Recommendations.....	157
9.3.1 Recommendations for NIR fluorophore evaluation.....	157
9.3.2 Recommendations for the Probe-based Parathyroid Detection	159
9.3.3 Recommendations for the Development of Fluorescence Imaging	159
9.3.4 Parathyroid Perfusion Imaging	161
9.4 Contributions to the Field and Societal Impact.....	162
9.4.1 Impact on Endocrine Surgery	162
9.4.2 Impact on Biophotonics	165
9.4.2.1 Characterization of a new endogenous fluorophore	165
9.4.2.2 Novel imaging approach.....	167
9.4.3 Commercialization.....	167
9.5 Protection of Research Subjects.....	168
9.6 References.....	169
APPENDIX A: ALTERNATIVE APPROACHES TO INVESTIGATE THE SOURCE OF FLUORESCENCE IN THE PARATHYROID: UNPUBLISHED RESULTS.....	171
A1.1 Abstract	172
A1.2 Background and Motivation.....	172
A1.3 Testing the Calcium-sensing receptor hypothesis.....	172
A1.3.1 Parathyroid homogenization with varying detergents	173
A1.3.2 A Detergent-free method for isolation of caveolar membranes.....	175
A1.3.3 NIR autofluorescence of medullary thyroid xenografts.....	176
A1.3.4 Immunoprecipitation with anti-CaSR	177
A1.3.5 CaSR overexpression lysates	177
A1.4 Photobleaching.....	178
A1.5 Troubleshooting Gel Electrophoresis Studies.....	180
A1.6 Multidimensional Protein Identification Technology Analysis	182
A1.7 Building a custom microscope for NIR autofluorescence microscopy.....	183
A1.8 Protein Over-expression Lysates.	184
A1.9 Pancreatic Islet Cell Autofluorescence	186
A1.10 Conclusions.....	187

LIST OF FIGURES

Figure	Page
2.1 Anatomy of the parathyroid and thyroid glands	8
2.2 Optical coherence tomography images of parathyroid and lymph node	15
2.3 Jablonski diagram representing fluorescence	17
2.4 Raman spectra of parathyroid and thyroid glands	21
3.1 Clinical near-infrared fluorescence spectroscopy system.....	33
3.2 Typical in vivo NIR fluorescence spectra from neck tissues.....	35
3.3 Distribution of parathyroid to thyroid peak ratios	37
4.1 Typical NIR fluorescence spectra from parathyroid and surrounding tissues	51
4.2 Pairwise comparisons showing effects of patient factors on fluorescence	55
4.3 Secondary hyperparathyroidism patient results and histology	56
4.4 Effects of additional sources of variability	58
5.1 Location of NIR autofluorescence in parathyroid microscopy images	74
5.2 Parathyroid autofluorescence intensity decay over time	75
5.3 Biophysical behavior of parathyroid fluorescence	77
5.4 Molecular weight of parathyroid fluorophore visualized with SDS-PAGE	78
5.5 Additional endocrine tissues with NIR autofluorescence	80
5.6 Electron microscopy and chromogranin-A immunohistochemistry images.....	82
6.1 Schematic of three fluorescence imaging systems.....	97
6.2 Spatial resolution comparison across fluorescence imaging systems.....	101
6.3 Contrast ratio comparison across fluorescence imaging systems	102
6.4 Signal validation of near-infrared dyes with fluorescence imaging systems.....	104
6.5 In vitro testing of fluorescence imaging systems on parathyroid and thyroid tissue.	104
6.6 Intraoperative parathyroid imaging with clinical endoscope camera	106
7.1 Near-infrared fluorescence spectroscopy system and results	119
7.2 Receiver operating characteristic curve for spectroscopy results	120
7.3 Near-infrared fluorescence imaging system using clinical endoscope camera	122
7.4 In vivo fluorescence images of the parathyroid with clinical endoscope camera.....	124
7.5 Healthy parathyroid and thyroid fluorescence images of canine subjects	125

8.1 Overlay Tissue Imaging System design.....	138
8.2 OTIS Imaging detects diseased and normal parathyroid glands.....	142
8.3 Indocyanine green fluorescence imaging with OTIS.....	143
A.1 Supernatant and pellet fluorescence in RIPA buffer.....	173
A.2 Fluorescence of Calcium-sensing receptor transfected cells	178
A.3 Photobleaching of thyroid tissue.....	179
A.4 SDS-PAGE of parathyroid in Triton X and Laemmli buffers	181
A.5 Autofluorescence of pancreatic beta cells.....	186

LIST OF TABLES

Table	Page
2.1 Summary of near-infrared imaging systems in literature	18
3.1 Patient summary of parathyroid fluorescence, visual inspection, and histology	39
4.1 Detection rate of parathyroid glands by disease state with NIR fluorescence.....	52
4.2 Clinical and demographic patient characteristics and statistical significance	53
6.1 Overview of clinical requirements and performance of three imaging systems.....	105
7.1 Individual demographics and intraoperative fluorescence imaging results	121
8.1 Characteristics of patients recruited for OTIS imaging	140

CHAPTER 1

INTRODUCTION

1.1 Goal

The goal of this research is to develop a technique to find the parathyroid glands during endocrine surgery and lower the barriers to its clinical translation. Patient care would be greatly improved by the widespread adoption of a tool to reduce surgical complications associated with inadequate parathyroid gland detection. Before any medical device can be adopted into clinical practice, it must overcome many hurdles such as showing higher efficacy than alternative methods, utility over a diverse patient population, easy integration into the clinical workflow, and a mechanism that does not harm the patient. In this dissertation, I demonstrate the clinical adoptability of a parathyroid detection device based on NIR autofluorescence. I show near-infrared (NIR) autofluorescence in parathyroid gland tissue can be detected intraoperatively with high accuracy regardless of disease state using fluorescence spectroscopy and imaging. Furthermore, this work advances our understanding of the biological basis of the autofluorescence within the parathyroid gland.

1.2 Motivation

Thyroid and parathyroid disease require thyroidectomy and parathyroidectomy to remove malignant glands in over 80,000 patients in the United States (1). Difficulty in detecting the parathyroid glands presents a significant challenge during thyroidectomies and parathyroidectomies. Complications with the parathyroid and thyroid glands are common, with 25-28 cases per 100,000 of hyperparathyroidism and approximately 20 million people affected by some sort of thyroid disease (2, 3). Surgical means are used to remove the affected gland(s) when the disease cannot be treated by other methods (4). Because parathyroid glands are small and variable in position, they are difficult to distinguish from thyroid and surrounding tissues in the neck. Existing parathyroid localization methods suffer from low sensitivity, require uptake of radiopharmaceuticals, or necessitate the use of expensive equipment. Surgeons ultimately rely on visual inspection to identify the different tissues, which can be subjective and inconclusive. Trauma, inadvertent removal or devascularization of parathyroid glands are recognized complications of this procedure (5). The incidence of inadvertent parathyroidectomy ranges from 8% to 19% of patients undergoing total thyroidectomy (6). Accidental removal or injury of the parathyroid can cause hypoparathyroidism and hypocalcemia, leading to long-term issues with calcium regulation. Hypocalcemia is the most common cause of malpractice litigation after

endocrine surgery (5). There is a critical need for a tool that provides sensitive real-time detection of parathyroid gland regardless of disease state. Such a tool should be highly effective at differentiating parathyroid glands from thyroid and other tissues in the region to avoid accidental injury or removal of the parathyroid glands.

Therefore, my overall motivation for this doctoral project is to further the development of an intraoperative technique using NIR fluorescence spectroscopy and imaging to guide surgical resection of the parathyroid and thyroid in real-time, regardless of disease state. A reliable and accurate parathyroid detection tool would minimize surgical error and improve patient outcome after endocrine surgery by supplementing the standard of visual inspection. This dissertation builds on previous work in our lab that demonstrated basic feasibility of NIR fluorescence detection of the parathyroid glands. This dissertation work will advance the development of this parathyroid detection technology by performing studies to lower the barriers to its clinical adoption.

1.3 Specific Aims

Specific Aim 1: Characterize the variability of fluorescence signatures of thyroid and parathyroid tissues. Previous studies have shown the feasibility of detecting a NIR autofluorescence signal in the parathyroid gland that has a higher intensity than all other surrounding neck tissues (7). In this aim, I performed a larger clinical study at Vanderbilt University Medical Center on patients undergoing parathyroidectomy and/or thyroidectomy to identify the effects of patient factors on variability in fluorescence signatures of thyroid and parathyroid tissues. Factors such as disease state, BMI, serum calcium levels, age, and gender were considered. The capability of probe-based NIR fluorescence spectroscopy in identifying parathyroid tissue across a diverse patient population was evaluated using histology as the gold standard when available and compared with the sensitivity of visual inspection. Changes associated with these factors were correlated to the parathyroid fluorescence intensity, and their effect on parathyroid identification was evaluated.

Specific Aim 2: Evaluate the biological basis of the NIR fluorescence signal in the parathyroid gland. Clinical adoption of a technique often requires some understanding of the mechanism behind its functioning. Therefore, I evaluated the biological basis of the fluorescence signal in the parathyroid gland. The behavior of the fluorescence signal was assessed over time

and in response to detergents, heat, and serum proteases. Gel electrophoresis, mass spectrometry, transmission electron microscopy, differential gradient centrifugation, and density gradient centrifugation were performed to understand the source of the NIR fluorescence. NIR fluorescence microscopy was performed on parathyroid tissue cross sections and correlated to immunohistochemical stains to determine the subcellular location of the fluorescence signal. Bulk tissue samples emitting similar NIR autofluorescence signals were identified. The behavior and structural location of the NIR fluorophore in parathyroid gland tissue was characterized.

Specific Aim 3: Develop a clinical fluorescence imaging system and test for discrimination of parathyroid tissue.

Images are more useful for surgical guidance than the point measurements acquired with fluorescence spectroscopy. In this aim, I furthered the development of the parathyroid detection technique by using fluorescence imaging. The minimum imaging system requirements needed for parathyroid detection were assessed by comparing three imaging sensors. Once established, the feasibility of intraoperative, real-time, wide-field NIR fluorescence imaging of the parathyroid gland was demonstrated using a commercial endoscope system. A novel imaging system was then designed to address the shortcomings of traditional methods of surgical NIR imaging by directly projecting NIR fluorescence information onto the surgical field. Hardware and software was developed for this projector imaging system that allows image collection from the tissue site, application of feature extraction algorithms, and direct projection of visible light overlaying areas of NIR autofluorescence in the surgical field. Images were collected and projected intraoperatively on patients at Vanderbilt University Medical Center.

The combination of these three aims investigates the use of NIR autofluorescence spectroscopy and imaging for intraoperative parathyroid detection. The outcomes of this research demonstrate a method to revolutionize endocrine surgeries by increasing accuracy of tissue resection and improving patient outcome. Development of an effective detection tool could lead to fewer complications in endocrine surgery due to accidental injury or incomplete removal of the parathyroid. Through this dissertation work, I achieved a greater depth in understanding of the autofluorescence in the parathyroid gland. In the future, these findings may lead to widespread clinical adoption of this technology for parathyroid detection.

1.4 Summary of Chapters

The material comprising this dissertation is organized in the following manner:

Chapter 1 gives an introduction to the problem motivating this work and provides justification for the technological development discussed in this dissertation. The specific aims used to guide this research are also summarized here.

Chapter 2 provides relevant background material for the research performed in this body of work. This chapter addresses the anatomy and physiology of thyroid and parathyroid glands, challenges in surgical treatment of thyroid and parathyroid disease, traditional methods for parathyroid localization, and the current landscape for near-infrared imaging and spectroscopy. The overall significance of this work is also discussed.

Chapter 3 provides a report on the feasibility of probe-based fluorescence spectroscopy for detecting the parathyroid glands *in vivo* on a pilot patient population. The sensitivity and specificity of the approach are discussed compared to traditional parathyroid detection methods.

Chapter 4 contains a larger, more in-depth patient study that determines the patient factors that affect the parathyroid gland autofluorescence signal intensity. Patient factors such as disease state, age, gender, ethnicity, serum calcium levels, parathyroid hormone levels, vitamin D levels, and body-mass index were investigated for their contribution to parathyroid signal variability.

Chapter 5 describes multiple approaches taken to understand the structural and biochemical nature of the near-infrared endogenous fluorophore present in parathyroid tissue including microscopy, gel electrophoresis, density gradient centrifugation, and transmission electron microscopy.

Chapter 6 contains details of a study testing three different near-infrared fluorescence imaging systems in order to characterize the system specifications needed for parathyroid visualization. This study informed the design requirements for a next generation parathyroid fluorescence imaging system

Chapter 7 describes the first *in vivo* pilot study for intraoperative detection of parathyroid glands during cervical endocrine surgery using a clinical endoscope camera adapted for use in near-infrared fluorescence imaging.

Chapter 8 describes a novel fluorescence imaging approach whereby invisible NIR information is converted to visible light and projected directly on the patient such that the

parathyroid gland are highlighted in a visible green overlay directly on the tissue site. A pilot study was conducted using this system to show feasibility of the approach.

Chapter 9 provides a summary of the major results presented in this dissertation and potential future directions for this project. It also contains information about the broader impact of the research in endocrine surgery, biophotonics, and society at large.

Appendix A is a short summary of alternative approaches explored that were aimed at the evaluation of the identity of the NIR fluorophore in parathyroid tissue.

1.5 References

1. Mohebati A, Shaha AR. Imaging techniques in parathyroid surgery for primary hyperparathyroidism. *American journal of otolaryngology*. 2012 Jul-Aug;33(4):457-68. PubMed PMID: 22154018. Pubmed Central PMCID: 3311773.
2. Kim LAAM. Hyperparathyroidism WebMD2008.
3. Sosa JA, Powe NR, Levine MA, Udelsman R, Zeiger MA. Profile of a clinical practice: Thresholds for surgery and surgical outcomes for patients with primary hyperparathyroidism: a national survey of endocrine surgeons. *The Journal of clinical endocrinology and metabolism*. 1998 Aug;83(8):2658-65. PubMed PMID: 9709928.
4. Doherty GM. *Oncology: An Evidence Approach*: Springer New York; 2006.
5. Pattou F, Combemale F, Fabre S, Carnaille B, Decoulx M, Wemeau JL, et al. Hypocalcemia following thyroid surgery: incidence and prediction of outcome. *World journal of surgery*. 1998 Jul;22(7):718-24. PubMed PMID: 9606288.
6. Sakorafas GH, Stafyla V, Bramis C, Kotsifopoulos N, Kolettis T, Kassaras G. Incidental parathyroidectomy during thyroid surgery: an underappreciated complication of thyroidectomy. *World journal of surgery*. 2005 Dec;29(12):1539-43. PubMed PMID: 16311857.
7. Paras C, Keller M, White L, Phay J, Mahadevan-Jansen A. Near-infrared autofluorescence for the detection of parathyroid glands. *J Biomed Opt*. 2011 Jun;16(6). PubMed PMID: WOS:000293086800038. English.

CHAPTER 2

BACKGROUND

2.1 Anatomy and Physiology of Parathyroid and Thyroid Glands

2.1.1 Parathyroid Gland Anatomy and Physiology

The parathyroid glands are small endocrine glands in the neck that play a key role in maintaining normal extracellular calcium concentration. The parathyroid glands are typically four in number, but there have been reports of patients with anywhere between 1 -12 parathyroid glands. The glands are typically located in the posterior aspect of the thyroid gland (Figure 2.1). The superior parathyroid glands typically lie at the level of the middle third of the thyroid, and the inferior parathyroid glands lie at the level of the inferior third (3). However, significant variations exist in parathyroid location. The parathyroid glands are soft and flabby yielding variable shape and dimensions. An average parathyroid gland is 5x3x1 mm in size and weighs approximately 35-50 mg (4). Parathyroid gland color varies with stromal fat, appearing reddish-brown when little fat is present and yellow-brown when fat is present (4).

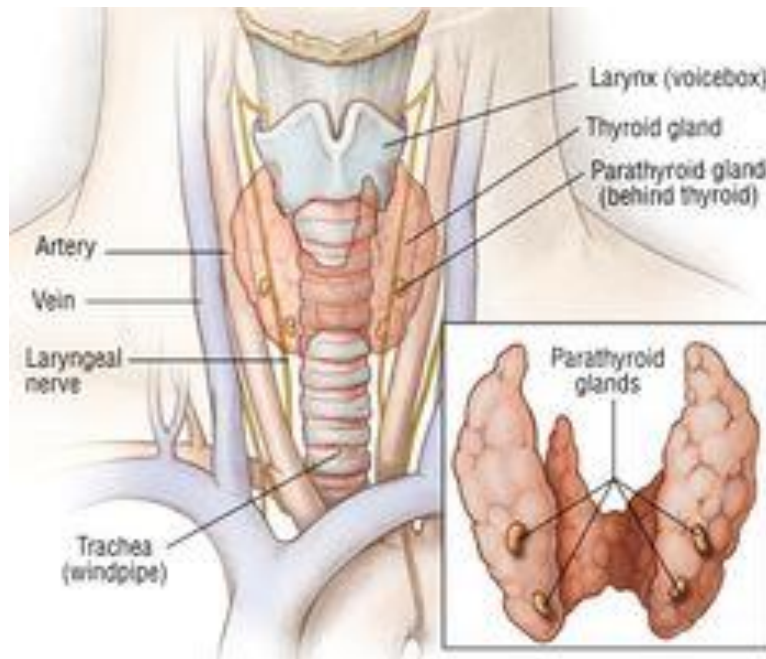


Figure 2.1: Anatomy of the parathyroid and thyroid glands (2)

Parathyroid glands regulate plasma calcium levels by sensing exquisitely small changes in Ca^{2+} and modulating the secretion of parathyroid hormone in response. Parathyroid hormone (PTH) is the principle secretory product of the parathyroid gland, and it is one of the two major hormones modulating calcium and phosphate homeostasis. PTH acts on the kidney, intestines, and bones to regulate calcium metabolism. PTH is essential to life due to its overall effect of increasing Ca^{2+} in the plasma. PTH acts on the bone to mobilize Ca^{2+} stores. Labile pools of Ca^{2+} in bone fluid provide a fast transfer of Ca^{2+} into the plasma, while dissolution of the stable pools of Ca^{2+} in bone minerals serves as a slow transfer of Ca^{2+} and PO_4^{3-} into the plasma. PTH has a rapid effect on renal tubular function in the kidney, leading to increased reabsorption of filtered Ca^{2+} and increased excretion of PO_4^{3-} (4). PTH also enhances the activation of vitamin D by the kidneys. In the intestines, PTH indirectly promotes absorption of Ca^{2+} and PO_4^{3-} by playing a role in vitamin D activation (5).

2.1.2 Thyroid Gland Anatomy and Physiology

The thyroid is a firm, richly vascularized, reddish-brown endocrine gland located on the anterior surface of the trachea just below the larynx. It consists of two lobes that are about 50-60 mm long and joined in the middle by a narrow section called the isthmus, giving it a butterfly shape. Occasionally, the isthmus is replaced by a pyramidal lobe whose apex points cranially due to its descent from the tongue during development (6). Important vocal nerves pass close to the thyroid capsule of the thyroid gland, including the recurrent laryngeal nerve and the external laryngeal nerve (7). In addition, the neck region contains an abundance of vascular, lymphatic, and musculoskeletal tissues.

The thyroid gland synthesizes and secretes thyroid hormones L-thyroxine (T4), L-triiodothyronine (T3), and calcitonin. Thyroid secretion of T3 and T4 regulate metabolic body processes, cellular respiration, total energy expenditure, growth and maturation of tissues as well as the turnover of hormones, substrates and vitamins. The functional unit of the thyroid is the follicle, which are made up of a ring of secretory cells called follicular cells. Follicular cells enclose a lumen called the colloid that serves as an extracellular storage site for thyroid hormones. Thyroglobulin is a large protein molecule found in the colloid that is essential for the synthesis of thyroid hormones. C-cells are a secretory cell type that secrete calcitonin, and are found in the interstitial spaces of the follicular cells (4).

The thyroid fulfills its role through the synthesis and secretion of thyroid hormones to regulate basal metabolic rate and calcitonin to regulate calcium metabolism (5). Thyroid hormones, T3 and T4, directly or indirectly affect nearly every tissue in the body by doing the following: 1) Increasing overall basal metabolic rate to produce a calorogenic effect, 2) Promoting intermediary metabolism of carbohydrates, fats, and proteins, 3) Increasing target cell response to catecholamines, 4) Increasing heart rate and force of contraction, 5) Stimulating growth hormone secretion and promoting the effects of growth hormone on its targets, 6) Assisting in normal nervous system development.

2.2 Parathyroid and Thyroid Disease

Over the past several decades, the incidence of surgical endocrine disorders affecting the parathyroid and thyroid glands has increased. **Primary hyperparathyroidism** is a disorder where one or more parathyroid glands become overactive and secrete excessive amounts of parathyroid hormone. It results in a rise in blood calcium levels (hypercalcemia). Hyperparathyroidism most frequently presents in older post-menopausal women with 1000,000 new cases developed each year (8). Approximately 85% of cases are caused by hyperparathyroidism is by a non-malignant adenoma of one of the parathyroid glands. An overgrowth of normal cells, called hyperplasia, can result in an enlargement of one or more of the glands and cause hyperparathyroidism. The rarest cause of hyperparathyroidism, is **parathyroid cancer**, accounting for less than 1% of all cases (9). Mild symptoms of hyperparathyroidism related to elevated calcium level include joint aches, weakness, fatigue, difficulty concentrating or loss of appetite. In more severe cases where PTH and blood calcium levels are higher, patients may develop impaired kidney function, kidney stones, bone disease, or rheumatologic symptoms such as gout (9). Non-surgical treatment suffices for people with minimal symptoms and mildly elevated blood calcium levels. **Secondary hyperparathyroidism (SHPT)** is the overproduction of parathyroid hormone secondary to a chronic abnormal process stimulating its production. The most common causes of SHPT are chronic kidney disease and vitamin D deficiency. SHPT is associated with four-gland hyperplasia, which is often treated surgically with either a total parathyroidectomy with autotransplantation or a 3.5 gland parathyroidectomy. **Tertiary hyperparathyroidism** occurs after longstanding secondary hyperparathyroidism and is a state of excessive secretion of parathyroid

hormone that results in hypercalcemia. Often times tertiary hyperparathyroidism is diagnosed when secondary hyperparathyroidism persists after a renal transplantation.

Diseases of the thyroid can be classified as structural, functional, or both. Functional disorders occur when the thyroid does not produce normal levels of thyroid hormone such as in hypothyroidism or hyperthyroidism. **Hypothyroidism** is a condition where the thyroid does not produce enough thyroid hormone. It primarily affects women over the age of 60 and can be treated with synthetic thyroid hormones. **Hyperthyroidism** is a disease of the thyroid gland characterized by an overproduction of free thyroid hormone. In over 70% of cases, hyperthyroidism is caused by **Graves' disease**. Graves' disease is an autoimmune disorder causing an overactive thyroid gland, which can affect metabolic rate. This disorder primarily affects women between the ages of 20 to 40. Common symptoms of hyperthyroidism include anxiety, weakness, tremors, excessive perspiration, rapid heartbeats, and weight loss. Medicine, radioiodine, or surgery can be used to treat hyperthyroidism, depending on age and severity of the condition.

Structural thyroid diseases include conditions such as thyroid nodules and goiters. **Thyroid nodules** are a collection of cells within the thyroid that grow to produce a lump. These are relatively common, occurring in 1.6% of adult women and 0.1% of adult men (10). The thyroid may contain a single nodule (uninodular goiter) or several nodules (multinodular goiter). A majority of thyroid nodules are benign but may be classified as malignant depending on their composition and potential to spread beyond the thyroid gland (10). A multinodular goiter is an enlarged thyroid gland with a goiter consisting of several thyroid nodules. Goiters may result if the thyroid is inefficient at making thyroid hormone, causing an enlargement of the gland to compensate. This commonly occurs in poverty-stricken areas due to dietary iodine deficiency, affecting over 100 million people worldwide (11). Goiters can also be caused by inflammation of the thyroid gland (thyroiditis) or thyroid tumors. Goiters may be non-toxic or toxic. Non-toxic goiters are a simple enlargement of the thyroid without an increase in thyroid hormone secretion. Toxic goiters are associated with hyperthyroidism and can be treated with anti-thyroid medication, iodine treatment, or surgery (12). **Thyroid cancer** is a malignant neoplasm that can arise from the parafollicular or follicular cells of the thyroid. In 2013, there were an estimated 60,000 new cases of thyroid cancer in the US alone, mostly affecting women between ages 25 to

65 (13). The most common management of thyroid cancer is surgical resection, radioactive iodine ablation, hormone treatment, and chemotherapy.

2.3 Challenge: Parathyroid Detection during Endocrine Surgery

For many endocrine disorders, removal of diseased tissue during parathyroidectomy or thyroidectomy procedures may be the only curative option. Patient outcome is strongly dependent on the ability of the surgeon to resect diseased tissue while conserving normal tissue. In the specific case of parathyroidectomy and thyroidectomy procedures, accurate localization of the parathyroid glands relies on visual inspection by the surgeon. Because of the small size and variable position of the parathyroid glands, they are difficult to distinguish from thyroid and surrounding tissues in the neck. As a result, parathyroidectomies and thyroidectomies often result in insufficient removal or damage to the parathyroid (14). Hypoparathyroidism from inadvertent parathyroidectomy during thyroidectomy is a potentially debilitating disorder occurring in up to 50% of cases (15). Patients who experience this may present with mild central nervous system symptoms such as numbness, spasm, confusion or seizures. It may also lead to respiratory compromise or in some cases congestive heart failure and arrhythmias. The treatment for these patients involves life-long administration of calcium and vitamin D supplements, significantly affecting their quality of life (16). Effective surgical treatment of thyroid and parathyroid disease is dependent on accurate localization of the parathyroid glands. However, parathyroid detection during surgery can be highly subjective and dependent on the experience of the surgeon. Studies have shown that surgeons whose practice is made up of less than 25% of endocrine procedures perform 82% of thyroidectomies and 78% of parathyroidectomies in the United States (17). Complications are particularly prevalent in these hospitals receiving a low volume of endocrine cases (18).

2.4 Current Parathyroid Detection Techniques

An ideal parathyroid localizing technique has yet to be established. Localization and identification of parathyroid glands has been attempted by a variety of invasive and non-invasive techniques such as preoperative ultrasound, Sestamibi scintigraphy, computed tomography (CT), magnetic resonance imaging (MRI) and intraoperative intact parathyroid hormone (iPTH) assay (19). These existing methods for identifying parathyroid glands are limited in their applicability and sensitivity, rendering them inadequate to fully prevent surgical complications (20). Most rely on preoperative identification of diseased parathyroid glands either by size or uptake of radiotracer, limiting their intraoperative utility. US is the most frequently used preoperative imaging technique due to its low cost and safety. However it is highly operator-dependent and not reliable for visualization of healthy parathyroid glands due to their small size and similarity in acoustic signal to thyroid. Though US is highly sensitive when detecting enlarged parathyroid glands, false-positives and false-negatives result from thyroid nodules, blood vessels, lymph nodes or esophagus. Sestamibi scintigraphy is a nuclear medicine technique where a radioactive agent is injected in the patient and selectively absorbed by the hypersecreting gland. It can convey broad information on gland location, but it is limited by its ability to only localize hypersecreting glands. Sestamibi also has the disadvantage of requiring radiotracers and providing little anatomical detail (21). The sensitivity of Sestamibi scintigraphy and preoperative ultrasound is only 47-61% as reported in most studies (22, 23). CT relies on the vascularity of parathyroid glands for imaging. Its sensitivity can range from 40 – 80% with high dependence on size of lesion and experience of the radiologist. In areas such as the sternal notch and mediastinum, CT can fail to identify parathyroid glands because of artifacts or confusion with lymph nodes. Imaging modalities such as CT and MRI are prone to false-negatives and false-positives and have low sensitivity (19). Cost, especially for CT scanning and MRI remains prohibitive for routine use. Intraoperative parathyroid hormone assay takes advantage of the short half-life of PTH to measure the amount of circulating hormone at the time and location a sample is obtained. The accuracy of iPTH is dependent on the surgeon's familiarity. It requires specialized centers close to the site of operation because of the 2 to 4 minute half-life of PTH (19). The turn-around time for iPTH monitoring with state-of-the-art assays still runs at least 9 minutes, not taking into account the travel time of the sample to the assay machine. There remains a need for a way to accurately identify parathyroid tissue intraoperatively.

2.5 Optical Imaging and Spectroscopy

Light based methods have been shown to provide fast, non-invasive characterization of tissues. Traditional optical techniques are applied to diagnosis of tissue pathology by detection biochemical, chemical, or physiological changes that occur as diseases progress. Optical spectroscopy and imaging techniques can improve the accuracy of clinical decisions by aiding visual inspection, which can be highly subjective and dependent on the experience of the surgeon. When compared to conventional imaging methods, optical imaging produces higher resolution images in real-time to inform surgical decisions while the patient is still in the operating room (24). Optical techniques have less extensive and relatively inexpensive instrumentation that can be easily adapted into the surgical suite. It offers high sensitivity detection (25) with low toxicity to the patient. Wavelength can be varied according to application in order to target a wide variety of intrinsic or exogenous tissue biomarkers (26).

This dissertation investigates the use of NIR fluorescence spectroscopy and imaging to detect the parathyroid gland. Rather than optically differentiating human pathology, fluorescence spectroscopy and imaging is used to detect anatomical differences between parathyroid and surrounding tissues based on an intrinsic fluorophore. In addition NIR fluorescence spectroscopy and imaging, several light based methods under investigation for the intraoperative identification of parathyroid tissue will be described.

2.5.1 Optical Coherence Tomography for Parathyroid Detection

Optical coherence tomography (OCT) is a non-invasive medical imaging technique that performs high resolution, cross-sectional tomographic imaging of tissue microstructure by measuring back-scattered or back-reflected light. OCT is the optical analog to ultrasound imaging in that it uses light rather than sound. OCT can provide image resolutions between 1 – 15 μm , which is several orders of magnitude higher than conventional ultrasound (27). In non-transparent tissues, OCT can image the micro-architectural features up to 2 mm in depth. This technique has been applied to obtain real-time, high spatial resolution images of tissues across multiple fields such as dermatology, urology, gynecology, ophthalmology, and gastroenterology (27-31). Recent investigators have applied OCT to parathyroid identification during surgery (1, 32-34). In one study, 32 patients undergoing parathyroidectomy, thyroidectomy, or lymphandectomy were recruited. Across all patients, 520 OCT images were collected from

normal and diseased glands and correlated with histopathology. Results showed OCT could differentiate the parathyroid glands from surrounding structures with a sensitivity and specificity of 84% and 94%. The thin, highly backscattering capsule surrounding parathyroid glands provided a bright source of contrast up to 0.5 mm in depth (Figure 2.2). No difference was found between normal and diseased glands (1). Difficulty in distinguishing parathyroid and lymph tissue was observed (33). Barriers to adoption of OCT in surgical identification of parathyroid glands includes low intraoperative image quality due to artifacts and difficulty handling intraoperative OCT probes, and the high cost of OCT systems (1, 33).

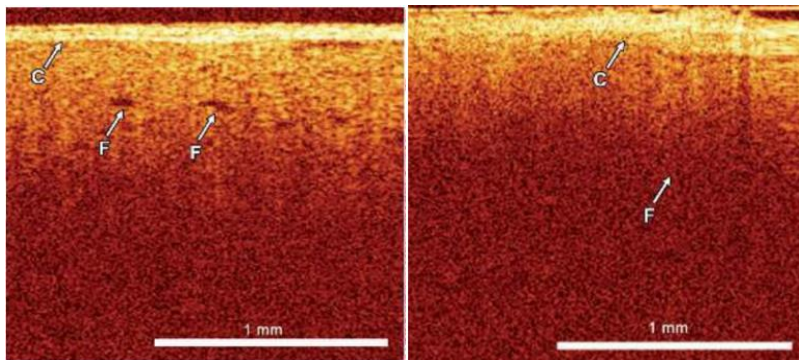


Figure 2.2. OCT images of parathyroid (left) and lymph node (right). C=capsule, F=fatty deposits. (1)

2.5.2 Optical Spectroscopy for Parathyroid Detection

Raman spectroscopy and diffuse reflectance have been used to discriminate endocrine tissues. Raman spectroscopy utilizes the inelastic scattering of monochromatic light from a laser source to detect a unique molecular “fingerprint” of a sample. Photons of laser light are absorbed by the sample and reemitted at a different frequency. This shifting in frequency is called the Raman Effect and provides information about the vibrational, rotation, and other low frequency transitions in molecules (35). Raman spectroscopy gives high molecular specificity and sensitivity to provide a differential diagnosis between tissues. This modality has been studied extensively for disease detection such as cervical dysplasia (36, 37), breast cancer (38, 39), skin cancer (40, 41), and more. Recently, researchers have attempted to apply Raman spectroscopy to parathyroid tissue to identify parathyroid tissue pathology. One group used near-infrared Raman spectroscopy specifically for the differentiation between parathyroid adenomas and parathyroid

hyperplasia due to the clinical difficulty in making this distinction (42). With a small sample size of 15 glands, their results showed a detection sensitivity of 95% for parathyroid adenomas and 93% for hyperplastic glands. The biochemical mechanism for the difference between adenomas and hyperplasia was not elucidated. This technique shows promise to distinguish between parathyroid disease type, and more samples must be measured for validation. This technique was not applied to the differentiation of parathyroid tissue and surrounding neck tissue such as thyroid, lymph nodes, fat, and muscle.

In addition to Raman spectroscopy, diffuse reflectance spectroscopy was attempted for tissue discrimination in the neck. Diffuse reflectance spectra acquired between 350-1850 nm were measured. The study successfully differentiate nerve tissue with 78% sensitivity, however, the ability of the technique to identify the parathyroid gland was limited (43).

2.5.3 NIR Fluorescence Spectroscopy and Imaging

This dissertation describes the use of NIR fluorescence spectroscopy and imaging for successful parathyroid detection. Fluorescence spectroscopy and imaging is one of the most widely used optical techniques for *in vivo* characterization of tissues especially in clinical oncology (26, 44, 45). Fluorescence spectroscopy employs the emission of light from an electronically excited state. Fluorescence is brought about by absorption of photons in the singlet ground state promoted to a singlet excited state (S₂). Excitation will occur when incident photons contain energy equal to gap between singlet states, allowing electrons to absorb enough energy to jump up to one of the higher states. The amount of energy required to excite each fluorophore differs, meaning wavelength can be optimized for maximal fluorescence depending on the molecule. The excited molecule initially undergoes non-radiative relaxation in which the excitation energy is dispersed as vibrations or heat to the solvent, and no photon is emitted. Subsequently, the excited molecule returns to ground state. This involves the emission of a photon of lower energy, which corresponds to a longer wavelength than the absorbed photon (Figure 2.3). The energy difference between the excited photon and the emitted photon is called the Stokes' Shift. The process of fluorescence occurs on a timescale of nanoseconds (46).

NIR fluorescence spectroscopy and imaging is particularly attractive because it takes advantage of an “optical window” between 700 – 900 nm. This wavelength range offers several millimeter penetration depth and decreased scattering and absorption of biomolecules relative to

ultraviolet and visible wavelengths (47), making the NIR region optimal for studies on the diagnosis and detection of disease.

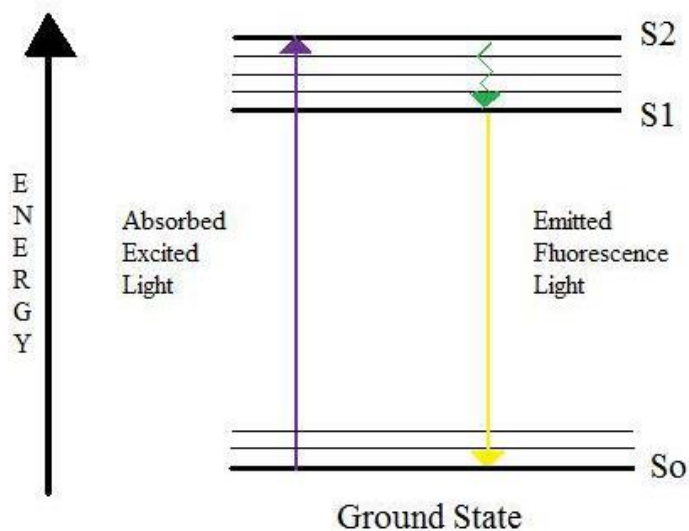


Figure 2.3: Jablonski diagram representing fluorescence

2.5.3.1 NIR Fluorophores: Extrinsic and Intrinsic

Fluorescence spectroscopy instrumentation must cater to applications based on properties of the fluorescing compound, called a fluorophore. Fluorophores can be intrinsic or extrinsic. Intrinsic fluorophores are naturally occurring and often emit weaker fluorescence than exogenous, or externally administered fluorophores that are added to provide contrast. Known sources of endogenous fluorescence include aromatic amino acids (i.e. tryptophan, tyrosine, phenylalanine), enzyme cofactors (NADH, FAD, pyridoxyl phosphate), and intact tissue components such as porphyrins, collagen, elastin, and lipofuscins. These well studied endogenous fluorophores are shown to have peak excitation and emission wavelengths in the visible and ultraviolet regions (46).

Specifically in the NIR region of the electromagnetic spectrum, intrinsic fluorophores are rare. There are few published accounts of near infrared autofluorescence beyond 680 nm being observed in tissues. In some studies NIR fluorescence has been reported in the fundus but there is not definitive evidence of the origin of the signal (48). Porphyrins and their derivatives are

endogenous fluorophores with the longest known emission wavelength, with peak emission between 620-700 nm (49).

Because NIR wavelengths are attractive for biomedical imaging due to their increased penetration depth in biological tissues due to low scattering, low absorption, and low background autofluorescence, research in NIR fluorescence most commonly involves extrinsic contrast agents. Common NIR contrast agents include cyanines like indocyanine green (50, 51), phthalocyanines / porphyrins / pyrroles (52), squaraines, or BODIPYs (53). However, exogenous dyes can suffer from false-positive results due to non-specific tissue targeting, potential toxicity, and elongated procedure time due to pre-administration (54). NIR fluorescence spectroscopy and imaging of parathyroid glands has been done with exogenous contrast agents. Contrast agents (T700-F and T800-F) were injected in animal models to image the thyroid and parathyroid glands (55). In another report, methylene blue was used as the contrast agent in rabbits (56) as well as humans (57). However these approaches, unlike the approach described in this dissertation, rely on extrinsic contrast and uptake of the agent for its success.

In this work, we have discovered a novel NIR endogenous fluorophore in the parathyroid gland that could be detected *in vivo* and avoid the challenges associated with the use of contrast agents while still taking advantage of the deeper penetration depth and low background autofluorescence unique to the longer NIR wavelength.

Device	Excitation Source	Fluorescence Collection	Dye imaging or autofluorescence?	Application
Photodynamic Eye (Hamamatsu)	LED at 760 nm	820 nm Bandpass filter	Dye	Intraoperative ICG imaging of blood vessels and lymph nodes ¹
SPY (Novadaq)	LED at 806 nm	835 nm "camera"	Dye	Blood flow in vessels, tissue and organ perfusion in coronary artery bypass, cardiovascular, plastic, reconstructive, organ transplant and gastrointestinal surgery ²
FLARE (Frangioni lab)	LED at 745-779nm	808-848 nm bandpass filter	Dye	Tumor delineation ³
HyperEye (Mizuho Medical)	LED at 760 nm	840 nm cut-on filter	Dye	ICG fluorescence angiography ⁴
Custom System (Ntziachristos lab)	Laser diode at 750 nm	795 nm bandpass filter	Dye	Sentinel lymph node detection, tumor delineation ⁵
Fluobeam (Fluoptics)	Laser at 750 nm	>800 nm	Dye	Visualization of the blood flow, lymphatic flow, identification of the bile ducts during hepatobiliary surgery, detection of primary liver tumors and/or hepatic metastases ⁶

Table 2.1: Summary of near-infrared imaging systems in literature

2.5.3.2 Current Near-infrared Fluorescence Imaging Systems

In the past decade, numerous NIR fluorescence imaging techniques have been developed for clinical applications such as tumor margin detection, sentinel lymph node mapping, and detection of brain vasculature (58). The growing popularity of NIR fluorescence imaging techniques can be partially attributed to its ability to deliver high sensitive and real-time information. The most prevalent approach for NIR fluorescence imaging has utilized exogenous contrast from indocyanine green (ICG) or methylene blue. Table 2.1 summarizes some of the most prominent NIR imaging systems reported in literature such as the Photodynamic Eye (59), SPY system (60), FLARE (61), Fluobeam (62), and NIR goggles (63). These system use a variety of approaches such as multiple cameras to capture NIR and color images simultaneously, or single cameras to capture images sequentially. The systems can be hand-held, mounted with remote display or worn in the form of goggles. The light sources vary from light emitting diodes (LEDs), filtered white light sources, or diode lasers. A majority of the NIR fluorescence imaging systems in use require dimming of the operating room lights, but some groups have utilized a method whereby pulsed excitation and gated acquisition allows NIR imaging with the room lights on (64). Although there have been many advances in the development of NIR imaging systems, a majority of these systems are used for dye imaging. There is a need for an NIR imaging system that can be used in autofluorescence applications that have lower intensities of NIR signal. This proposal discusses the development and testing of an NIR imaging system for NIR autofluorescence.

2.5.4 Previous work on NIR fluorescence detection of the parathyroid

The high NIR autofluorescence signal in the parathyroid glands was discovered prior to this dissertation work by members of the biophotonics lab at Vanderbilt University. At the time of the discovery, very little work was being done at the intersection of endocrine surgery and biophotonics. Initial *in vitro* studies used Raman spectroscopy to determine differences between the parathyroid gland and thyroid gland in a canine model. These experiments were conducted with a portable Raman spectroscopy system comprised of a 785 nm diode laser (Innovative Photonic Solutions, NJ), a fiber optic probe (EMVision, FL) delivering 80 mW of light to tissue, an imaging spectrograph (Kaiser Optical Systems, Inc., MI), and back-illuminated, deep-depletion, charge coupled device (CCD) camera (Andor Technology, CT), all controlled with a

laptop computer. The results revealed a striking background fluorescence from the parathyroid gland that saturated the detector with a 30 ms integration time. The integration time was reduced from 3 s to 30 ms before a non-saturated signal could be acquired and processed for Raman signal extraction. Conversely, the raw Raman spectra of the other tissue types did not saturate with an integration time of 3 s. An *in vivo* Raman study on patients undergoing parathyroid and thyroid surgery revealed similar results with high background autofluorescence emitted from parathyroid tissue (Figure 2.4). The results indicated that NIR fluorescence spectroscopy with 785 nm excitation was a superior optical method to Raman spectroscopy because clear autofluorescence was observed, which obscured the Raman signal.

The fluorescence of the parathyroid and thyroid was characterized in the lab by performing optical property measurements such as excitation-emission matrices (EEM), reduced scattering coefficient, and absorption coefficient. The EEM revealed the presence of a single prominent emission peak at 822 nm in both thyroid and parathyroid tissues. Results indicated the fluorophore in the parathyroid gland has an optimal emission peak at 822 nm under 785 nm excitation. The reduced scattering coefficient, μ_s' , of both the thyroid and parathyroid is relatively constant over the 700-900 nm wavelength range. Parathyroid tissue shows greater scattering, with a $\mu_s' \approx 2\text{mm}^{-1}$ across this entire wavelength range. Thyroid scattering was lower, at $\mu_s' \approx 1.1\text{mm}^{-1}$. The absorption coefficient of both thyroid and parathyroid was approximately equal across the NIR. Absorption decreases linearly from $\mu_a \approx 0.02\text{ mm}^{-1}$ at 700 nm to less than $\mu_a \approx 0.005\text{ mm}^{-1}$ at 800 nm. Parathyroid absorption increases slightly starting at 860 nm up to $\mu_a \approx 0.01\text{ mm}^{-1}$ at 900 nm.

Finally, an *in vivo* pilot study of NIR fluorescence spectroscopy for parathyroid detection was performed on 21 patients. Results validated NIR fluorescence spectroscopy for parathyroid detection. The feasibility studies performed set the stage for this dissertation work which is aimed at lowering the barriers to clinical translation of this technique.

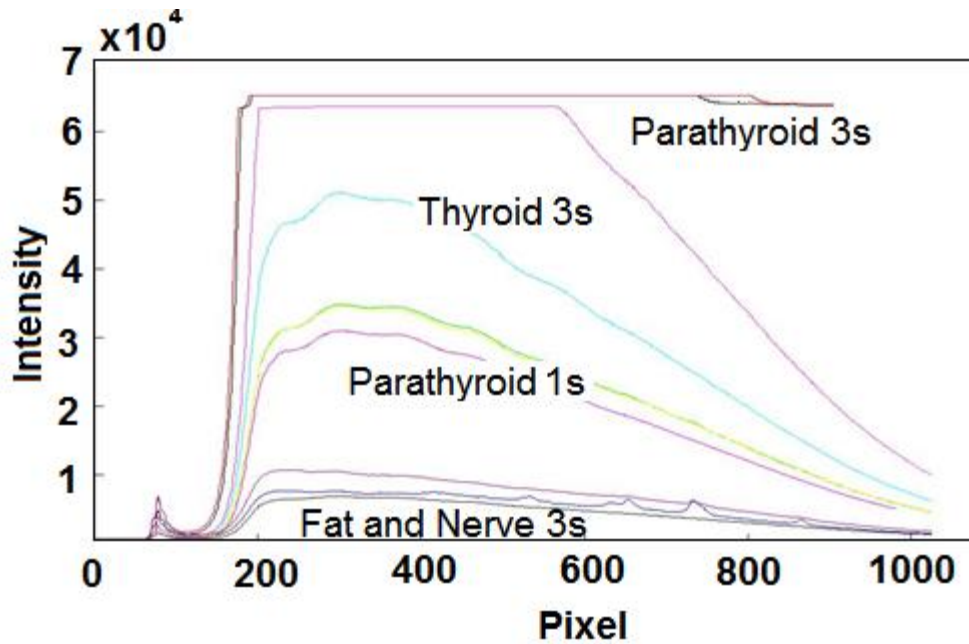


Figure 2.4: *In vivo* Raman spectra of the parathyroid and thyroid glands of a typical patient during endocrine surgery

2.6 Significance and Impact

2.6.1 Novel intraoperative method for parathyroid gland identification

This dissertation addresses an unmet need in endocrine surgery for intraoperative identification of the parathyroid gland during thyroidectomy and parathyroidectomy procedures using a unique application of fluorescence spectroscopy and imaging. In thyroidectomy cases, the prevalence of transient hypocalcemia ranges from 19 to 38% and the prevalence of permanent hypoparathyroidism is as high as 3% (65). This results from insufficient identification of the parathyroid gland during surgery leading to trauma or devascularization. The consequences of insufficient parathyroid identification during parathyroidectomy procedures can lead to re-operation or morbidity. Current methods of parathyroid identification are solely focused on detection of diseased glands. This dissertation focuses on parathyroid gland anatomical identification regardless of disease state. Furthermore, many of the current methods for diseased parathyroid gland identification require preoperative imaging, frozen section analysis or assay

measurements, all of which do not provide real-time intraoperative information. The method described in this dissertation identifies the parathyroid gland in real-time during the procedure. Such a method has the potential to transform the gold standard approach to endocrine procedures. It could reduce the risk of parathyroidectomy and thyroidectomy in low volume centers and in cases with residents and surgeons with little experience who typically have higher rates of inadvertent parathyroid removal in thyroidectomy cases (14).

2.6.2 Novel endogenous near-infrared fluorophore

Near-infrared spectroscopy and imaging has largely focused on dye based applications using indocyanine green or methylene blue due to the lack of endogenous fluorophores in the near-infrared region. This dissertation uncovers a source of endogenous near-infrared fluorescence that enables medical imaging without synthetic dyes. The fluorophore described here has near-infrared fluorescence at 785nm excitation and 822nm emission. Porphyrins are the longest emitting biological fluorophore known (46). Peak fluorescence emission emitting in the 800 nm range is not commonly reported in literature. Therefore, a new NIR endogenous fluorophore provides a new source of contrast that can be used as an alternative to exogenous contrast in select applications. Researchers and clinicians may benefit from this robust tissue-specific intrinsic contrast in applications such as fluorescence microscopy, whole animal imaging, or surgical imaging modalities. Because the excitation and emission wavelengths are very similar to the widely used ICG dyes, the biomedical community may benefit from using very similar instrumentation to that which is already used. This fluorophore could present a new tool to enhance fundamental understanding of endocrine physiology. This endogenous fluorophore may provide a molecular probe that can be studied to learn more about basic endocrine physiology and pathophysiology.

2.6.3 A Unique Approach to Surgical Imaging

Near-infrared fluorescence imaging is a rapidly growing field in medicine and surgery. Many of the imaging systems under development and in use have two common attributes. First, they require the use of synthetic dyes. Second, they relay information to the end-users via a remote display (i.e. monitor). As a result, clinicians receive the visual image in a separate location from the point-of-care, thereby disrupting the flow of the procedure. This dissertation presents a unique

overlay method of projecting the processed near-infrared image back on the surgical field in real-time to guide the procedure. The method discussed focuses on near-infrared fluorescence imaging of the parathyroid gland, but the approach could be widely applied to many different disease applications and types of imaging.

2.7 References

1. Ladurner R, Hallfeldt KK, Al Arabi N, Stepp H, Mueller S, Gallwas JK. Optical coherence tomography as a method to identify parathyroid glands. *Lasers in surgery and medicine*. 2013 Dec;45(10):654-9. PubMed PMID: 24249200.
2. LearnBones. Primary Hyperparathyroidism www.learnbones.com2012.
3. Daniel Oertil RU. *Surgery of the Thyroid and Parathyroid Glands*: Springer; 2012.
4. Livolsi VA, Asa, Syliva L.,. *Endocrine Pathology*: Saunders; 2002.
5. Sherwood L. *Human Physiology: From Cells to Systems*: Cengage Learning; 2006.
6. Schuenke M, Schulte Erik, Schumacher, Udo. *Neck and Internal Organs (THIEME Atlas of Anatomy)*. Thieme, editor2011.
7. Fancy T, Daniel Gallagher, and Joshua D. Hornig. *Surgical anatomy of the thyroid and parathyroid glands*. *Otolaryngologic clinics of North America*. 2010;43(2):221-7.
8. Lal G CO. *Textbook of Endocrine Surgery*: Philadelphia: Elsevier; 2005. 384-92 p.
9. Patient information: Primary hyperparathyroidism (Beyond the Basics) [Internet]. 2013.
10. Golden SH, Robinson KA, Saldanha I, Anton B, Ladenson PW. Clinical review: Prevalence and incidence of endocrine and metabolic disorders in the United States: a comprehensive review. *The Journal of clinical endocrinology and metabolism*. 2009 Jun;94(6):1853-78. PubMed PMID: 19494161.
11. Zimmermann MB, Jooste PL, Pandav CS. Iodine-deficiency disorders. *Lancet*. 2008 Oct 4;372(9645):1251-62. PubMed PMID: 18676011.
12. Nygaard B. Hyperthyroidism. *American family physician*. 2007 Oct 1;76(7):1014-6. PubMed PMID: 17956073.
13. *Cancer Facts & Figures 2013* [Internet]. American Cancer Society. 2013.
14. Rajinikanth J, Paul MJ, Abraham DT, Ben Selvan CK, Nair A. Surgical audit of inadvertent parathyroidectomy during total thyroidectomy: incidence, risk factors, and outcome.

Medscape journal of medicine. 2009;11(1):29. PubMed PMID: 19295950. Pubmed Central PMCID: 2654678.

15. Asari R, Passler C, Kaczirek K, Scheuba C, Niederle B. Hypoparathyroidism after total thyroidectomy: a prospective study. Archives of surgery. 2008 Feb;143(2):132-7; discussion 8. PubMed PMID: 18283137.

16. Khan MI, Waguespack SG, Hu MI. Medical management of postsurgical hypoparathyroidism. Endocrine practice : official journal of the American College of Endocrinology and the American Association of Clinical Endocrinologists. 2011 Mar-Apr;17 Suppl 1:18-25. PubMed PMID: 21134871.

17. Saunders BD, Wainess RM, Dimick JB, Doherty GM, Upchurch GR, Gauger PG. Who performs endocrine operations in the United States? Surgery. 2003 Dec;134(6):924-31; discussion 31. PubMed PMID: 14668724.

18. Sosa JA, Bowman HM, Tielsch JM, Powe NR, Gordon TA, Udelsman R. The importance of surgeon experience for clinical and economic outcomes from thyroidectomy. Ann Surg. 1998 Sep;228(3):320-30. PubMed PMID: 9742915. Pubmed Central PMCID: 1191485.

19. Mohebati A, Shaha AR. Imaging techniques in parathyroid surgery for primary hyperparathyroidism. American journal of otolaryngology. 2012 Jul-Aug;33(4):457-68. PubMed PMID: 22154018. Pubmed Central PMCID: 3311773.

20. Antakia R, Edafe O, Uttley L, Balasubramanian SP. Effectiveness of preventative and other surgical measures on hypocalcemia following bilateral thyroid surgery: a systematic review and meta-analysis. Thyroid : official journal of the American Thyroid Association. 2015 Jan;25(1):95-106. PubMed PMID: 25203484.

21. Whitcroft KL, Sharma A. Sestamibi scintigraphy for parathyroid localisation: a reminder of the dangers of false positives. BMJ case reports. 2014;2014. PubMed PMID: 24618871.

22. Nichols KJ, Tomas MB, Tronco GG, Palestro CJ. Sestamibi parathyroid scintigraphy in multigland disease. Nuclear medicine communications. 2012 Jan;33(1):43-50. PubMed PMID: 22001718.

23. Patel CN, Salahudeen HM, Lansdown M, Scarsbrook AF. Clinical utility of ultrasound and 99mTc sestamibi SPECT/CT for preoperative localization of parathyroid adenoma in patients with primary hyperparathyroidism. Clinical radiology. 2010 Apr;65(4):278-87. PubMed PMID: 20338394.

24. Kherlopian AR, Song T, Duan Q, Neimark MA, Po MJ, Gohagan JK, et al. A review of imaging techniques for systems biology. BMC systems biology. 2008;2:74. PubMed PMID: 18700030. Pubmed Central PMCID: 2533300.

25. Muller J, Wunder A, Licha K. Optical imaging. Recent results in cancer research Fortschritte der Krebsforschung Progres dans les recherches sur le cancer. 2013;187:221-46. PubMed PMID: 23179883.

26. Wagnieres GA, Star WM, Wilson BC. In vivo fluorescence spectroscopy and imaging for oncological applications. *Photochemistry and photobiology*. 1998 Nov;68(5):603-32. PubMed PMID: 9825692.
27. Fujimoto JG, Pitris C, Boppart SA, Brezinski ME. Optical coherence tomography: an emerging technology for biomedical imaging and optical biopsy. *Neoplasia*. 2000 Jan-Apr;2(1-2):9-25. PubMed PMID: 10933065. Pubmed Central PMCID: 1531864.
28. Gambichler T, Jaedicke V, Terras S. Optical coherence tomography in dermatology: technical and clinical aspects. *Archives of dermatological research*. 2011 Sep;303(7):457-73. PubMed PMID: 21647692.
29. Tsai TH, Lee HC, Ahsen OO, Liang K, Giacomelli MG, Potsaid BM, et al. Ultrahigh speed endoscopic optical coherence tomography for gastroenterology. *Biomedical optics express*. 2014 Dec 1;5(12):4387-404. PubMed PMID: 25574446. Pubmed Central PMCID: 4285613.
30. Kharchenko S, Adamowicz J, Wojtkowski M, Drewa T. Optical coherence tomography diagnostics for onco-urology. Review of clinical perspectives. *Central European journal of urology*. 2013;66(2):136-41. PubMed PMID: 24579012. Pubmed Central PMCID: 3936153.
31. Ascencio M, Collinet P, Cosson M, Mordon S. [The role and value of optical coherence tomography in gynecology]. *Journal de gynécologie, obstétrique et biologie de la reproduction*. 2007 Dec;36(8):749-55. PubMed PMID: 17822859. Place et interet de la tomographie par coherence optique en gynécologie.
32. Sommerey S, Ladurner R, Al Arabi N, Mortensen U, Hallfeldt K, Gallwas J. Backscattering intensity measurements in optical coherence tomography as a method to identify parathyroid glands. *Lasers in surgery and medicine*. 2015 Aug;47(6):526-32. PubMed PMID: 26032506.
33. Sommerey S, Al Arabi N, Ladurner R, Chiapponi C, Stepp H, Hallfeldt KK, et al. Intraoperative optical coherence tomography imaging to identify parathyroid glands. *Surgical endoscopy*. 2015 Sep;29(9):2698-704. PubMed PMID: 25475518.
34. Conti de Freitas LC, Phelan E, Liu L, Gardecki J, Namati E, Warger WC, et al. Optical coherence tomography imaging during thyroid and parathyroid surgery: a novel system of tissue identification and differentiation to obviate tissue resection and frozen section. *Head & neck*. 2014 Sep;36(9):1329-34. PubMed PMID: 23956009.
35. Colthup N. *Introduction to infrared and Raman Spectroscopy*. Elsevier, editor2012.
36. Robichaux-Viehoever A, Kanter E, Shappell H, Billheimer D, Jones H, 3rd, Mahadevan-Jansen A. Characterization of Raman spectra measured in vivo for the detection of cervical dysplasia. *Appl Spectrosc*. 2007 Sep;61(9):986-93. PubMed PMID: 17910796.

37. Kanter EM, Vargis E, Majumder S, Keller MD, Woeste E, Rao GG, et al. Application of Raman spectroscopy for cervical dysplasia diagnosis. *Journal of biophotonics*. 2009 Feb;2(1-2):81-90. PubMed PMID: 19343687. Pubmed Central PMCID: 3960286.
38. Keller MD, Vargis E, de Matos Granja N, Wilson RH, Mycek MA, Kelley MC, et al. Development of a spatially offset Raman spectroscopy probe for breast tumor surgical margin evaluation. *J Biomed Opt*. 2011 Jul;16(7):077006. PubMed PMID: 21806286. Pubmed Central PMCID: 3144975.
39. Bi X, Rexer B, Arteaga CL, Guo M, Mahadevan-Jansen A. Evaluating HER2 amplification status and acquired drug resistance in breast cancer cells using Raman spectroscopy. *J Biomed Opt*. 2014 Feb;19(2):025001. PubMed PMID: 24496495. Pubmed Central PMCID: 3913568.
40. Lieber CA, Majumder SK, Ellis DL, Billheimer DD, Mahadevan-Jansen A. In vivo nonmelanoma skin cancer diagnosis using Raman microspectroscopy. *Lasers in surgery and medicine*. 2008 Sep;40(7):461-7. PubMed PMID: 18727020. Pubmed Central PMCID: 2782422.
41. Lieber CA, Majumder SK, Billheimer D, Ellis DL, Mahadevan-Jansen A. Raman microspectroscopy for skin cancer detection in vitro. *J Biomed Opt*. 2008 Mar-Apr;13(2):024013. PubMed PMID: 18465976.
42. Das K, Stone N, Kendall C, Fowler C, Christie-Brown J. Raman spectroscopy of parathyroid tissue pathology. *Lasers in medical science*. 2006 Dec;21(4):192-7. PubMed PMID: 17024320.
43. Schols RM, ter Laan M, Stassen LP, Bouvy ND, Amelink A, Wieringa FP, et al. Differentiation between nerve and adipose tissue using wide-band (350-1,830 nm) in vivo diffuse reflectance spectroscopy. *Lasers in surgery and medicine*. 2014 Sep;46(7):538-45. PubMed PMID: 24895321.
44. Atyaoui M, Dimassi W, Tounsi N, Jaidan NE, Ezzaouia H. Fluorescence spectroscopy and imaging to improve diagnosis of normal and tumoral cytological pancreatic cells. *Pathology, research and practice*. 2013 Jan 15;209(1):1-5. PubMed PMID: 23177616.
45. Ebenezar J, Ganesan S, Aruna P, Muralinaidu R, Renganathan K, Saraswathy TR. Noninvasive fluorescence excitation spectroscopy for the diagnosis of oral neoplasia in vivo. *J Biomed Opt*. 2012 Sep;17(9):97007-1. PubMed PMID: 23085924.
46. Lakowicz JR. *Principles of Fluorescence Spectroscopy*: Springer Science & Business Media; 2013.
47. Hadjipanayis CG, Jiang H, Roberts DW, Yang L. Current and future clinical applications for optical imaging of cancer: from intraoperative surgical guidance to cancer screening. *Seminars in oncology*. 2011 Feb;38(1):109-18. PubMed PMID: 21362519. Pubmed Central PMCID: 3061227.

48. Keilhauer CN, Delori FC. Near-infrared autofluorescence imaging of the fundus: visualization of ocular melanin. *Investigative ophthalmology & visual science*. 2006 Aug;47(8):3556-64. PubMed PMID: 16877429.
49. Schneckenburger H, Wustrow TP. Intracellular fluorescence of photosensitizing porphyrins at different concentrations of mitochondria. *Photochemistry and photobiology*. 1988 Mar;47(3):471-3. PubMed PMID: 2967982.
50. Kokudo N, Ishizawa T. Clinical application of fluorescence imaging of liver cancer using indocyanine green. *Liver cancer*. 2012 Jun;1(1):15-21. PubMed PMID: 24159568. Pubmed Central PMCID: 3747548.
51. Benson J. Indocyanine Green Fluorescence for Sentinel Lymph Node Detection in Early Breast Cancer. *Annals of surgical oncology*. 2015 Aug 11. PubMed PMID: 26259758.
52. Ghoroghchian PP, Frail PR, Susumu K, Park TH, Wu SP, Uyeda HT, et al. Broad spectral domain fluorescence wavelength modulation of visible and near-infrared emissive polymersomes. *Journal of the American Chemical Society*. 2005 Nov 9;127(44):15388-90. PubMed PMID: 16262400.
53. Luo S, Zhang E, Su Y, Cheng T, Shi C. A review of NIR dyes in cancer targeting and imaging. *Biomaterials*. 2011 Oct;32(29):7127-38. PubMed PMID: 21724249.
54. Choi HS, Liu W, Liu F, Nasr K, Misra P, Bawendi MG, et al. Design considerations for tumour-targeted nanoparticles. *Nature nanotechnology*. 2010 Jan;5(1):42-7. PubMed PMID: 19893516. Pubmed Central PMCID: 2797834.
55. Hyun H, Park MH, Owens EA, Wada H, Henary M, Handgraaf HJ, et al. Structure-inherent targeting of near-infrared fluorophores for parathyroid and thyroid gland imaging. *Nature medicine*. 2015 Feb;21(2):192-7. PubMed PMID: 25559343. Pubmed Central PMCID: 4319985.
56. Antakia R, Gayet P, Guillermet S, Stephenson TJ, Brown NJ, Harrison BJ, et al. Near infrared fluorescence imaging of rabbit thyroid and parathyroid glands. *The Journal of surgical research*. 2014 Dec;192(2):480-6. PubMed PMID: 24980856.
57. Tummers QR, Schepers A, Hamming JF, Kievit J, Frangioni JV, van de Velde CJ, et al. Intraoperative guidance in parathyroid surgery using near-infrared fluorescence imaging and low-dose Methylene Blue. *Surgery*. 2015 Nov;158(5):1323-30. PubMed PMID: 25958068. Pubmed Central PMCID: 4603995.
58. Frangioni JV. In vivo near-infrared fluorescence imaging. *Current opinion in chemical biology*. 2003 Oct;7(5):626-34. PubMed PMID: 14580568.
59. Noura S, Ohue M, Seki Y, Tanaka K, Motoori M, Kishi K, et al. Feasibility of a lateral region sentinel node biopsy of lower rectal cancer guided by indocyanine green using a near-infrared camera system. *Annals of surgical oncology*. 2010 Jan;17(1):144-51. PubMed PMID: 19774415.

60. Tobis S, Knopf JK, Silvers CR, Marshall J, Cardin A, Wood RW, et al. Near infrared fluorescence imaging after intravenous indocyanine green: initial clinical experience with open partial nephrectomy for renal cortical tumors. *Urology*. 2012 Apr;79(4):958-64. PubMed PMID: 22336035.
61. Troyan SL, Kianzad V, Gibbs-Strauss SL, Gioux S, Matsui A, Oketokoun R, et al. The FLARE intraoperative near-infrared fluorescence imaging system: a first-in-human clinical trial in breast cancer sentinel lymph node mapping. *Annals of surgical oncology*. 2009 Oct;16(10):2943-52. PubMed PMID: 19582506. Pubmed Central PMCID: 2772055.
62. Dutour A, Josserand V, Jury D, Guillermet S, Decouvelaere AV, Chotel F, et al. Targeted imaging of alpha(v)beta(3) expressing sarcoma tumor cells in vivo in pre-operative setting using near infrared: a potential tool to reduce incomplete surgical resection. *Bone*. 2014 May;62:71-8. PubMed PMID: 24530474.
63. Liu Y, Bauer AQ, Akers WJ, Sudlow G, Liang K, Shen D, et al. Hands-free, wireless goggles for near-infrared fluorescence and real-time image-guided surgery. *Surgery*. 2011 May;149(5):689-98. PubMed PMID: 21496565. Pubmed Central PMCID: 3079879.
64. Sexton K, Davis SC, McClatchy D, 3rd, Valdes PA, Kanick SC, Paulsen KD, et al. Pulsed-light imaging for fluorescence guided surgery under normal room lighting. *Optics letters*. 2013 Sep 1;38(17):3249-52. PubMed PMID: 23988926. Pubmed Central PMCID: 4051311.
65. Edafe O, Antakia R, Laskar N, Uttley L, Balasubramanian SP. Systematic review and meta-analysis of predictors of post-thyroidectomy hypocalcaemia. *The British journal of surgery*. 2014 Mar;101(4):307-20. PubMed PMID: 24402815.

CHAPTER 3

A NOVEL OPTICAL APPROACH TO INTRAOPERATIVE DETECTION OF PARATHYROID GLANDS

Melanie A. McWade¹, Constantine Paras¹, Lisa M. White², John E. Phay³,
Anita Mahadevan-Jansen¹, James T. Broome⁴

¹ Department of Biomedical Engineering, Vanderbilt University, Nashville, TN

² General Surgery, Murfreesboro Medical Clinic, Murfreesboro, TN

³ Division of Surgical Oncology, The Ohio State University, Columbus, OH

⁴ Division of Surgical Endocrinology, St. Thomas Midtown Hospital, Nashville, TN

This chapter was published in:

“A novel optical approach to intraoperative detection of parathyroid glands.”

Surgery. 2013.

3.1 Abstract

Background: Inadvertent removal of parathyroid glands is a challenge in endocrine surgery. There is a critical need for a diagnostic tool that provides sensitive, real-time parathyroid detection during procedures. We have developed an intraoperative technique using near-infrared (NIR) fluorescence for *in vivo*, real-time detection of the parathyroid regardless of its pathologic state.

Methods: NIR fluorescence was measured intra-operatively from 45 patients undergoing parathyroidectomy and thyroidectomy. Spectra were measured from the parathyroid and surrounding neck tissues during surgery using a portable, probe-based fluorescence system at 785-nm excitation. Accuracy was evaluated by comparison to histology or visual recognition by the surgeon.

Results: NIR fluorescence detected the parathyroid in 100% of patients. Parathyroid fluorescence was significantly stronger (1.2 – 18 times) than that of the thyroid with peak fluorescence at 822-nm. Surrounding tissues showed no auto-fluorescence. Disease state did not affect the ability to discriminate parathyroid glands but may account for signal variability.

Conclusions: NIR fluorescence spectroscopy can intraoperatively detect the parathyroid regardless of tissue pathology. The signal may be due to calcium-sensing receptors present in the parathyroid. The signal strength and consistency indicates the simplicity and effectiveness of this method. Its implementation may limit surgical time, cut costs, and improve surgical success rates.

3.2 Introduction

Thyroid and parathyroid diseases require thyroidectomy and parathyroidectomy to remove both benign and malignant glands in over 80,000 patients per year in the United States (1). These procedures require careful resection of the diseased gland(s) while preserving healthy tissues in the neck. Problems arise because of the small size and variable position of the parathyroid glands, making them difficult to distinguish from thyroid and surrounding tissues in the neck. Accidental removal or injury of the parathyroid glands during thyroidectomy can cause long-term issues with calcium regulation due to hypoparathyroidism and subsequent hypocalcemia. Incomplete removal of or inability to identify hypersecreting parathyroid tissue during parathyroidectomy may require reoperation due to persisting hyperparathyroidism. Surgeons must rely on visual inspection to distinguish tissues, which can be subjective and inconclusive. In many cases, patients fail to achieve postoperative normocalcemia because of the infrequency of cases and limited experience of the individual surgeon (1,2).

Localization and identification of parathyroid glands has been attempted by a variety of techniques such as preoperative ultrasound, Sestamibi scintigraphy, computed tomography (CT), magnetic resonance imaging (MRI) and intraoperative intact parathyroid hormone (iPTH) assay (1). These existing methods for identifying parathyroid glands are limited in their applicability and sensitivity, rendering them inadequate to prevent surgical complications (3). Most rely on preoperative identification of diseased parathyroid glands either by size or uptake of radiotracer, limiting their intraoperative utility. Cost, especially for CT scanning and MRI remains prohibitive for routine use. The turn-around time for iPTH monitoring with state-of-the-art assays still runs at least 9 minutes, not taking into account the travel time of the sample to the assay machine. The sensitivity of Sestamibi and preoperative ultrasound is only 47-61% as reported in most studies (4,5). Therefore, there remains a need for a way to accurately identify parathyroid tissue intraoperatively.

Fluorescence spectroscopy has been used in several other applications for the identification of tissues. It has been utilized to detect and diagnose many diseases such as brain tumors (6), skin conditions (7), and esophageal disease (8) as well as evaluate surgical margins after resections for breast cancer (9). We have previously conducted a pilot study using NIR fluorescence spectroscopy to detect the parathyroid during surgical procedures (10). NIR wavelengths are attractive in biomedical applications due to their increased penetration depth and decreased

scattering and absorption in tissues relative to ultraviolet and visible wavelengths (11). Furthermore, the NIR region is considered the optical window because there are no naturally occurring fluorophores known to emit peak fluorescence at NIR wavelengths. This makes the NIR region optimal for medical applications (12).

We have developed an optical method to detect the parathyroid from other tissues in the neck in a way that overcomes limitations of surgeon-based identification and current localization techniques. Using NIR fluorescence spectroscopy, we hypothesize that we can provide sensitive, real-time information to the surgeon about the location of the parathyroid regardless of disease state.

3.3 Patients and Methods

Patients with primary thyroid or parathyroid disease undergoing parathyroidectomy or thyroidectomy at the Vanderbilt Endocrine Surgery Center were considered for this study. The operating endocrine surgeon determined the eligibility of each patient by evaluating their overall health in a preoperative assessment at the Vanderbilt Clinic. Under the approval of the Institutional Review board, written consent was obtained for a total of 35 patients between the ages of 18 – 99, regardless of gender or race.

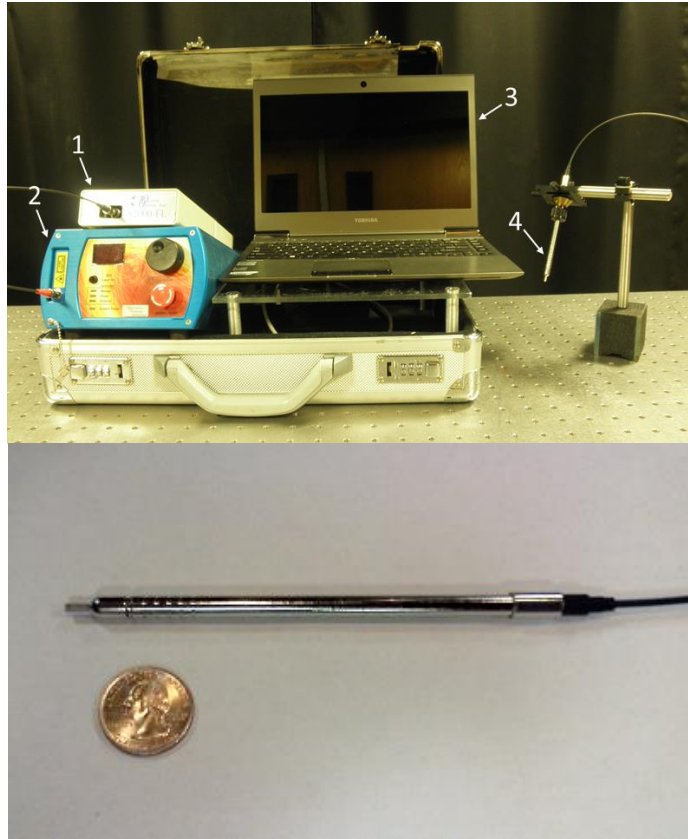


Figure 3.1: Top- Near-infrared fluorescence spectroscopy system showing a (1) spectrometer, (2) 785-nm diode laser, (3) laptop computer, and (4) hand-held fiber optic probe. Bottom- Fiber optic probe next to a quarter to show scale

3.3.1 Fluorescence Measurement

For optical detection of the parathyroid gland during surgery, we used a portable fluorescence spectroscopy system designed for clinical use shown in Figure 3.1. The system is comprised of a NIR diode laser (U-type, IPS, Monmouth Junction, NJ) coupling 785-nm light through a 7-around-1 sterilized fiber optic probe. Tissue was irradiated with 80 mW of light in a 400 μm spot size. Fluorescence was detected by a spectrometer (S2000-FL, Ocean Optics, Dundelin, FL) via the collection fibers. Inline filtering at the tip of the fiber optic and at the port of the spectrometer ensured that no visible or laser light interfered with the fluorescence signal. Fluorescence measurements were controlled by a laptop computer running custom software in LabView (National Instruments, Austin, TX).

Measurements were collected in the operating room after the parathyroid and thyroid were exposed. The surgeon placed the pencil-sized fiber optic probe onto multiple tissue sites while fluorescence spectra were measured. Spectra from the parathyroid and thyroid were measured for all patients, as well as fat, muscle, lymph, and trachea, depending on accessibility. All measurements were made with the overhead lights turned off and the operating lights directed away. Background measurements were collected with the laser off. Six spectra were collected from each tissue site with an integration time of 300 ms per spectra. The confidence level (high, medium, or low) of the surgeon in visually identifying each tissue type was recorded. Because visual identification is the most commonly employed technique for intraoperative parathyroid detection, it was used as a point of comparison to assess the performance of this technology. Tissue sites with a low surgical confidence level were excluded from analysis, unless there was available histology from that tissue. Histology was compared to the measured fluorescence spectra and used as the gold standard for parathyroid detection. It was not feasible to collect parathyroid gland histology from every patient because tissue determined to be healthy is not removed during surgery.

3.3.2 Data Processing and Statistical Analysis

Processing and analysis of the NIR spectra were performed post-operatively. In MATLAB software (Mathworks, Inc., Natick, MA), the spectra for each tissue site were averaged and processed for noise smoothing and background subtraction. Day to day variations in the system were corrected by performing spectral calibration with a neon argon lamp. The wavelength-dependent response of the system was corrected using a National Institute of Standards and Technology (NIST)-calibrated tungsten lamp. Following data processing, the spectra were normalized to the maximum fluorescence intensity of the thyroid to account for intensity variability across the patient population. The peak parathyroid to thyroid fluorescence intensity ratio (P/T ratio) was calculated for each patient. A P/T ratio equal to or less than one indicates that NIR fluorescence spectroscopy is incapable of distinguishing between tissue types.

The normalized spectra were categorized according to the following disease states: benign thyroid disease, malignant thyroid disease, hyperthyroidism, and hyperparathyroidism. The data was analyzed using a 2-sample *t*-test to examine the differences in the peak parathyroid and thyroid autofluorescence intensities. The level of significance was defined as $P < 0.01$.

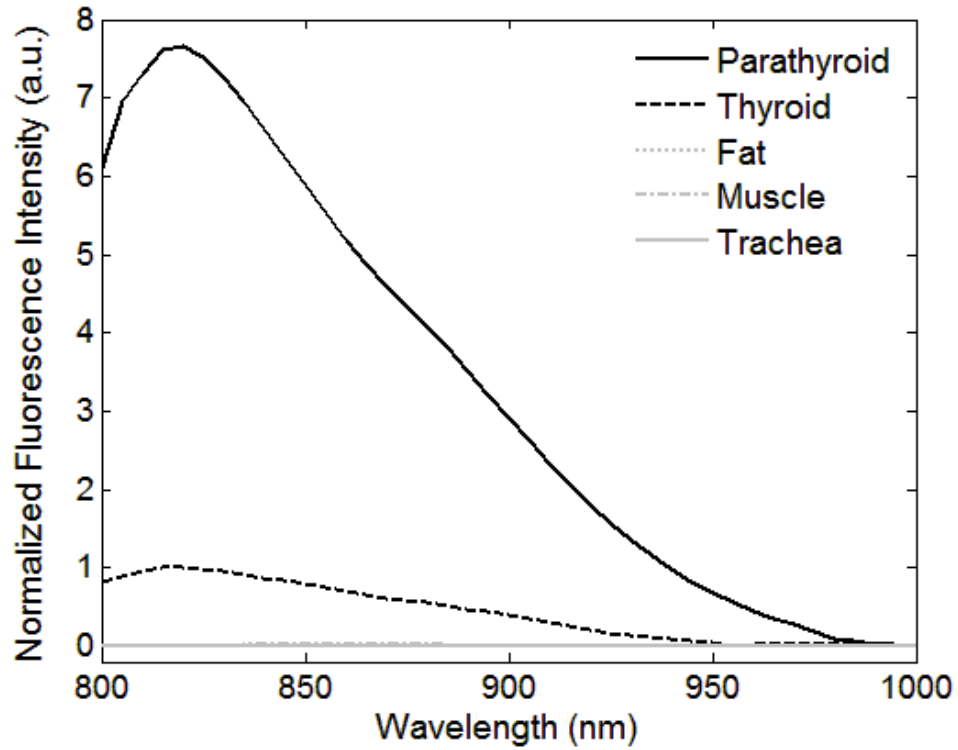


Figure 3.2: Typical normalized near-infrared spectra. Each spectrum is taken as the average of 6 measurements at the site of investigation. The parathyroid signal is significantly stronger than anything else in the neck. It is 7.5 times greater than the thyroid peak intensity.

3.4 Results

The goal of this study was to determine if NIR fluorescence spectroscopy could distinguish the parathyroid gland from the thyroid and all other tissues in the neck during surgery, regardless of disease type. Fluorescence spectra of these tissues were obtained from 45 patients. Of these patients, 14 (31%) underwent thyroidectomy for benign thyroid disease, 6 (13%) underwent thyroidectomy for malignant disease, 9 (20%) underwent thyroidectomy for hyperthyroidism, and 16 (36%) underwent parathyroidectomy for primary or secondary hyperparathyroidism. Three patients fell in two disease categories.

For all patients, the fluorescence intensity of the parathyroid was greater than all other tissues regardless of disease state. The thyroid exhibited a weaker fluorescence signal than the parathyroid but consistently stronger than that of muscle, fat, and surrounding tissues, which showed no fluorescence. Using a 2-sample *t*-test at a 99.9% significance level, the parathyroid fluorescence intensity was found to be significantly higher than thyroid fluorescence with a *p*-value of 5.91×10^{-14} . A typical spectrum collected during surgery shows a fluorescence peak at about 822 nm for the thyroid and the parathyroid (Figure 3.2). The spectral shape of the parathyroid and thyroid curves shows similarity when normalized to their respective peaks. The P/T ratio ranged from 1.2 to 18 for patients in all disease categories as shown in Figure 3.3. A one-way ANOVA test was performed to determine whether the observed auto-fluorescence signal was affected by disease state. Results showed no significant difference in P/T ratio across disease types (*P*-value < 0.01).

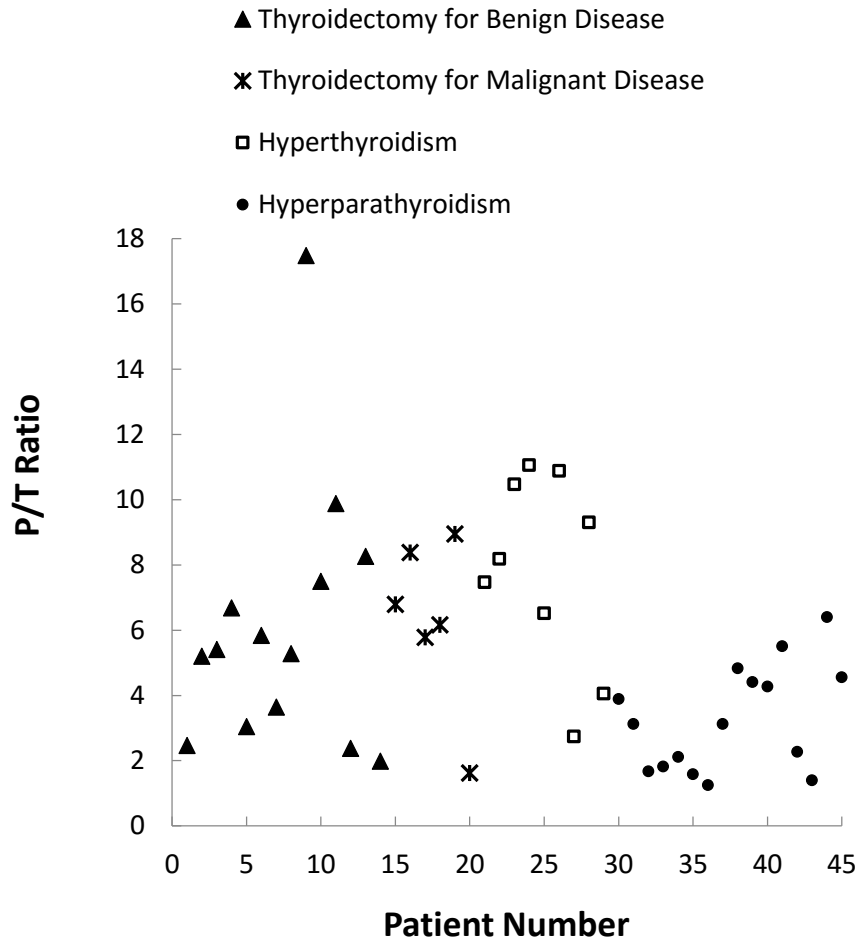


Figure 3.3: The ratio of peak parathyroid to thyroid fluorescence intensity ranges from 1.2 to 18 for all disease types. Patients are broken down by disease type to show variation in parathyroid autofluorescence. *Indicates patient also underwent parathyroidectomy for hyperparathyroidism.

Histological validation of the parathyroid gland was available for 22 of the 45 patients. In these patients, spectral measurements were collected prior to resection. Tissue histology confirmed the finding that parathyroid tissue exhibits stronger fluorescence than thyroid tissue. Table 1 shows NIR fluorescence spectroscopy can identify tissue type with higher accuracy than visual inspection by the surgeon. This is evident in cases 3, 5 and 18 in which visual assessment of the surgeon incorrectly identified tissues which NIR fluorescence spectroscopy correctly identified as compared to histology. With 22 patients who have histology to confirm the tissue identity determined from spectral measurements, the power of this study is 99.89% for detecting a 5% difference in NIR auto-fluorescence between thyroid and parathyroid tissue. However, more patients must be measured in each disease category before further conclusions can be drawn on the source of the variability across patients as is relates to disease state.

The parathyroid was accurately detected with NIR fluorescence spectroscopy in 100% of patients. When the detection threshold is set to a P/T ratio of 1.2 the sensitivity is 1.0 and the specificity is 1.0. Peak sensitivity and specificity for common parathyroid detection modalities are 60% and 81% for CT (13), 47% and 87% for ultrasound (4), and 61% and 84% for Sestamibi scintigraphy (5). NIR fluorescence spectroscopy was able to detect parathyroid tissue with higher sensitivity and specificity than all other modalities.

Table 3.1: Tissue identification using fluorescence spectroscopy compared to visual inspection and histology

Case #	Surgeon Assessment (by visual assessment)	Confidence	P/T Ratio	Histology
1	Parathyroid	High	1.63	Parathyroid
2	Parathyroid	Medium	3.969	Parathyroid
3	Parathyroid	High	7.9	Parathyroid
	Parathyroid	Low/Medium	0.23	Benign fatty tissue
4	Parathyroid	High	11.3	Parathyroid
5	Unknown	Low	3.63	Parathyroid
6	Parathyroid	Medium/High	3.12	Parathyroid
7	Parathyroid	Medium/High	4.55	Parathyroid
8	Parathyroid	Medium	1.82	Parathyroid
9	Parathyroid	High	3.64	Parathyroid
10	Parathyroid	High	1.57	Parathyroid
11	Parathyroid	High	8.95	Parathyroid
12	Parathyroid	Medium	1.2	Parathyroid
13	Parathyroid	High	3.12	Parathyroid
14	Parathyroid	High	4.82	Parathyroid
15	Parathyroid	High	4.41	Parathyroid
16	Parathyroid	High	4.28	Parathyroid
17	Parathyroid	High	5.51	Parathyroid
18	Parathyroid	High	0.88	Thyroid
	Parathyroid	High	2.69	Parathyroid
19	Parathyroid	High	1.98	Parathyroid
20	Parathyroid	High	4.55	Parathyroid
21	Parathyroid	High	1.36	Parathyroid
22	Parathyroid	High	6.40	Parathyroid

In cases 1-22, Near-infrared spectroscopy results are confirmed by tissue histology. In cases 3, 5 and 18 highlighted in bold, visual inspection by the surgeon incorrectly identifies tissue type.

3.5 Discussion

We present a novel tool utilizing the intrinsic NIR autofluorescence to detect parathyroid tissue and guide surgeons in real-time during endocrine surgeries. The results reported here show that NIR fluorescence spectroscopy is capable of reliable and repeatable detection of the parathyroid gland in patients undergoing thyroidectomy and parathyroidectomy regardless of the disease state. For all patients, parathyroid fluorescence intensity is significantly higher than thyroid fluorescence for all patients. Fat, muscle, lymph node and other surrounding neck tissues do not exhibit any fluorescence, allowing surgeons to distinguish parathyroid glands from fat or other tissues. When normalized to their respective peaks, the spectra from the parathyroid and thyroid exhibit similarity in their spectral line shape. Both tissue types show only one emission peak at 822 nm upon excitation with 785 nm light, indicating that the autofluorescence is a result of a single, naturally occurring fluorophore present in both the parathyroid and thyroid. The identity of the fluorophore is presently unknown, and there are no reports of biological fluorophores with peak fluorescence around 822 nm. Our leading hypothesis is that the NIR autofluorescence in the parathyroid is due to the calcium-sensing receptor (CaSR). Calcium-sensing receptors are involved in controlling synthesis and secretion of PTH and calcitonin. The highest levels of CaSR expression are found in parathyroid cells and smaller concentrations are found in the C-cells of the thyroid but nowhere else in the muscle, fat or lymph of the neck region. This provides a fluorophore that is present in high concentrations in parathyroid tissue and low concentrations in thyroid tissue making CaSR a highly probable candidate for the observed fluorescence. Cell culture studies must be done to determine the mechanism of the parathyroid autofluorescence.

The variability in the parathyroid to thyroid fluorescence intensity ratio (P/T ratio) ranges from 1.2 to 18. There are many factors that may contribute to the inter-patient variability in the P/T ratio, the most prominent being patient disease state. Insufficient visual diagnosis may also contribute to variability in the P/T ratio across patients. Six patients demonstrated a P/T ratio between 1 and 2. While the degree of variability in the ratio needs to be better understood and could be potentially related to the inter-patient variability or fat overlaying the parathyroid during measurement, even the 20% difference was found to be statistically significant ($p\text{-value} = 5.91 \times 10^{-14}$) and reproducible.

We have shown that NIR fluorescence spectroscopy of the parathyroid can improve upon the visual inspection of the surgeon during endocrine procedures. On its own, visual diagnosis of

the parathyroid is highly subjective and depends heavily on the experience and frequency in which the surgeon performs these procedures. Our analysis of 22 tissue samples identified on the basis of either visual diagnosis or NIR fluorescence spectroscopy and compared to histology confirm visual inspection is insufficient as a stand-alone detection method. In 3 of the 22 cases shown in Table 1, the tissue was misdiagnosed by the surgeon and properly diagnosed by NIR fluorescence spectroscopy. Case 3 shows an example of the surgeon improperly labeling fat tissue as parathyroid tissue. Case 5 shows an example of the surgeon unable to identify a sample of tissue as the parathyroid gland. In case 18, the surgeon misidentifies thyroid as parathyroid tissue. If these cases went uncorrected, the error could result in persistent hyperparathyroidism and the necessity of reoperation due to inadequate removal of all abnormal tissue at the time of initial operation. Also, during thyroid resections, inaccurate identification of parathyroid tissue could lead to inadvertent resection of one or more parathyroid glands leading to potential hypoparathyroidism and permanent dependence on calcium salts and vitamin D analogs.

NIR fluorescence spectroscopy can achieve a sensitivity and specificity of 100% when the detection threshold is set to a P/T ratio > 1 . This result shows higher accuracy in parathyroid detection than preoperative imaging techniques such as CT, ultrasound and Sestamibi scintigraphy (1,14). Unlike Sestamibi scintigraphy, NIR autofluorescence can distinguish both normal and abnormal functioning parathyroid glands. Current intraoperative detection methods such as frozen section analysis and needle aspiration with parathyroid hormone (PTH) analysis do not offer the time, cost and safety benefits of NIR fluorescence spectroscopy. Frozen section analysis requires high cost to the patient and long waiting times associated with pathological processing. This method also risks damaging/destroying the parathyroid when tissue is removed for analysis. Needle aspiration with PTH assay allows for accurate identification of the parathyroid gland, but the false negative rate is as high as 13% (15,16). Alternatively, NIR fluorescence spectroscopy is capable of identifying the parathyroid in 30 – 40 seconds without damage to the tissue. The briefcase sized spectroscopy system is associated with a one-time cost of approximately \$8,000. Since the tissue discrimination can be automated yielding an answer in real time and data acquisition can be performed by clinical personnel, a trained technician is not required and will not add to the cost of this device. Because the system is fully reusable, the upfront cost can be defrayed over its lifetime. It has the added benefits of being portable and requiring minimal set-up

time (3 minutes) in the operating room. With further investigations of this technology, the added steps of turning off room lights and diverting overheads lights may be able to be bypassed as well.

The parathyroid detection tool proposed here is unique because it relies on intrinsic fluorescence in the NIR region, excluding the need for exogenous chemicals. Fluorescence detection modalities operating on the autofluorescence of biological tissue are commonly used clinically for applications such as breast tumors (17), gliomas (18), and cervical precancers (19). However, many of these tools use ultraviolet or visible light because biological fluorophores typically exhibit peak autofluorescence in this range. The NIR region is considered an ideal optical window because it provides a deep penetration depth in tissue and there are few known biological fluorophores that emit at these wavelengths.

This method may have some limitations. Though NIR light at 785 nm penetrates several millimeters deep in tissue, the tissue must be exposed in order for the optical probe to deliver light and collect the signal. If the other tissue such as fat is overlaying the parathyroid, the fluorescence signal will be affected. However, this issue can be addressed by altering the collection geometry of the probe to allow for subsurface parathyroid gland and adenoma detection. Second, the probe-based system provides point measurements in tissue. This means surgeons are unable to scan the surgical field and receive spatial information about the location of the parathyroid. However, the fiber optic probe has the advantage of allowing the surgeon to reach under layers of tissue to obtain a measurement. Visual inspection is necessary to provide guidance to the point of measurement. The development of an imaging device could improve the diagnostic capacity of this technology by allowing the surgeon to view the entire operative field in two dimensions. Work is being done to develop such an imaging system that would provide intuitive information to the surgeons to detect the glowing parathyroid gland(s) in real-time.

3.6 Conclusions

This study presents a novel tool using NIR autofluorescence spectroscopy to detect the parathyroid gland in real-time during endocrine surgeries. We have shown its ability to accurately detect the parathyroid regardless of disease state with greater sensitivity and specificity than other imaging modalities, including visual diagnosis. The mechanism of the autofluorescence is still unknown, but this technique shows promise as an intraoperative tool for improving success of parathyroidectomies and thyroidectomies.

3.7 Acknowledgements

This study was supported by NCI 1R25CA136440-01 and NIH R41 EB015291

3.8 References

1. Mohebati A, Shaha AR. Imaging techniques in parathyroid surgery for primary hyperparathyroidism. *American Journal of Otolaryngology*. 2012;33(4):457-468.
2. Malmaeus J, Granberg PO, Holvorsen J, Akerstrom G, Johansson H. Parathyroid Surgery in Scandanavia. *Acta Chir Scand*. 1988; 33:1364-1367
3. R. L. Prosst, J. Gahlen, P. Schnuelle, S. Post and F. Willeke. Fluorescence-guided minimally invasive parathyroidectomy: a novel surgical therapy for secondary hyperparathyroidism. *Am J Kidney Dis*. 2006; 48(2):327-331
4. Patel CN, Salahudeen HM, Lansdown M, Scarsbrook AF. Clinical Utility of Ultrasound and ^{99m}Tc Sestamibi SPECT/CT for Preoperative Localization of Parathyroid Adenoma in Patients with Primary Hyperparathyroidism. *Clinical Radiology*. 2010; 65(4):278-287.
5. Nichols KJ, Tomas MB, Tronco GG, Palestro CJ. Sestamibi Parathyroid Scintigraphy in Multigland Disease. *American Journal of Otolaryngology*. 2012;33(1):43-50.
6. Butte PV et al. Fluorescence lifetime spectroscopy for guided therapy of brain tumors. *Neurimage*. 2011; 54(1):125-135.
7. Lemos MC. Fluorescence spectroscopy as a tool to detect and evaluate glucocorticoid-induced skin atrophy. *Lasers in Medical Science*. 2012;27(5):1059.
8. DaCosta RS, Wilson BC. Spectroscopy and fluorescence in esophageal disease. Best practice and research *Clinical Gastroenterology*. 2006; 20(1):41-57.
9. Keller MD et al., Autofluorescence and diffuse reflectance spectroscopy and spectral imaging for breast surgical margin analysis. 2010;42(1):15-23.
10. Paras C, Keller M, White L, Phay J, Mahadevan-Jansen A. Near-Infrared Auto-fluorescence for the Detection of Parathyroid Glands. *Journal of Biomedical Optics*. 2011;16(6).
11. Mahadevan-Jansen A et al., Near-infrared Raman Spectroscopy for in vitro Detection of Cervical Pre-cancers. *Photochemistry and Photobiology*. 1998;68(1): 123-132.
12. Umezawa K, Nakamura Y, Makino H, Citterio D, Suzuki K. Bright, Color-Tunable Fluorescent Dyes in the Visible-Near-Infrared Region. *Journal of the American Chemical Society*. 2008;130(5): 1550.

13. Zald PB, Hamilton BE, Larsen ML, Cohen JI. The Role of Computed Tomography for Localization of Parathyroid Adenomas. *The Laryngoscope*. 2008;118(8):1405-1410.
14. Hunter GJ, Schellingerhout D, Vu TH, Perrier ND, Hamberg LM. Accuracy of four-dimensional CT for the localization of abnormal parathyroid glands in patients with primary hyperparathyroidism. *Radiology*. 2012;264(3):789-795
15. Rose J, Guerrero MA. Management of Primary Hyperparathyroidism, Thyroid and Parathyroid Diseases – New Insights into Some Old and Some New Issues, Dr. Laura Ward (Ed.), InTech. 2012.
16. Bancos I et al., Risks and benefits of parathyroid fine-needle aspiration with parathyroid hormone washout. *Endocrine Practice*. 2012;18(4):441-449
17. Gupta KP, Majumder K, Uppal A. Breast Cancer Diagnosis using N2 Laser Excited Autofluorescence spectroscopy. *Lasers in Surgery and Medicine*. 1997; 22(5):417-422.
18. Toms S, Lin W, Weil RJ, Mahlon J, Jansen ED, Mahadevan-Jansen A. Intraoperative Optical Spectroscopy Identifies Infiltrating Glioma Margins with High Sensitivity. *Neurosurg*. 2005; 57(4):382-391.
19. Ramanujam N et al. Cervical Precancer Detection Using a Multivariate Statistical Algorithm Based on Laser-Induced Fluorescence Spectra at Multiple Excitation Wavelengths. *Photochemistry and Photobiology*. 1996; 64(4):720-735.

CHAPTER 4

ESTABLISHING THE CLINICAL UTILITY OF AUTOFLUORESCENCE SPECTROSCOPY FOR PARATHYROID DETECTION

Melanie A. McWade¹, M.S., Melinda E. Sanders², M.D., James T. Broome³, M.D.,
Carmen C. Solórzano⁴, M.D., Anita Mahadevan-Jansen¹, Ph.D.

¹ Department of Biomedical Engineering, Vanderbilt University, Nashville, TN

² Department of Pathology, Microbiology and Immunology, Vanderbilt University, Nashville, TN

³ Division of Surgical Endocrinology, St. Thomas Midtown Hospital, Nashville, TN

⁴ Division of Surgical Oncology and Endocrine Surgery, Vanderbilt University, Nashville, TN

This chapter was published in:

“Establishing the clinical utility of autofluorescence spectroscopy for parathyroid detection.”

Surgery. 2016

4.1 Abstract

Background: Inability to accurately identify parathyroid glands during cervical endocrine surgery hinders patients from achieving post-operative normocalcemia. An intrinsic near-infrared fluorescence method was developed for real-time parathyroid identification with high accuracy. This study assesses the clinical utility of this approach.

Methods: Autofluorescence measurements were obtained from 137 patients (264 parathyroid glands) undergoing parathyroidectomy and/or thyroidectomy. Measurements were correlated to disease state, calcium levels, parathyroid hormone (PTH), vitamin D levels, age, sex, ethnicity and body-mass index (BMI). Statistical analysis identified which factors significantly affect parathyroid detection.

Results: High parathyroid fluorescence was consistently detected and showed wide variability across patients. Near-infrared fluorescence was used to correctly identify 256/264 (97%) of glands. The technique showed high accuracy over a wide variety of disease states, though patients with secondary hyperparathyroidism demonstrated confounding results. Analysis revealed BMI ($P<0.01$), disease state ($P<0.01$), vitamin D ($P<0.05$), and calcium levels ($P<0.05$) account significantly for variability in signal intensity. Age, gender, PTH, and ethnicity had no effect.

Conclusions: This intrinsic fluorescence-based intraoperative technique can accurately detect nearly all parathyroid glands in real-time. Its discrimination capacity is largely unlimited by patient variables, but several factors affect signal intensity. These results demonstrate potential clinical utility of optical guidance for parathyroid detection.

4.2 Introduction

Insufficient or inaccurate identification of the parathyroid glands during thyroidectomy and parathyroidectomy procedures can lead to surgical complications. The incidence of inadvertent parathyroidectomy during thyroidectomy ranges from 8 - 19% (1) and may result in post-operative hypocalcemia. Surgical cure for patients with hyperparathyroidism is dependent on adequate resection of hypersecreting parathyroid glands. If not accomplished, patients may suffer from persistent hyperparathyroidism and require reoperation. Development of preoperative parathyroid imaging modalities has improved surgical success rate (2); however, surgeons must still rely on visual assessment during surgery to identify parathyroid glands. The accuracy of this approach is highly dependent on the experience level of the surgeon (3).

Parathyroid detection presents greatest difficulty in cases such as total thyroidectomy (TT), completion thyroidectomy (CT), central neck lymph node dissection, and reoperative thyroid and parathyroid procedures. The larger extent of dissection during TT and central neck lymphadenectomy poses greater risk of inducing iatrogenic surgical trauma and compromised blood supply to the parathyroid glands (4). Difficulty in reoperative and CT procedures is due to the formation of scar tissue and fibrosis, which distorts normal dissection planes and anatomic relationships (5). During parathyroidectomy, ectopic glands and multiple gland disease also present obstacles to adequate resection and surgical success (3). Intraoperative rapid parathyroid hormone assay is one technique for confirming complete removal of hyper-functioning glands and in some cases to confirm the correct identification of parathyroid tissue. Intraoperative parathyroid aspiration is another technique for confirmation that requires finding the gland, aspirating it with a needle, and analyzing the aspirate for PTH (6). There remains a clinical need for an intraoperative technique to detect the parathyroid gland instantly and with high accuracy.

To fill this clinical need, we have previously demonstrated the capability of a novel parathyroid detection technique using near-infrared (NIR) fluorescence spectroscopy (7-9). The parathyroid glands have been shown to emit a NIR autofluorescence signal that is stronger than that of the thyroid and all surrounding tissues in the surgical bed. Unlike current preoperative parathyroid detection modalities, this method provides real-time, intraoperative feedback with high accuracy. Intrinsic fluorescence is the basis of this technique, which obviates the need for potentially non-specific or toxic external contrast agents. The fluorophore in the parathyroid gland is currently unknown. A more thorough understanding of the sources contributing to

variability in parathyroid fluorescence intensity is necessary and may provide insight into the fluorescence etiology.

This new surgical technique must be proven to be capable of handling the full spectrum of inter-patient variability prior to clinical adoption. The goal of this study then is to establish the clinical utility for this novel intraoperative parathyroid detection technique. This will be determined by assessing the effects of pathologic, clinical and demographic patient variables on the parathyroid fluorescence signal. We present NIR fluorescence spectra acquired from patients undergoing cervical endocrine surgery. Patient factors such as body-mass index, metabolite levels, disease type, or hormone levels, age, and gender underwent statistical analysis for their effects on the parathyroid detection rate. The results suggest NIR fluorescence spectroscopy is ready for clinical implementation as a parathyroid detection tool by showing its effectiveness over a variety of clinical presentations.

4.3 Materials and Methods

4.3.1 Patient Selection.

Informed written consent from all patients enrolled in the study which was approved by the Institutional Review Board (IRB) of Vanderbilt University (# 070795). All patients 18 – 99 years of age who presented at the Vanderbilt Endocrine Surgery Center for thyroidectomy and/or parathyroidectomy were eligible for enrollment into the study. Patient eligibility was evaluated by the attending surgeon during preoperative assessment at the Vanderbilt University Endocrine Surgery Center. One hundred thirty-seven patients were enrolled for intraoperative fluorescence detection of the parathyroid glands.

4.3.2 Fluorescence Measurement.

The surgical procedure was conducted as called for by the disease presentation. During dissection, at least one parathyroid gland was identified. The tissue was exposed such that the 2 mm tip of the optical probe could directly contact the surface of the tissue. NIR autofluorescence spectra were collected from parathyroid, thyroid, muscle, and fat using a custom, portable NIR fluorescence spectroscopy system (7, 9). A total of 264 parathyroid glands from 137 patients were measured with one to four glands measured per patient. The system consists of a 785-nm

diode laser (IPS, Monmouth Junction, NJ, I0785SL0050PA), sterile fiber optic probe (EMVision, Loxahatchee, FL), and spectrometer (Ocean Optics, Dunedin, FL, S2000-FL) all controlled by a laptop computer. The fiber optic probe irradiated tissue with 80 mW of light and a 400- μm spot size for an integration time of 300 ms. Six spectra were collected per tissue site with the overhead lights turned off, taking approximately 4 seconds for each spot measured. Fluorescence measurements were validated using tissue histology as the gold standard when available. In cases where the parathyroid was not removed, the confidence level of the surgeon in their visual identification was noted (high, medium, or low). Low confidence measurements were excluded from the study. To account for day-to-day system variations, each fluorescence spectra from a given patient was divided by the peak fluorescence intensity of the thyroid of that same patient to yield what is referred to throughout the study as normalized fluorescence. Further calibration and post-processing was performed as described previously (7). Parathyroid glands were deemed “undetectable” if their normalized peak fluorescence intensity was less than 1, because this indicated the parathyroid fluorescence was not greater than thyroid fluorescence of that individual patient.

4.3.3 Data Analysis.

Patient variables were collected and maintained in an IRB-approved database. To assess the effect of pathology on parathyroid detection, the detection rate was characterized as a function of disease state. Detection rate is defined as the number of parathyroid glands identified with NIR fluorescence spectroscopy divided by the number of glands identified using histology or visual identification by the surgeon. For further statistical analysis, patients were then stratified according to demographic and clinical variables to determine their effects on the NIR fluorescence signal in the parathyroid. Variables included age (continuous between 18-99 years of age), gender (male or female), ethnicity (Caucasian or not Caucasian), and body-mass index (BMI) (normal or overweight/obese) at time of surgery, disease state (benign thyroid disease, malignant thyroid disease, hyperthyroidism, hyperparathyroidism or concurrent parathyroid and thyroid disease), total 25-hydroxyvitamin D level (low or normal), serum calcium levels (normal or high), and parathyroid hormone (PTH) levels (normal and high) measured preoperatively.

A multi-way analysis of variance (ANOVA) test was used to analyze the effect of patient variables on normalized peak parathyroid fluorescence measurements. Before analysis, outlier

measurements were identified and excluded using Cook's distance analysis (10). Unavailability of all lab tests across patients precluded a fully balanced design so two separate ANOVAs were carried out: (1) Effect of disease state, calcium, BMI, age, gender, and ethnicity on parathyroid signal across all patients; (2) Effect of vitamin D and PTH levels on parathyroid signals of patients undergoing parathyroidectomy procedures. Multiple t-tests were performed for pairwise comparison of patient variables showing significance in the ANOVA. Overall significance was 0.05, and Bonferroni's correction was applied to account for multiple comparisons.

4.3.4 Alternative sources of variability.

Alternative sources of variability including intraglandular spatial variability and effect of contact pressure were investigated. For analysis of the intraglandular differences, fluorescence measurements were collected at five different locations within the same tissue specimen of a patient in five patients. In each location, 6 consecutive spectra were measured to get an average fluorescence spectra. The effect of probe-to-tissue contact pressure on parathyroid fluorescence intensity was also examined *in vivo* and *in vitro*. During surgery, fluorescence measurements were collected where the surgeon indicated the probe contact pressures qualitatively to be "light", "medium", and "heavy". Additionally, *in vitro* measurements were performed on excised fresh frozen human parathyroid tissue while controlling probe pressure from 0 – 60 Newtons/cm² using a scale to measure the force of the probe on the tissue. Differences in peak fluorescence intensity were determined as a function of probe contact pressure.

4.4 Results

Fluorescence measurements were collected from 264 parathyroid glands in 137 patients undergoing parathyroidectomy and/or thyroidectomy. The fluorescence measurements of 69 parathyroid glands were confirmed with histology. Of the glands that could not be confirmed with histology, 88% were identified as parathyroid glands with high confidence and 12% with medium confidence using the visual assessment of the surgeon. A typical fluorescence spectra is shown in **Figure 4.1A**. The normalized peak parathyroid fluorescence intensity varied from 1.2 to 29 times greater than peak thyroid fluorescence for the detectable parathyroid glands (**Figure 4.1B**). Parathyroid NIR autofluorescence was consistently greater than the thyroid and all

surrounding tissues in 97% (256 of 264) of glands measured. Muscle, fat, lymph nodes, thymus, and trachea showed little to no fluorescence signal.

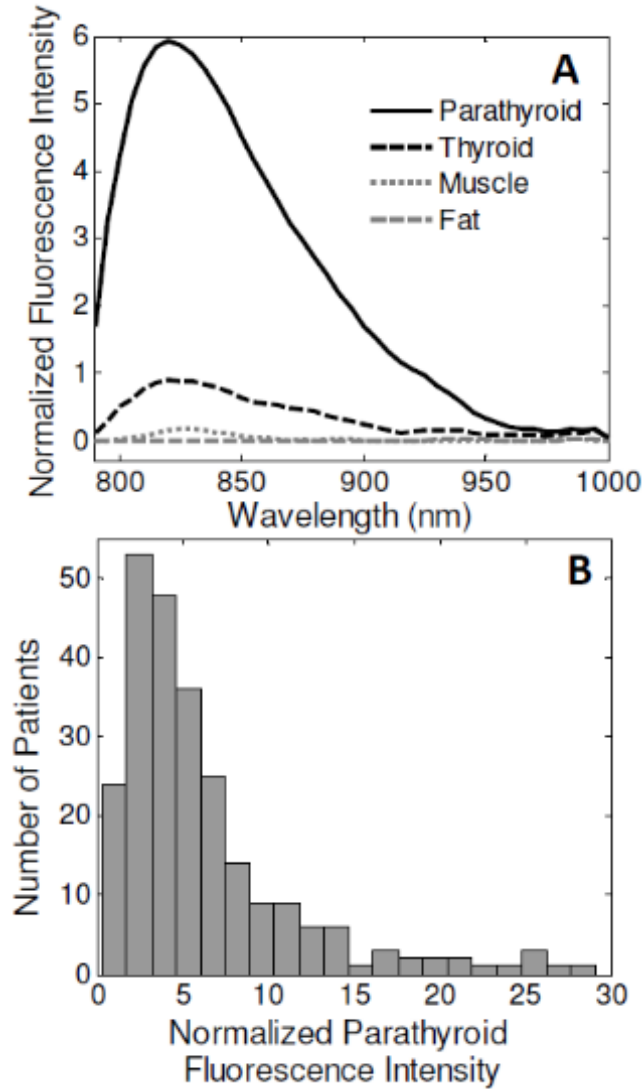


Figure 4.1. (A) Typical NIR fluorescence spectra of parathyroid, thyroid, muscle, and fat in a single patient. (B) Variability in parathyroid signal across 137 patients.

Disease Type	Total patients (Total glands)	Average Normalized Parathyroid Fluorescence	Standard Error	Detection rate
Nontoxic nodular goiter	16 (25)	7.34	1.12	100% (25 of 25)
Toxic multinodular goiter	8 (20)	7.30	0.81	100% (20 of 20)
Hashimoto's thyroiditis	8 (19)	6.55	0.91	100% (19 of 19)
Graves disease	16 (28)	8.67	1.51	100% (28 of 28)
Differentiated thyroid cancer	30 (57)	5.53	0.51	98.2% (56 of 57)
Thyroid adenoma (follicular or hurthle cell)	9 (16)	7.36	1.29	100% (16 of 16)
Medullary thyroid cancer	1 (1)	3.47	NA	100% (1 of 1)
Primary hyperparathyroidism	34 (60)	4.91	0.61	100% (60 of 60)
Primary hyperparathyroidism with multigland hyperplasia	2 (5)	3.07	0.53	100% (5 of 5)
Secondary hyperparathyroidism	4 (13)	1.15	0.13	53.8% (7 of 13)
Tertiary hyperparathyroidism	1 (3)	2.99	0.44	100% (3 of 3)
Concurrent parathyroid and thyroid disease	8 (17)	7.71	2.38	94% (16 of 17)

Table 4.1. Detection rate of parathyroid glands with the use of near-infrared fluorescence spectroscopy in patients across all disease states

4.4.1 Accuracy of Parathyroid Detection

NIR fluorescence spectroscopy demonstrated 100% parathyroid detection accuracy in patients with toxic and non-toxic nodular goiter, Hashimoto's thyroiditis, follicular and Hürthle cell thyroid adenoma, medullary thyroid carcinoma, Graves' disease, and primary and tertiary hyperparathyroidism (**Table 4.1**). Patients with well-differentiated thyroid cancer showed 98% detection accuracy (56 of 57 glands), and patients with concomitant parathyroid and thyroid disease exhibited a 94% detection accuracy (16 of 17 glands). The lower accuracy observed in each of these two disease states was a result of a single gland emitting low fluorescence signal. Reduced performance was recorded in the specific case of patients with renal-induced secondary hyperparathyroidism (sHPT), where NIR fluorescence spectroscopy was able to detect 54% of parathyroid glands (7 of 13 glands). All parathyroid glands with low signal were histologically confirmed to be parathyroid tissue, with the exception of the gland from the patient with well-differentiated thyroid cancer. Because parathyroid fluorescence was not significantly different from thyroid fluorescence in secondary hyperparathyroidism patients, measurements from the four sHPT patients were excluded from subsequent analysis and discussed separately in more detail.

Patient Factor (Mean, Range)	No. of patients in category (No. of glands)	P-value
BMI ($\mu=30 \text{ kg/m}^2$, Range=18.5-56 kg/m^2)		0.0018
<i>Normal (18.5-24.9 kg/m^2)</i>	26 (52)	
<i>Overweight/Obese (>25 kg/m^2)</i>	106 (195)	
Age ($\mu=53$ years, Range=20-87 years)		0.64
Disease state		0.008
<i>Benign thyroid disease</i>	33 (60)	
<i>Malignant thyroid disease</i>	29 (54)	
<i>Hyperthyroidism</i>	25 (49)	
<i>Hyperparathyroidism</i>	37(68)	
<i>concurrent thyroid and parathyroid disease</i>	8 (16)	
Ethnicity		0.57
<i>Caucasian</i>	125 (237)	
<i>Not caucasian</i>	8 (10)	
Gender		0.32
<i>Male</i>	21 (42)	
<i>Female</i>	112 (205)	
Serum Calcium Level ($\mu=9.9 \text{ mg/dL}$, Range=8.5-13.6 mg/dL)		0.012
<i>Normal (8.5 - 10.5 mg/dL)</i>	93 (177)	
<i>High (>10.5 mg/dL)</i>	33 (47)	
Parathyroid Hormone ($\mu = 365 \text{ pg/mL}$, Range = 21-2500 pg/mL)		0.67
<i>Normal (10 - 65 pg/mL)</i>	3 (7)	
<i>High (65 - 200 pg/mL)</i>	22 (40)	
<i>Very High (>200 pg/mL)</i>	22 (42)	
Vitamin D ($\mu=34 \text{ ng/mL}$, Range=8-66 ng/mL)		0.026
<i>Low (<30 ng/mL)</i>	25 (41)	
<i>Normal (30 - 80 ng/mL)</i>	32 (65)	

μ is the mean value for each patient factor

Table 4.2. Clinical and demographic patient characteristics and results of a Multi-way ANOVA test

4.4.2 Analysis of Variability in Parathyroid Fluorescence

Pertinent patient demographics and clinical characteristics are summarized in **Table 4.2**. Multi-way ANOVA tests showed the following factors have a significant effect on parathyroid fluorescence intensity: disease state ($P = 0.008$), BMI ($P = 0.0018$), preoperative calcium levels ($P = 0.012$), and preoperative vitamin D levels ($P = 0.026$). No significant differences in the parathyroid signal were found due to age, gender, ethnicity, and parathyroid hormone levels. Prior to conducting ANOVA tests, four parathyroid measurements were determined to be outliers using Cook's distance. Though these four glands were detected with NIR fluorescence spectroscopy, they were excluded from analysis due to their high fluorescence signal. The high normalized fluorescence intensity in these glands were due to low levels of thyroid fluorescence in these patients. Low thyroid fluorescence may be due to measurements localized in cystic or high fat areas of the thyroid gland.

Pairwise comparisons were performed to assess the individual effects of each factor identified to be statistically significant different in the ANOVA analysis (**Figure 4.2A-D**). These tests disclosed that patients with hyperparathyroidism have significantly lower peak parathyroid signal compared to patients with hyperthyroidism ($P < 0.01$) and malignant thyroid disease ($P < 0.05$). Parathyroid glands of patients with overweight/obese BMI have significantly lower peak fluorescence signal than that of patients with normal BMI ($P < 0.001$). Significantly lower parathyroid fluorescence signals were measured in patients with high serum calcium levels compared to patients with normal calcium levels ($P < 0.01$). Finally, patients with low vitamin D levels showed significantly lower parathyroid fluorescence signals than patients with normal vitamin D levels ($P < 0.05$). It should be noted that in all these patients, the parathyroid intensities were consistently greater than thyroid intensities.

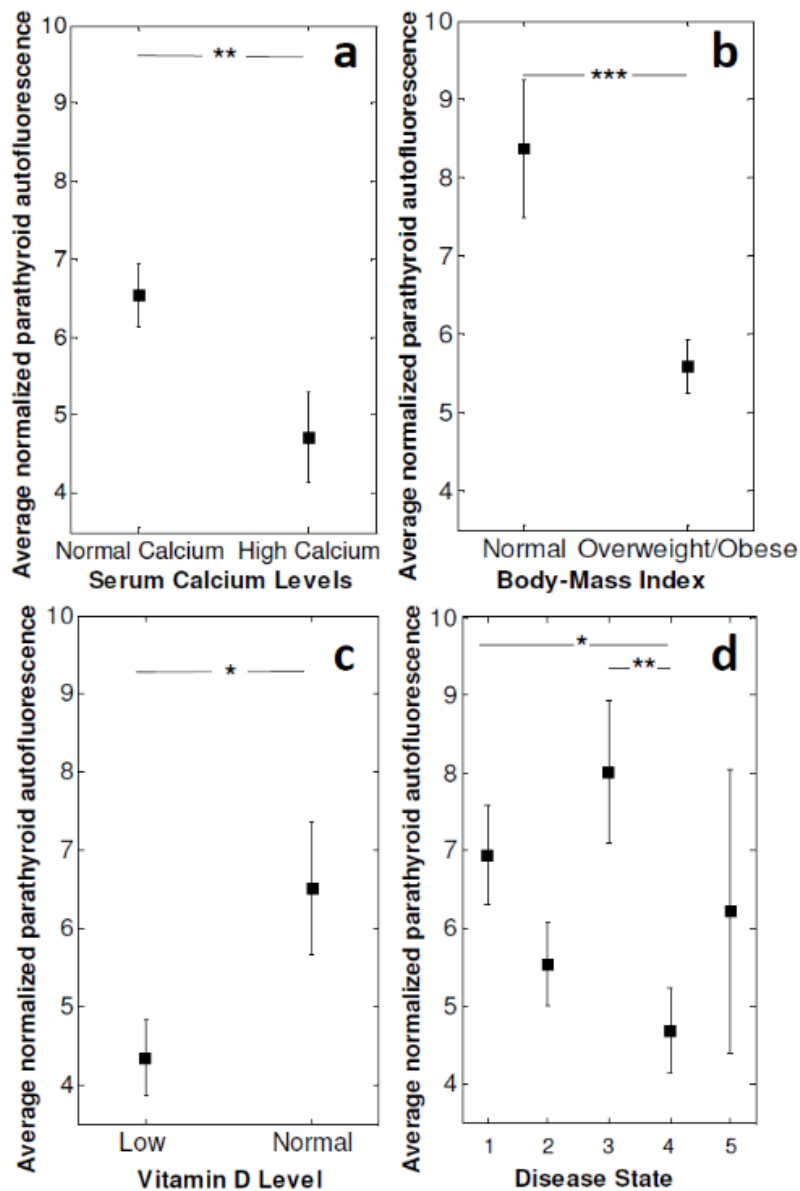


Figure 4.2. Average near infrared auto-fluorescence signal from parathyroid glands of patients with A) Normal (8.5 -10.5 mg/dL) and high (>10.5 mg/dL) serum calcium levels, B) Normal BMI (18.5 – 24.9 kg/m²) and high BMI (>25 kg/m²), C) Low (< 30 ng/dL) and high (30 – 80 ng/dL) total vitamin D levels, D) Benign thyroid disease-1, malignant thyroid disease-2, hyperthyroidism-3, hyperparathyroidism-4. Error bars indicate standard error of mean. Asterisks indicate significant differences (*p<0.05, **p<0.01, ***p<0.001)

4.4.3 Low Fluorescence in Secondary Hyperparathyroidism Patients

When patients with sHPT are separated out from patients with other disease states, the accuracy of fluorescence spectroscopy for parathyroid detection is 54% in sHPT patients compared to 99% in all other disease states. A closer look at the four sHPT patients revealed that each patient had at least one gland with high autofluorescence signal (**Figure 4.3A**). Histopathological analysis was performed on two glands that showed high and low fluorescence signals within the same sHPT patient to evaluate the cellular differences for the observed reduction in fluorescence signal. The gland with low fluorescence signal (**Figure 4.3B**) showed diffuse chief cell hyperplasia with expanded lobules and some fibrosis with very little fat. In contrast, the parathyroid gland with higher fluorescence (**Figure 4.3C**) showed water clear nodules and oxyphil patterns amidst the diffuse chief cell hyperplasia. Both glands were made up of 1 - 5% fat, which is much lower than normocellular parathyroid glands which typically has 10 -25% fat content.

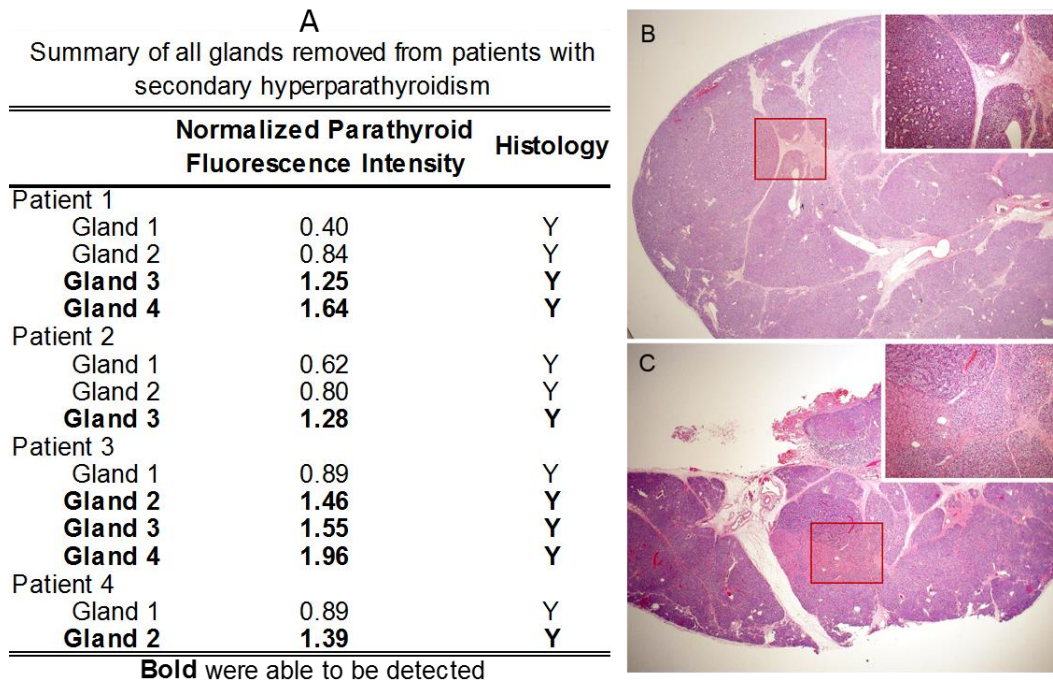


Figure 4.3. (A) Summary of glands removed from secondary hyperparathyroidism patients. Patient 4 had two glands removed with varying signal intensity. (B) Hematoxylin and eosin (H&E) stain of gland 1 of Patient 4 shows diffuse chief cell hyperplasia. (C) H&E stain of gland 2 of patient 4 shows water clear cell and oxyphil cell nodules amidst diffuse chief cell hyperplasia. (2x magnification with 10x inset).

4.4.4 Alternative sources of variability

Additional factors that add to the variability in parathyroid fluorescence of all patients were also characterized. Intraglandular spatial heterogeneity in both parathyroid and thyroid measurements contributed to the variability in peak fluorescence intensity. As exemplified in one patient shown in **Figure 4.4A**, the fluorescence signal in five unique locations across the surfaces of both the parathyroid and thyroid gland showed a wide spread. In this patient, the mean and standard deviation of parathyroid and thyroid peak fluorescence was 4.99 ± 0.97 and 1.00 ± 0.10 a.u, respectively. This same trend was observed across all five patients measured. In another patient, the lowest intensity parathyroid fluorescence measurements overlapped the highest intensity thyroid measurement, indicating if those two points were collected in isolation, that particular parathyroid gland would not have been detected by NIR fluorescence spectroscopy. However, the parathyroid intensity is greater than the thyroid when multiple measurements from each tissue are averaged. Probe contact pressure demonstrated a consistent inverse relationship to peak parathyroid fluorescence intensity (**Figure 4.4B**). A decreasing trend in parathyroid fluorescence from 1 to 0.86 (relative to peak fluorescence at 0 N/cm^2) was observed *in vitro* when varying probe contact pressure on the parathyroid from $0 - 60 \text{ N/cm}^2$. This decreasing trend in parathyroid fluorescence was also observed *in vivo* when the probe contact pressure varied from surgeon-determined “light”, “medium”, and “heavy” levels.

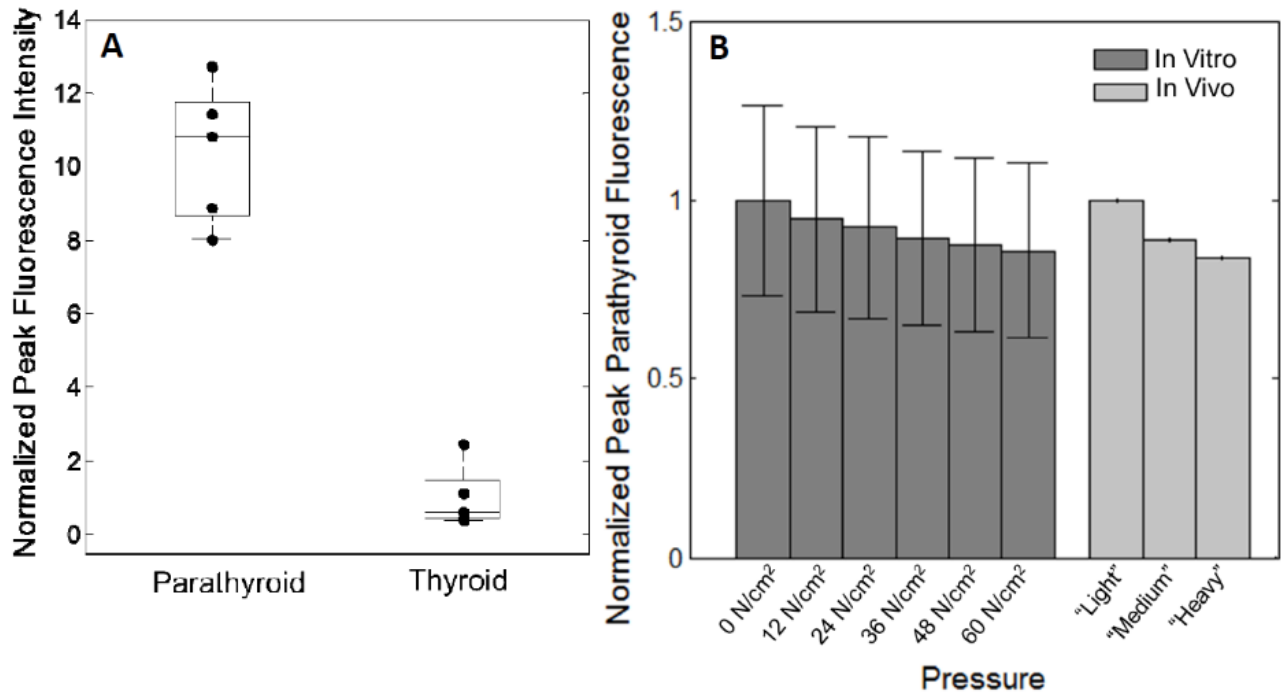


Figure 4.4. Additional sources of variability. (A) Intragland spatial heterogeneity contributes to variability in parathyroid and thyroid fluorescence signal. Each black dot corresponds to the fluorescence peak measured from a different location in a single gland. (B) Probe contact pressure is inversely related to parathyroid fluorescence. *In vitro* measurements performed with controlled pressure from 0 to 60 N/cm². *In vivo* measurements performed with surgeon’s assessment of “light,” “medium,” and “heavy” contact pressure.

4.5 Discussion

Parathyroid detection during cervical endocrine procedures can pose difficulty to even the most experienced surgeons. Inadvertent parathyroid trauma or removal during thyroidectomy and insufficient removal of hypersecreting glands during parathyroidectomy are well-recognized surgical complications (5). To address this problem, we have developed a tool for real-time intraoperative parathyroid detection using NIR autofluorescence spectroscopy. The basis for this technique is an intrinsic fluorescence signal emitted from the parathyroid gland at a higher intensity than all other surrounding neck tissues (7-9). Although the feasibility of the technique has been shown over a large patient population (9), the wide variability in the intensity of the high NIR autofluorescence signal has not been characterized thus far.

This study determines whether pathologic, clinical and demographic patient factors correlate with the variability in the signal intensity of parathyroid glands using NIR fluorescence spectroscopy. The results indicate that this technique offers high levels of accuracy for parathyroid detection in patients presenting with a variety of thyroid and parathyroid disease states and regardless of clinical and demographic factors. Studies show that parathyroidectomy for primary hyperparathyroidism has a >95% success rate in the hands of an experienced endocrine surgeon. Failure to detect the parathyroid gland is more prevalent in centers with lower volumes of parathyroidectomy and thyroidectomy cases (3). Furthermore, lack of clear parathyroid identification during thyroidectomy can lead to an increased incidence of permanent hypoparathyroidism (4). NIR fluorescence spectroscopy has demonstrated detection accuracy ranging from 94% to 100% in all but 4 patients studied thus far which include patients with toxic and non-toxic nodular goiter, Hashimoto's thyroiditis, follicular and Hürthle cell thyroid adenoma, well-differentiated and medullary thyroid carcinoma, primary and tertiary hyperparathyroidism, Graves' disease, and concurrent parathyroid and thyroid disease. The accuracy of this technique indicates its potential utility to improve parathyroid detection and hence surgical outcomes.

This study included four patients (13 glands) with renal-induced sHPT (out of 137 patients), where a low parathyroid detection rate was observed in each of these patients. Twenty-six million American adults have chronic kidney disease, and over 60% of these patients are at risk for the development of sHPT and 10% will require parathyroidectomy (11). In this study, 54% of glands from the four patients with sHPT emitted detectable levels of normalized

fluorescence compared to 94-100% of glands in all other patients. Each patient had 2 to 4 hypersecreting glands measured and 1 to 3 of those glands in each patient emitted high levels of detectable autofluorescence while the remaining glands showed a low intensity. Interestingly, the parathyroid glands of three patients with multigland hyperplasia unrelated to sHPT (i.e. tertiary hyperparathyroidism and familial hypocalciuric hypercalcemia) emitted high levels of fluorescence, indicating that some sHPT parathyroid glands may have a unique molecular composition that causes the down-regulation of the fluorescence signal. Varying patterns of chief cell, water clear cell or oxyphil cell hyperplasia as seen in the histological analysis sHPT glands may contribute to varying fluorescence signals. Fat content may also play a role, as parathyroid glands in sHPT patients have decreased fat compared to normocellular glands. Future analysis of the histological features from all disease states will further elucidate these findings.

The performance of traditional parathyroid preoperative imaging techniques such as Sestamibi scintigraphy (SS) and ultrasound (US) is affected by patient factors such as preoperative serum calcium, parathyroid hormone, disease severity, and vitamin D levels (12, 13). Other studies have also reported the influence of factors such as BMI and hormone levels on detection accuracy of optical techniques (14). Based on these studies, we selected age, ethnicity, disease state, preoperative serum calcium, vitamin D, BMI, and PTH levels as patient factors that could potentially be responsible for the variability in the observed parathyroid fluorescence and therefore affect the detection rate of NIR fluorescence spectroscopy. The results reported here show that NIR fluorescence spectroscopy is capable of reliable real-time detection of the parathyroid glands during thyroidectomy and parathyroidectomy regardless of clinical and demographic characteristics of the patient. Certain patient factors, including BMI, disease state, calcium levels, and vitamin D levels, were found to significantly affect the variability in the parathyroid fluorescence across the patient population. However, the parathyroid signal variability associated with these patient factors did not preclude the ability of this technique to successfully detect the parathyroid gland with 94-100% accuracy.

Disease state, BMI, preoperative vitamin D levels and serum calcium levels were shown to contribute to the variability in the parathyroid fluorescence signal, which ranged from 1.2 to 29 times higher than thyroid fluorescence. Patients with normal BMI are shown to emit a significantly higher parathyroid fluorescence signal than in patients who have overweight or

obese BMIs. These results suggest that parathyroid compositional changes such as increase in stromal fat at high BMIs (15) may be responsible for the change in fluorescence signal. Patient disease state showed an effect on parathyroid fluorescence intensity with lower signal emitted from patients with primary hyperparathyroidism compared to those with benign thyroid disease or hyperthyroidism. Furthermore, the glands of patients with normal preoperative serum calcium (not low and not high) exhibited significantly higher fluorescence than glands of patients with high serum calcium. This finding along with the low detection rates in sHPT indicate a down-regulation of the parathyroid fluorophore in cases of hypersecreting parathyroid glands. Results indicate that this phenomenon that may be dependent more on the calcium level than the PTH level.

Although the biological basis for the fluorescence signal is not currently known, these results provide indications for potential fluorophore candidates. Calcium-sensing receptors and vitamin D receptors are tentative fluorophore candidates because the levels of these proteins in tissue correspond to the trends observed in the parathyroid fluorescence signal. These proteins show slight down-regulation in primary hyperparathyroidism and more severe down-regulation in secondary hyperparathyroidism (16). Though we believe identifying the fluorophore is not essential for the widespread use of this technology, future knowledge of the biological basis for the fluorescence can expand the use of NIR fluorescence spectroscopy as a surgical guidance tool. Biochemical studies are ongoing to narrow this hypothesis and identify the contributing fluorophore.

Parathyroid detection with NIR fluorescence spectroscopy is not affected by user-induced variability and spatial heterogeneities within a given gland, though these factors did contribute to variability in the fluorescence across patients. The fluorescence signal was shown to decrease as probe contact pressure on the tissue increased both *in vitro* and *in vivo*. Increased probe pressure is likely to alter fluorescence intensity due to changes in the absorption and scattering properties of the tissue (17). The range of probe contact pressures applied did not alter the parathyroid gland fluorescence measurement to the extent that it was no longer detected, indicating this technique is capable of handling user-induced variability. The effects of probe contact pressure can be minimized if users are trained to operate at low pressures. Intraglandular spatial heterogeneity was also observed to cause variability in fluorescence measurement at different points within the same gland of the same patient. The reason for the discrepancies in

fluorescence across locations may be due to heterogeneous distribution of the fluorophore across the tissue. In one case, the lowest of five parathyroid measurements across a single gland was lower than the highest of five thyroid measurements in the same patient. If these measurements had been collected in isolation, the parathyroid signal would have been considered undetectable by NIR fluorescence spectroscopy. This finding indicates the need for at least three measurements in each gland for accurate identification of the parathyroid gland. Multiple measurements would also minimize the error due to the probe unknowingly slipping off the small gland during surgery. Each fluorescence measurement takes only 300 ms, and as such multiple measurements can be made intraoperatively without adding appreciable time to the procedure. It is also important to note that the parathyroid gland fluorescence is maintained regardless of its vascularity. No change in the parathyroid gland fluorescence was observed when the measurements were made on *in vivo* vascularized glands versus glands that had been removed and de-vascularized.

Overall, NIR fluorescence spectroscopy is a promising method for parathyroid detection across a diverse patient population. Clinical acceptance of such a technique requires an understanding of all factors present in the patient population. This study shows that this system is able to handle disease, user-induced, and physiologic variability. This study also demonstrated a unique reduction in signal in some of the glands of sHPT patients. This finding will be critical to our improved understanding of the basis of the observed fluorescence. Even though the fluorophore is unknown, this comprehensive study validates the use of this technique in the typical patient population at most major hospitals. This technology is ready for clinical translation through the regulatory process while ongoing research seeks to understand the etiology of the observed autofluorescence. This study gives evidence that use of this device has the potential to improve patient outcome and minimize complications in parathyroid and thyroid procedures.

4.6 Acknowledgments

We would like to thank the hospital staff at the Vanderbilt Endocrine Surgery center for their assistance in data collection. This material is based upon work supported by the National Science Foundation Graduate Research Fellowship Program under Grant No. 0909667 and the National Institute of Health under Grant No. NIHR41 EB015291.

4.7 References

1. Gourgiotis S, Moustafellos P, Dimopoulos N, Papaxoinis G, Baratsis S, Hadjiyannakis E. Inadvertent parathyroidectomy during thyroid surgery: the incidence of a complication of thyroidectomy. *Langenbeck's archives of surgery / Deutsche Gesellschaft fur Chirurgie*. 2006 Nov;391(6):557-60. PubMed PMID: 16951969.
2. Mohebati A, Shaha AR. Imaging techniques in parathyroid surgery for primary hyperparathyroidism. *American journal of otolaryngology*. 2012 Jul-Aug;33(4):457-68. PubMed PMID: 22154018. Pubmed Central PMCID: 3311773.
3. Chen H, Wang TS, Yen TWF, Doffek K, Krzywda E, Schaefer S, et al. Operative Failures After Parathyroidectomy for Hyperparathyroidism The Influence of Surgical Volume. *Ann Surg*. 2010 Oct;252(4):691-4. PubMed PMID: WOS:000282369400015. English.
4. Bergamaschi R, Becouarn G, Ronceray J, Arnaud JP. Morbidity of thyroid surgery. *Am J Surg*. 1998 Jul;176(1):71-5. PubMed PMID: WOS:000074852100020. English.
5. Lin DT, Patel SG, Shaha AR, Singh B, Shah JP. Incidence of inadvertent parathyroid removal during thyroidectomy. *Laryngoscope*. 2002 Apr;112(4):608-11. PubMed PMID: WOS:000174970600003. English.
6. Perrier ND, Ituarte P, Kikuchi S, Siperstein AE, Duh QY, Clark OH, et al. Intraoperative parathyroid aspiration and parathyroid hormone assay as an alternative to frozen section for tissue identification. *World J Surg*. 2000 Nov;24(11):1319-22. PubMed PMID: 11038200.
7. McWade MA, Paras C, White LM, Phay JE, Mahadevan-Jansen A, Broome JT. A novel optical approach to intraoperative detection of parathyroid glands. *Surgery*. 2013 Dec;154(6):1371-7. PubMed PMID: WOS:000327571200059. English.
8. Paras C, Keller M, White L, Phay J, Mahadevan-Jansen A. Near-infrared autofluorescence for the detection of parathyroid glands. *J Biomed Opt*. 2011 Jun;16(6). PubMed PMID: WOS:000293086800038. English.
9. McWade MA, Paras C, White LM, Phay JE, Solorzano CC, Broome JT, et al. Label-free Intraoperative Parathyroid Localization With Near-Infrared Autofluorescence Imaging. *The Journal of clinical endocrinology and metabolism*. 2014 Dec;99(12):4574-80. PubMed PMID: 25148235.
10. Cook RD. Detection of Influential Observation in Linear-Regression. *Technometrics*. 1977;19(1):15-8. PubMed PMID: WOS:A1977CV78500002. English.
11. Stack BC. Secondary Hyperparathyroidism: BMJ Best Practice; 2014 [updated January 14, 2014; cited 2015 February 13, 2015]. Available from: <http://bestpractice.bmj.com/best-practice/monograph/1107/basics/epidemiology.html>.

12. Hughes DT, Sorensen MJ, Miller BS, Cohen MS, Gauger PG. The biochemical severity of primary hyperparathyroidism correlates with the localization accuracy of sestamibi and surgeon-performed ultrasound. *J Am Coll Surg*. 2014 Nov;219(5):1010-9. PubMed PMID: 25086814.
13. Berber E, Parikh RT, Ballem N, Garner CN, Milas M, Siperstein AE. Factors contributing to negative parathyroid localization: an analysis of 1000 patients. *Surgery*. 2008 Jul;144(1):74-9. PubMed PMID: 18571587.
14. Vargis E, Byrd T, Logan Q, Khabele D, Mahadevan-Jansen A. Sensitivity of Raman spectroscopy to normal patient variability. *J Biomed Opt*. 2011 Nov;16(11). PubMed PMID: WOS:000298546500038. English.
15. Iwasaki A, Shan L, Kawano I, Nakamura M, Utsuno H, Kobayashi A, et al. Quantitative analysis of stromal fat content of human parathyroid glands associated with thyroid diseases using computer image analysis. *Pathology international*. 1995 Jul;45(7):483-6. PubMed PMID: 7551007.
16. Rodriguez M, Nemeth E, Martin D. The calcium-sensing receptor: a key factor in the pathogenesis of secondary hyperparathyroidism. *American journal of physiology Renal physiology*. 2005 Feb;288(2):F253-64. PubMed PMID: 15507543.
17. Ti Y, Lin WC. Effects of probe contact pressure on in vivo optical spectroscopy. *Optics express*. 2008 Mar 17;16(6):4250-62. PubMed PMID: 18542520.

CHAPTER 5

CHARACTERIZATION OF AN ENDOGENOUS NEAR-INFRARED FLUOROPHORE IN PARATHYROID AND OTHER ENDOCRINE TISSUES

Melanie A. McWade¹, Melinda E. Sanders², Carmen C. Solórzano³,
W. Hayes McDonald⁴, Anita Mahadevan-Jansen¹

¹Biomedical Photonics Center, Department of Biomedical Engineering, Vanderbilt University, 5824 Stevenson Center, Nashville, TN, 37235.

²Department of Pathology, Microbiology and Immunology, Vanderbilt University, Nashville, Tennessee 37232

³Division of Surgical Oncology and Endocrine Surgery, Vanderbilt University 2220 Pierce Avenue, 37232, Nashville, Tennessee.

⁴Department of Biochemistry and Mass Spectrometry Research Center, Vanderbilt University, 465 21st Ave South, Nashville, TN, 37203.

This chapter was submitted as:

“Characterization of a Near-infrared Endogenous Fluorophore in Parathyroid and other Endocrine Tissues.” *Proceedings of the National Academy of Science*, 2016

5.1 Abstract

Biomedical imaging with near-infrared (NIR) wavelengths is highly favorable due to deep light penetration (1). NIR imaging has relied on exogenous dyes because endogenous NIR fluorophores are rare (2-4). Here we introduce a robust, endogenous NIR fluorophore present in the parathyroid gland, adrenal medulla, pancreas, and thyroid gland. We present the characterization of this NIR endogenous fluorophore that was initially observed in the parathyroid glands of patients undergoing endocrine surgery with peak excitation and emission of 785-nm and 822-nm (5-7). Fluorescence microscopy reveals NIR autofluorescence emitted from the cytoplasmic region of parathyroid cells. Differential centrifugation indicates the fluorophore is present in an organellar-size structure. After SDS-PAGE, the majority of fluorescence was at approximately 15-kDa. Broad spectrum protease treatment shows loss of fluorescence, indicating the fluorescence likely originates from a protein or protein co-factor. Results show the fluorophore is not heat-labile. The robust behavior of the fluorophore, its localization in the cytoplasmic region, and its observation in a variety of endocrine tissues led to the hypothesis that this fluorophore is housed in the secretory granules. Electron microscopy of fluorescent fractions of adrenal and parathyroid tissue revealed granular, electron-dense structures with diameters similar to that of endocrine secretory granules (8). Autofluorescence microscopy of parathyroid tissue was compared to chromogranin-A stains, which revealed co-localization of NIR fluorescence and granular structures. This work is the first to unveil and characterize a novel NIR fluorophore in endocrine tissues. This study uncovers a new intrinsic target for fluorescence imaging and informs NIR dye developers of autofluorescence to avoid.

5.2 Introduction

In the past decade, the widespread adoption of fluorescence-based techniques in biology and medicine has generated an increased interest in endogenous and exogenous fluorophores. Endogenous fluorescence applications have primarily focused on ultraviolet and visible wavelengths because endogenous NIR fluorophores are uncommon. However, because the NIR region (650 – 900 nm) enables exceptionally deep tissue penetration due to low levels of absorption, scattering, and autofluorescence (9), exogenous NIR dyes have been developed to utilize the benefits of this “optical window” (1-3). Exogenous dyes can suffer from false-positive results due to non-specific tissue targeting, potential toxicity, and elongated procedure time due to pre-administration (10). We have uncovered an endogenous source of NIR fluorescence in endocrine tissue that presents a singular exception to the long-held notion that NIR biological fluorophores are rare.

Here we report the discovery of a novel endogenous NIR fluorophore present in the parathyroid glands. Our previous studies using NIR fluorescence spectroscopy and imaging have targeted this fluorophore to identify the parathyroid gland intraoperatively in over 130 patients with 99% accuracy (5-7). Despite consistent and robust measurements of this fluorophore in the parathyroid gland, the molecular basis for the fluorescence signal remains unknown. Studies thus far have shown the fluorophore has a peak fluorescence emission at 822-nm with 785-nm excitation. Furthermore, clinical fluorescence measurements indicate that the fluorophore has a 1.2 to 29 times higher concentration in the parathyroid than the thyroid (5). These clinical results imply an unknown endogenous fluorophore and motivates further investigation to characterize this apparently endogenous fluorophore in the parathyroid gland.

Known sources of endogenous fluorescence include aromatic amino acids (i.e. tryptophan, tyrosine, phenylalanine), enzyme cofactors (NADH, FAD, pyridoxyl phosphate), and intact tissue components such as porphyrins, collagen, elastin, and lipofuscins. These fluorophores have been ruled out as potential candidates for the NIR fluorophore we observe in parathyroid tissue due to their well-characterized emission peaks at ultraviolet and visible wavelengths (11). Porphyrins and their derivatives are the exception, as they have the longest known emission peak between 620-700 nm (12). However, porphyrins are an unlikely candidate because the peak parathyroid fluorescence emission is observed at 822-nm, and porphyrins are not present in parathyroid or

thyroid tissue. The NIR fluorophore observed in parathyroid studies (5-7) has never been characterized.

In both research and clinical applications such as microscopy, whole animal and deep tissue imaging, disease diagnosis, flow cytometry, surgical guidance, and dye development, the knowledge of a new endogenous fluorophore has the potential to change traditional practices. This NIR fluorophore provides a potential alternative to synthetic dyes, which induce a moderate risk to patients undergoing imaging procedures. Risk reduction justifies proposals to fast-track its application development. Conversely, exogenous dye approaches may need to adapt to avoid high background autofluorescence due to this endogenous fluorophore. Finally, a deeper understanding of the nature of this NIR fluorophore in the parathyroid gland is a potential tool for the study of physiological processes in endocrine biology.

The goal of this study was to evaluate the biological characteristics of the NIR endogenous fluorescence signal in order to expand and inform biomedical applications utilizing this fluorophore. A variety of approaches were employed to accomplish this goal. Fluorescence microscopy was used to achieve subcellular localization of the fluorophore within tissue. Biochemical studies characterized fluorophore behavior in response to gel electrophoresis, centrifugation, heat, and proteases. NIR autofluorescence was tested in endocrine tissues beyond parathyroid and thyroid. Finally, the structural origin of the fluorophore was studied using density gradient centrifugation, transmission electron microscopy, and immunohistochemistry.

5.3 Materials and Methods

5.3.1 Fluorescence microscopy

Fresh frozen de-identified human endocrine tissues were obtained from the Cooperative Human Tissue Network (CHTN) at Vanderbilt University with approval from the Vanderbilt Institutional Review Board (IRB #070795). A majority of studies were performed on parathyroid adenoma tissue. Tissue was embedded in optimal cutting temperature compound, sliced in 5- μ m thick sections, and placed on quartz microscope slides (Electron Microscopy Sciences). Tissue sections were stored at -80°C and were not fixed or stained prior to fluorescence imaging. Parathyroid adenoma sections were thawed to room temperature before imaging. Imaging was performed with a Zeiss Axiovert 135 (Carl Zeiss) fluorescence microscope equipped with a

PhotonMax 512B (Princeton Instruments) cooled CCD camera cooled to -70°C . Images were first collected under transmitted bright field illumination. Corresponding autofluorescence images were then collected using a NIR 785-nm diode laser (Innovative Photonic Solutions), which provided sample trans-illumination via an optical fiber delivering an average 4.7 mW to sample. A 785-nm edge long-pass filter (Semrock) was placed in the optical path to filter excitation light. Images were acquired with WinView/32 software (Roper Scientific) with 3 accumulations and 15 s exposure times. Dark current images were collected at each location in the tissue. Fluorescence images of unstained sections were collected within 1 hour of thawing in order to minimize tissue degradation. Low magnification images were collected using a $2.5\times / 0.075$ objective (Carl Zeiss). High magnification images were collected using a $40\times / 0.60$ objective (Carl Zeiss).

5.3.1.1 Histopathology

Tissue slices were immediately fixed in 10% formalin buffer after imaging and prepared for histopathology using standard protocols. Hematoxylin and eosin (H&E) stained sections were obtained from each tissue slice for overall morphology. Co-registration of fluorescence image with H&E image was achieved by imaging the H&E stained section using a color CMOS detector (Basler AG) in the same spot that NIR fluorescence images were collected.

5.3.1.2 Image Analysis

Fluorescence and bright field images were analyzed using a custom MATLAB program. Dark current images were subtracted from each fluorescence image. The fluorescence image was laid over the corresponding bright light image of the unstained section. The features of the unstained section were used to align the fluorescence image and the H&E stained section. To enhance visualization of the tissue fluorescence in the images, false color was added to the fluorescence images.

5.3.2 Fluorescence over time

Bulk samples of fresh frozen human parathyroid tissue were thawed to 4°C and placed in 150 μL of phosphate-buffered saline to avoid dehydration. Tissue fluorescence was initially measured using a NIR fluorescence scanner with 785-nm excitation (LI-COR Biosciences) and at

10 additional time points over 150 hours. Parathyroid and thyroid tissue fluorescence were quantified, and the fluorophore half-life was calculated by linear regression analysis against time.

5.3.3 Fluorescence response to proteases

Frozen human parathyroid adenoma tissue samples were pulverized to a fine powder using a mortar and pestle precooled in liquid nitrogen. Ground tissue was homogenized with 20 strokes of a Potter-Elvehjem tissue grinder (Wheaton Industries, Inc.) in ice cold RIPA buffer (50 mM 72Tris-HCl, 150 mM NaCl, 0.1% SDS, 1% IGEPAL CA-630, 0.5% sodium deoxycholate, pH 8) (Sigma). Parathyroid homogenate was centrifuged at 10,000g for 10 minutes. The parathyroid supernatant was separated in two equal aliquots. Proteinase K was added at a volume of 100 µg per mL of tissue lysate to one aliquot, and the other aliquot served as a control. Both samples were incubated for 1 hour at 23 °C before imaging with a near-infrared scanner at 1, 5, 20, and 50 hours. Fluorescence intensities of each sample were quantified to determine effects of a broad spectrum protease on autofluorescence signal.

5.3.4 Fluorescence response to heat

Parathyroid tissue lysate was prepared with RIPA buffer as previously described. Sample was heated for 5 min at 95 °C and cooled to 23°C. Heated samples were imaged with NIR scanner along with an unheated control sample of parathyroid lysate. Fluorescence intensities of each sample were quantified to determine effects of temperature on autofluorescence signal.

5.3.5 Differential centrifugation

Bulk parathyroid adenoma tissue samples were homogenized in cold homogenization buffer (50 mM Hepes/NaOH pH 7.5, 0.33 M sucrose) in a 2:1 weight-volume ratio. Differential centrifugation was performed to separate subcellular particles based on the differences in the sedimentation coefficients of these particles. The sedimentation coefficient is a function of the shape, density, and volume of the particle, also considering the viscosity and density of the medium (13). Tissue homogenates were centrifuged at 500 g for 5 minutes. The supernatant was removed, and the nuclear pellet, which contained nuclei, unbroken cells, and cell debris, was set aside. The low speed supernatant was centrifuged at 10,000 g for 10 minutes. The resulting medium speed supernatant, which contains the soluble components of the tissue, was set aside. The resulting

medium speed pellet contained mitochondria, lysosomes, peroxisomes, and other similar-sized subcellular organelles (13). All three fractions were diluted to the same volume and placed in a 96 well plate. Fractions were imaged using a near-infrared scanner to determine the subcellular location of the parathyroid fluorophore. Experiments were performed in triplicate.

5.3.6 SDS-PAGE

Sodium dodecyl sulfate-polyacrylamide gel electrophoresis (SDS-PAGE) was conducted on the XCell SureLock Mini-Cell System (Invitrogen) using NuPAGE Novex 4 to 12% Bis-Tris Zoom gels (Invitrogen) with MES running buffer. Parathyroid tissue was homogenized in 2X Laemmli buffer (4% SDS, 20% glycerol, 0.5% Beta-mercaptoethanol, 120 mM Tris-Cl, pH 6.8), incubated at 4°C for 24 hours, and cleared by centrifugation at 10,000g for 15 minutes. Twenty-five µg of each parathyroid sample and controls (sample buffer without protein content) were mixed with LDS sample buffer (Invitrogen) containing 1% (w/v) DTT for 15 minutes and heated at 95°C for 5 minutes. Parathyroid samples, controls, and molecular weight standards (Bio-Rad) were run at 100 V until the tracking dye front reached the bottom of the well. Gel was immediately imaged under a NIR scanner prior to staining. The fluorescent bands were quantified for each sample and compared to molecular weight standards. Gels were stained with Coomassie blue dye to ensure proper running of the samples.

5.3.7 Autofluorescence measurement of additional endocrine tissues

Parathyroid adenoma, benign thyroid, normal pancreas, and adrenal pheochromocytoma samples were thawed to 23°C and imaged under a NIR fluorescence scanner. Chicken breast was used as a negative control. Relative fluorescence intensities were quantified for each tissue type. Fluorescence spectra were measured using a probe-based NIR fluorescence spectroscopy system previously described (6, 7, 35). The spectroscopy system delivered 785-nm diode laser light (Innovative Photonic Solutions) via a fiber optic probe (EMVision) to each tissue. Fluorescence was collected and detected by a Visible/NIR spectrometer (Ocean Optics). The spectra were processed and plotted in MATLAB to compare peak wavelength and fluorescence intensity for each tissue.

5.3.8 Parathyroid and Adrenal tissue fractionation

Experimental findings led to the hypothesis that the fluorophore originates from within the secretory granules of endocrine tissues. Subsequent experiments aimed to probe the validity of that hypothesis. Parathyroid adenoma and adrenal pheochromocytoma tissue was fractionated for crude isolation of secretory granules using the density gradient centrifugation protocol described by Bartlett and Smith (14). Tissues were pulverized in liquid nitrogen and placed in Potter-Elvehjem homogenizers with 0.3 M sucrose solution at a 1:5 weight-to-volume ratio. Homogenates were centrifuged at 400 g for 20 minutes. Supernatants were aspirated and placed in a polypropylene tube (Beckman Coulter). The supernatants were centrifuged in an L-90 K Beckman Coulter ultracentrifuge for 20 minutes at 4°C at 8720 g (Type 70.1 Ti rotor, Beckman Coulter), then aspirated from pellets and set aside. The remaining sediment was resuspended with 8.9 mL of 0.3M sucrose solution and centrifuged again for 20 min. at 4°C at 8720 g. The supernatants were removed and combined with previous supernatants. The combined supernatants were added to an ultracentrifuge tube and spun for 60 min. at 4°C at 80,790 g. The supernatants were discarded, and the pellets were resuspended in 2 mL of 0.3 M sucrose solution. A volume of 6.5 mL of 1.6 M sucrose solution was added to the bottom of an ultracentrifuge tube, and the 2 mL supernatant solution was layered on top. The samples were ultracentrifuged for 60 min. at 4°C at 80,790 g through this hyperosmotic sucrose solution. The contents of the tubes could be visually distinguished into five fractions, which were decanted and imaged with a NIR fluorescence scanner. Discarded tissue components were also measured for fluorescence signal to ensure the fluorescent component harvested at the end of the experiment.

5.3.9 Transmission Electron Microscopy (TEM) of Isolated Fluorescent Tissue Fraction

The fluorescent fraction isolated with density gradient centrifugation was prepared for TEM using negative staining. A formvar-coated, 200-mesh, copper grid was floated on to of a 40 µL drop of sample for 30 s. The grid was then removed, and excess fluid was wicked away. The grid, with adsorbed particles, was then floated on a 40 µL drop of 2% aqueous phosphotungstic acid (pH 5.1) for 30 s before wicking away excess fluid. Samples were then imaged using a Phillips/FEI T-12 transmission electron microscope. Particle diameters were quantified for 30 particles across the sample.

5.3.10 Chromogranin A (CgA) Immunohistochemistry

Unstained parathyroid sections on quartz slides were imaged as previously described using a NIR fluorescence microscope. After imaging, all slides were placed in 10% neutral buffered formalin for fixation. Slides were then incubated with Ready-To-Use anti-Chromogranin A (Leica) for one hour. The Bond Polymer Refine detection system (Leica) was used for visualization as follows: the slides were placed in rabbit anti-mouse secondary for 8 min. and a goat anti-rabbit (HRP) for 8 min. A peroxide block was placed on the slides for 5 min., and then the DAB solution was placed on the slides for 10 min. A counterstain of Hematoxylin was applied for 8 min. Slides were dehydrated, cleared, and cover-slipped. Identical regions of tissue imaged for NIR autofluorescence were then imaged with bright light illumination. NIR autofluorescence images were laid over CgA stained images to assess the correlation between fluorescence and CgA expression.

5.4 Results

5.4.1 Fluorescence Microscopy Reveals Cytoplasmic Autofluorescence.

Fluorescence microscopy was performed to determine subcellular location of fluorescence emission. NIR autofluorescence images (Fig. 5.1A) overlaying H&E stained bright field images of the same tissue location (Fig. 5.1B) revealed the morphological location of the emitted fluorescence (Fig. 5.1C). At 2.5X magnification, images reveal fluorescence emission from parenchymal cells of the parathyroid gland (Fig. 5.1A-C). No fluorescence is emitted from connective tissue, lymphatic space, vacuoles, fibrotic tissue and extracellular fat. The parathyroid section in Fig. 5.1A-C reveals a normal rim of parathyroid tissue comprised of chief cells and an adenomatous region comprised primarily of more eosinophilic oxyphil cells. Both cell types emit NIR autofluorescence. Fluorescence images collected under 40X magnification show a punctate pattern of fluorescence (Fig. 5.1D). Correlation of NIR autofluorescence with cellular structures by overlaying fluorescence and H&E images of the same section at 40X magnification (Fig. 5.1E) revealed strongest fluorescence is emitted from cytoplasmic region rather than the cell membrane or nucleus (Fig. 5.1F).

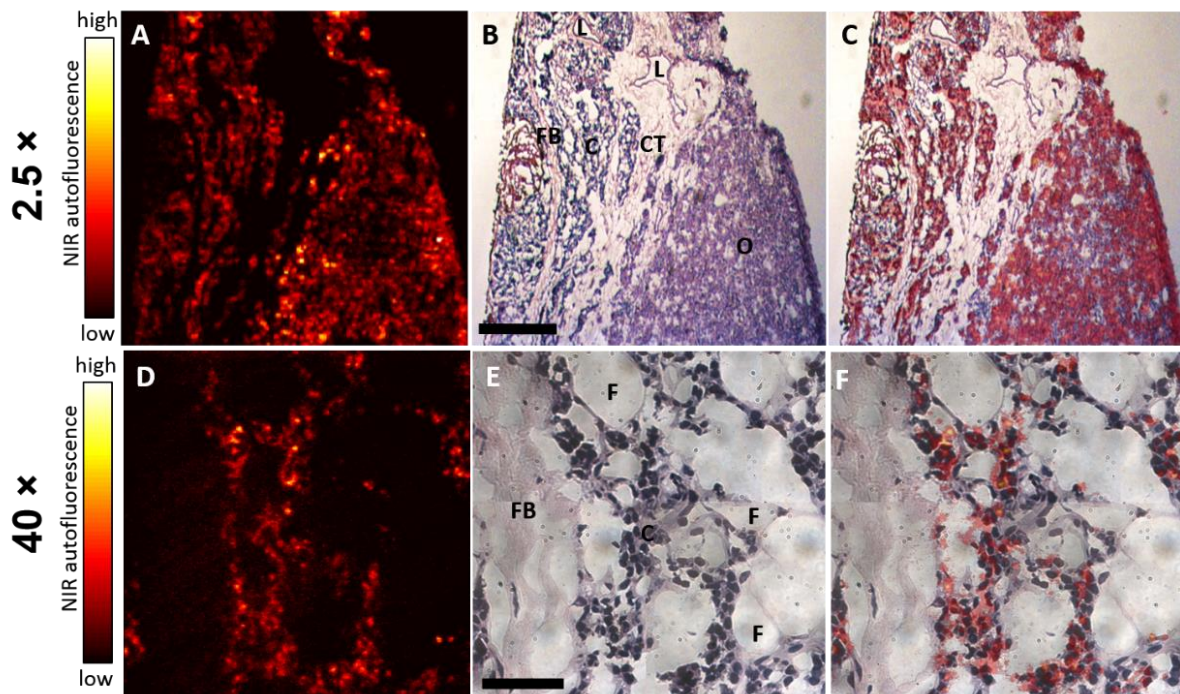


Figure 5.1: Location of autofluorescence using fluorescence microscopy of human parathyroid tissue cross sections. Images at 2.5X magnification show A) NIR fluorescence of unstained section, B) H&E stain, C) overlay of fluorescence and H&E stain. Scale bar is 500 μm for A-C. Images at 40X show D) NIR fluorescence of unstained section, E) H&E stain, F) overlay of fluorescence and H&E stain. Scale bar is 50 μm for D-F. Labelled on images: C-chief cells, O-oxyphil cells, L-lymphatic space, CT-connective tissue, FB-fibrosis, F-fat.

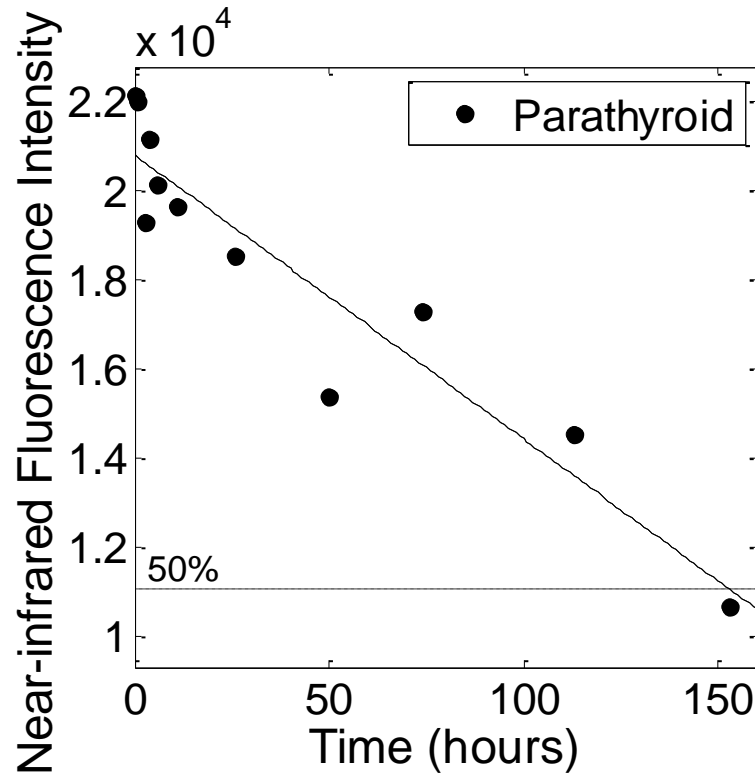


Figure 5.2: Parathyroid tissue near-infrared autofluorescence is reduced over time. Linear regression line is shown ($R^2=0.89$). Parathyroid autofluorescence has a half-life of 152 hours shown by dotted line indicating 50% drop in fluorescence signal.

5.4.2 NIR Fluorophore Heat-Stable with Mild Proteinase-Sensitivity

Parathyroid bulk tissue fluorescence measured over a 150 hour time period indicates that the near-infrared fluorophore is relatively stable over time. Parathyroid fluorescence demonstrated a linear decrease over time, resulting in 48% of initial fluorescence after 150 hours (Figure 5.2).

Parathyroid homogenates exposed to proteinase K exhibited complete loss of fluorescence after a 50 hour incubation time compared to parathyroid homogenates without proteinase K (Fig. 5.3A). Fluorescence intensity in proteinase K sample was 93 a.u. compared to 6532 a.u. in the control sample, which is a 98.6% decrease in autofluorescence signal as a result of proteinase K treatment. Fluorescence intensity between proteinase K homogenate and positive control was not significantly different after shorter incubation periods ranging from 1 to 20 hours. The stark drop in fluorescence in proteinase K sample could be attributed to protein digestion by proteinase K, suggesting a proteinaceous nature of the fluorophore.

Heating parathyroid homogenates yielded no decrease in fluorescence compared to unheated parathyroid homogenate (Fig. 5.3B). After 95°C heat treatment, heated parathyroid homogenate maintained a fluorescence intensity that was 8665 a.u. compared to 8900 a.u. in unheated samples.

5.4.3 Differential Centrifugation Suggests NIR Fluorophore Housed In Organellar-Sized Subcellular Structure

Differential centrifugation was performed on parathyroid homogenates to isolate the subcellular fraction in which the fluorescent component is located. The separation of subcellular particles by differential centrifugation is based on the differences in the sedimentation coefficients of these particles. The sedimentation coefficient is a function of the shape, density, and volume of the particle, also considering the viscosity and density of the medium (13). The NIR fluorescence intensity of the organelle pellet containing mitochondria, secretory granules, lysosomes, peroxisomes and other organelles of similar size measured 140.71 ± 14.52 a.u and was found to be significantly greater than the NIR fluorescence in the nuclear pellet or supernatant after differential centrifugation (Fig. 5.3C). The nuclear pellet, containing cell nuclei, debris, and unbroken cells emitted a fluorescence intensity of 34.41 ± 7.46 a.u, while a NIR fluorescence intensity of 48.90 ± 13.16 a.u. was measured from the supernatant, containing remaining cellular components.

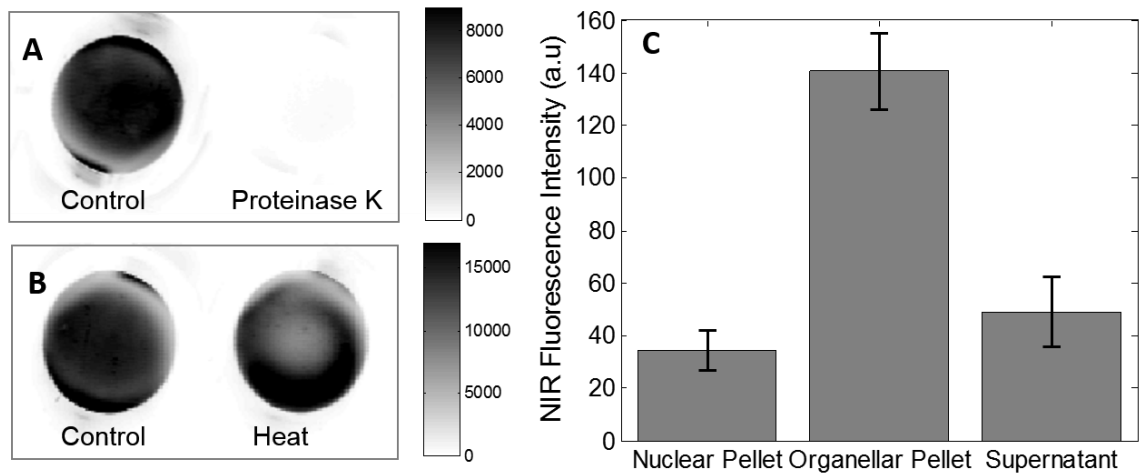


Figure 5.3: Biophysical studies on parathyroid fluorophore. A) Parathyroid lysate mixed with proteinase K shows reduced fluorescence compared to parathyroid lysate without proteinase K. B) Parathyroid lysate subject to 95°C heating shows similar fluorescence to control. C) Parathyroid homogenates that underwent low speed (500 x g) and medium speed (10,000 x g) centrifugation reveal highest fluorescence in medium speed pellet, containing unbroken subcellular membrane bound organelles. Error bars represent standard errors (N=3).

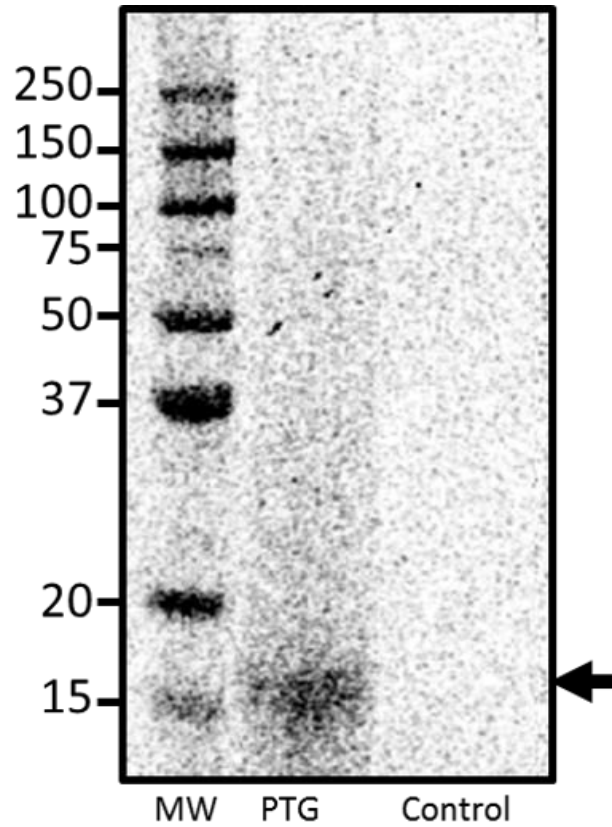


Figure 5.4: Parathyroid fluorophore autofluorescence in an unstained SDS-PAGE gel shows fluorescent band at approximately 15 kDa. Lanes from left to right: MW- Molecular weight standards, PTG- Parathyroid tissue homogenized in 2X Laemmli buffer, Control.

5.4.4 SDS-PAGE reveals Molecular Weight of NIR Fluorophore

Separation of parathyroid homogenates in SDS-PAGE revealed the presence of autofluorescence in a 15-kDa after homogenization of parathyroid samples in 2x Laemmli (Fig. 5.4). Because only 25 μ g protein could be loaded onto the gel, a low signal-to-noise ratio of autofluorescence was observed. Remarkably, the NIR autofluorescence was not quenched by the denaturation, heating, and reducing conditions prior to separation in the polyacrylamide gel.

5.4.5 Multiple Endocrine Tissues Emit NIR Autofluorescence

To determine other tissue expressing this NIR fluorophore beyond the parathyroid gland, NIR fluorescence of benign thyroid, normal pancreas, and adrenal pheochromocytoma tissue were measured and compared to parathyroid. Fluorescence images and spectra revealed NIR autofluorescence signal was present at varying levels in each endocrine tissue type (Fig. 5.5A). Figure 5.5B shows a typical fluorescence spectra of these endocrine tissue types when excited with 785-nm. Parathyroid adenoma, thyroid, pancreas, and adrenal pheochromocytoma tissue clearly show a single peak at 822-nm. Adrenal pheochromocytoma tissue emitted the highest fluorescence signal, with peak intensity 3.9 times higher than parathyroid peak intensity. Pancreas and thyroid exhibited peak fluorescence intensities 0.59 and 0.46 times parathyroid peak intensity, respectively. Chicken breast served as the negative control and demonstrated no autofluorescence signal in either imaging or spectroscopy measurements.

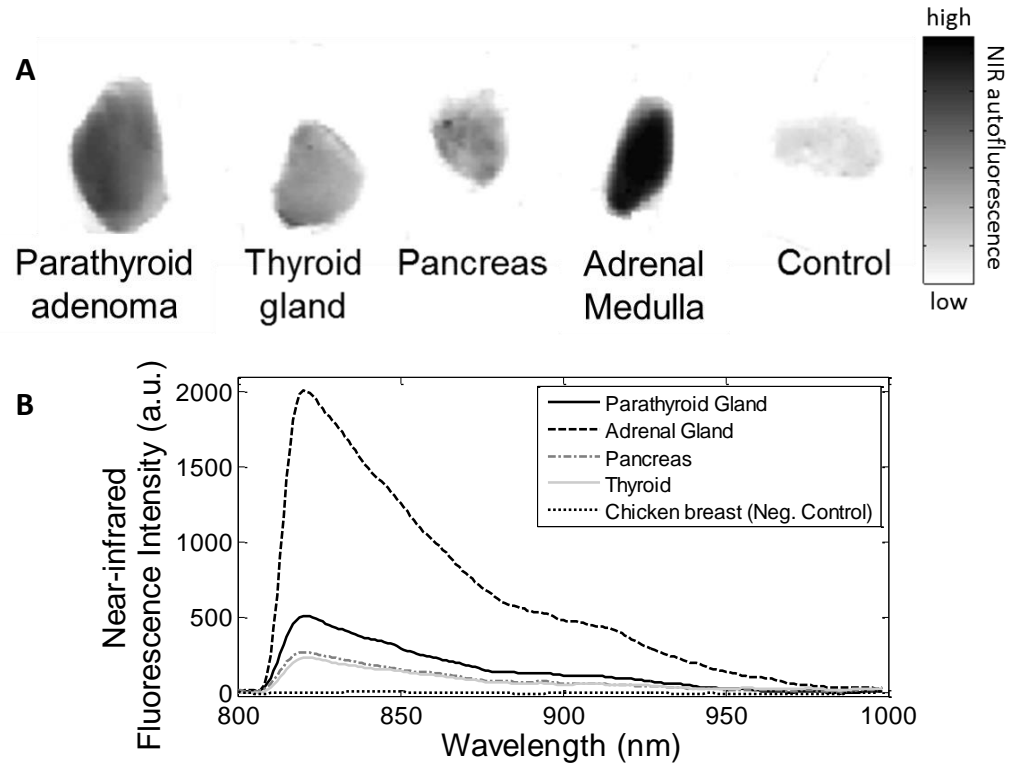


Figure 5.5: Additional tissues with intrinsic NIR fluorescence. Pancreas, adrenal glands, and thyroid emit intrinsic near-infrared fluorescence at excitation 785 nm and emission 822 nm. Fluorescence measured using A) NIR fluorescence imaging, and B) NIR fluorescence spectroscopy

5.4.6 Fluorophore Localized in Electron-Dense Granular Structure

Fluorescence measured in multiple endocrine tissues, along with the punctate pattern of fluorescence observed in fluorescence microscopy images and the biochemical studies results suggested the localization of the NIR fluorophore in secretory granules. For further validation, subcellular fractionation and electron microscopy was performed. A tissue fractionation protocol utilizing density gradient centrifugation and ultracentrifugation through a hyperosmotic sucrose solution for the isolation of secretory granules successfully isolated the fluorescent tissue component from adrenal and parathyroid tissue (Fig. 5.6A). Fluorescence measurements of the five tissue fractions isolated after ultracentrifugation revealed the highest fluorescence intensity was found in fraction 5, which was the most dense tissue fraction. According to the protocol described by Bartlett and Smith (14), fraction 5 contains highly purified secretory granules. Tissue fractions discarded during density gradient centrifugation did not emit NIR fluorescence, thereby ensuring that the fluorescence component was maintained in the tissue lysate undergoing ultracentrifugation.

Transmission electron microscopy images of samples of fraction 5 prepared with a negative staining technique revealed electron-dense granular structures in parathyroid and adrenal tissue extracts (Fig. 5.6B-C). In adrenal gland fractions, the granular structures had an average diameter of 341 ± 171 nm, while the granular structures in parathyroid gland fractions had an average diameter of 426 ± 168 nm. In both the parathyroid and adrenal gland images, granular features were the most prominent feature that displayed varying electron densities.

The NIR autofluorescence patterns in human parathyroid tissue cross sections were then compared to CgA immunohistochemical staining patterns. CgA staining was used to serve as a marker for secretory granule activity in the cytoplasm parathyroid parenchyma cells because CgA is widely expressed in parathyroid tissue (15). NIR fluorescence displayed an overlap in regions where chromogranin A is expressed in the tissue (Fig. 6D-F). However, CgA staining was also present in areas where no fluorescence signal was detected. The punctate pattern of fluorescence was localized in the cytoplasm region of the parathyroid parenchyma cells.

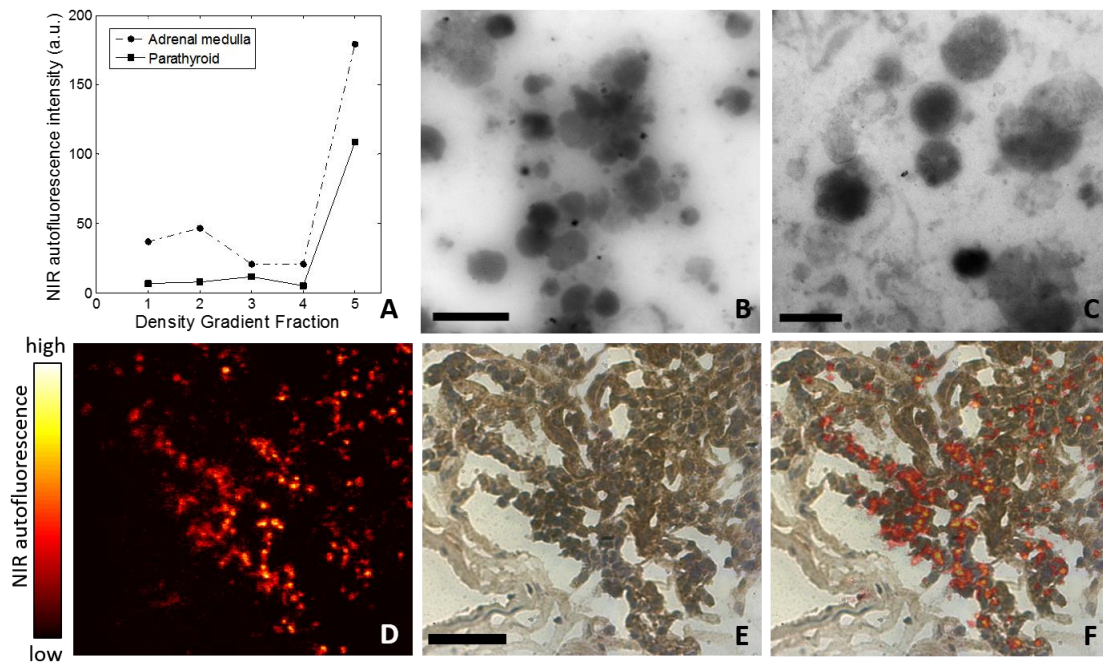


Figure 5.6: Secretory granules are hypothesized to contribute to NIR autofluorescence in parathyroid and other endocrine tissues. A) Parathyroid and adrenal medulla tissue fractionated with density gradient centrifugation yielded a dense fluorescent fraction. Fluorescent fractions were imaged with transmission electron microscopy revealing electron-dense granular structures in both B) Parathyroid tissue (scale bar=2 μ m, 11000X magnification) and C) adrenal medulla tissue (scale bar = 0.5 μ m, 30000X magnification), D) NIR fluorescence microscopy image of parathyroid tissue showed similar patterns as E) Chromogranin-A (a secretory granule marker) staining of parathyroid tissue. F) The distribution of fluorescence material across the Scale bar is 500 μ m for D-E.

5.5 Discussion

Our discovery of NIR autofluorescence in the parathyroid provides an exception to the traditional understanding that endogenous NIR fluorophores are not common. These results present the discovery of a new NIR endogenous fluorophore present in the parathyroid, adrenal medulla, pancreas, and thyroid. This paper is the first to report the biochemical and cell biological characterization of this novel endogenous NIR fluorophore. Characterization of the NIR fluorophore suggests that it is present in the cytoplasmic region in an organellar-sized structure and has a molecular weight of 15-kDa. Biochemical studies reveal it is highly robust and was digestible by proteinase K, although at a period of 50 hours. This initial discovery and characterization has the potential to transform fluorescence imaging by providing an endogenous alternative to exogenous NIR dyes and adding a precaution to exogenous NIR dye users looking to avoid background autofluorescence.

Although the fluorescence peak at 822-nm has been consistently observed *in vivo* during intraoperative endocrine procedures (5-7), the characteristics of the NIR fluorophore remains unknown. NIR fluorescence microscopy images of unstained parathyroid tissue reveal fluorescence emission from the cytoplasmic region of the parathyroid parenchyma cells. This result narrows the pool of potential fluorophore candidates showing that fluorescence is not strongly emitted from either the cell nucleus or plasma membrane. Chief cells are regarded as the functional cells of the parathyroid gland, rather than the oxyphil cells. Fluorescence images reveal both chief and oxyphil cells emit this fluorescence signal, indicating fluorescence is not unique to a single cell type. This may be due to the fact that parathyroid chief and oxyphil cells are thought to be derivatives of one another with similar secretory products and expression profiles of proteins such as parathyroid hormone, calcium-sensing receptors, and vitamin D receptors (16).

NIR autofluorescence of parathyroid tissue measured over approximately one week revealed the fluorophore is highly stable and resistant to degradation. A half-life of 152 hours indicates higher photostability even compared to, for example, the 26 hour half-life of green fluorescent protein, which is known to be highly stable (17). Fluorophore stability may be due to its localization within a degradation-resistant molecular architecture in tissue such as secretory vesicles (8) or protein aggregates (18).

Characterization approaches are different for small molecules and proteins (19, 20). Fluorophore response to proteinase K, a broad spectrum protease, was observed to determine the

nature of the fluorophore and inform future experiments. Proteinase K is known to cleave peptide bonds with broad specificity for general digestion of proteins in biological samples (21). Therefore, the quenching of tissue autofluorescence after protein digestion using proteinase K suggests either that the NIR fluorescence originates from a protein rather than a small molecule or that it requires a protein co-factor to maintain its fluorescence signal. Protocols for protein digestion with proteinase K are reported to typically require 15 minutes to 3 hours of incubation time, sometimes requiring as much as overnight incubation. Fluorescence quenching via proteinase K was not observed in parathyroid homogenates until 50 hours after application, which is a large increase in incubation time compared to incubation times reported in traditional protocols (22). The longer time course for proteinase K induced fluorescence quenching indicates that the NIR fluorophore in parathyroid tissue has protective mechanisms in place that resist degradation by proteinase K for a period of time. The possibility cannot be eliminated, however, that protein digestion delivered downstream effects resulting in the quenching of fluorescence activity of non-protein origin.

The inability of heat to diminish NIR fluorescence in parathyroid homogenates further displays the robust nature of the fluorophore. Protein autofluorescence has been shown to alter in response to denaturation due to change in protein conformation. For example, green fluorescent protein and tryptophan autofluorescence decreases after heating due to loss of proper folded structure (23, 24), while tryptophan shows an increase in fluorescence intensity upon denaturation (1). The lack of change in fluorescence of the NIR parathyroid fluorophore in response to heat suggests this fluorophore may be in the class of proteins that is known to be stable even at the boiling temperature of water. This stability has been attributed to a variety of characteristics such as increased packing density that reduces cavities in the hydrophobic core, small solvent exposed surface area an increase of hydrophobicity in the core region, decreased length of surface loops, and increased hydrogen bonds between polar residues (25). The resilience of this fluorophore to degradation due to heat, time and protease activity is a potentially attractive quality for applications that require a robust and stable source of contrast. These results also show that modification of standards protocols (i.e. incubation times, choice of detergents, etc.) is necessary for fluorophore isolation due to its degradation resistant properties.

Recovery of various subcellular fractions by differential centrifugation revealed the greatest NIR autofluorescence to be present in the organellar-fraction that is rich with mitochondria

and other subcellular organelles with a size, density, and volume similar to that of subcellular organelles such as mitochondria, peroxisomes, lysosomes, and secretory granules. The nuclear fraction contained 75% less fluorescence than the organellar-fraction, which is consistent with the NIR fluorescence microscopy images in Fig. 5.1 that did not reveal nuclear fluorescence. Small amounts of fluorescence in the nuclear fraction after differential centrifugation may be due to the fluorophore present in unbroken cells. The remaining supernatant containing the microsomal fraction, soluble cytosolic proteins, fragments of the Golgi apparatus, and endoplasmic reticulum also revealed very low fluorescence that was 68% less than in the organellar fraction. Small amounts of NIR fluorescence in this supernatant fraction may be due to break down of organellar structures during homogenization, which could release components into the less dense fraction.

Separation of the NIR fluorophore in parathyroid tissue showed strong NIR fluorescence at 15-kDa. Laemmli buffer, which is ionic and highly denaturing due to high concentration of sodium dodecyl sulfate, homogenized the parathyroid tissue facilitating the migration of the fluorescent material to a 15-kDa band. The maintenance of the NIR fluorescent signal through the SDS-PAGE protocol was validated by the previously experiments showing fluorescence is not hindered by heat or denaturing detergents. Knowledge of the molecular weight of this fluorophore can be used in further studies to identify the precise fluorescent protein or peptide.

The fluorescence emission peak for parathyroid adenoma, thyroid, pancreas, and adrenal pheochromocytoma tissue was observed at 822-nm, suggesting that the NIR endogenous fluorophore is the same for each of these endocrine tissues. This also may indicate that the fluorophore is a subcellular component required to carry out production, secretion, or regulation of hormones. Consistently higher NIR fluorescence intensities observed in adrenal pheochromocytoma tissue samples reveals increased expression of the NIR fluorophore in this tissue type above parathyroid and the other endocrine tissues measured. The results suggest that the application of this endogenous source of contrast can be expanded to endocrine tissues beyond parathyroid glands. It is possible that researchers reporting high levels of background NIR autofluorescence in tissue measurements of, for example, soft-tissue sarcomas (26) and colon (27), are detecting the same NIR fluorophore, indicating potential applications of this endogenous fluorophore beyond endocrine tissues.

The results of aforementioned experiments led to a hypothesis that the NIR fluorophore is localized within the secretory granules common to the parathyroid gland, thyroid, pancreas, and

adrenal medulla. The punctate cytoplasmic pattern of NIR fluorescence observed in microscopy images is similar to that observed in other studies imaging secretory granules (28). Furthermore, because the robustness of the fluorescence in response to heat, protease, and time is consistent with secretory granule behavior (8), a more in-depth investigation of these secretory granules was investigated.

Endocrine tissues are known to be characterized by the presence of two types of secretory organelles: large electron-dense secretory granules and smaller electron-lucent synaptic-like microvesicles (29). A protocol to isolate secretory granules from chromaffin cells resulted in the harvesting of a fluorescent fraction in the component of tissue thought to be large impure secretory granules (14). Transmission electron microscopy images of the fluorescent fractions of both parathyroid and adrenal medulla tissue yielded large electron dense granular structures of comparable size, shape, and electron density to secretory granules in literature which have been reported to range from 200 – 700 nm in diameter in parathyroid and 100 – 300 nm in adrenal glands (30, 31). The fluorescent fractions obtained from parathyroid tissue revealed granular structures of greater diameter than those from fractionated adrenal tissue, which is consistent with the larger size of secretory granules in adrenal tissue than parathyroid tissue.

Further investigation of the secretory granule hypothesis was performed using chromogranin A stain as a marker for secretory granules in the parathyroid tissue because of its high expression in parathyroid secretory granules (15). Much of the observed fluorescence overlapped with areas stained with chromogranin A. Though there were some areas of the tissue exhibiting chromogranin A staining without fluorescence, this does not exclude secretory granules as the location of the NIR fluorophore. Due to non-specific staining, the chromogranin A antibody could have additionally stained non-fluorescent members from the family of granin-like proteins. Additionally, other proteins localized in secretory granules such as the granin family of proteins and granin-derived peptides may be potential candidates, as many members of this family are present in adrenal medulla, pancreas, thyroid, and parathyroid (32, 33). Immunohistochemical studies show that the expression patterns of different secretory granule components such as chromogranin A, chromogranin B, secretogranin I and secretogranin II are shown to have distinct expression patterns and levels in endocrine tissues that are sometimes overlapping and sometimes complementary (15, 28). This suggests the possibility of a secretory granule component whose expression pattern matches more closely to the NIR fluorescence observed in tissue. Certain

members of the granin family are reported to be heat-stable. This quality is consistent with the resistance of the observed NIR fluorescence in response to heat. Heat-stable proteins in this family include secretogranin II, secretogranin IV (HISL-19 antigen), secretogranin V (endocrine secretory protein 7B2), secretogranin VI (NESP55), and secretogranin VII (28, 34).

Furthermore, chromogranin A is known to have down-regulated expression in parathyroid adenomas and parathyroid glands that are hyperplastic from uremic secondary hyperparathyroidism. Even though the plasma levels of chromogranin A are higher in these patients, immunohistochemistry has shown lower levels of chromogranin A expression in these glands (36). This is consistent with the low fluorescence signal observed in patients with primary and secondary hyperparathyroidism. Future work will be done to explore fluorophore candidates by correlating immunohistochemical staining of these proteins with NIR fluorescence in parathyroid and other endocrine tissues.

This novel endogenous NIR fluorophore is potentially intriguing for two primary reasons. First, those working in the NIR “optical window” with the expectation of low biological autofluorescence should account for this NIR endogenous fluorophore prior to the development and application of exogenous NIR dyes such as indocyanine green (ICG). This NIR fluorophore may account for high background autofluorescence or false-positives in dye applications in and around the endocrine tissues where it was observed. Second, this biological fluorophore provides a new source of contrast that can be used as an alternative to exogenous contrast agents in select endocrine applications. Researchers and clinicians utilizing fluorescence microscopy, whole animal imaging, or surgical imaging modalities, for example, may benefit from this robust, tissue specific, and intrinsic source of contrast. Imaging of pancreatic islets in diabetes research, for example, may be enhanced by this NIR fluorophore. Because the excitation and emission wavelengths are very similar to the widely used ICG dyes, the biomedical community may benefit from using very similar instrumentation to that which is already used. It is important to note, however, that though the observed NIR fluorescence is bright relative to tissue background, exogenous dyes such as ICG are designed to emit a much higher intensity signal. Therefore, higher exposure times and excitation powers may be required to visualize this endogenous NIR fluorophore. Finally, this fluorophore could present a new tool to enhance fundamental understanding of endocrine physiology. Previous clinical studies showing a downregulation of the NIR fluorophore in certain disease states such as primary hyperparathyroidism (5) indicates this

fluorophore is affected by disease processes. This fluorophore, then, may provide a molecular probe that can be studied to learn more about basic endocrine physiology and pathophysiology.

5.6 Conclusion

We have discovered the presence of a novel endogenous fluorophore with peak emission in the NIR region. This study shows the distribution of this fluorophore in the parathyroid, thyroid, pancreas, and adrenal pheochromocytoma. Characterization of this NIR fluorophore reveal location in an organellar-sized structure within the cytoplasmic region of the cell. Results suggest this fluorophore may be a 15-kDa protein that is resistant to heat and degradation over time. Future studies will be aimed at determining the precise biochemical identity of this fluorophore, which we hypothesize to be present within the secretory granules of endocrine tissues. Presently, the distribution of this NIR fluorophore across multiple endocrine tissues will open the door to many future applications utilizing this endogenous source of contrast for biomedical imaging.

5.7 Acknowledgements

We would like to thank the hospital staff at the Vanderbilt Endocrine Surgery center for their assistance in data collection. This material is based upon work supported by the National Science Foundation Graduate Research Fellowship Program under Grant No. 0909667 and the National Institute of Health under Grant No. NIHR41 EB015291.

5.8 References

1. Lakowicz JR. Principles of Fluorescence Spectroscopy: Springer Science & Business Media; 2013.
2. Choi HS, Gibbs SL, Lee JH, Kim SH, Ashitate Y, Liu F, et al. Targeted zwitterionic near-infrared fluorophores for improved optical imaging. *Nature biotechnology*. 2013 Feb;31(2):148-53. PubMed PMID: 23292608. Pubmed Central PMCID: 3568187.
3. Welsher K, Liu Z, Sherlock SP, Robinson JT, Chen Z, Daranciang D, et al. A route to brightly fluorescent carbon nanotubes for near-infrared imaging in mice. *Nature nanotechnology*. 2009 Nov;4(11):773-80. PubMed PMID: 19893526. Pubmed Central PMCID: 2834239.
4. Escobedo JO, Rusin O, Lim S, Strongin RM. NIR dyes for bioimaging applications. *Current opinion in chemical biology*. 2010 Feb;14(1):64-70. PubMed PMID: 19926332. Pubmed Central PMCID: 2819555.

5. McWade MA, Sanders ME, Broome JT, Solorzano CC, Mahadevan-Jansen A. Establishing the clinical utility of autofluorescence spectroscopy for parathyroid detection. *Surgery*. 2015 Oct 7. PubMed PMID: 26454675.
6. McWade MA, Paras C, White LM, Phay JE, Solorzano CC, Broome JT, et al. Label-free Intraoperative Parathyroid Localization With Near-Infrared Autofluorescence Imaging. *The Journal of clinical endocrinology and metabolism*. 2014 Dec;99(12):4574-80. PubMed PMID: 25148235.
7. McWade MA, Paras C, White LM, Phay JE, Mahadevan-Jansen A, Broome JT. A novel optical approach to intraoperative detection of parathyroid glands. *Surgery*. 2013 Dec;154(6):1371-7. PubMed PMID: WOS:000327571200059. English.
8. Bajpai S, Hamilton J. The isolation and partial characterization of bovine parathyroid secretory granules. *Bone and mineral*. 1990 Apr;9(1):9-22. PubMed PMID: 2337691.
9. Weissleder R. A clearer vision for in vivo imaging. *Nature biotechnology*. 2001 Apr;19(4):316-7. PubMed PMID: 11283581.
10. Choi HS, Liu W, Liu F, Nasr K, Misra P, Bawendi MG, et al. Design considerations for tumour-targeted nanoparticles. *Nature nanotechnology*. 2010 Jan;5(1):42-7. PubMed PMID: 19893516. Pubmed Central PMCID: 2797834.
11. Richards-Kortum R, Sevick-Muraca E. Quantitative optical spectroscopy for tissue diagnosis. *Annual review of physical chemistry*. 1996;47:555-606. PubMed PMID: 8930102.
12. Schneckenburger H, Wustrow TP. Intracellular fluorescence of photosensitizing porphyrins at different concentrations of mitochondria. *Photochemistry and photobiology*. 1988 Mar;47(3):471-3. PubMed PMID: 2967982.
13. Hooper NM. *Protein Purification Applications*. Oxford University Press; 2001. p. 119-22.
14. Bartlett SF, Smith AD. Adrenal chromaffin granules: isolation and disassembly. *Methods in enzymology*. 1974;31:379-89. PubMed PMID: 4422250.
15. Rosa P, Gerdes HH. The granin protein family: markers for neuroendocrine cells and tools for the diagnosis of neuroendocrine tumors. *Journal of endocrinological investigation*. 1994 Mar;17(3):207-25. PubMed PMID: 8051343.
16. Ritter CS, Haughey BH, Miller B, Brown AJ. Differential gene expression by oxyphil and chief cells of human parathyroid glands. *The Journal of clinical endocrinology and metabolism*. 2012 Aug;97(8):E1499-505. PubMed PMID: 22585091. Pubmed Central PMCID: 3591682.
17. Corish P, Tyler-Smith C. Attenuation of green fluorescent protein half-life in mammalian cells. *Protein engineering*. 1999 Dec;12(12):1035-40. PubMed PMID: 10611396.

18. Chi EY, Krishnan S, Randolph TW, Carpenter JF. Physical stability of proteins in aqueous solution: mechanism and driving forces in nonnative protein aggregation. *Pharmaceutical research*. 2003 Sep;20(9):1325-36. PubMed PMID: 14567625.
19. Marshak DR, Kadonaga, James T., Burgess, Richard R., Knuth, Mark W., Brennan Jr., William A., Lin Sue-Hwa. *Strategies for Protein Purification and Characterization: A Laboratory Course Manual*. Press CSHL, editor1996.
20. *Small Molecule Medicinal Chemistry: Strategies and Technologies*. Werngard Czechtizky PH, editor: Wiley; 2015.
21. Ebeling W, Hennrich N, Klockow M, Metz H, Orth HD, Lang H. Proteinase K from *Tritirachium album* Limber. *European journal of biochemistry / FEBS*. 1974 Aug 15;47(1):91-7. PubMed PMID: 4373242.
22. Andreou LV. Preparation of genomic DNA from bacteria. *Methods in enzymology*. 2013;529:143-51. PubMed PMID: 24011042.
23. Permyakov EA, Burstein EA. Some aspects of studies of thermal transitions in proteins by means of their intrinsic fluorescence. *Biophysical chemistry*. 1984 May;19(3):265-71. PubMed PMID: 6722276.
24. Waldo GS, Standish BM, Berendzen J, Terwilliger TC. Rapid protein-folding assay using green fluorescent protein. *Nature biotechnology*. 1999 Jul;17(7):691-5. PubMed PMID: 10404163.
25. Kim TD, Ryu HJ, Cho HI, Yang CH, Kim J. Thermal behavior of proteins: heat-resistant proteins and their heat-induced secondary structural changes. *Biochemistry*. 2000 Dec 5;39(48):14839-46. PubMed PMID: 11101300.
26. Nguyen JQ, Gowani Z, O'Connor M, Pence I, Nguyen TQ, Holt G, et al. Near-infrared autofluorescence spectroscopy of in vivo soft tissue sarcomas. *Optics letters*. 2015 Dec 1;40(23):5498-501. PubMed PMID: 26625035.
27. Shao X, Zheng W, Huang Z. In vivo diagnosis of colonic precancer and cancer using near-infrared autofluorescence spectroscopy and biochemical modeling. *J Biomed Opt*. 2011 Jun;16(6):067005. PubMed PMID: 21721826.
28. Rosa P, Hille A, Lee RW, Zanini A, De Camilli P, Huttner WB. Secretogranins I and II: two tyrosine-sulfated secretory proteins common to a variety of cells secreting peptides by the regulated pathway. *The Journal of cell biology*. 1985 Nov;101(5 Pt 1):1999-2011. PubMed PMID: 4055903. Pubmed Central PMCID: 2113975.
29. *Surgical Endocrinology*. Bloom JLaSR, editor: Butterworth-Heinemann; 2013.
30. Isono H, Shoumura S, Emura S. Ultrastructure of the parathyroid gland. *Histology and histopathology*. 1990 Jan;5(1):95-112. PubMed PMID: 2134362.

31. Krstic RV. Human Microscopic Anatomy: An Atlas for Students of Medicine and Biology: Springer; 1994.
32. Portela-Gomes GM, Grimelius L, Stridsberg M. Secretogranin III in human neuroendocrine tumours: a comparative immunohistochemical study with chromogranins A and B and secretogranin II. Regulatory peptides. 2010 Nov 30;165(1):30-5. PubMed PMID: 20550951.
33. Weiler R, Fischer-Colbrie R, Schmid KW, Feichtinger H, Bussolati G, Grimelius L, et al. Immunological studies on the occurrence and properties of chromogranin A and B and secretogranin II in endocrine tumors. The American journal of surgical pathology. 1988 Nov;12(11):877-84. PubMed PMID: 2847571.
34. Helle KB. Chromogranins A and B and secretogranin II as prohormones for regulatory peptides from the diffuse neuroendocrine system. Results and problems in cell differentiation. 2010;50:21-44. PubMed PMID: 20217490.
35. Paras C, Keller M, White L, Phay J, Mahadevan-Jansen A. Near-infrared autofluorescence for the detection of parathyroid glands. J Biomed Opt. 2011 Jun;16(6). PubMed PMID: WOS:000293086800038. English.
36. Tanaka, R., Umemura, S., Kakuta, T., Fujisaki, T., Sakai, H., Saitoh, A., & Osamura, R. Y. (2003). Co-expression of Parathyroid Hormone and Chromogranin A in Secondary Hyperparathyroidism: A Functional Marker for Secretory Activity of Hyperplastic Nodules. Pathology-Research and Practice, 199(2), 93-99.

CHAPTER 6

IMAGING SYSTEM DESIGN FOR SURGICAL GUIDANCE WITH NEAR-INFRARED AUTOFLUORESCENCE

Melanie McWade, Isaac Pence, Constantine Paras, and Anita Mahadevan-Jansen

Department of Biomedical Engineering, Vanderbilt University, Nashville, TN

This chapter was published in:

“Imaging system design for surgical guidance with near-infrared autofluorescence.”

SPIE Proceedings. 2015.

6.1 Abstract

We present a study to evaluate and compare three near-infrared (NIR) fluorescence imaging systems designed to provide intraoperative guidance around anatomical structures. The three systems adapted specifically for the application of endogenous NIR fluorescence detection were (i) a photomultiplier tube based NIR viewer, (ii) a thermoelectrically cooled electron-multiplying charge-coupled device (CCD) camera, and (iii) a clinical endoscope CCD camera system. Each system was evaluated on the basis of ease-of-use, cost, and system performance. The cooled CCD camera showed the highest contrast ratio, but is limited in utility by its bulk interface and high cost. The clinical endoscope camera showed flexibility in its field-of-view and provides the benefit of being sterilized to allow easy integration into the surgical suite; however, it exhibits signal nonlinearity that would distort quantitative analysis. The NIR viewer shows optimal performance, exhibiting high spatial resolution, linearity, and sufficient contrast to differentiate between tissue types. This low-cost design proves to be the optimal system for parathyroid detection, offering ease-of-use in a surgical setting while meeting system performance requirements.

6.2 Introduction

Intraoperative guidance methods offering real-time feedback have the potential to improve accuracy of tissue resection during surgery. Optical methods have gained widespread use in surgical guidance applications over the last decade, primarily for the resection of diseased tissue (1-3). One study reports brain tumor margins identified intraoperatively using reflectance and fluorescence spectroscopy, preventing local tumor recurrence by guiding the complete resection of cancerous cells (4). In another study, Raman spectroscopy distinguishes breast tumors from normal tissue with high sensitivity during partial breast mastectomy (5). Optical imaging can improve the accuracy of clinical decisions by aiding visual inspection, which can be highly subjective and dependent on the experience of the surgeon. When compared to conventional imaging methods, optical imaging produces higher resolution images in real-time to inform surgical decisions while the patient is still in the operating room (6). Optical techniques have less extensive and relatively inexpensive instrumentation that can be easily adapted into the surgical suite. It offers high sensitivity detection with low toxicity to the patient (7). Furthermore, wavelength can be varied according to application in order to target a wide variety of intrinsic or exogenous tissue biomarkers (8).

NIR optical imaging is particularly attractive because it takes advantage of an “optical window” between 700 – 900 nm. This wavelength range offers a tissue penetration depth of several millimeters and decreased scattering and absorption of biomolecules relative to ultraviolet and visible wavelengths (9), making the NIR region optimal for studies on the diagnosis and detection of disease. In fluorescence imaging, optical signals can originate from extrinsic contrast agents or endogenous tissue fluorophores. Because endogenous NIR fluorophores are rare, research in NIR fluorescence has mostly involved exogenous contrast agents, the most common of which are polymethines. In particular, indocyanines, such as indocyanine green (ICG) and cardio-green have been used extensively as contrast agents for many applications (10,11). Several intraoperative NIR fluorescence imaging systems are in pre-clinical and clinical use for detecting margins of cancerous tissue using exogenous dyes (12-14).

Current fluorescence detection systems are limited in two ways. First, many of the current systems used for exogenous dye imaging have inadequate sensitivity to detect weaker fluorescence emitted from endogenous fluorophores. Second, the functionality of these imaging systems is dependent on tissue disease state. There is a need for a method to visualize anatomical

structures beyond tumor margins. Particularly in endocrine procedures, surgeons would greatly benefit from an imaging system that provides anatomical guidance for identification of the parathyroid gland. Other modalities such as ultrasound (15) and MRI (16) have been used for intraoperative anatomical guidance, but the requirement of a trained operator, low sensitivity, and extensive instrumentation hinder widespread use. Because of the small size (3-5 millimeters) and variable location of parathyroid glands in the neck, endocrine surgeries can often result in insufficient removal or damage to the parathyroid. These patients may fail to achieve normocalcemia, which can necessitate re-operation and lower patient quality of life (17,18). A previous study demonstrates the use of NIR fluorescence spectroscopy for anatomical guidance during endocrine procedures by detecting auto-fluorescence in the parathyroid gland. The study shows that the parathyroid consistently emits a NIR auto-fluorescent signal 1.2 – 29 times greater than the thyroid regardless of the disease state (19). Fluorescence spectroscopy offers a fast, highly sensitive *in vivo* method for distinguishing the parathyroid gland from surrounding neck tissues by detecting an unknown endogenous NIR fluorophore. Detection of endogenous fluorescence avoids the potential problems associated with exogenous contrast agents such as toxicity, photobleaching, and localization. However, spectroscopy is inherently limited by its inability to give spatial information without time prohibitive measurements over the entire region of interest. Surgeons must still rely on visual guidance to lead them to the correct points for measurement.

Driven by the need for a surgical guidance tool that provides anatomical guidance without the use of exogenous dyes, we have translated the NIR fluorescence spectroscopy technology into an imaging system that can be implemented in an operating room. The goal of this study is to determine the optimal NIR fluorescence imaging system design for this application. Three imaging systems were built for the detection of endogenous NIR fluorophores: the NIR viewer, cooled CCD camera, and clinical endoscope camera. Designs were evaluated based on imaging system performance metrics used in literature (20-22) and clinical specifications given by endocrine surgeons at Vanderbilt University. The optimal system design for intraoperative surgical guidance was determined by assessing systems based on three criteria: ease-of-use, cost, and system performance. System performance was determined by the compliance of each system to the following specifications: a minimum field-of-view (FOV) of 9 cm to allow visualization of the entire surgical incision, linearity of measured intensities, spatial resolution of at least 500 μm to

resolve a single parathyroid, sufficient contrast to distinguish fluorescence from background, and retention of the intensity ratio of parathyroid to thyroid fluorescence captured by spectroscopy. The ease-of-use criteria accounts for sterilizability of the system and ease of integration into the surgical suite. The cost of the imaging system must not outweigh the benefits of the device that arise from lower rates of re-operation and reduced legal fees from potential failed operations. The system determined to provide best performance was used for intraoperative parathyroid autofluorescence detection during cervical endocrine surgery.

6.3 Materials and Methods

6.3.1 System Description

Three systems were built as tools for real-time anatomical guidance during operation (Figure 6.1). The key design criteria for the systems were ease of use, cost, and system performance. The first system is the NIR Viewer, which was built using a commercial infrared viewer (Find-R-Scope, FJW Optical) with a high resolution photomultiplier tube to amplify the signal. Images were captured using a 7 x 7 mm CCD camera with 480 x 640 pixels and 10-bit resolution (Sony). Images were processed by custom-made LabView software and displayed on a laptop computer screen for the surgeon to view during the procedure. The NIR viewer is a hand-held system and can be mounted by the arm onto the operating room lights above the surgical field for clinical measurements. This system cannot be sterilized and therefore is designed to remain outside the 90 cm sterile halo. The second system is a cooled CCD camera system, which was designed using a 512 x 512 pixel cooled CCD camera (PhotonMax 512, Princeton Instruments). The CCD camera is capable of single photon sensitivity and thermoelectric cooling to suppress dark current. During imaging, the system was mounted on a surgical microscope (Wild Heerbrugg M690, Leica), which can be positioned over the surgical field. The cooled CCD camera cannot be sterilized, but it can be adapted to the operating room either by overlaying a sterile drape or remaining outside the sterile halo. The third fluorescence imaging system is the clinical endoscope camera, which was adapted from an endoscope camera (PDD camera, Karl Storz) commonly used in surgery for gastrointestinal, general surgery, urology, and gynecology applications. It is composed of a 3-chip color camera with an integrated parfocal zoom lens with a focal range of 25 – 50 mm. The camera was driven by a camera

control unit (Tricam SL, Karl Storz). This hand-held system was designed to withstand the sterilization process, offering the flexibility of either being held in hand during intraoperative imaging or mounted on the overhead surgical lights.

A diode laser ($\lambda=785$ nm) coupled through a fiber optic probe (EMVision) onto the field of interest provided the fluorescence excitation for all systems. A notch filter was positioned in front of the detector in each system to block the fluorescence excitation. For parathyroid detection, this filter has a center wavelength of 785 nm (Supernotch-Plus, Kaiser Optical Systems). For the cooled CCD camera and NIR viewer, filtered light was focused through a C-mount macro zoom lens (Zoom 7000, Navitar), which allows 6X magnification power over a focal range of 18 – 108 mm. Fluorescence images were captured with each system and displayed on a monitor.

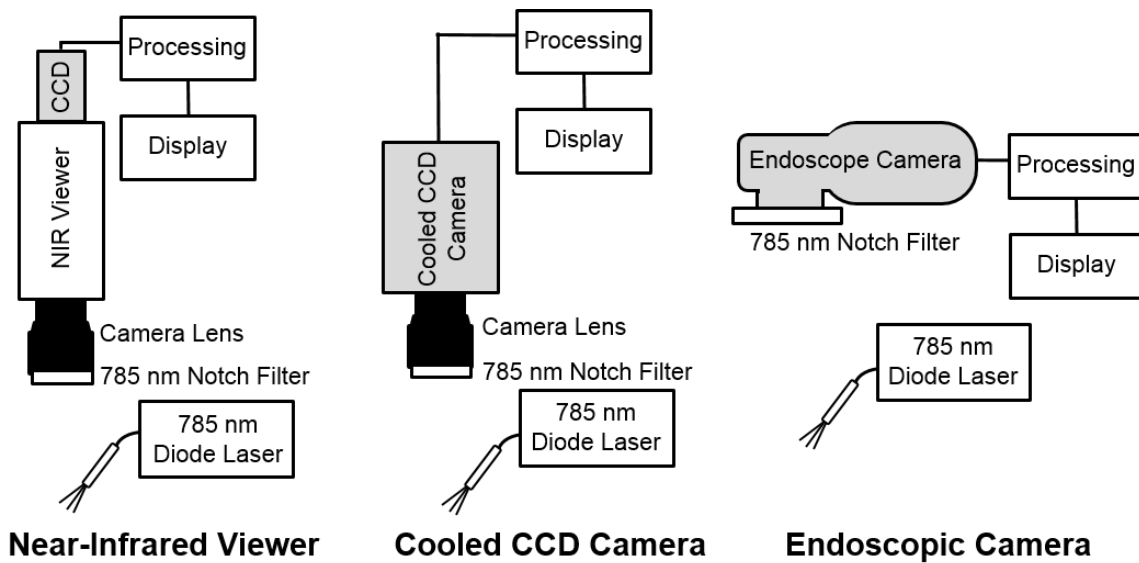


Figure 6.2: System Overview of the cooled CCD camera, NIR viewer and clinical endoscope camera

6.3.2 System Performance Tests

A series of tests were carried out to characterize the imaging system performance based on metrics important in clinical imaging. The following metrics were assessed for all systems: field-of-view (FOV), linearity, contrast ratio, spatial resolution, and feature retention as compared to the probe-based spectroscopy system.

The FOV of the imaging systems were measured as a function of distance between the detector and surgical field to determine which systems could image the entire field of interest at clinically relevant working distances. A clinically relevant working distance is 90 cm for non-sterilizable instruments to remain outside of the sterile surgical halo. Systems must capture at least a 9 cm FOV during endocrine procedures in order to visualize the entire surgical incision in the neck. A 2D phantom consisting of a 1 mm Cartesian grid was imaged from a maximum distance of 110 cm. The distance was decreased in 5 mm increments until focusing was no longer possible. With the filter removed, the phantom was imaged under ambient illumination. The maximum FOV at which the NIR viewer could resolve the phantom was measured and recorded. The focal length of the lens was set to its maximum focal length ($f = 108$ mm) for measurements with the NIR viewer and cooled CCD camera. The focal length of the clinical endoscope camera was set to its maximum ($f = 50$ mm).

Linearity of an imaging system is important because it ensures that the output signal is linearly proportional to the input intensity. Linearity is determined by the ability of the detector to convert incident photons into an electrical signal. Particularly for quantitative photometric analysis in fluorescence imaging, a detector must respond linearly to the fluorescent intensity of the sample. To determine the linearity of each system, the fluorescent intensity was measured as a function of laser power irradiating a fluorescent dye (DLS790D, Crystalyn) diluted in methanol in a quartz cuvette. The dye fluorescence is similar to that of parathyroid tissue, having equal excitation and emission wavelengths. Light from a 785 nm diode laser excited the sample with powers ranging from 0 to 130 mW in a 35 mm excitation spot. Three images at each irradiation level were acquired at a 90 cm working distance, averaged and background subtracted. The mean intensity over the area of the cuvette was calculated, and least squares regression lines were fit to the data at each irradiation level. Baseline intensity was subtracted to account for the offset due to noise in dark conditions.

Contrast ratio is a quality metric that is defined as the ratio of the intensity of the brightest area to the darkest area of an image. The ability to distinguish the signal from the background improves as contrast ratio increases. Contrast ratio was measured from the images collected by the three systems in the experiment described above. It was calculated across the collected images, as the ratio of the difference in brightest and darkest intensity to darkest intensity.

Spatial resolution determines the clarity of an image. It is defined as the minimum distance between two points in an image that can be detected by the system. An imaging system suitable for parathyroid detection during endocrine surgery must have spatial resolution of approximately 500 μm . To measure spatial resolution, a 99% diffuse reflectance standard (Spectralon, Labsphere) was placed behind a positive glass resolution target card (USAF 1951, Edmund Optics) with vertical and horizontal elements made up of lines ranging from 1.0 – 645.0 line pairs/mm. An image of the resolution card was acquired with each system from a 90 cm working distance under ambient illumination. To quantitatively assess vertical and horizontal spatial resolution, the mean intensity profiles were extracted across the horizontal and vertical bars of the ruling elements, which correspond to varying line pairs/mm. The peak to valley ratio (PVR) was calculated from the local peaks and valleys of the intensity profiles for each ruling element. Spatial resolution was determined to be the separation distance between lines that yielded a PVR equal to the square root of 2 (22).

6.3.3 Signal Validation Tests

Signal validation tests were performed to demonstrate the capability of each imaging system to capture differences in fluorescence intensity between two tissue types. First, system validation was demonstrated by imaging two dye phantoms. The phantoms were made with the same fluorescent dye used in previous studies, diluted to concentrations that optically mimic parathyroid and thyroid tissue. The dyes were measured with the three imaging systems and the fluorescence spectroscopy system. Fluorescence intensities were quantified to determine if a difference in fluorescence could be distinguished between the parathyroid and thyroid phantoms.

The second functional test demonstrates the endogenous fluorescence contrast between canine parathyroid and thyroid tissue *ex vivo*. As mentioned previously, clinical measurements with probe-based fluorescence spectroscopy show that parathyroid tissue exhibits an auto-

fluorescence signal 2 – 21 times greater than the thyroid (19). This functional test demonstrates the utility of a two-dimensional imaging system for intraoperative guidance to identify the parathyroid during endocrine surgeries. Discarded canine parathyroid and thyroid tissue were acquired from the Vanderbilt University animal research facilities in the Division of Surgical Research. Canine tissue was chosen because parathyroid and thyroid tissues from the same subject could not be acquired from humans. Canine and human parathyroid and thyroid tissue exhibit similar levels of NIR auto-fluorescence, and both species have similar endocrine anatomy. The samples were snap-frozen and stored at -80°C until imaging. Prior to image collection, samples were thawed in phosphate buffered saline at room temperature. Tissue was illuminated with 80 mW, and images were collected from a 90 cm working distance to account for the operating room requirement that non-sterile instruments remain outside of the sterile surgical halo. Baseline images with no sample excitation were collected for background subtraction after measurement. Two-dimensional false-color images were created by converting pixel intensities into a color scale. Each image was normalized to the maximum pixel intensity to maximize color contrast and allow comparison across systems.

Clinical measurement was performed as an *in vivo* validation of the system performance. One patient was recruited from the Vanderbilt Medical Center under IRB approval (#070795) after being determined eligible by the operating endocrine surgeon. Clinical images were obtained after parathyroid gland was exposed on surface of the surgical bed.

6.4 Results

6.4.1 System Performance Tests

The FOV of the NIR viewer and cooled CCD camera is linearly related to the distance between the face of the lens and the sample. Over object distances from 20 – 110 cm, FOV varied from 4 – 35 mm and 6 – 35 mm for the NIR viewer and cooled CCD, respectively. Below 20 cm, focused images could not be obtained for these systems. At a clinically relevant working distance of 90 cm, a maximal FOV of 29 cm, 29.5, and 21 cm is obtained from the NIR viewer, cooled CCD camera, and endoscope camera, respectively. All imaging systems are able to achieve the minimum 9 cm FOV required to image the surgical incision during endocrine procedures.

The intensity measured from the NIR viewer and cooled CCD camera is linear with excitation power. A linear least squares fit through the measured data. The goodness of fit is R-squared value of 0.998 and 0.999 for the NIR viewer and cooled CCD camera, respectively. The clinical endoscope camera did not show a linear relationship between excitation power and measured fluorescence intensity. The spatial resolution for all three imaging systems was found to be sufficient for imaging the 3 – 5 mm diameter of a typical healthy parathyroid gland from a 90 cm working distance. Sample images of the resolution target card and intensity profiles are shown in Figure 6.2A-F. Overall, the NIR viewer showed the highest spatial resolution compared to the other two systems. A separation distance of 198 μm and 177 μm in the vertical and horizontal directions, respectively, yielded a PVR just above the square root of 2. The results show that the PVR increases as the space between rulings increases (Figure 6.2G).

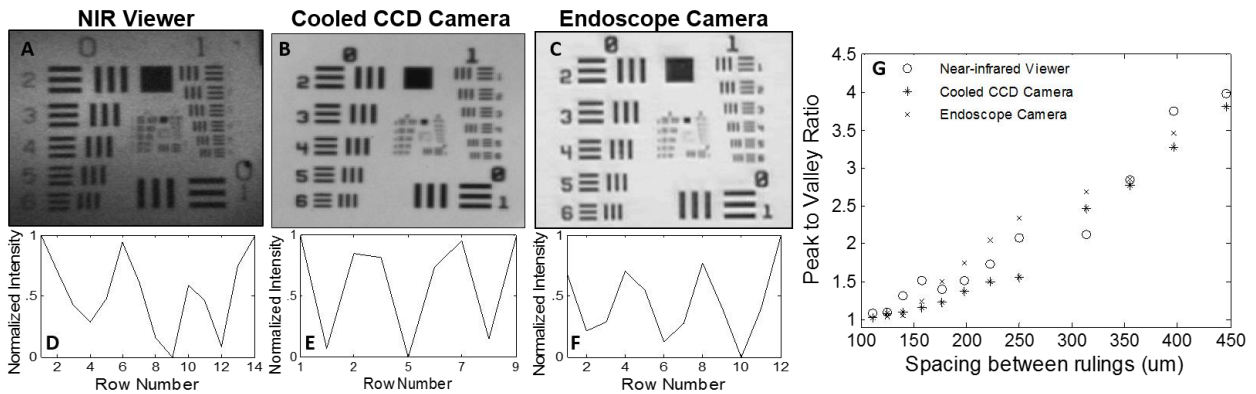


Figure 6.2: A-C) Images of USAF 1951 spatial resolution target from 90 cm distance for near-infrared viewer, cooled CCD camera, and endoscope camera, respectively. D-F) Sample intensity profile across a set of vertical rulings for each imaging system at 177 μm resolution. G) Peak to valley ratio as a function of spacing between rulings.

The contrast ratio of the images of the dye phantoms varies linearly with excitation power for all three systems (Fig. 6.3, displayed in log-scale to capture differences in scale). At higher powers, the images displayed a higher contrast ratio. The cooled CCD camera demonstrated a large dynamic range compared to the NIR viewer and the endoscope camera. At 80 mW excitation power, the cooled CCD camera demonstrated a contrast ratio approximately 450 times greater than the other two systems. A much higher contrast ratio is expected from a cooled CCD camera, because cooling reduces the dark current and therefore lowers background signal. The phantom and tissue validation tests determine whether contrast ratios as high as that seen with the cooled CCD camera is necessary to differentiate between tissue types.

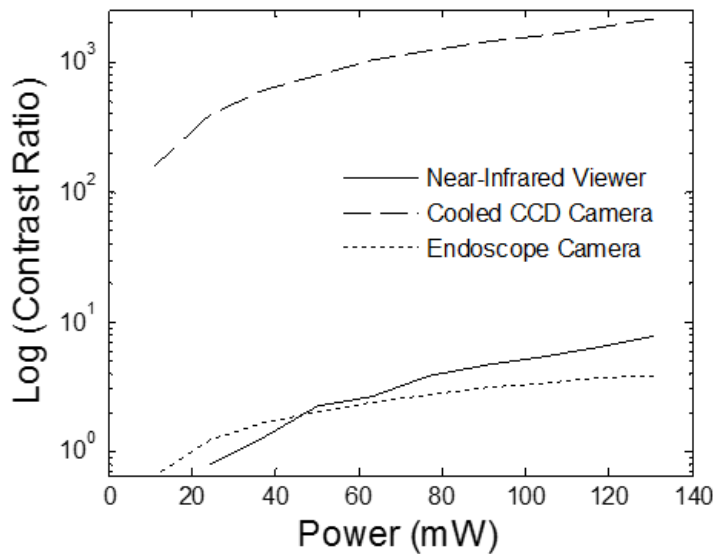


Figure 6.3: Contrast ratio of the NIR viewer, cooled CCD camera and endoscope camera with varying excitation power.

6.4.2 Signal Validation Tests

Fluorescence images of two dye phantoms designed to mimic the fluorescence of the parathyroid and thyroid demonstrate the feasibility of visualizing contrast between the two tissue types (Fig. 6.4A-F). The mean fluorescence intensity was analyzed across each pixel in the area of the cuvettes. The ratio of intensity between the parathyroid and thyroid phantoms (P/T ratio) was compared to the fluorescence spectra (Fig. 6.4G). The parathyroid phantom was successfully distinguished from the thyroid phantom for all three imaging systems with a P/T ratio of 3.15, 3.64, and 2.76 for the NIR viewer, cooled CCD, and clinical endoscope camera, respectively. These values vary 0.5 – 23% from the P/T ratio of the spectroscopy system, which was 3.62. This comparison is important because of the previous success of NIR fluorescence spectroscopy in distinguishing the parathyroid in patients *in vivo* (19). The results indicate the feasibility of using all three fluorescence imaging systems for parathyroid identification as well as applications using exogenous dyes.

The fluorescence images of parathyroid and thyroid canine tissue samples show increased emission levels in the parathyroid relative to the thyroid (Fig. 6.5A-C). The P/T ratios are 2.07, 1.99, and 2.26 for the NIR viewer, cooled CCD camera, and endoscope camera, respectively. These values are consistent across imaging systems and comparable to a P/T ratio of 2.1, which was obtained using fluorescence spectroscopy (Fig. 6.5D).

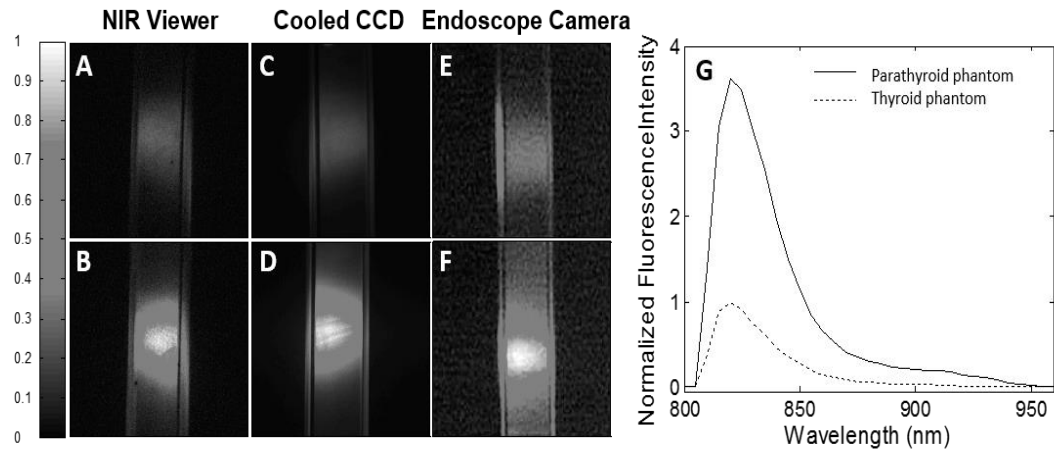


Figure 6.4: Fluorescence images of parathyroid (bottom row) and thyroid equivalent dye phantoms (top row) using the A-B) NIR Viewer, C-D) cooled CCD, and E-F) endoscope camera. G) Spectra of phantoms collected with spectroscopy system.

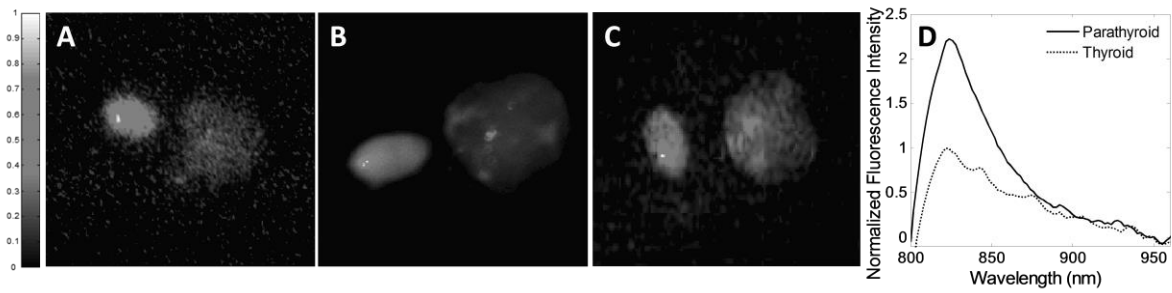


Figure 6.5: Fluorescence images of the parathyroid (left) and thyroid (right) using the A) NIR viewer, B) cooled CCD camera, and C) endoscope camera. D) Fluorescence spectra from the same tissue using fluorescence spectroscopy.

An overview of the performance of each system is described in Table 6.1. Based on all clinical specifications described for fluorescence imaging of endogenous fluorophores, the clinical endoscope camera outperforms the cooled CCD camera and NIR viewer. The bulk of the cooled CCD camera makes it difficult to use in the operating room, while the clinical endoscope camera suffers from nonlinearity. The NIR viewer meets all clinical requirements and has been identified as the optimal imaging system design of the three configurations tested.

The clinical endoscope camera was used during a parathyroidectomy procedure to collect near-infrared autofluorescence measurements on the parathyroid gland on a patient presenting with non-toxic multinodular goiter. The fluorescence (shown in green) and white light images collected were overlaid and demonstrated the sensitivity of this system to detect low levels of intrinsic biological fluorescence for anatomical guidance to the parathyroid gland (Figure 6.6).

Table 6.1: Overview of clinical requirements and imaging performance for NIR viewer, cooled CCD camera, and clinical endoscope camera.

	Linearity	Field-of-View	Contrast Ratio	Spatial Resolution	Feature Retention (P/T ratio)	Cost	Ease-of-use
Clinical Requirement	Yes	≥ 9 cm at 90 cm	High enough to detect PT	≤ 500 μm	Similar to spectroscopy system	Low	Sterilizable, easy to manipulate
NIR Viewer	Yes	29 cm	4	177 μm	2.07	low	Not sterilizable, hand-held
Cooled CCD camera	Yes	30 cm	77	223 μm	1.99	high	Not sterilizable, bulky
Clinical endoscope camera	No	21 cm	3	177 μm	2.26	low	Sterilizable, hand-held

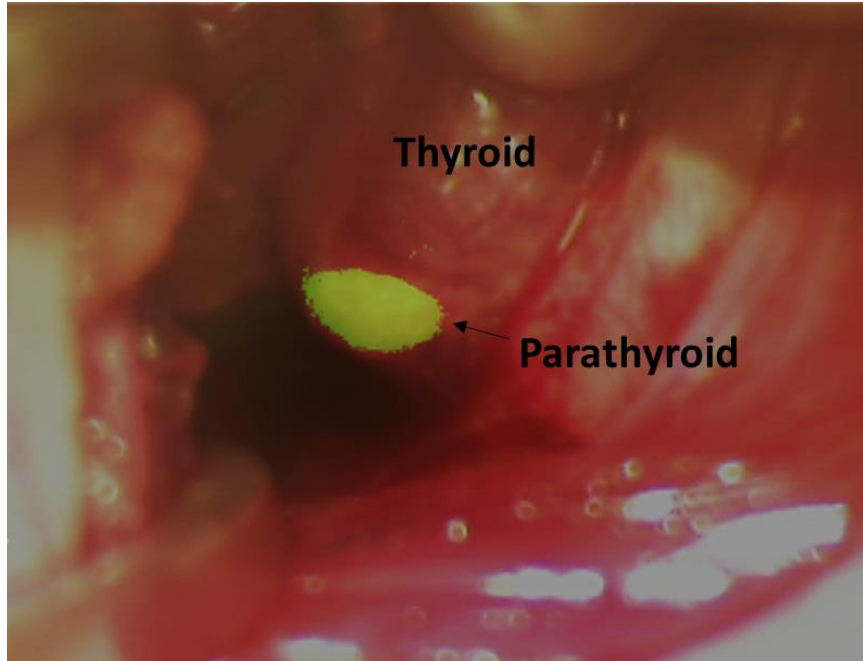


Figure 6.6: Intraoperative near infrared imaging of parathyroid autofluorescence during thyroidectomy. Green overlay shows area of near-infrared fluorescence corresponding to parathyroid gland.

6.5 Discussion

Three NIR fluorescence imaging systems designed for anatomical guidance using endogenous fluorophores were compared for the suitability of clinical use. The optimal system design for intraoperative surgical guidance was determined by assessing systems based on ease-of-use, cost, and system performance. System performance was determined by the compliance of each system to the following specifications: a minimum FOV of 9 cm to allow visualization of the entire surgical incision, linearity of measured intensities, spatial resolution of at least 500 μm to resolve a single parathyroid, enough contrast to distinguish fluorescence from background, and retention of the intensity ratio of parathyroid to thyroid fluorescence captured by spectroscopy.

It was found that at a clinically relevant working distance of 90 cm, all imaging systems had a FOV greater than 20 cm. This FOV allows visualization of the entire surgical incision, which is approximately 7 x 9 cm for endocrine procedures. Each system provides the focus to allow visualization of fine precision movements without compromising the working distance necessary for a surgeon to move freely around the surgical field. The wide focal range of the lens in the cooled CCD and NIR viewer systems offers the capability to alter the FOV and match the unique specifications of each procedure. The clinical endoscope camera is not capable of as wide a range of focus. However, it can be sterilized and moved closer to the surgical field during imaging. This feature of the clinical endoscope system allows the greatest flexibility and ease-of-use out of all imaging systems tested.

The linearity tests show that the NIR viewer and cooled CCD camera measure intensities that are linear with emission intensity over the range of 0 – 130 mW. This is in contrast to the clinical endoscope camera that does not show a constant gain in response to increasing incident intensity. Linearity of system measurements in response to incident light is necessary for accurate photometric analysis. Such is the case in parathyroid detection where the ratio between parathyroid and thyroid fluorescence is calculated to provide guidance during surgical resection.

The spatial resolution of the NIR viewer is the highest of the three systems. However, all systems were able to detect features within 177 – 250 μm in size, far exceeding the minimum 500 μm criteria for parathyroid detection. Electrical noise is the largest limiting factor dictating the smallest detectable feature of an imaging system. No noticeable difference is seen in the resolution of the cooled CCD camera compared to the other two systems, despite its thermoelectric cooling that is designed to eliminate background noise. Resolution differences across systems are on the

micron level, which is indiscernible when projected on a display monitor in the operating room. With the spatial resolution demonstrated in this test, all imaging systems can also be applied to imaging smaller more detailed tissue structures in other applications.

Characterization of the contrast ratio allowed quantification of the ease at which tissue structures can be observed during surgery. For imaging during parathyroidectomy and thyroidectomy procedures, it is important that an imaging system has enough contrast to distinguish varying levels of fluorescence in the parathyroid and thyroid to aid resection. The cooled CCD camera has a lower background signal which provided a higher contrast ratio than the NIR viewer or clinical endoscope. However, the relatively lower levels of contrast exhibited by the clinical endoscope have been previously shown to be adequate for fluorescence visualization in the operating room (23). At 80 mW excitation power, a contrast ratio of 3.85 for the NIR viewer proves to be adequate for parathyroid and thyroid visualization in the functional imaging tests described in this paper. Though the cooled CCD camera captures images with lower background signal and higher contrast ratios, results show that more involved imaging systems are not necessary to aid surgical resection for applications like parathyroid detection.

The fluorescence images acquired from the parathyroid and thyroid dye phantoms demonstrate the feasibility of using these three imaging systems to distinguish between varying fluorescence intensities at levels comparable to real tissue (Fig. 6.4A-F). The P/T ratio for the dye phantoms measured with the NIR viewer fell within 13% of the P/T ratios measured using the cooled CCD, clinical endoscope camera and point-based spectroscopy system (Fig. 6.4G). Similarity in P/T ratios for imaging and spectroscopy systems indicates that feature retention may be maintained across detection modalities despite differences in illumination-collection geometry and source-detector separation distance. Lower excitation powers are associated with higher safety margins, which is promising for the eventual clinical application of these imaging systems.

In addition to its implications for auto-fluorescence measurements *in vivo*, the phantom dye tests point to the utility of the NIR viewer in exogenous NIR dye applications. In some surgical procedures, exogenous NIR dyes are administered to give contrast to tissue structures that do not exhibit intrinsic contrast. For cases such as sentinel lymph node mapping with indocyanine green (24), cancer detection with fluorescent beacons (25), or imaging of tumor vasculature with NIR quantum dots (26), the NIR viewer may be able to provide intraoperative fluorescence imaging.

The fluorescence images collected from *in vitro* canine parathyroid tissue establish the capability of the imaging systems to discriminate between tissue types with varying intrinsic fluorescence (Fig. 6.5). Parathyroid tissue exhibited a higher average fluorescence intensity than thyroid tissue in the fluorescence images collected with the NIR viewer. In endocrine cases where the point-based spectroscopy system is used for parathyroid detection, a P/T ratio of 1.2 is considered the threshold for distinguishing parathyroid from thyroid. All three images produced a P/T ratio above threshold, which coincided with the results collected using the spectroscopy system. The fluorescence images collected with the clinical endoscope camera and NIR viewer (Fig. 6.5A-B) show a higher background signal, resulting in a lower contrast ratio than was calculated from the image collected by the cooled CCD camera (Fig. 6.5B). Despite the discrepancy in contrast ratio, the differences in fluorescence intensity between the two tissue types are distinguished with both systems. In the case of parathyroid detection, both systems fulfill their primary purpose, which is to guide the surgeon to the correct location for surgical resection. These images indicate that lower cost detectors can be used for this application, providing the benefit of affordability in a clinical setting.

The largest limitation of the fluorescence imaging system is variability due to the lack of uniform light distribution. Measured fluorescence intensity will change as a function of the tissue curvature. As a result, there is a need to control for depth during measurement. Error may also arise from points of specular reflectance, which may skew the P/T ratios by inaccurately increasing the intensity of the measured signal. However, specular reflectance can be minimized by altering the illumination-collection geometry as well as post-processing the images.

The results presented here show that the performance of all three imaging systems can capture the differential in tissue fluorescence between the parathyroid and thyroid. By also taking ease-of-use and system cost into consideration, the clinical endoscope camera was determined to be the optimal system design for this surgical imaging application (Table 6.1). The cooled CCD camera shows the highest image quality, resulting from the high contrast achieved by the noise-reducing cooling of its back-illuminated detector. However, the bulk and high cost of the system limit its usefulness in the operating room. The weight of the 9 pound cooled CCD camera system necessitates mounting on a free-standing surgical microscope, which creates a large footprint that is potentially intrusive in a clinical setting. Though not practical for an operating room, the cooled CCD camera can be useful as a standard for other imaging systems in the laboratory. The clinical

endoscope system is the most easily integrated into the surgical environment because of its hand-held size and capacity for sterilization. The NIR viewer is high performing as shown by its linearity, flexible FOV, high spatial resolution and ability to differentiate tissue auto-fluorescence. However, because it does not have the capability of sterilization, its use is constrained in a sterile operating room setting. The clinical endoscope camera was determined to be a useful tool for imaging low levels of intrinsic near-infrared autofluorescence. This system demonstrated successful tissue contrast in real-time during thyroidectomy procedure, without compromising surgical sterility and with minimal disruption to the surgical procedure. Unlike the currently established parathyroid imaging techniques, the clinical endoscope camera is capable of providing real-time guidance to the surgeon, giving the potential to minimize surgical error and reduce high rates of re-operation. The results achieved here will inform future investigations aimed towards more in-depth clinical implementation of the fluorescence imaging system

6.6 Acknowledgements

This material is based upon work supported by the National Science Foundation Graduate Research Fellowship Program under Grant No. 0909667 and the National Institute of Health under Grant No. NIHR41 EB015291.

6.7 References

1. M. D. Keller, et al., "Autofluorescence and Diffuse Reflectance Spectroscopy and Spectral Imaging for Breast Surgical Margin Analysis," *Lasers in Surgery and Medicine*, vol. 42, pp. 15–23, 2010.
2. A. N. Yaroslavsky, V. Neel, and R. R. Anderson. "Fluorescence polarization imaging for delineating nonmelanoma skin cancers," *Optics Letters*, vol. 29, no. 17, pp. 2010-2012, 2004.
3. S. P. Lerner, et al., "Optical Coherence Tomography as an Adjunct to White Light Cystoscopy for Intravesical Real-Time Imaging and Staging of Bladder Cancer," *Urology*, vol. 72, no. 1, pp. 133–137, 2008.
4. W. Lin, et al., "In Vivo Brain Tumor Demarcation Using Optical Spectroscopy," *Photochemistry and Photobiology*, vol. 73, pp. 396–402, 2001.
5. A. S. Haka, et al., "In vivo Margin Assessment during Partial Mastectomy Breast Surgery Using Raman Spectroscopy" *Cancer Res.*, vol. 66, pp. 3317-3322, 2006.

6. A. R. Kherlopian, et al. "A review of imaging techniques for systems biology," *BMC Systems Biology*, vol. 2, no. 74, 2008.
7. J. Muller, "Optical Imaging," *Recent Results Cancer Res.*, vol. 187, pp. 221-246, 2013.
8. G. A. Wagnieres, et al., "In Vivo Fluorescence Spectroscopy and Imaging for Oncological Applications," *Photochemistry and Photobiology*, vol. 68, no. 5, pp. 603-632, 1998.
9. G. Costas et al., "Current and Future Clinical Applications for Optical Imaging of Cancer: From Intraoperative Surgical Guidance to Cancer Screening," *Molecular Imaging in Oncology*, vol. 38, pp. 109–118, 2011.
10. T Ishizawa et al., "Real-time identification of liver cancers by using indocyanine green fluorescent imaging," *Cancer*, vol. 115, no. 11, pp. 2491–2504, 2009.
11. C. Hirche et al., "ICG fluorescence-guided sentinel node biopsy for axillary nodal staging in breast cancer," *Breast Cancer Res Treat*, vol. 121, pp. 373–378, 2010.
12. T. Handa et al., "New device for intraoperative graft assessment: HyperEye charge-coupled device camera system," *Gen. Thorac. Cardiovasc. Surg.*, vol. 58, pp. 68–77, 2010
13. S. L. Troyan et al., "The FLARE Intraoperative Near-Infrared Fluorescence Imaging System: A First-in-Human Clinical Trial in Breast Cancer Sentinel Lymph Node Mapping," *Ann. Surg. Oncol.*, vol. 16, pp. 2943–2952, 2009.
14. S. Noura et al., "Feasibility of a Lateral Region Sentinel Node Biopsy of Lower Rectal Cancer Guided by Indocyanine Green Using a Near-Infrared Camera System," *Ann. Surg. Oncol.*, vol. 17, pp 144-151, 2010.
15. G. Rostaminia et al., "Surgical repair of bilateral levator ani muscles with ultrasound guidance," *International Urogynecology Journal*, vol. 24, no. 7, pp 1237-1239. 2013.
16. M. R. Van Den Bosch, et al., "MRI-guided robotic system for transperineal prostate interventions: proof of principle," *Phys. Med. Biol.*, vol. 55, pp. N133–N140, 2010.
17. A Mohebati, A.R. Shaha, "Imaging techniques in parathyroid surgery for primary hyperparathyroidism," *Amer J. of Otolaryngology*. Vol. 33, pp. 457-468, 2012.
18. J. Malmaeus, et al., "Parathyroid Surgery in Scandanavia," *Acta Chir Scand*. vol. 33, pp. 1364-1367, 1988.
19. M. McWade, et al., "A Novel Optical Approach to Intraoperative Detection of Parathyroid Glands," *Surgery*, vol. 154, no. 6, 2013.

20. S.S. Young, R.G. Driggers, and E.L. Jacobs. *Signal Processing and performance Analysis for imaging Systems*. Artech House, 2008.
21. T. M. Bydlon, "Performance metrics of an optical spectral imaging system for intra-operative assessment of breast tumor margins," *Optics Express*., vol. 18, pp. 8058-8076, 2010.
22. S. C. Gebhart, R. C. Thompson, A. Mahadevan-Jansen, "Liquid-crystal tunable filter spectral imaging for brain tumor demarcation," *Applied Optics*, vol. 46, pp. 1896-1910. 2007.
23. J. A. Witjes, et al., "Comparison of Hexaminolevulinate Based Flexible and Rigid Fluorescence Cystoscopy with Rigid White Light Cystoscopy in Bladder Cancer: Results of a Prospective Phase II Study," *European Urology*, vol. 47, pp. 319-322, 2005.
24. N. Tagaya, et al., "Intraoperative identification of sentinel lymph nodes by near-infrared fluorescence imaging in patients with breast cancer," *Amer. J. of Surg.*, vol. 195, pp. 850-853, 2008.
25. U. Mahmood and R. Weissleder, "Near-infrared optical imaging of proteases in cancer," *Molecular Cancer Therapeutics*, vol. 2, pp. 489-496, 2003.
26. W. Cai et al., "Peptide-Labeled Near-Infrared Quantum Dots for Imaging Tumor Vasculature in Living Subjects," *Nano Letters*, vol. 6, pp. 669-676, 2006.

CHAPTER 7

LABEL-FREE INTRAOPERATIVE PARATHYROID LOCALIZATION WITH NEAR- INFRARED AUTOFLUORESCENCE IMAGING

Melanie A. McWade¹, Constantine Paras¹, Lisa M. White², John E. Phay³, Carmen C. Solórzano⁴, James T. Broome⁵, Anita Mahadevan-Jansen¹

¹Biomedical Photonics Laboratory, Department of Biomedical Engineering Vanderbilt University, 5824 Stevenson Center, 37235 Nashville, Tennessee.

²Murfreesboro Surgical Center, 1272 Garrison Drive, 37129 Murfreesboro, Tennessee.

³Division of Surgical Oncology, Ohio State University, 410 W 10th Ave, 43210 Columbus, Ohio.

⁴Division of Surgical Oncology and Endocrine Surgery, Vanderbilt University 2220 Pierce Avenue, 37232, Nashville, Tennessee.

⁵Division of Surgical Endocrinology, Saint Thomas Midtown Hospital, 300 20th Ave N Suite 601, 37203, Nashville, Tennessee.

This chapter was published in:

“Label-free intraoperative parathyroid localization with near-infrared autofluorescence imaging.”

Journal of Clinical Endocrinology and Metabolism. 2014.

7.1 Abstract

Context: The inability to accurately localize the parathyroid glands during parathyroidectomy and thyroidectomy procedures can prevent patients from achieving post-operative normocalcemia. There is a need for an improved method for parathyroid identification.

Objective: The objective of the study was to test the accuracy of a real-time, label-free technique that uses near-infrared (NIR) autofluorescence imaging to localize the parathyroid gland.

Subjects and Methods: Patients undergoing parathyroidectomy and/or thyroidectomy were included in this study. To validate the intrinsic fluorescence signal in parathyroid gland, point measurements from 110 patients undergoing parathyroidectomy and/or thyroidectomy were collected using NIR fluorescence spectroscopy. Fluorescence imaging was performed on six patients. Imaging contrast is based on a previously unreported intrinsic NIR fluorophore that exists in highest concentration in the parathyroid gland. The accuracy of fluorescence imaging was analyzed in comparison with visual assessment and histological findings.

Results: The parathyroid glands in 100% of patients measured with fluorescence imaging were successfully detected in real-time. Fluorescence images consistently showed 2.4 – 8.5 times higher emission intensity from the parathyroid than surrounding tissue. Histological validation confirmed that the high intrinsic fluorescence signal in the parathyroid gland can be used to localize the parathyroid gland regardless of disease state.

Conclusion: NIR fluorescence imaging represents a highly sensitive, real-time tool for parathyroid localization during surgery. This novel solution does not require administration of contrast agents, which reduces procedure time and eliminates potential toxicity risks. The elegance and effectiveness of NIR autofluorescence imaging of the parathyroid gland makes it highly attractive for clinical application in endocrine surgery.

7.2 Introduction

One of the most common complication in surgical intervention of patients with parathyroid and thyroid disease is the inability to localize parathyroid glands (1-3). Intraoperative parathyroid identification is difficult due to their small size, inconspicuous coloring, and variable location (4).

The challenge of parathyroid localization is heightened in patients undergoing reoperation or presenting with ectopic and/or supernumerary abnormal glands (5). Accidental removal of healthy parathyroid glands during thyroidectomy results in postoperative hypocalcemia in 20 – 30% of thyroidectomy cases (6). Conversely, insufficient removal of diseased parathyroid glands during parathyroidectomy can require reoperation due to persistent hypercalcemia (7).

High complication rates during cervical endocrine procedures have spurred efforts to image parathyroid location (8-10). Currently, the most commonly employed image guidance techniques for parathyroid localization are Sestamibi scintigraphy, ultrasound, computed tomography and magnetic resonance imaging (11). However, these methods are limited by their inability to reliably localize healthy glands or provide real-time intraoperative information. In the case of Sestamibi scintigraphy, the administration of radiotracers requires an additional step and can suffer from non-selective tissue uptake (11,12). There is currently no intraoperative method for identifying the parathyroid gland in real-time regardless of disease state. Surgeons must therefore rely on visual inspection, which is highly subjective and dependent on experience level (13-15).

Optical imaging methods can improve the accuracy of surgical resection by producing higher resolution images in real-time (16). NIR fluorescence imaging is particularly attractive because it takes advantage of an “optical window” between 700–900 nm where light can penetrate deep into tissue with relatively little scattering or absorption (17). Because reports of endogenous NIR fluorophores are rare, clinical use of NIR fluorescence has mostly involved exogenous contrast agents such as indocyanine green and methylene blue (18,19). A method that relies on intrinsic NIR fluorescence could avoid the challenges associated with the use of contrast agents such as potential toxicity, photobleaching and localization, while taking advantage of the longer NIR wavelength.

A promising target for parathyroid localization is a novel, intrinsic, NIR fluorophore that has been discovered in high concentrations the parathyroid gland regardless of disease state (20,21). In this study, the nature of this fluorophore is investigated over a large patient population using NIR fluorescence spectroscopy. To allow improved visualization, a detector is designed for intraoperative anatomical guidance to the parathyroid gland via this fluorescence signal. We report the results of the first real-time intraoperative intrinsic fluorescence imaging of the parathyroid gland to guide cervical endocrine surgery in human patients.

7.3 Materials and Methods

The central goal of this study was to evaluate the ability of NIR autofluorescence imaging to localize the parathyroid gland intraoperatively. We began by measuring the spectral properties of the fluorescence signal from neck tissues in humans ($n = 110$) during parathyroidectomy and thyroidectomy. We then showed proof-of concept using a custom intraoperative NIR fluorescence imaging system to image the parathyroid glands ($n = 6$). Next, we used histology to validate the high fluorescence signals imaged in healthy parathyroid glands of canine subjects ($n = 6$). Finally, we measured NIR fluorescence from kidney and colon ($n = 5$), due to their role in calcium homeostasis, to evaluate other tissues that express the NIR fluorophore of interest.

7.3.1 Patient Recruitment

Patients undergoing parathyroidectomy and/or thyroidectomy were recruited for this study. Approval was obtained from the Investigational Review Board (IRB) at Vanderbilt University. Study inclusion criteria included (i) adult patients between the ages of 18 – 99 years, (ii) presenting with primary thyroid or parathyroid pathophysiology. The attending surgeon at the Vanderbilt Clinic conducted a preoperative evaluation to ensure each subject was a safe and acceptable candidate for the study. Informed written consent was obtained from each patient enrolled. All optical procedures were performed such that patient care was not compromised.

7.3.2 Clinical Fluorescence Spectroscopy

A near-infrared fluorescence spectroscopy system was assembled using a 785 nm diode laser (Innovative Photonic Solutions, I0785SL0050PA) connected to a fluorescence spectrometer (Ocean Optics, S2000-FL) through a fiber optic probe. The probe consists of 7-around-1 fibers

with inline filtering to attenuate the signals generated in the delivery and collection fibers. The parathyroidectomy or thyroidectomy procedure was performed per routine. When the parathyroid was exposed, fluorescence spectra were acquired from parathyroid, thyroid, muscle and fat. The visual diagnosis and level of confidence of the surgeon on the type of tissue and pathology was recorded. Six measurements were collected at each tissue site by the attending surgeon at an integration time of 300 ms. All measurements were made with the overhead operating room lights off. The data was corrected for the spectral response of the system measured with a calibrated tungsten white light source. Each spectrum was normalized to peak thyroid fluorescence to account for day to day variations in the source and system response. Spectra were background subtracted, and the six recordings for each site were averaged together.

7.3.3 Intraoperative Fluorescence Imaging

The near-infrared fluorescence imaging system developed at Vanderbilt University by customizing a clinical endoscope camera. It is composed of a 3-chip color camera with an integrated parfocal zoom lens (Karl Storz, PDD Camera). The camera was driven by a camera control unit (Tricam SL, Karl Storz). A long-pass 808 nm filter was placed in front of the detector to block excitation light while enabling white light and fluorescence image capture. The light source was the same 785 nm diode laser used for spectroscopy. The hand-held detector and fiber optic probe were sterilized prior to each surgery. The system obtains a field-of-view of 25 cm² with a spatial resolution of 170 μm from a working distance of 15 cm.

Images were collected after the surgeon had identified and exposed parathyroid tissue on the surface of the surgical field. The camera was held stationary 15 cm above the tissue, and white light images were collected. Near-infrared fluorescence images were captured with the operating room lights were turned off and the laser evenly irradiated the surgical field at 1 W/cm². Intraoperative images were displayed on a screen that was not visible to the attending surgeon for the ethical reason that the research study should not dictate decisions during surgery. Histopathology of all tissues removed during the course of the surgery served as the gold standard to compare fluorescence measurements. Normal parathyroid diagnosis was based on visual inspection only. Raw images were processed post-operation, and parathyroid contrast was calculated as the ratio of fluorescence intensity of the parathyroid compared to fluorescence of all other surrounding tissues

7.3.4 Ex vivo Tissue Measurements

Because histological validation of the fluorescence signal cannot be performed on healthy human parathyroid tissue, canine tissues were used due to their similarity in structure and function. Healthy mongrel canines of either sex were euthanized and parathyroid and thyroid tissue was excised. Excised tissues were cut in two and half was snap frozen and maintained at -80°C for further analysis. The other half was immediately fixed in 10% neutral buffered formalin and processed for histological analysis. For measurement, samples were thawed to room temperature in phosphate buffered saline.

7.3.5 Statistical Analysis

Statistical analysis was performed with a Student's *t*-test to detect significant differences in the fluorescence signal from parathyroid and surrounding neck tissue. The sample size of 6 patients for the imaging study was chosen as the minimum sample size needed to provide at least 80% power to detect the mean difference between parathyroid fluorescence and background as seen in the clinical spectroscopy study. Statistical significance was assigned for *P* values ≤ 0.05 .

7.4 Results

7.4.1 Validation of Parathyroid Autofluorescence in a Large Patient Population

The presence of the NIR fluorescence signal in parathyroid tissue was confirmed during surgery using single point spectroscopy. Measurements were collected from various neck tissues of 110 patients undergoing parathyroidectomy and thyroidectomy. Results show that the parathyroid glands in all patients exhibited a significantly higher fluorescence signal than thyroid, muscle, and fat. Fluorescence detection of the parathyroid showed 100% sensitivity when measured with spectroscopy, with the parathyroid signal ranging from 1.2 – 25 times higher than thyroid, and all surrounding tissues emitted no signal (Figure 7.1).

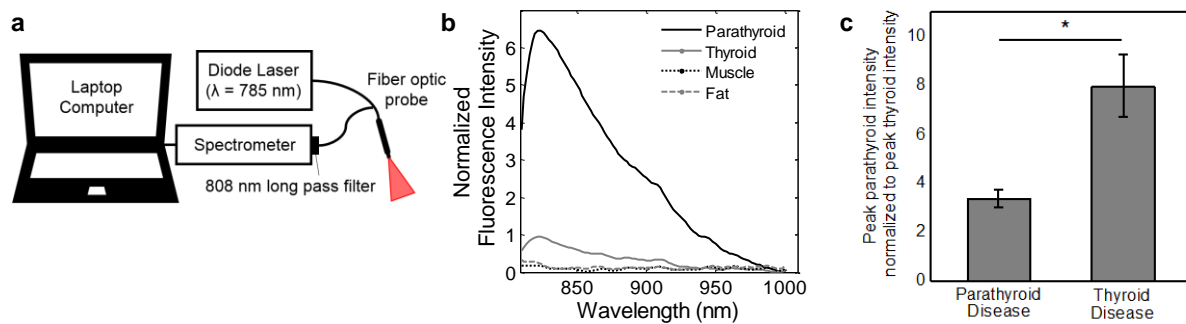


Figure 7.1 Near-infrared fluorescence spectroscopy detects parathyroid tissue intraoperatively on 110 patients undergoing parathyroidectomy or thyroidectomy. A) Portable fluorescence spectroscopy system comprised of a spectrometer, NIR laser diode, laptop computer, hand-held fiber optic probe. B) Representative fluorescence spectra from patient undergoing thyroidectomy shows highest level of fluorescence in parathyroid. C) Average normalized parathyroid signal across patients presenting with four different disease types.

High NIR fluorescence signals from parathyroid tissue were confirmed with histology when available. Histological validation was available for the diseased parathyroid in 47 patients, for the diseased thyroid in 81 patients, and for both diseased tissue types in 14 patients. The efficacy of using this technique to localize the parathyroid was assessed using a receiver operating characteristic (ROC) curve (Figure 7.2). Results showed the area under the ROC curve, a measure of predictive power, was 0.9945. For a tissue to be identified as parathyroid, the optimal cutoff value of the fluorescence signal when normalized to the thyroid was determined to be 1.29 based on the appropriate trade-off between sensitivity and specificity from the ROC curve.

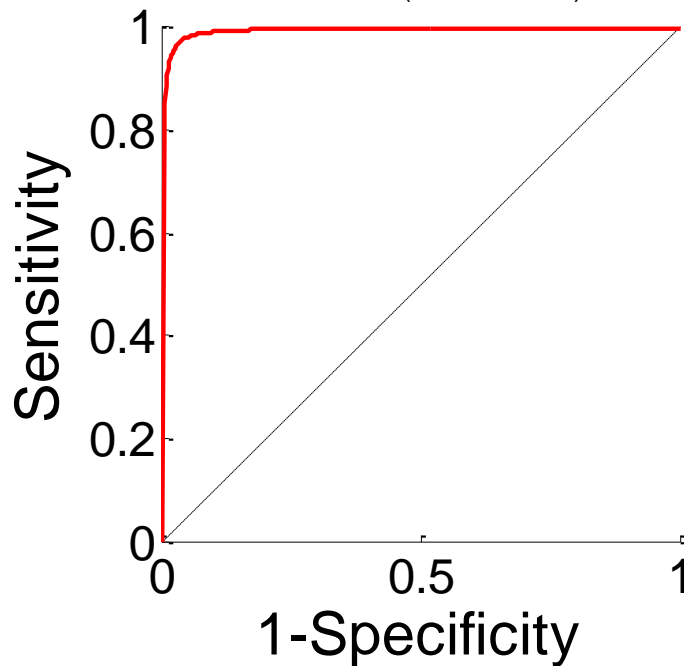


Figure 7.2. Receiver operating characteristic (ROC) curve of the near-infrared parathyroid fluorescence signal normalized to thyroid fluorescence. The area under the curve is 0.9945

7.4.2 Patient Characteristics

Intraoperative imaging was performed on six patients undergoing either thyroidectomy or parathyroidectomy. Three patients were diagnosed with primary hyperparathyroidism, two patients with non-toxic nodular thyroid goiters, and one patient with papillary thyroid cancer (Table 7.1).

Postoperative Diagnosis	Age (year)	Sex	Race	Surgeon Assessment (by visual observation)	Confidence level of surgeon in visual assessment	Parathyroid contrast using fluorescence imaging	Histopathological confirmation of parathyroid?
Parathyroid disease							
Primary hyperparathyroidism	65	Male	White	Parathyroid	high	2.53	Yes
Primary hyperparathyroidism	67	Male	White	Parathyroid	high	4.17	Yes
Primary hyperparathyroidism	53	Female	Black	Parathyroid	high	3.71	Yes
Thyroid disease							
Nontoxic multinodular goiter	40	Female	White	Parathyroid	high	8.48	No
Nontoxic uninodular goiter	29	Female	White	Parathyroid	high	5.9	No
Papillary thyroid cancer	75	Male	White	Parathyroid	high	2.91	No

Table 7.1 Individual demographics and intraoperative fluorescence imaging results for six patients undergoing parathyroidectomy or thyroidectomy.

7.4.3 Intraoperative Imaging of the Parathyroid

To capture NIR parathyroid fluorescence, an imaging system was adapted from a clinical endoscope camera typically used for visible fluorescence applications in gynecology, urology and gastrointestinal surgeries (Karl Storz, PDD camera) (Figure 7.3). The time for fluorescence image capture during surgery ranged from 4 to 9 minutes with a mean time of 6 minutes. Measurements did not interfere with the flow of the surgical procedure. Because the source of contrast is intrinsic, no preoperative preparation was needed for intraoperative imaging.

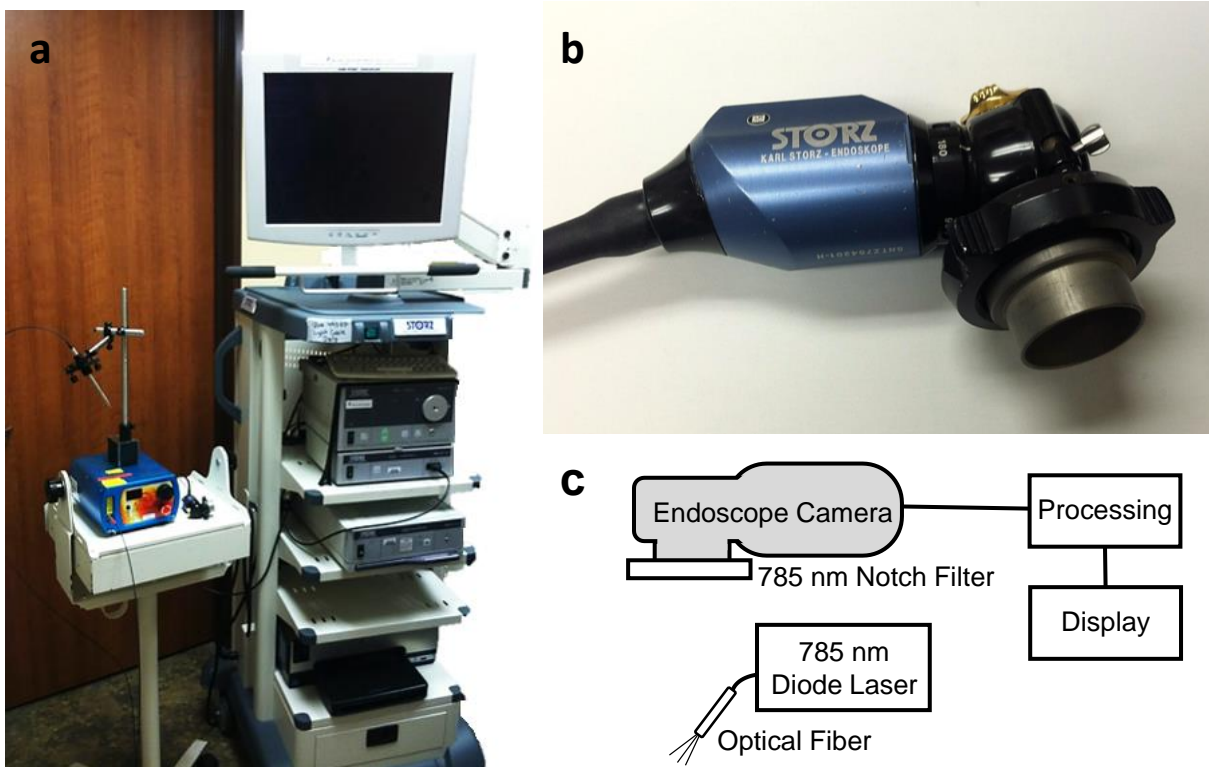


Figure 7.3 Intraoperative near-infrared fluorescence imaging system. A) Surgical cart with fluorescence processing and display (right) and detector with NIR diode laser (left). B) Close up of fluorescence imaging detector with band-pass filter. C) Schematic of fluorescence imaging system for parathyroid detection.

Intrinsic parathyroid fluorescence was detected on all six patients regardless of disease state. In a patient with a nontoxic multinodular goiter, parathyroid fluorescence (shown in red) overlaid on a bright light color image of the surgical field clearly delineated the parathyroid gland from surrounding tissue (Figure 7.4a-c). The parathyroid signal intensity exceeded the fluorescence from all surrounding tissue such as fat, muscle, thyroid, nerve, and trachea in each patient measured. While in some cases a low level signal from the thyroid was imaged, the detector was optimized to image parathyroid fluorescence with maximum contrast. Point measurements with fluorescence spectroscopy collected after imaging confirm the presence of a high fluorescence signal in the parathyroid (Figure 7.4d). Imaging results show parathyroid glands from thyroidectomy patients on average emit stronger fluorescence signal than that of parathyroidectomy patients. The average parathyroid contrast (fluorescence intensity of parathyroid to that of surrounding tissue) for the parathyroid glands measured across six patients was 5.76 for patients with primary thyroid disease and 3.47 for patients with primary parathyroid disease. These results show that thyroidectomy patients had a statistically significantly higher parathyroid signal than patients undergoing parathyroidectomy (P-value < 0.021), which is also confirmed in the 110 patients measured with probe-based spectroscopy (Figure 7.1).

Accuracy of parathyroid identification using fluorescence imaging was compared to the gold standard of histopathology in cases where diseased parathyroid tissue was removed. A representative example of histopathological analysis is depicted in Fig. 7.4e from an excised parathyroid gland that exhibited a parathyroid contrast of 3.71 with intraoperative fluorescence imaging. If parathyroid glands were not excised, the identity of the parathyroid was confirmed by visual inspection of an experienced surgeon who rated their confidence as high, medium, or low. Surgeons were highly confident in their visual identification of all fluorescent parathyroid tissues imaged.

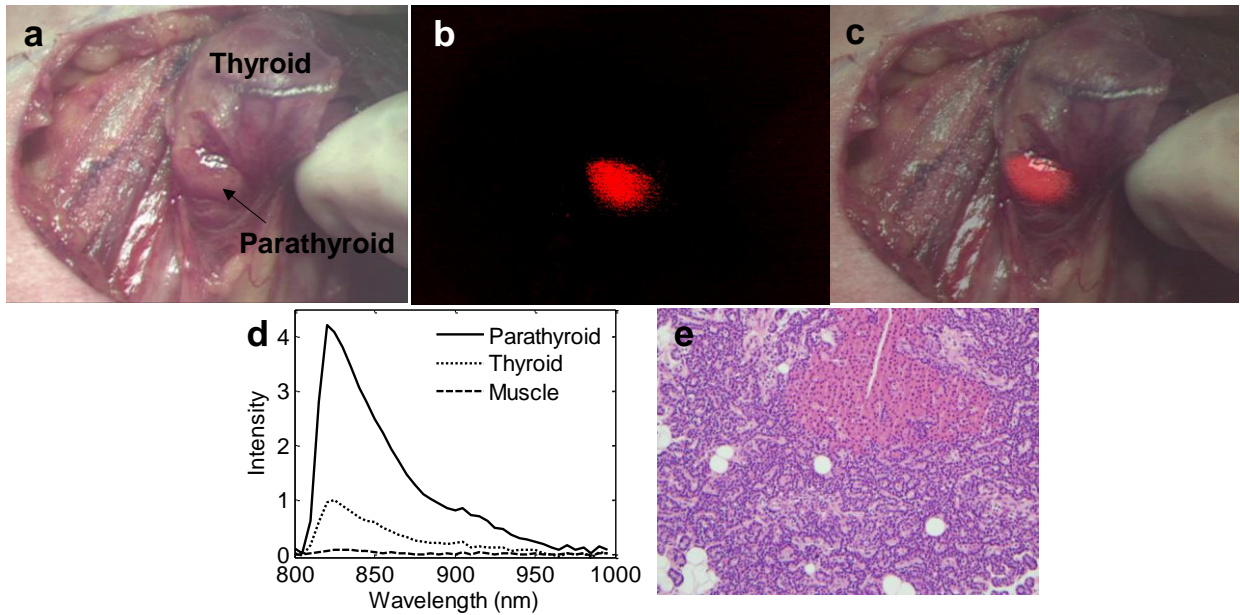


Figure 7.4 Intraoperative fluorescence images of the parathyroid gland. A) Bright field image of parathyroid and thyroid from patient undergoing thyroidectomy. B) Near-infrared fluorescence image shows parathyroid in red. C) Bright field and fluorescence images overlaid shows parathyroid fluorescence. D) Fluorescence spectra of tissues show in A-C confirm fluorescence signal. E) H&E stained slide of parathyroid gland from patient undergoing parathyroidectomy confirms that intraoperative fluorescence signal successfully identified parathyroid tissue.

7.4.4 *Ex vivo* fluorescence imaging of healthy canine parathyroid tissue

In order to histologically validate the fluorescence signal of normal tissue, near-infrared fluorescence imaging was performed *ex vivo* on the parathyroid and thyroid glands of six healthy canine subjects. Imaging permitted real-time identification of the healthy parathyroid gland by detecting higher fluorescence than thyroid tissue and background (Figure 7.5a). The fluorescence signal of healthy tissue was measured with fluorescence spectroscopy (Figure 7.5b). Histological analysis of the same sample measured in Fig. 7.5a-b confirmed that healthy parathyroid tissue exhibits a high NIR fluorescence signal (Figure 7.5c).

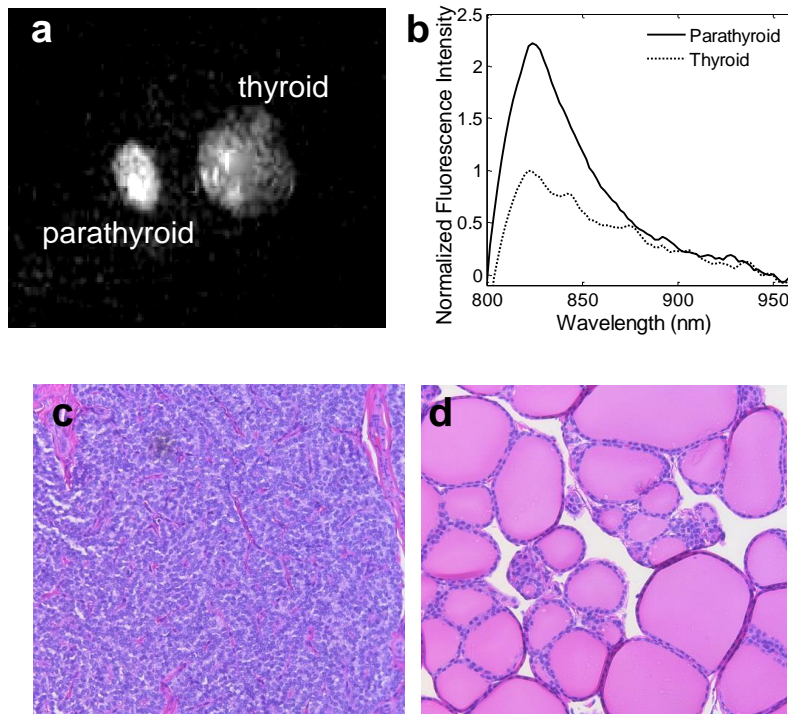


Figure 7.5 Healthy parathyroid and thyroid fluorescence in canine subjects. A) Representative near-infrared fluorescence image of parathyroid (left) and thyroid (right) shows a higher fluorescence intensity from parathyroid *in vitro*. B) NIR fluorescence spectra collected from the same samples confirm high level of fluorescence in parathyroid with peak emission at 822 nm. Microphotographs of H&E stained slide of C) healthy canine parathyroid and D) thyroid tissue (20x magnification) provide histological validation that healthy tissues exhibit NIR fluorescence.

7.5 Discussion

Insufficient parathyroid localization during cervical endocrine surgery can irreversibly damage the body's calcium-regulation, which has led it to become one of the principal causes of surgical malpractice litigation (22). In this study, we investigate the utility of near-infrared autofluorescence imaging of the parathyroid using a previously undiscovered source of biological contrast. Intraoperative detection of the parathyroid glands is aimed at improving the rates of post-operative normocalcemia.

Validation of the robust and consistent nature of NIR parathyroid autofluorescence was performed in 110 patients undergoing parathyroidectomy and thyroidectomy. The NIR fluorescence signal in the parathyroid and thyroid indicate a novel, NIR fluorophore that is excited at 785 nm and emits at 822 nm. The higher intensity signal in the parathyroid than the thyroid suggests the fluorophore is present at a greater concentration in the parathyroid gland. The high fluorescence of the parathyroid gland is present both in patients with primary thyroid disease and primary parathyroid disease, indicating this surgical navigation technique is valid regardless of disease state. Fluorescence spectroscopy was used to characterize the NIR signal rather than imaging because spectral analysis offers more comprehensive insight on both the shape and intensity of the fluorescence signal. Though spectroscopy shows high accuracy in parathyroid identification, it is inherently restricted because it can only provide measurements at a single points in the surgical field. NIR fluorescence imaging provides a more useful surgical guidance tool because it can capture spatial information on parathyroid fluorescence intraoperatively.

Here we present for the very first time *in vivo*, real-time, intraoperative surgical guidance of endocrine surgery using NIR fluorescence imaging to provide specific and sensitive localization of the parathyroid gland. Though the parathyroid glands of all six patients imaged showed higher fluorescence than surrounding tissues, patients with primary thyroid disease showed significantly greater parathyroid contrast than patients with primary parathyroid disease. Patients undergoing thyroidectomy traditionally present with the most difficult to find parathyroid glands due to the small size of healthy glands (23). The utility of this imaging technique is therefore emphasized in patients with thyroid disease because the hardest to find parathyroid glands emit the greatest fluorescence contrast.

One limitation of human validation of the NIR fluorescence imaging is that there is no way to validate the fluorescence of healthy parathyroid tissue because healthy tissue is not routinely removed during surgery. Therefore, the ability of NIR fluorescence imaging to identify parathyroid glands was confirmed using *ex vivo* parathyroid and thyroid tissue from healthy canine subjects. This result combined with *in vivo* human results confirms that NIR fluorescence imaging is capable of identifying both healthy and diseased parathyroid glands.

In addition to a robust, real-time solution to intraoperative parathyroid detection, we postulate the discovery of a unique NIR fluorophore with potentially wide-spread therapeutic

applications. Though the previous imaging and spectroscopy studies give insight into the optical properties and location of this intrinsic fluorophore in healthy and diseased parathyroid tissue, its identity remains invalidated. Typically, intrinsic fluorophores originate from amino acids and cofactors (24). A primary fluorophore candidate is the extracellular calcium-sensing receptor, which are G-protein coupled receptors present at highest concentrations in the chief cells of the parathyroid gland, lower concentrations in the parafollicular cells of the thyroid, and not present in other neck tissues (25-27). Calcium-sensing receptors are known to be down-regulated in patients with hyperparathyroidism (28). This is consistent with the lower fluorescence intensity measured in the parathyroid glands of patients with hyperparathyroidism.

The discovery of an intrinsic NIR fluorophore is transformational in the fields of both surgical imaging and biomedical photonics because endogenous NIR fluorophores with emission greater than 800 nm have not been reported in literature. Potentially, this NIR fluorophore could replace the use of exogenous contrast agents in specific applications and become a new target for surgical imaging beyond parathyroidectomy and thyroidectomy procedures. With future knowledge of the fluorophore identity, the benefits of NIR fluorescence imaging can be expanded beyond intraoperative parathyroid detection to other surgical guidance applications involving tissues expressing this NIR fluorophore.

In this pilot study, NIR autofluorescence of the parathyroid was effectively imaged despite the use of a clinical endoscope camera that was manufactured for applications with visible contrast agents. While this detector showed sufficient contrast for parathyroid detection, an imaging system optimized for (i) weaker signals emitted from biological fluorophores and (ii) near-infrared wavelengths could potentially further increase parathyroid contrast. Near-infrared wavelengths are especially useful in surgical imaging because of their relatively deep penetration depth into tissue (~2–3 mm) compare to ultraviolet and visible wavelengths (29). Accordingly, an optimized detector may also offer the sensitivity to detect signals emitted from a greater depth in tissue, forgoing the need to expose the parathyroid at the surface of the surgical field.

The intraoperative method for parathyroid detection described in this study holds major advantages over current intraoperative methods such as frozen section analysis and fine-needle aspiration with intact parathyroid hormone (iPTH) assay. NIR fluorescence imaging offers intraoperative parathyroid detection, delivering information on parathyroid identity in real-time without administration of contrast agents or the excision of samples for analysis. In contrast,

frozen section analysis may require partial excision of a gland, which risks damage to its blood supply (30). Fine needle aspiration with iPTH assay suffers from high false negative rates and is not employed when the parathyroid is not removed (31). Both fine needle aspiration and frozen section analysis add significant time and cost to a procedure. NIR fluorescence imaging would be especially useful in cases of parathyroid auto-transplantation where it is necessary to accurately and quickly identify the resected tissue as parathyroid before re-implanting (32).

In summary, our study is the first to report real-time intraoperative imaging of the parathyroid gland during surgery using intrinsic biological fluorescence. Furthermore, our results indicate a novel, near-infrared biological fluorophore that has not previously been reported in literature. The high levels of this fluorophore in the parathyroid gland offers the unique opportunity for tissue-selective imaging without administered contrast agents. Future analysis must be performed on parathyroid tissue specimen to uncover the biochemical mechanism of the fluorescence signal.

7.6 References

1. Gourgiotis S, Moustafellos P, Dimopoulos N, Papaxoinis G, Baratsis S, Hadjiyannakis E. Inadvertent parathyroidectomy during thyroid surgery: the incidence of a complication of thyroidectomy. *Langenbeck's Archives of Surgery*, 2006;391(6): 557-560.
2. Sakorafas GH, Stafyla V, Bramis C, Kotsifopoulos N, Kolettis N, Kassaras G, Incidental parathyroidectomy during thyroid surgery: an underappreciated complication of thyroidectomy. *World J Surg*. 2005;29(12):1539-43.
3. Kowalski LP, Surgical complications after thyroid surgery performed in a cancer hospital. *Otolaryngology-Head and Neck Surgery*, 2005;132(3): 490-494.
4. Mariani G, Gulec SA, Rubello D, Boni G, Puccini M, Pelizzo MR, Giuliano AE, Preoperative localization and radioguided parathyroid surgery. *Journal of Nuclear Medicine*, 2003;44(9):1443-1458
5. Sebag F, Shen W, Brunaud L, Kebebew E, Duh QY, Clark OH. Intraoperative parathyroid hormone assay and parathyroid reoperations. *Surgery*, 2003;134(6):1049-1055.
6. Christou N, Mathonnet M, Complications after total thyroidectomy, *Journal of visceral surgery*, 2013;150(4): 249-256.
7. Nadine CR, Sturgeon C, Clark OH. Persistent and recurrent hyperparathyroidism, *Current treatment options in oncology*, 2004;5(4): 335-345.

8. O'Doherty MJ, Kettle AG, Wells P, Collins RE, Coakley AJ, Parathyroid imaging with technetium-99m-sestamibi: preoperative localization and tissue uptake studies. *Journal of nuclear medicine: official publication, Society of Nuclear Medicine*, 1992;33(3): 313-318.
9. Majithia A, Stearns MP, Methylene blue toxicity following infusion to localize parathyroid adenoma. *The Journal of Laryngology & Otology*, 2006;120(2):138-140.
10. Prosst RL, Weiss J, Hupp L, Willeke F, Post S, Fluorescence-guided minimally invasive parathyroidectomy: clinical experience with a novel intraoperative detection technique for parathyroid glands. *World journal of surgery*, 2010;34(9): 2217-2222.
11. Mohebati A, Shaha AR, Imaging techniques in parathyroid surgery for primary hyperparathyroidism. *Am J Otolaryngol*, 2012;33:457-68.
12. Taillefer R, Boucher Y, Potvin C, Lambert R, Detection and localization of parathyroid adenomas in patients with hyperparathyroidism using a single radionuclide imaging procedure with technetium-99m-sestamibi (double-phase study), *J Nucl Med*, 1992;33(10):1801–1807.
13. Zarebczan B, Chen H, Influence of surgical volume on operative failures for hyperparathyroidism, *Advances in surgery*, 2011;45:237.
14. Erbil Y, Barbaros U, Ozbey N, Aral F, Özarmağan S, Risk factors of incidental parathyroidectomy after thyroidectomy for benign thyroid disorders, *International Journal of Surgery* 2009; 7(1): 58-61.
15. Sosa JA, Bowman HM, Tielsch JM, Powe NR, Gordon TA, Udelsman R, The importance of surgeon experience for clinical and economic outcomes from thyroidectomy, *Annals of surgery*, 1998; 228(3): 320.
16. Kherlopian AR, Song T, Duan Q, Neimark MA, Po MJ, Gohagan JK, Laine AF, A review of imaging techniques for systems biology, *BMC Systems Biology*, 2(1), 74, (2008).
17. Hadjipanayis CG, Jiang H, Roberts DW, Yang L, Current and Future Clinical Applications for Optical Imaging of Cancer: From Intraoperative Surgical Guidance to Cancer Screening, *Molecular Imaging in Oncology*, 2011;38:109–118.
18. Matsui A, Tanaka E, Choi HS, Kianzad V, Gioux S, Lomnes SJ, Frangioni JV, Real-time, near-infrared, fluorescence-guided identification of the ureters using methylene blue. *Surgery*, 2010;148(1): 78-86.
19. Hirche C, Murawa D, Mohr Z, Kneif S, Hünerbein M, ICG fluorescence-guided sentinel node biopsy for axillary nodal staging in breast cancer, *Breast Cancer Res Treat*, 2010;121;373–378.
20. Paras C, Keller M, White LM, Phay JE, Mahadevan-Jansen A, Near-Infrared Auto-fluorescence for the Detection of Parathyroid Glands, *J Biomed Optics*, 2011;16(6).

21. McWade MA, Paras C, White LM, Phay JE, Mahadevan-Jansen A, Broome JT, A novel optical approach to intraoperative detection of parathyroid glands, *Surgery*, 2013; 154(6):1371-1377.
22. Dralle H, Lorenz K, Machens A, Verdicts on malpractice claims after thyroid surgery: Emerging trends and future directions, *Head & neck*, 2012;34(11):1591-1596.
23. Lee NJ, Blakey JD, Bhuta S, Calcaterra TC, Unintentional parathyroidectomy during thyroidectomy. *The Laryngoscope*, 1999;109(8): 1238-1240.
24. Lakowicz JR, *Principles of fluorescence spectroscopy*. Springer, 2007.
25. Brown EM, MacLeod RJ, Extracellular calcium sensing and extracellular calcium signaling, *Physiological reviews*, 2001; 81(1): 239-298.
26. Chattopadhyay N, Cheng I, Rogers K, Riccardi D, Hall A, Diaz R, Brown EM, Identification and localization of extracellular Ca²⁺-sensing receptor in rat intestine, *American Journal of Physiology-Gastrointestinal and Liver Physiology*, 1998;274(1): G122-G130.
27. Riccardi D, Hall AE, Chattopadhyay A, Xu JZ, Brown EM, Hebert SC, Localization of the extracellular Ca²⁺/polyvalent cation-sensing protein in rat kidney. *American Journal of Physiology-Renal Physiology*, 1998;274(3): F611-F622.
28. Gogusev J, Duchambon P, Hory B, Giovannini M, Goureau Y, Sarfati E, Drüeke TB, Depressed expression of calcium receptor in parathyroid gland tissue of patients with hyperparathyroidism, *Kidney international*, 1997;51(1): 328-336.
29. Stolik S, Delgado JA, Perez A, Anasagasti L, Measurement of the penetration depths of red and near infrared light in human “ex vivo” tissues, *Journal of Photochemistry and Photobiology B: Biology*, 2000; 57(2): 90-93.
30. Perrier ND, Ituarte P, Kikuchi S, Siperstein AE, Duh QY, Clark OH, Hamill T, Intraoperative parathyroid aspiration and parathyroid hormone assay as an alternative to frozen section for tissue identification. *World journal of surgery*, 2000;24(11): 1319-1322.
31. Bancos I, Grant CS, Nadeem S, Stan MN, Reading CC, Sebo TJ, Dean DS, Risks and benefits of parathyroid fine-needle aspiration with parathyroid hormone washout, *Endocrine Practice*, 2012;18(4):441-449.
32. Lo CY, Parathyroid autotransplantation during thyroidectomy. *ANZ journal of surgery*, 2002; 72(12): 902-907.

CHAPTER 8

FLUORESCENCE-GUIDED SURGERY WITH OVERLAY TISSUE IMAGING SYSTEM: FIRST IN-HUMAN RESULTS FOR LABEL-FREE PARATHYROID LOCALIZATION

Melanie A. McWade¹, Carmen C. Solórzano², Anita Mahadevan-Jansen¹

¹Biomedical Photonics Laboratory, Department of Biomedical Engineering Vanderbilt University, 5824 Stevenson Center, 37235 Nashville, Tennessee.

²Division of Surgical Oncology and Endocrine Surgery, Vanderbilt University 2220 Pierce Avenue, 37232, Nashville, Tennessee.

This chapter was submitted as:

“Fluorescence-guided surgery with Overlay Tissue Imaging System: First in-human results for label-free parathyroid localization.” *Science Translational Medicine*, 2016.

8.1 Abstract

Patient quality of life suffers when surgeons are unable to detect their parathyroid glands during parathyroid and thyroid surgery. Healthy parathyroid glands damaged or removed during thyroid surgery can cause debilitatingly low blood calcium levels. Previously developed imaging tools for parathyroid detection have not adequately mitigated this problem due to their poor integration into the real-time surgical workflow. Recently, an endogenous near-infrared (NIR) fluorescence signal has been discovered at uniquely high levels parathyroid glands regardless of disease state. We have developed an Overlay Tissue Imaging System (OTIS) that detects parathyroid NIR autofluorescence and projects the image back on the patient for direct parathyroid visualization within the surgeon's line of sight. Diseased and normal parathyroid glands were detected and overlaid with visible green light in real-time in 12 patient undergoing endocrine surgery. OTIS imaging holds great potential to reduce surgical complications and presents a paradigm shift in both parathyroid detection and fluorescence imaging.

8.2 Introduction

Patients can be sentenced to lifelong issues with calcium regulation if their parathyroid glands are not detected during parathyroid and thyroid surgery (1, 2). Up to 12% of patients experience permanently low blood calcium levels due to damage or accidental removal of healthy parathyroid glands during thyroid surgery (3). Thyroid cancer is the cancer with the fastest-growing number of new cases in women (4), thereby increasing the concern for surgical complications. Conversely, insufficient removal of all hypersecreting parathyroid glands occurs in up to 30% of parathyroid surgeries, leading to persisting imbalances in parathyroid hormone levels and the need for reoperation (5). Failure to find the parathyroid glands is a major cause of morbidity during both parathyroid and thyroid surgery (6, 7).

Preoperative Sestamibi scintigraphy and ultrasound imaging are commonly used to localize enlarged diseased parathyroid glands (8), but the remote image displays during surgery are not dynamic nor are the modalities capable of localizing these glands in the absence of disease. Surgeons, therefore, must rely on their eyes and experience to detect parathyroid tissue during surgery, which is especially difficult for trainees and surgeons in low-volume centers (9). There is a significant unmet clinical need for a reliable intraoperative tool to detect parathyroid glands during thyroid and parathyroid surgery.

We have developed a non-invasive, intrinsic optical method based on NIR autofluorescence for reliable and consistent identification of diseased *and normal* parathyroid glands (10-12). This signal has been demonstrated to be present at higher levels in parathyroid tissue compared to all the tissues in the neck creating an internal beacon. This method has been intra-operatively validated in over 140 patients *in vivo* by collecting point measurements with probe-based fluorescence spectroscopy. However, parathyroid gland imaging would provide more useful information for surgical decision making. Clinical acceptance of parathyroid fluorescence detection requires an imaging system that can be seamlessly integrated into the operating room.

The recent boom in near-infrared (NIR) fluorescence imaging system development has begun to transform surgical guidance. Dynamic NIR images collected during surgery enables real-time decision making that traditional pre-operative imaging has not allowed. Both current NIR imaging and traditional pre-operative imaging systems, however, introduce errors due to image interpretation that can prevent surgeons from taking full advantage of information-rich

images (13). These errors rise from issues such as lack of image context, time-consuming image analysis, and remote image displays and lessen the effectiveness of image-guided surgery (14-16). This challenge is especially prominent when surgeons must translate images on a distant display monitor with the anatomy at their fingertips (17, 18). An estimated 30-40% of errors in surgical imaging are due to such interpretive errors. Therefore, there is a significant need for imaging systems with better image visualization and ergonomics at the center of the design (17, 19).

The most recent approaches to improve image visualization rely on the heads-up display, a semi-transparent image display strategy. Heads-up displays prevent surgeons from diverting attention away from the patient by virtually merging fluorescence images with the visual field when the surgeon is looking through microscope oculars (20, 21), semi-transparent mirrors (22), or wearable goggles. However, endocrine surgery and other procedures that do not require display monitors, microscopes, or preadministered contrast agents are highly unlikely to adapt these new fluorescence imaging strategies. Our solution is a direct overlay technique for label-free NIR autofluorescence imaging that projects the image directly on the surgical field without hardware between the surgeon and patient. Direct image overlay is a nascent idea (23) but has never been done on humans. (24, 25). Furthermore, direct overlay imaging and NIR fluorescence imaging in general has previously been constrained by use with extrinsic NIR dyes, because label-free fluorescence is largely confined to ultraviolet and visible wavelengths (26).

Here we present a novel imaging system for parathyroid detection that projects the optical image directly on to surgical field eliminating the need for a display system. We have designed, built and validated an overlay tissue imaging system (OTIS) that projects NIR autofluorescence images acquired of the surgical field of view in the neck during endocrine procedures, directly onto the patient during surgery. We showcase the first in-human results of OTIS in fluorescence guided surgical procedures by enabling naked-eye visualization of the endogenous near-infrared fluorescence of the parathyroid glands during thyroid and parathyroid procedures with 100% accuracy. OTIS has unique sensitivity to detect endogenous biological fluorescence, which is typically weaker than dye fluorescence. This motivates the use of OTIS to image low concentrations of NIR dyes that cannot be detected with traditional imaging systems. We demonstrate OTIS imaging for enhancing dye contrast in surgery using reduced concentrations of indocyanine green (ICG), an FDA approved NIR dye, *in vitro*. This surgical

imaging platform for projecting images directly on patient tissue is potentially transformative for a wide range of imaging techniques and clinical applications.

8.3 Materials and Methods

8.3.1 Study Design

This study was designed to investigate the potential of our NIR fluorescence-based overlay tissue imaging system (OTIS) to detect and enhance intraoperative visualization of the parathyroid gland compared to surrounding tissues during parathyroidectomy and thyroidectomy. An intraoperative imaging pilot study was conducted patients undergoing parathyroidectomy and/or thyroidectomy (n=12) at the Vanderbilt University Endocrine Surgery Center after approval from the Institutional Review Board at Vanderbilt University (#070795). Study inclusion criteria included adult patients between the ages of 18-99 years undergoing endocrine surgery due to presentation of thyroid or parathyroid disease. The attending surgeon at the Vanderbilt Clinic conducted preoperative evaluations on each subject to ensure their safety and acceptability for this study. Informed written consent was obtained for all enrolled patients. Imaging was performed during surgery such that patient care was not compromised. The surgeon was blinded to all fluorescence information provided by the overlay imaging system. Samples were excluded from the study if the surgeon had low confidence in the identity of the tissue sample and no histology was available or if the overhead lights were not turned completely off.

8.3.2 Overlay Tissue Imaging System

The overlay tissue imaging system (OTIS) was designed to enhance visualization of the surgical field by overlaying NIR fluorescence with visible light in real-time. Image collection with OTIS is accomplished via a NIR CMOS camera (Basler AG), a fixed focal length lens ($f=50$ mm, Navitar), and a long-pass filter (808 nm, Semrock). Images are collected with an exposure time of 100 ms. The surgical field is illuminated with an NIR diode laser ($\lambda = 785$ nm, Innovative Photonics Solutions) coupled through a 400- μ m fiber optic patch cable, filtered with a laser clean-up filter (Semrock), and focused with a plano-convex lens ($f=75$ mm, Thorlabs) to achieve a 5-cm diameter spot size with power density of 11.5 mW/cm². The raw NIR image is

sent to a laptop computer (Toshiba) for real-time image processing using custom feature extraction algorithm in LabVIEW software. The processed image will be sent to a high-lumen light-emitting diode (LED) projector (AAXA Technologies). The image is sent through a fixed focal-length lens ($f=50$ mm, Navitar) through a dichroic filter (801 nm, Semrock) and on to the surgical field. Areas of high NIR fluorescence are overlaid with green light from the projector. The distance of the camera and projector from the dichroic mirror as well as the lenses coupled to the projector and the NIR camera are matched such that the collected and projected image are aligned. A color CMOS detector (Basler AG) was mounted to the side of OTIS in order to detect images that could be visualized with the naked eye.

A custom LabVIEW based software program performs real-time feature extraction of NIR fluorescence images. Images collected by the NIR camera are sent to the laptop computer and a user-defined mask around the surgical incision is selected to minimize the effects of NIR light reflections off surgical tools. A dark frame is subtracted, and the image is sent through a convolution filter and a feature extraction algorithm to achieve morphological transformation. This series of steps achieves maximal signal intensity in the areas of low level fluorescence present in the surgical field. The processed image will be sent to the projector and converted to a green color intensity before projection on the tissue. The software will also allow co-registration of the projected image with real space using a series of x and y manipulation controls. Image co-registration is performed prior to each procedure using a fluorescent grid phantom to account for slight changes in image alignment

8.3.3 Intraoperative Overlay Imaging

During parathyroidectomy and/or thyroidectomy procedures, parathyroid glands were exposed. Using a disposable sterile handle, the surgeon positioned OTIS approximately 50 cm above the surgical incision such that it remained outside the sterile field. A visible white grid was projected onto the patient to add in positioning and focusing of OTIS. All overhead lights were turned off and surgical headlights directed away to minimize light interference. Images were collected, processed, and projected directly on the tissue. The surgeon looked away during projection to avoid being influenced by the results. The confidence level (high, medium, or low) of the surgeon in visually identifying each parathyroid gland was recorded. Because visual identification is the most commonly employed technique for intraoperative parathyroid detection,

it was used as a point of comparison to assess the performance of this technology. Tissue sites with a low surgical confidence level were excluded from analysis, unless there was available histology from that tissue. Histology was compared to the measured fluorescence images and used as the gold standard for parathyroid detection. It was not feasible to collect parathyroid gland histology from every patient because tissue determined to be healthy is not removed during surgery.

8.3.4 Dye Imaging

Indocyanine green (Sigma) diluted with intralipid to concentrations of 10, 5, 1, 0.5, 0.25, 0.125, 0.06, and 0 μM . One hundred μL of each ICG concentration was imaged with OTIS *in vitro*. Real-time feature extraction was performed by the imaging system the same manner as in *in vivo* imaging. OTIS projected green overlay on the dye samples at varying intensities for each concentration, which was recorded by the color camera. The signal to background ratio was measured for each dye sample.

8.3.5 Statistical Analysis

Data are presented as mean \pm standard deviation. Paired Student's *t* tests were used to assess statistical significance. Values of $P < 0.05$ were considered statistically significant.

8.4 Results

8.4.1 Design of overlay tissue imaging system (OTIS)

We developed a real-time intraoperative overlay tissue imaging system (OTIS) (Fig. 8.1) to project NIR fluorescence images on the surgical field during surgery. OTIS is a hands-free imaging system containing a high sensitivity NIR camera aligned to a visible projector with precision matched fields-of-view of 5×6.25 cm for image collection and overlay during surgery. OTIS collects NIR images of the surgical field illuminated with a NIR diode laser ($\lambda = 785$ nm) and relays them through a refinement algorithm to reduce noise and extract NIR fluorescent features. The refined NIR image is converted to a green color scale and overlaid directly on the NIR fluorescent tissues via the projector. Images are continuously processed and projected on the patient at a rate of 4 fps, allowing real-time, dynamic visualization of the fluorescence information at the surgical site. OTIS has a resolution of 176 μm , which is well over the required

resolution to visualize normal parathyroid glands (2-4 mm diameter). Immediately prior to each procedure, projections of a NIR fluorescent reference grid were spatially shifted to ensure precise alignment of the projected image with the visual field.

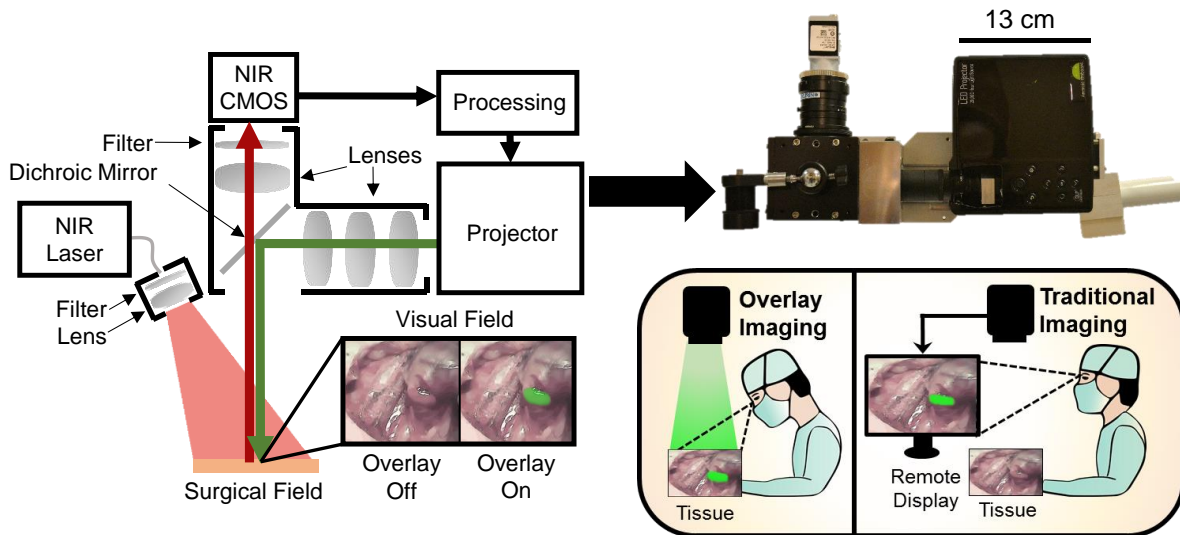


Figure 8.1: Overlay tissue imaging system design

8.4.2 OTIS Deployment in Operating Room

Real-time intraoperative OTIS imaging was performed during parathyroidectomy and thyroidectomy surgeries after parathyroid glands were exposed on the surface of the surgical field. Overhead lights and surgical headlights were turned off or directed away from the tissue site. OTIS was positioned approximately 50 cm above the exposed glands and then imaged and overlaid with green for direct fluorescence visualization. OTIS allows for completely hands-free operation and was integrated into the endocrine surgical workflow for live identification of parathyroid glands. Because OTIS is not yet an FDA approved device, surgeons looked away from the surgical field during imaging so that surgical decision-making was not affected by the OTIS overlay. The average time for fluorescence-based OTIS imaging was 5 minutes.

8.4.3 Patient characteristics

Twelve patients undergoing parathyroidectomy and/or thyroidectomy were recruited for intraoperative OTIS imaging. Six patients were diagnosed with thyroid disease, five patients with hyperparathyroidism, and one patient with concurrent parathyroid and thyroid disease (Table 8.1). Thirty-three parathyroid glands were measured. Four parathyroid glands were excluded due to incidental surgical light interference that drowned out NIR fluorescence signal.

8.4.4 Intraoperative OTIS imaging in Endocrine Surgery

We demonstrate the feasibility of real-time, label-free OTIS imaging to enhance intraoperative visualization of invisible endogenous NIR fluorescence by overlaying fluorescent parathyroid glands with visible green light directly on the patient. Across all twelve patients, 100% of parathyroid glands (29 of 29) were detected based on their endogenous NIR fluorescence signal. OTIS feature extraction was accomplished in real-time for all but two parathyroid glands, which required alterations to the feature extraction algorithm post-surgery. Each of the glands measured were confirmed as true parathyroid tissue using histopathology, or highly confident visual assessment by the endocrine surgeon when histopathology was not possible.

Table 8.1: Characteristics of patients recruited for OTIS imaging

Patient	Disease	Age	Sex	BMI (kg/m ²)	Parathyroid Histopathology	Surgeon confidence	Parathyroid in vivo fluorescence	OTIS overlay
Thyroidectomy					Not available			
3	Papillary thyroid cancer	70	F	28.5	Not available	High	++	Yes
4	Benign thyroid goiter	55	F	29.9	Not available	High	++	Yes
					Not available	High	+	Yes
					Not available	High	+	Yes
					Not available	High	+	Yes
6	Papillary thyroid cancer	32	F	25.1	Not available	High	++	Yes
					Not available	High	+	Yes
7	Graves' Disease	51	F	26.6	Not available	High	+	No*
					Not available	High	+	Yes
					Not available	High	+	Yes
					Not available	High	+	Yes
8	Benign thyroid goiter	62	M	25.2	Not available	High	++	Yes
					Not available	High	++	Yes
10	Papillary thyroid cancer	55	M	26.6	Not available	High	++	Yes
					Not available	High	++	Yes
Parathyroidectomy					Not available		++	
1	1° hyperparathyroidism	66	F	26.1	Not available	High	++	Yes
					PTG adenoma	High	++	Yes
					Normal PTG	High	+++	Yes
					Benign thyroid	Low	-	No
5	Hyperparathyroidism (MEN-1)	57	M	25.7	Hyperplastic PTG	High	+++	Yes
					Hyperplastic PTG	High	++	Yes
9	1° hyperparathyroidism	70	F	22.8	PTG adenoma	High	++	No*
					PTG adenoma	High	++	Yes
					PTG adenoma	High	++	Yes
11	2° hyperparathyroidism	46	F	36.8	PTG adenoma	High	++	Yes
					PTG adenoma	High	++	Yes
12	1° hyperparathyroidism	67	F	47.8	PTG adenoma	High	++	Yes
					Normal PTG	High	++	Yes
Parathyroidectomy/Thyroidectomy								
2	1° hyperparathyroidism	73	F	28	PTG adenoma	High	+++	Yes
	Benign thyroid goiter							

* Feature extraction of two glands occurred after surgery due to changes in processing algorithm.
Parathyroid in vivo fluorescence based on SBR: + (1.5 to 2.2), ++ (2.3 to 4.9) , +++ (5 to 16), - (<1.5)

Figure 8.2A-B conveys how difficult it is to distinguish unenhanced parathyroid glands with the naked eye due to the visual homogeneity of tissues in the surgical incision. OTIS imaging of the neck incision directly highlighted NIR fluorescent parathyroid glands in visible green light such that the contrast enhancement could be visualized at the surgeon's fingertips. (Fig. 8.2C-D). A green color was chosen for the overlay because it provides stark visual contrast against the surrounding tissues. Results show a uniform green color map whereby the intensity of the fluorescence signal is proportional to the intensity of the green overlay. OTIS detected normal functioning parathyroid glands as small as 2 mm (Fig. 8.2D) as well as larger hypersecreting parathyroid adenomas up to 30 mm in diameter (Fig. 8.2C). Surrounding muscle, thyroid gland, fat, nerves and blood vessels within the surgical incision did not show an NIR fluorescence signal, as shown in previous studies (12), and therefore were not overlaid in green for visualization via OTIS.

Seventeen hypercellular parathyroid glands had an average signal-to-background ratio (SBR) of 5.97 ± 1.71 a.u., which was not significantly different from the SBR for twelve normal parathyroid glands of 5.77 ± 2.31 a.u. (Figure 8.2E). However, the thyroid glands had a SBR of 1.28 ± 0.08 a.u, which was significantly lower than both normal parathyroid glands ($P < 0.05$) and hypersecreting parathyroid glands ($P < 0.01$). Figure 8.1 demonstrates the ability of OTIS imaging to provide both quantitative information in the form of SBR as well as qualitative information in the form of the green overlay on the surgical field. In Patient 1 (Table 8.1), a suspected parathyroid candidate imaged with OTIS revealed no fluorescence signal and hence received no OTIS overlay. Frozen section analysis of the tissue biopsy confirmed this result showing the specimen was comprised of benign thyroid tissue. OTIS imaging projected visible green overlay to highlight parathyroid tissue immediately after resection, demonstrating the feasibility of NIR fluorescence based OTIS imaging *ex vivo*. Four glands were excluded from the study because the lights were left on in the surgical suite, which masked NIR fluorescence signal. This can be addressed in future iterations of NIR fluorescence based OTIS imaging by subtracting surgical light noise during image processing. Intraoperative overlay imaging using OTIS did not impede the surgical workflow.

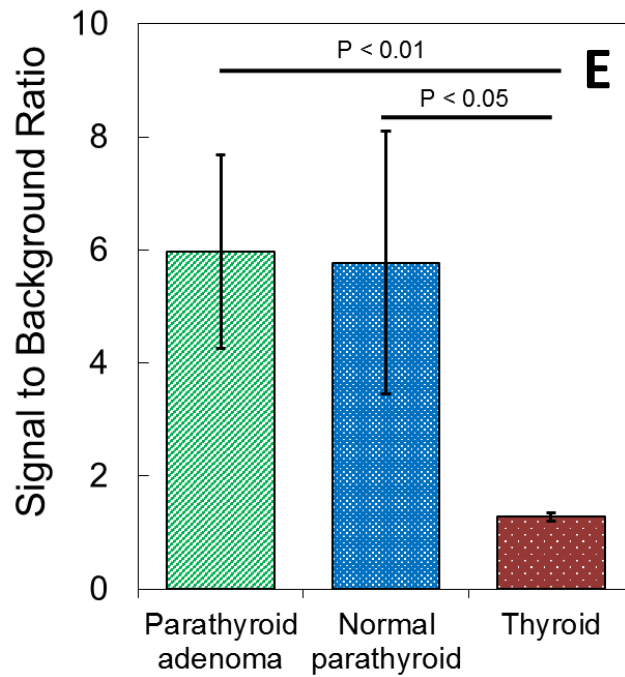
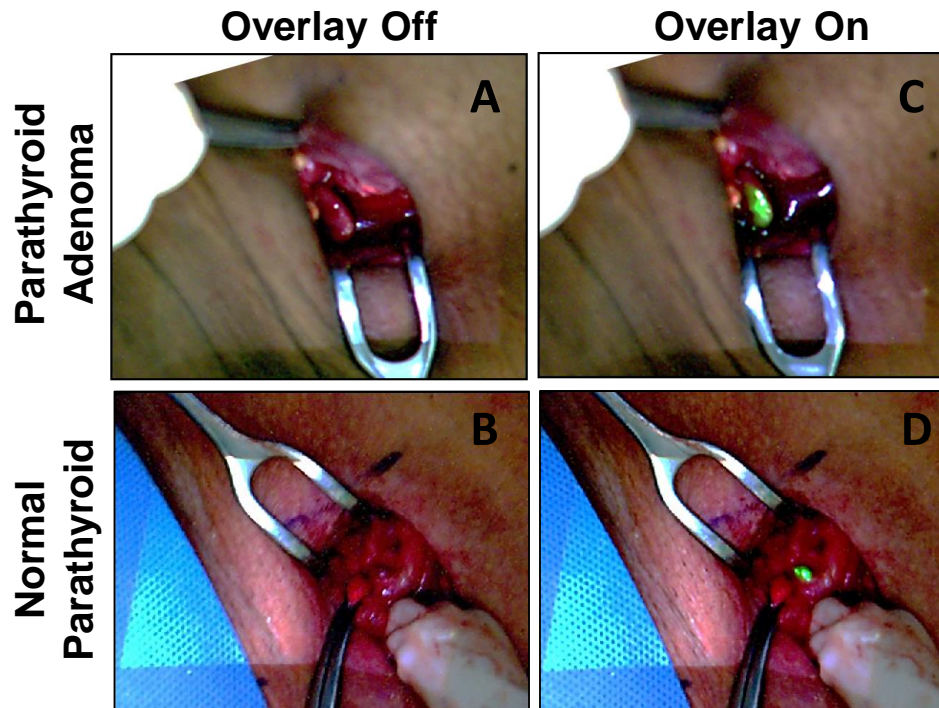


Figure 8.2: OTIS imaging detects diseased and normal parathyroid glands by overlaying with green light

8.4.5 Enhancing dye contrast with OTIS imaging

Results showed successful OTIS imaging of low concentrations of ICG. OTIS detected invisible NIR fluorescence ICG concentrations ranging from 0.06 – 10 μ M. Each sample was overlaid with a visible green light intensity proportional to its fluorescence signal *in vitro* (Fig. 8.3A-C). The visual field is therefore directly enhanced with OTIS imaging. A clinically relevant ICG concentration of 5 μ M demonstrated a SBR of 100.8. However, concentrations as low as 0.06 μ M ICG emitted fluorescence detectable by OTIS with SBR of 8.06 (Fig. 8.3D). Though fluorescence emission of the 0.06 μ M sample was weak relative to higher concentrations, the intensity of the green OTIS overlay could be increased for brighter visualization by utilizing real-time changes to the OTIS processing algorithm. Results show low level fluorescence contrast can be visualized with high intensity OTIS overlay for optimal visualization via the real-time feature extraction algorithm (Fig 8.3E).

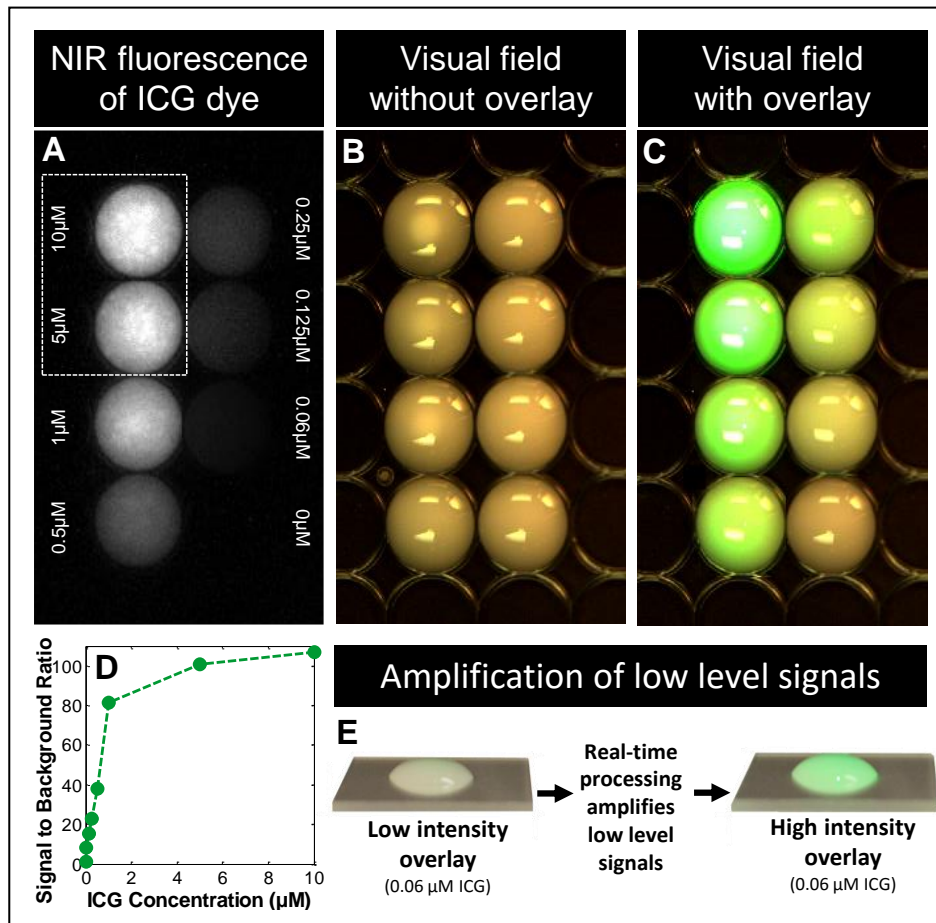


Figure 8.3: Indocyanine fluorescence imaging with OTIS

8.5 Discussion

The key innovations of our overlay tissue imaging system are the ability to project fluorescence images directly on the patient in real-time and the ability to achieve label-free parathyroid gland detection at the tissue site regardless of disease state. Reliable intraoperative localization of healthy and diseased parathyroid glands could improve the patient outcomes cervical endocrine surgery by reducing rates of postoperative hypocalcemia and reoperation. Decreased error during parathyroidectomy and thyroidectomy would reduce the rates of post-operative emergency department visits (27), cut healthcare costs associated with extended medical care (28), and limit one of the largest sources of post-operative litigation (29). The current clinical imaging methods rely on the parathyroid gland being diseased. Surgical imaging systems at large rely on remote displays, proven to induce interpretive error and complicate patient outcomes. In this proof-of concept study, we show our Overlay Tissue Imaging System (OTIS) design is capable of rapid intraoperative high accuracy parathyroid detection through direct overlay of NIR fluorescence signal on patients in real-time to reduce error in image interpretation.

We showcase OTIS as a novel visualization strategy for fluorescence guided surgery that supplies intuitive intraoperative images to supplement visual inspection and reduce surgical complications. OTIS performs real-time NIR fluorescence imaging, feature extraction, and projection of images directly onto the patient at 4 fps. Hands-free, continuous image collection and overlay allows surgeons to view fluorescence at the tissue site while conducting the surgery. Rather than overlaying the surgical field with the entire NIR fluorescence image, OTIS projects a refined image that highlights only the NIR fluorescent signal from features of interest, which is the parathyroid gland in this case. The intraoperative extraction algorithm performs this process in real-time to amplify low-level signals and reduce noise associated with stray operating room light and background autofluorescence. The OTIS imaging system is easily mobilized over the surgical incision, making it convenient to identify the parathyroid with minimal disruption to the workflow. The initial success of OTIS imaging for intraoperative tissue visualization opens the door for its use as a platform technology in a range of fluorescence-guided surgery applications.

In the first in-human clinical pilot study, we demonstrate NIR fluorescence-based OTIS imaging provides high accuracy, label-free parathyroid detection visualized with a novel real-time tissue overlay strategy during parathyroidectomy and thyroidectomy procedures. OTIS can

distinguish diseased and normal parathyroid glands from surrounding tissues (i.e. thyroid gland, muscle, fat, blood vessels) with 100% accuracy based on NIR autofluorescence emission. The OTIS processing algorithm extracted fluorescent parathyroid glands for low background noise projection. Because we were in the process of refining the system throughout the study, we found that the feature extraction algorithm was not optimized for real-time image projection during measurement of two parathyroid glands. Because of time constraints during measurement, alterations to the processing parameters made post-operation to account for altered light conditions and depth of the glands in the incision causing fainter fluorescence. Additionally, the issue of false positives due to NIR light reflections on the surgical tools was addressed by creating a user-defined mask to eliminate projection of elements outside the incision. The green OTIS overlay provided a stark contrast directly over both diseased and normal parathyroid tissue to facilitate clear visual identification in the surgeon's line of site. OTIS co-registered these refined parathyroid fluorescence images with tissue in the operating field. This eliminates the mental gymnastics associated with orienting remotely displayed preoperative Sestamibi scintigraphy, computed tomography or ultrasound images with live tissue that has been distorted due to the surgical procedure.

The high resolution of NIR fluorescence-based OTIS (176 μm) enables the detection of both larger diseased glands and smaller normal glands, which can be as small as 2 to 4 mm in diameter. OTIS imaging therefore reveals its capacity to meet a clinical need by detecting smaller normal glands which go undetected by preoperative imaging modalities such as Sestamibi scintigraphy and ultrasound because of their small size and insufficient tracer uptake and acoustic difference compared to surrounding tissue (8). With resolution as high as 176 μm , OTIS imaging would be useful for cancer applications where precise resection of tumor margins is needed. Beyond spatial localization, OTIS can quantify parathyroid gland fluorescence in real-time. In this pilot study, normal and diseased parathyroid glands had a significantly higher autofluorescence than thyroid and surrounding tissues. Quantification of fluorescence intensity could in the future be encoded in the color scale and overlaid by OTIS to simultaneously depict both location and disease state of each parathyroid gland.

OTIS imaging rapidly and non-invasively identifies parathyroid gland location without the need for intraoperative parathyroid hormone assay or frozen section analysis, which require long wait times due to sample analysis several times during the procedure (30). In a patient with

primary hyperparathyroidism, NIR-based OTIS imaging exhibited improved specificity compared to visual inspection by immediately identifying a parathyroid adenoma candidate as being negative for parathyroid tissue based on its lack of NIR fluorescence and OTIS overlay. Due to uncertainty with visual inspection, the specimen was sent for frozen tissue analysis during surgery and determined to be benign thyroid tissue. This is a retrospective study designed only to gather data, rather than affective patient outcome. However, in the future, OTIS could provide real-time, non-invasive, intraoperative parathyroid detection to supplement visual inspection and avoid wait time and risk associated with unnecessary removal of normal tissue. Furthermore, NIR fluorescence-based OTIS imaging itself poses no risk to the patient. Endogenous parathyroid NIR fluorescence could be visualized with an 11.5 mW/cm^2 power density comparable to the 11 mW/cm^2 reportedly needed for parathyroid gland imaging with exogenous contrast (31). Thus, OTIS can improve the workflow of NIR fluorescence guided surgery by removing the need for exogenous contrast agents while maintaining safe levels of laser irradiation.

NIR based OTIS imaging is capable of detecting parathyroid glands regardless of perfusion status and at depths of 0.5 cm in tissue (32). The depth of detection of the 785 nm light used in NIR fluorescence-based OTIS imaging is greater than that of visible or ultraviolet light due to the low absorption and scattering of NIR light in tissue (cite). In this study, however, all parathyroid glands were exposed prior to measurement. Further studies will explore the depth dependent detection limit at which NIR fluorescence based OTIS imaging can identify the parathyroid gland. OTIS imaging of devascularized parathyroid tissue was demonstrated on an *ex vivo*, histologically confirmed parathyroid adenoma immediately after resection. Successful fluorescence detection and overlay validated the feasibility of the approach independent of tissue perfusion. It also demonstrates the potential utility of OTIS imaging in the pathology suite for rapid identification of tissue.

OTIS imaging is versatile for use with both endogenous and exogenous fluorescent compounds. A majority of fluorescent imaging systems in development are designed solely for imaging exogenous compounds such as ICG or methylene blue and have failed to detect low level endogenous fluorescence signals (31). While signal-to-background ratios increase when background autofluorescence is not detected during fluorescence dye imaging, detection of endogenous parathyroid gland fluorescence is a premier example where the ability of OTIS

imaging to detect low level endogenous signal replaces the need for exogenous dyes. In many surgical guidance applications such as angiography (33), perfusion monitoring (34), or sentinel lymph node detection (35), ICG is the optimal source of contrast. *In vitro* results validate NIR fluorescence based OTIS imaging for low concentration ICG fluorescence detection and contrast enhancement through false coloring such that even weak signals can be directly visualized. The ability of OTIS imaging to detect and amplify low level signals has the potential to simplify clinical applications by avoiding use of exogenous dyes or reducing dye dosage.

OTIS imaging is a platform approach that can be customized and extended beyond NIR fluorescence imaging for surgical guidance. The idea of projecting a full or feature extracted image directly in line with patient tissue would be transformative for a wide range of imaging techniques and clinical applications. For example, simple, well-validated changes to the detector, light source, and processing would make OTIS imaging applicable to laser Doppler flowmetry for perfusion imaging (36), multispectral imaging for cancer diagnosis (37), or optical metabolic imaging to monitor drug response (38). The uniform overlaying color map can be altered such that the intensity of the feature of interest (i.e. dye concentration, fluorescence emission, speckle contrast, etc.) is encoded in the chromaticity of the color scale rather than the intensity of a single color. Speckle contrast based OTIS imaging for vascular access detection may find a red-to-blue color scale optimal to identify relative velocity and location of blood flow. The presentation of OTIS overlay can be customized based on surrounding tissue color and the user's visual deficiencies. Future iterations of this technology are under development to operate with the operating room lights on in addition to providing these customizations in overlay visualization.

The ability of NIR fluorescence based OTIS imaging to detect and enhance visualization of parathyroid glands regardless of disease state fills a needed role in endocrine surgery and fluorescence guided surgery at large. Only recently have intraoperative fluorescence imaging system developers given attention to the importance of image presentation on patient outcomes. The overlay of extracted NIR fluorescence on the patient provides a significant leap forward for image guided surgery. Diseased and normal parathyroid glands visualization is enhanced by OTIS overlay directly on the tissue in real-time and without dyes, distant display monitors, or obstructive hardware to complicate the surgical workflow. This overlay imaging system presents a paradigm shift in surgical guidance as it allows direct visualization to aid tissue discrimination and thereby improve the outcome of endocrine neck surgery. The applications of OTIS extend

beyond anatomical detection of the parathyroid glands and may ultimately be extended to transform the standard-of-care for tissue diagnosis or tumor margin detection.

8.6 References

1. Sippel RS, Ozgul O, Hartig GK, Mack EA, Chen H. Risks and consequences of incidental parathyroidectomy during thyroid resection. *Anz J Surg.* 2007;77(1-2):33-6. doi: DOI 10.1111/j.1445-2197.2006.03972.x. PubMed PMID: WOS:000243634000009.
2. Gourgiotis S, Moustafellos P, Dimopoulos N, Papaxoinis G, Baratsis S, Hadjiyannakis E. Inadvertent parathyroidectomy during thyroid surgery: the incidence of a complication of thyroidectomy. *Langenbeck Arch Surg.* 2006;391(6):557-60. doi: DOI 10.1007/s00423-006-0079-8. PubMed PMID: WOS:000241612300003.
3. El Malki HO, Abouqal R. Systematic review and meta-analysis of predictors of post-thyroidectomy hypocalcaemia (*Br J Surg* 2014; 101: 307-320). *The British journal of surgery.* 2014;101(7):883. doi: 10.1002/bjs.9537. PubMed PMID: 24817656.
4. SEER Cancer Statistics Review, 1975-2012 [Internet]. National Cancer Institute. 2014. Available from: http://seer.cancer.gov/csr/1975_2012/.
5. Caron NR, Sturgeon C, Clark OH. Persistent and recurrent hyperparathyroidism. *Current treatment options in oncology.* 2004;5(4):335-45. PubMed PMID: 15233910.
6. Bhattacharyya N, Fried MP. Assessment of the morbidity and complications of total thyroidectomy. *Archives of otolaryngology--head & neck surgery.* 2002;128(4):389-92. PubMed PMID: 11926912.
7. Wells SA, Jr., Debenedetti MK, Doherty GM. Recurrent or persistent hyperparathyroidism. *Journal of bone and mineral research : the official journal of the American Society for Bone and Mineral Research.* 2002;17 Suppl 2:N158-62. PubMed PMID: 12412795.
8. Mohebati A, Shaha AR. Imaging techniques in parathyroid surgery for primary hyperparathyroidism. *American journal of otolaryngology.* 2012;33(4):457-68. doi: 10.1016/j.amjoto.2011.10.010. PubMed PMID: 22154018; PubMed Central PMCID: PMC3311773.
9. Chen H, Wang TS, Yen TW, Doffek K, Krzywda E, Schaefer S, et al. Operative failures after parathyroidectomy for hyperparathyroidism: the influence of surgical volume. *Ann Surg.* 2010;252(4):691-5. doi: 10.1097/SLA.0b013e3181f698df. PubMed PMID: 20881776.
10. McWade MA, Sanders ME, Broome JT, Solorzano CC, Mahadevan-Jansen A. Establishing the clinical utility of autofluorescence spectroscopy for parathyroid detection. *Surgery.* 2015. doi: 10.1016/j.surg.2015.06.047. PubMed PMID: 26454675.

11. McWade MA, Paras C, White LM, Phay JE, Solorzano CC, Broome JT, et al. Label-free Intraoperative Parathyroid Localization With Near-Infrared Autofluorescence Imaging. *The Journal of clinical endocrinology and metabolism*. 2014;99(12):4574-80. doi: 10.1210/jc.2014-2503. PubMed PMID: 25148235.
12. McWade MA, Paras C, White LM, Phay JE, Mahadevan-Jansen A, Broome JT. A novel optical approach to intraoperative detection of parathyroid glands. *Surgery*. 2013;154(6):1371-7. doi: DOI 10.1016/j.surg.2013.06.046. PubMed PMID: WOS:000327571200059.
13. Elliott JT, Dsouza AV, Davis SC, Olson JD, Paulsen KD, Roberts DW, et al. Review of fluorescence guided surgery visualization and overlay techniques. *Biomedical optics express*. 2015;6(10):3765-82. doi: 10.1364/BOE.6.003765. PubMed PMID: 26504628; PubMed Central PMCID: PMC4605037.
14. Krupinski EA. The role of perception in imaging: past and future. *Seminars in nuclear medicine*. 2011;41(6):392-400. doi: 10.1053/j.semnuclmed.2011.05.002. PubMed PMID: 21978443.
15. Manning DJ, Gale A, Krupinski EA. Perception research in medical imaging. *The British journal of radiology*. 2005;78(932):683-5. doi: 10.1259/bjr/72087985. PubMed PMID: 16046417.
16. Krupinski EA. Current perspectives in medical image perception. *Attention, perception & psychophysics*. 2010;72(5):1205-17. doi: 10.3758/APP.72.5.1205. PubMed PMID: 20601701; PubMed Central PMCID: PMC3881280.
17. Berguer R. Surgery and ergonomics. *Archives of surgery*. 1999;134(9):1011-6. PubMed PMID: 10487599.
18. Hanna GB, Shimi SM, Cuschieri A. Task performance in endoscopic surgery is influenced by location of the image display. *Ann Surg*. 1998;227(4):481-4. PubMed PMID: 9563533; PubMed Central PMCID: PMC1191300.
19. Stone R, McCloy R. Ergonomics in medicine and surgery. *Bmj*. 2004;328(7448):1115-8. doi: 10.1136/bmj.328.7448.1115. PubMed PMID: 15130981; PubMed Central PMCID: PMC406327.
20. Killory BD, Nakaji P, Gonzales LF, Ponce FA, Wait SD, Spetzler RF. Prospective evaluation of surgical microscope-integrated intraoperative near-infrared indocyanine green angiography during cerebral arteriovenous malformation surgery. *Neurosurgery*. 2009;65(3):456-62; discussion 62. doi: 10.1227/01.NEU.0000346649.48114.3A. PubMed PMID: 19687689.
21. Watson JR, Gainer CF, Martirosyan N, Skoch J, Lemole GM, Jr., Anton R, et al. Augmented microscopy: real-time overlay of bright-field and near-infrared fluorescence images.

J Biomed Opt. 2015;20(10):106002. doi: 10.1117/1.JBO.20.10.106002. PubMed PMID: 26440760.

22. Blackwell M, Nikou C, DiGioia AM, Kanade T. An image overlay system for medical data visualization. *Medical image analysis*. 2000;4(1):67-72. PubMed PMID: 10972322.

23. Sarder P, Gullicksrud K, Mondal S, Sudlow GP, Achilefu S, Akers WJ. Dynamic optical projection of acquired luminescence for aiding oncologic surgery. *J Biomed Opt*. 2013;18(12):120501. doi: 10.1117/1.JBO.18.12.120501. PubMed PMID: 24284472; PubMed Central PMCID: PMC4019413.

24. Mondal SB, Gao S, Zhu N, Sudlow GP, Liang K, Som A, et al. Binocular Goggle Augmented Imaging and Navigation System provides real-time fluorescence image guidance for tumor resection and sentinel lymph node mapping. *Scientific reports*. 2015;5:12117. doi: 10.1038/srep12117. PubMed PMID: 26179014; PubMed Central PMCID: PMC4503986.

25. Liu Y, Zhao YM, Akers W, Tang ZY, Fan J, Sun HC, et al. First in-human intraoperative imaging of HCC using the fluorescence goggle system and transarterial delivery of near-infrared fluorescent imaging agent: a pilot study. *Translational research : the journal of laboratory and clinical medicine*. 2013;162(5):324-31. doi: 10.1016/j.trsl.2013.05.002. PubMed PMID: 23747795; PubMed Central PMCID: PMC3805674.

26. Lakowicz JR. *Principles of Fluorescence Spectroscopy*: Springer Science & Business Media; 2013.

27. FitzGerald RA, Sehgal AR, Nichols JA, McHenry CR. Factors Predictive of Emergency Department Visits and Hospitalization Following Thyroidectomy and Parathyroidectomy. *Annals of surgical oncology*. 2015;22 Suppl 3:707-13. doi: 10.1245/s10434-015-4797-4. PubMed PMID: 26259757.

28. Cote V, Sands N, Hier MP, Black MJ, Tamilya M, MacNamara E, et al. Cost savings associated with post-thyroidectomy parathyroid hormone levels. *Otolaryngology--head and neck surgery : official journal of American Academy of Otolaryngology-Head and Neck Surgery*. 2008;138(2):204-8. doi: 10.1016/j.otohns.2007.11.021. PubMed PMID: 18241717.

29. Ready AR, Barnes AD. Complications of thyroidectomy. *The British journal of surgery*. 1994;81(11):1555-6. PubMed PMID: 7827875.

30. Conrad DN, Olson JE, Hartwig HM, Mack E, Chen H. A prospective evaluation of novel methods to intraoperatively distinguish parathyroid tissue utilizing a parathyroid hormone assay. *The Journal of surgical research*. 2006;133(1):38-41. doi: 10.1016/j.jss.2006.02.029. PubMed PMID: 16603189.

31. Hyun H, Park MH, Owens EA, Wada H, Henary M, Handgraaf HJ, et al. Structure-inherent targeting of near-infrared fluorophores for parathyroid and thyroid gland imaging.

Nature medicine. 2015;21(2):192-7. doi: 10.1038/nm.3728. PubMed PMID: 25559343; PubMed Central PMCID: PMC4319985.

32. Gerhard J. Müller AR. Laser-induced Interstitial Thermotherapy: SPIE Press; 1995.

33. Yannuzzi LA. Indocyanine green angiography: a perspective on use in the clinical setting. American journal of ophthalmology. 2011;151(5):745-51 e1. doi: 10.1016/j.ajo.2011.01.043. PubMed PMID: 21501704.

34. Hoffmann C, Compton F, Schafer JH, Steiner U, Fuller TF, Schostak M, et al. Intraoperative assessment of kidney allograft perfusion by laser-assisted indocyanine green fluorescence videography. Transplantation proceedings. 2010;42(5):1526-30. doi: 10.1016/j.transproceed.2010.01.069. PubMed PMID: 20620468.

35. Pitsinis V, Provenzano E, Kaklamanis L, Wishart GC, Benson JR. Indocyanine green fluorescence mapping for sentinel lymph node biopsy in early breast cancer. Surgical oncology. 2015. doi: 10.1016/j.suronc.2015.10.002. PubMed PMID: 26555151.

36. Wang RK, An L. Doppler optical micro-angiography for volumetric imaging of vascular perfusion in vivo. Optics express. 2009;17(11):8926-40. PubMed PMID: 19466142; PubMed Central PMCID: PMC2714191.

37. Qiu L, Pleskow DK, Chuttani R, Vitkin E, Leyden J, Ozden N, et al. Multispectral scanning during endoscopy guides biopsy of dysplasia in Barrett's esophagus. Nature medicine. 2010;16(5):603-6, 1p following 6. doi: 10.1038/nm.2138. PubMed PMID: 20383155; PubMed Central PMCID: PMC3052700.

38. Walsh AJ, Cook RS, Manning HC, Hicks DJ, Lafontant A, Arteaga CL, et al. Optical metabolic imaging identifies glycolytic levels, subtypes, and early-treatment response in breast cancer. Cancer research. 2013;73(20):6164-74. doi: 10.1158/0008-5472.CAN-13-0527. PubMed PMID: 24130112; PubMed Central PMCID: PMC3801432.

CHAPTER 9

CONCLUSIONS AND FUTURE DIRECTIONS

9.1 Summary and Integration

The overall objective of this dissertation is to develop an innovative optical technique for intraoperative parathyroid detection and lower the barriers to its clinical adoption. The parathyroid glands were previously shown to emit high levels of near-infrared (NIR) autofluorescence (1). In this work, I established NIR fluorescence spectroscopy as a highly accurate method to detect the parathyroid gland regardless of disease state. The NIR autofluorescence signal in the parathyroid gland was characterized across a large diverse patient population to determine the effects of patient factors like age, BMI, hormone levels, etc. In the second part of this dissertation, I evaluated the biological basis for the NIR fluorescence signal observed in parathyroid tissue. The behavior and sub-cellular location of the parathyroid fluorophore was characterized. Although the exact identity of the fluorophore is still unknown, these studies provide a sufficient basis for the clinical adoption of the parathyroid detection technique. This work brings the field one step closer to discovering the identity of a novel NIR endogenous fluorophore with potential applications beyond parathyroid detection. The last part of this dissertation involved the design and validation of a NIR fluorescence imaging approach to detect endogenous parathyroid fluorescence. I developed a novel projector-based fluorescence imaging approach to improve image visualization by overlaying autofluorescence images directly on the patient during surgery.

In Chapter 3, the feasibility of intraoperative NIR fluorescence spectroscopy for parathyroid detection was verified. The results of this study confirmed previous work done by Paras et al. (1), and shows parathyroid glands of patients with parathyroid and thyroid disease emits consistently higher peak autofluorescence at 822 nm than that of thyroid and surrounding tissues (n=45 patients) (2). Though parathyroid autofluorescence was consistently higher than thyroid across all patients, the ratio of parathyroid fluorescence to thyroid fluorescence varied from 1.2 to 18. The primary conclusion of this study is that NIR fluorescence spectroscopy is capable of reliable and repeatable detection of the parathyroid gland in patients undergoing thyroidectomy and parathyroidectomy regardless of the disease state.

In Chapter 4, a larger patient population was recruited for probe-based fluorescence spectroscopy measurements to determine the effects of normal patient variables on the clinical utility of this approach. Clinical adoption of this technique will require its utility across diverse patient characteristics. Over 260 parathyroid gland measurements (n=137 patients) demonstrated

the accuracy of this technique to be 97% for patients with benign thyroid disease, malignant thyroid disease, and hyperparathyroidism, with the lowest accuracy in patients with secondary hyperparathyroidism. The variability in parathyroid fluorescence intensity relative to thyroid fluorescence intensity was evaluated by correlating peak parathyroid intensities with body-mass index (BMI), vitamin D levels, serum calcium levels, age, gender, disease state, and parathyroid hormone levels. Hyperparathyroidism, low vitamin D levels, overweight or obese BMI, and high calcium levels were correlated with lower (but still detectable) parathyroid fluorescence signals. This study demonstrates the clinical utility of fluorescence guidance for parathyroid detection. Furthermore, the patient factors contributing to signal variability were critical to improving the understanding of the biological basis of the parathyroid fluorophore in future studies.

Chapter 5 and Appendix A characterized the endogenous near-infrared fluorophore in parathyroid gland tissue. NIR endogenous fluorophores with emission peaks greater than 800 nm are not common in literature. The observed parathyroid fluorophore we observe, therefore, is a novel finding. This chapter improved the understanding of parathyroid fluorescence behavior and location. This work was aimed at expanding and informing biomedical applications utilizing this novel fluorophore. NIR fluorescence microscopy was used to show subcellular localization of the fluorophore within the cytoplasmic regions of parathyroid gland tissue sections. Biochemical studies revealed the NIR fluorophore is highly robust and resistant to solubilization. The fluorescence signal is not easily quenched in response to heat, proteases, and denaturation with ionic detergents. The molecular weight of the fluorescence component was 15 kDa after SDS-PAGE. Autofluorescence at 822 nm was also observed in adrenal pheochromocytoma tissue, normal bulk pancreas and isolated pancreatic beta cells, and thyroid tissue, indicating the fluorophore may be involved in endocrine processes such as hormone synthesis and secretion. Secretory granules were identified as the leading hypothesis for the origin of the autofluorescence based on results of density gradient centrifugation, transmission electron microscopy, and immunohistochemistry. The primary conclusion of this chapter is that this NIR fluorophore is very resilient to quenching and present in multiple endocrine tissues. Secretory granules must be further explored as the origin of the signal.

In Chapter 6 and 7, the feasibility of NIR fluorescence imaging of endogenous parathyroid fluorescence was validated. The studies described in previous chapters used probe-based fluorescence spectroscopy and were therefore limited by their ability to provide only point

measurements. Parathyroid fluorescence detection was taken one step further by demonstrating the ability of imaging to convey the full spatial extent of fluorescence in the neck. In Chapter 6, lab validations established feasibility of endogenous NIR fluorescence imaging on three different imaging systems: a laboratory grade cooled-CCD camera, a photomultiplier tube based detector, and an adapted clinical endoscope camera. The clinical endoscope camera showed optimal NIR fluorescence imaging, despite not being designed specifically for NIR imaging. In Chapter 7, this adapted endoscope camera system achieved the first ever reported results of intraoperative parathyroid autofluorescence imaging on humans *in vivo*. The conclusion of Chapters 6 and 7 are that we can accomplish real-time intraoperative autofluorescence imaging of the parathyroid glands regardless of disease state.

Chapter 8 describes a novel approach to fluorescence imaging using a projector to overlay fluorescence images on the patient for direct tissue visualization in the surgeon's line of sight. Traditional fluorescence imaging systems, such as the one tested in Chapter 7, relies on a remote display monitor to deliver tissue information to surgeons during operation. In this study, I developed a novel projector imaging system, called Overlay Tissue Imaging System (OTIS). OTIS achieved real-time NIR fluorescence imaging, feature extraction, and projection of fluorescence images directly onto the patient undergoing parathyroid and thyroid surgery. Hands-free, continuous image collection and overlay allows surgeons to view fluorescence in the neck while conducting the procedure. Rather than overlaying the surgical field with the entire NIR fluorescence image, OTIS projects a refined image that highlights only the NIR fluorescent signal from parathyroid tissue. The intraoperative extraction algorithm effectively amplifies low-level endogenous fluorescence and reduces noise associated with stray operating room light and background autofluorescence. The results of OTIS imaging in this study presents a paradigm shift in surgical guidance by enabling direct visualization to aid tissue discrimination and thereby improving the outcome of endocrine neck surgery. OTIS is a platform technology that could be broadly applicable to disease indications and imaging modalities beyond NIR fluorescence parathyroid detection.

9.2 Major Conclusions

- We have developed a new method for detecting the parathyroid glands during surgery using NIR autofluorescence imaging and spectroscopy. This technology identifies both diseased and normal glands, providing a much needed real-time supplement to visual inspection.
- Fluorescence detection of the parathyroid gland has an accuracy of 97% and is largely unaffected by patient demographics and clinical characteristics.
- Disease state, BMI, preoperative serum calcium levels, and preoperative vitamin D levels were determined to significantly contribute to the variability in parathyroid fluorescence intensity relative to thyroid intensity. Though these variables did not hinder parathyroid fluorescence detection, future clinical systems could incorporate these variables into the parathyroid detection algorithm.
- Fluorescence detection of parathyroid glands in patients with secondary hyperparathyroidism had a much lower accuracy of 54%. The likely down-regulation of the parathyroid fluorophore provides an avenue for future studies to identify its exact biological source.
- A NIR endogenous fluorophore has been discovered with the longest red emission wavelength peak (822 nm) ever before reported, to our knowledge.
- Biochemical studies have revealed the endogenous parathyroid fluorophore is likely a protein or protein co-factor with fluorescence that is highly resistant to quenching in response to heat, proteases, and denaturation with stringent detergents.
- The endogenous NIR fluorophore is present in the parathyroid gland, thyroid gland, adrenal pheochromocytoma, and pancreas, indicating its identity is likely due to endocrine functioning like hormone synthesis or secretion. The secretory granules are the leading hypothesis.
- NIR fluorescence imaging of the endogenous fluorophore in diseased and normal parathyroid glands can achieve 2D spatial fluorescence information over the entire surgical incision in real-time. The parathyroid autofluorescence is strong enough to be imaged by non-NIR optimized detectors.
- Overlay Tissue Imaging System (OTIS) is a novel imaging approach that can overlay fluorescence information directly on the patient using a projector for intraoperative

parathyroid detection. We were the first to show overlay imaging of NIR endogenous fluorescence in humans. This platform technology can be expanded to applications beyond parathyroid imaging.

9.3 Recommendations

The results of this dissertation lead to a number of recommendations for future research directions in the area of fluorophore evaluation and technology development for surgical guidance.

9.3.1 Recommendations for NIR fluorophore evaluation

The fluorophore evaluation studies described in this dissertation lay the groundwork for future work to identify the precise source of NIR fluorescence. Significant efforts described in this dissertation identify the subcellular location and biochemical behavior of the autofluorescence. The studies suggest the fluorophore may be a protein or protein co-factor localized in the secretory granules of endocrine tissue. For this work to be fully utilized by the fields of endocrinology, surgery, and biophotonics, the precise identity of this fluorophore must be established. This task is not trivial and will require significant biochemical expertise. I recommend several approaches to identify the fluorophore.

First, I recommend a large scale study replicating the SDS-PAGE results that showed autofluorescence at 15 kDa in parathyroid gland tissue homogenates. This study should be expanded to adrenal pheochromocytoma and pancreatic islet samples because of the high autofluorescence observed in these tissue samples. Parathyroid adenoma, adrenal pheochromocytoma, and pancreas tissue homogenates should be separated by molecular weight using SDS-PAGE. Mass spectrometry can be performed on excised bands to identify common components across fluorescent samples in each tissue type. This study should be replicated to achieve high enough power to discern which tissue components are consistently expressed across all samples in order to distinguish true results from tissue variability and contamination.

Moving forward, fluorophore purification efforts may experience better traction when performed on isolated cell lines such as parathyroid chief cells, pancreatic beta cells, and human pheochromocytoma cell lines. Cell lines are not contaminated with the same extracellular debris (i.e. extracellular fat, connective tissues, blood vessels) that distort the results of purification

experiments with bulk tissue samples. Parathyroid cells are reportedly very difficult to culture, which may require studies to move towards pancreatic and adrenal pheochromocytoma cell lines. The abundance of diabetes related research on Vanderbilt's campus make pancreatic beta cells relatively easy to obtain for future studies.

The multidimensional protein identification technology (MudPIT) analysis described in Appendix A did not yield useful results because of the abundance of proteins present in the parathyroid and thyroid homogenates that were initially run. Inputting more refined tissue homogenates, with a more narrow range of tissue components, into MudPIT may produce more informative results. The past study compared differential expressions of parathyroid and thyroid samples. In future studies, differential expression profiles of parathyroid adenoma and adrenal pheochromocytoma tissue could be compared because pheochromocytoma tissue has higher autofluorescence than thyroid, which may yield more conclusive results. Purified parathyroid and adrenal pheochromocytoma samples can be obtained using ion exchange chromatography to separate samples based on affinity to the ion exchange column. An array of samples can be collected as they are eluted from the ion exchange column over time and their NIR fluorescence measured. The eluted samples with the highest NIR autofluorescence can then be input into the MudPIT analysis to generate differential expression profiles for parathyroid and adrenal pheochromocytoma. This experiment could yield more definitive candidates for the NIR fluorophore.

The secretory granule hypothesis can be further explored by reproducing the density gradient centrifugation experiments from Chapter 5 to achieve large volumes of the granular components previously shown in transmission electron microscopy images. This can be performed with adrenal pheochromocytoma, parathyroid and pancreas tissue. Large volumes of these fluorescent granular structures can be disrupted, and the contents can be run through SDS-PAGE. Autofluorescent bands can be trypsinized and measured with mass spectrometry. Previous experiments were limited by small volumes of granular material, which could not provide enough protein for accurate measurements. This experiment may validate the secretory granule hypothesis and determine the fluorescent component within the granules.

Finally, clinical parathyroid fluorescence measurements can be correlated to Sestamibi Scintigraphy uptake. Sestamibi Scintigraphy is one of the most commonly used preoperative imaging modalities for localization of hypersecreting parathyroid glands in patients with primary

hyperparathyroidism (PHPT). The exact mechanism of selective radiotracer uptake in abnormal parathyroid glands remains debatable. High mitochondrial activity is considered to be the major component of tracer uptake by human parathyroid tissue in patients with PHPT (3). Furthermore, it is widely accepted that Sestamibi scintigraphy poorly uptakes in parathyroid glands that are hyperplastic as a result of secondary hyperparathyroidism (4). It may yield interesting information to study the parathyroid fluorescence intensity across all 140 patients measured with probe-based NIR spectroscopy and correlate the signals with the radiotracer uptake of the abnormal parathyroid glands.

Identification of the exact nature of the NIR endogenous fluorophore observed in parathyroid tissue will require a multi-pronged approach. The experiments outlined in this section provide initial steps to continue to work in this dissertation.

9.3.2 Recommendations for the Development of Probe-based Parathyroid Detection

The development of probe-based detection of the parathyroid gland for research purposes has largely been wrapped up. This work has culminated in the development of a commercial parathyroid detection system, PTEye, in partnership with Anasys Biomedical Instruments. While much of the research and development work is being done by the engineers at Anasys, Vanderbilt researchers will evaluate the validity of the PTEye system before sending it out to other centers for clinical testing. FDA safety studies in patients will need to be conducted at the Vanderbilt Endocrine Surgery Center. It is important that the student involved in this study has a solid knowledge of the engineering behind the device as well as the clinical workflow to bridge a connection between the company and clinicians during this testing.

9.3.3 Recommendations for the Development of Fluorescence Imaging

The Overlay Tissue Imaging System (OTIS) for parathyroid detection is a promising surgical guidance tool that is ripe for further development. To begin with, the effects of non-flat visual fields on projector image alignment need to be characterized. While the parathyroid glands in the reported study with OTIS imaging required the exposure of the parathyroid gland on the surface of the operative field, the reality of surgery is that tissue can be located deep within the surgical incision. Advanced calibration processes could be included for 3D imaging, such as the use of 3D calibration phantoms. Another concern regarding tissue located deep within the

surgical incision is the ability to deliver light to these locations. Currently, the imaging system has an expanded beam illuminating the surgical field from one side of the imaging system. Shadowing effects can occur if a surgical tool or surgeon's hand is in the way or if the tissue is deep in the incision. A ring of lights could replace the current illumination scheme to minimize this problem. NIR light emitting diodes (LEDs) may prove to be the most compact and efficient way to integrate this illumination scheme.

The first generation OTIS technology was perceived to be bulky by the surgeons and residents who tested it during endocrine surgery. The sizeable form factor was largely due to the large LED projector used for image overlay. The projector was an off the shelf consumer model typically used for watching movies. Recently, several companies have been developing pico-projectors that are much smaller and could be integrated into OTIS to minimize its size.

Another significant area of development for OTIS is adaptation such that it can operate with the room lights on. Although our partnering surgeons are accustomed to turning the surgical lights off during data collection due to their experience with the probe-based spectroscopy study, the requirement for darkness in the operating room is not practical. The overhead room lights, the surgical lights, and the surgeon's head lamp all have significant intensity in the NIR wavelength range that causes obstruction of the endogenous fluorescence signal. This problem can be bypassed in several ways. The easiest solution would be to integrate a custom surgical overhead light that does not have high intensity in the NIR spectrum. Many LED white light sources are designed without NIR components and could prove to be quick solution. This approach would still require the lights native to the operating room to be turned off, but it would still allow surgeons to visualize the field under normal brightness conditions. Another solution is to integrate an illumination and image processing scheme whereby successive bright light frames are collected and subtracted from consecutive NIR fluorescence images while strobing NIR and white light sources similar to Kittle et al (5). Rapid processing hardware and software to achieve real-time images would be needed for this approach.

Anasys Biomedical Instruments is building a next generation commercial system based on the success of the first-generation OTIS results. They are implementing several proprietary changes to the projection, processing, and illumination. Anasys relies on our access to the clinical environment and well-outfitted optical laboratory space. The next researcher working on

this project at Vanderbilt will need to work closely with the company to troubleshoot these changes.

The final recommendation for the development of the OTIS system is to extend its use to applications beyond parathyroid detection by testing it on adrenal surgeries. Chapter 5 of this dissertation discussed the highest levels of NIR autofluorescence were found in adrenal pheochromocytoma tissues. OTIS could be used to overlay fluorescence information on tumor tissue to help delineate tumor margins. This is just one potential application for the extension of the device. As the mechanism of the NIR autofluorescence is uncovered, further applications of OTIS will be made obvious.

9.3.4 Parathyroid Perfusion Imaging

A related area of development with high clinical need is the adaptation of perfusion imaging to the parathyroid detection technology. We have consistently received feedback from endocrine surgeons both at Vanderbilt and outside medical centers that understanding the perfusion status of the parathyroid glands during surgery is very important. The inferior and superior parathyroid glands receive their blood supply from the inferior and superior thyroid arteries, respectively. Especially during thyroid resection, attempts to isolate the thyroid gland may result in accidental devascularization of the parathyroid glands. When this occurs, many surgeons rely on parathyroid gland autotransplantation, a process whereby the parathyroid glands are taken from their normal location and placed in the muscle bed on the side of the neck or in the forearm. The parathyroid glands will develop a new blood supply and regain function in 4 to 6 weeks (6). The efficacy of this precautionary approach is difficult to quantify because it is hard to determine whether normocalcemia is regained due to the autotransplanted parathyroid gland or the parathyroid glands still present in the neck.

Endocrine surgeons desire a tool that can inform them on the perfusion status of the parathyroid glands to help them decide whether to perform autotransplantation. Our clinical studies have shown that the NIR autofluorescence signal of the parathyroid gland at 822 nm is not affected by the perfusion status of the parathyroid glands. However, laser speckle imaging is an optical technique that could be integrated into the OTIS system to provide information on the perfusion status of the parathyroid glands. Laser speckle imaging has shown success for perfusion imaging in several applications such as brain microvasculature imaging (7). When an

object is illuminated by laser light, the backscattered light will form a random interference pattern consisting of dark and bright areas. This pattern is called a speckle pattern. If the illuminated object is static, the speckle pattern is stationary. When there is movement in the object, such as red blood cells in a tissue, the speckle pattern will change over time (8). Previous work by other research groups have shown the success of laser speckle imaging with 785 nm light (9). Therefore, both the light source and the NIR camera that is already in place in the OTIS system can be used to garner perfusion information. Changes will need to be made to the processing algorithms to extract the speckle contrast. Another concern is the band-pass filter in front of the NIR camera is designed to filter out the 785 nm light for fluorescence imaging. In speckle imaging, the 785 nm light is necessary to provide contrast. Therefore, a motor could be implemented in front of the NIR camera such that the band-pass filter is in place while in parathyroid detection (NIR fluorescence) mode and the filter is removed while in perfusion detection (laser speckle) mode. The speckle information could be encoded in a separate color than the fluorescence information. For example, NIR fluorescence could be overlaid on the tissue in green, positive perfusion could be overlaid in blue, and negative perfusion could be overlaid in red. A dual modality imaging system has the potential to transform endocrine surgery and capture the attention of the biophotonics field.

9.4 Contributions to the Field and Societal Impact

Through this dissertation, I have made many contributions to the fields of endocrine surgery and biophotonics. I have developed a technique to detect the parathyroid glands during surgery and avoid complications associated with inadequate localization. I have discovered and characterized a novel fluorophore in the NIR spectrum that is the first of its kind. Finally, I have developed a paradigm-shifting imaging approach that overlays the fluorescence images directly on the patient, replacing the need for distracting surgical monitors. The details and widespread implications of these contributions are described below.

9.4.1 Impact on Endocrine Surgery

First and foremost, the most profound impact this dissertation work may have is on the individual lives of men and women undergoing parathyroid or thyroid surgery. Without a suitable means to detect the parathyroid glands, a patient can leave the operating room with a

“life sentence”, which was the description given by one woman suffering from permanent hypocalcemia after complications in thyroid surgery. She describes her condition further saying, “My life changed in a matter of hours [after surgery]. I went from being a healthy, active, productive wife and working mother of three, to a ‘sick’ person with a rare disease” (10). This woman and many others have experienced a drastically decreased quality of life due to difficulty finding parathyroid glands during surgery.

Accidental removal or damage to parathyroid glands can cause transient and permanent hypocalcemia in 5% and 1%, respectively, of patients undergoing thyroid surgery. These patients experience numbness, tingling, muscle twitching, spasms, cramps, abnormal heart rhythms, and seizures as a result of accidental parathyroid removal or damage. In the long term, the side effects become much more serious such as kidney damage, cataracts, and calcification of soft tissues. Especially patients in rural settings receiving surgery in low-volume centers may especially benefit from this dissertation work. Studies have shown there is higher risk of surgical error due to improper parathyroid identification from surgeons with low experience levels (11). In the US alone, over 60,000 patients permanently affected by this condition must rely on daily supplementation of calcium and vitamin D or parathyroid hormone to replace the natural regulation of the parathyroid gland (12). While drug companies have poured millions of dollars into development of parathyroid hormone replacement therapies (13), ***this dissertation provides an intraoperative parathyroid detection tool to prevent the hypoparathyroidism before it even starts.***

We are the first to develop a label-free parathyroid detection tool for real-time intraoperative guidance during thyroid and parathyroid surgeries. This technology is unique, and there is no predicate to the device. Our method holds several clear advantages over current methods that I believe will allow it to gain market traction and find a permanent place in the operating room in the future. First, our method provides ***intraoperative*** surgical guidance to the parathyroid glands. The current parathyroid imaging modalities such as MRI, ultrasound, Sestamibi scintigraphy, and CT are limited because they can only provide preoperative images (14). Tissue is distorted during surgery, which can make it difficult to correlate with preoperative images. NIR autofluorescence detection of the parathyroid gland provides relevant images during the procedure. Furthermore, this method gives ***real-time*** information on parathyroid gland location. Intact parathyroid hormone (PTH) assay and frozen section analysis provide intraoperative —

but not real-time — information on whether the parathyroid gland was removed. Due to the short half-life of PTH, Intact PTH assays can confirm the removal of all hyperfunctioning parathyroid tissue by measuring PTH levels in blood samples obtained 5, 10, and 15 minutes after excision of adenomas (15). Frozen section analysis requires time to excise tissue and send to the pathology suite for analysis. Both of these methods add time to the surgical procedure that NIR parathyroid autofluorescence detection does not. These methods also rely on the removal of patient samples, unlike our *non-invasive* method. NIR parathyroid autofluorescence detection is the first imaging tool that can find parathyroid glands *regardless of disease state* unlike pre-operative imaging modalities that can only detect diseased glands. NIR fluorescence detection, therefore, fills a large unmet clinical need for detection of normal parathyroid glands in order to avoid hypocalcemia as a result of accidental parathyroid removal or injury during thyroid surgery. Finally, our method works *without tracers or dyes*. Sestamibi scintigraphy relies on the uptake of the radio tracer Technetium, and previous research efforts have relied on methylene blue (16), 5-aminolevulinic acid (17), and T700/T800 (18) to provide sufficient contrast for parathyroid gland imaging. Due to autofluorescence in the parathyroid gland, no pre-administered extrinsic dye or tracer is necessary. As a result, the technique is safer, takes less time, and is less prone to false positives.

The overlay imaging approached I achieved through the design and testing of the OTIS imaging system provides an attractive alternative to current image visualization methods used in endocrine surgery. Rather than viewing ultrasound images or Sestamibi scans on a remote screen, OTIS will provide real-time overlay directly on the patient. Endocrine surgeons will no longer need to divert their attention away from the neck incision to collect information on parathyroid location. OTIS will provide a supplement to their visual inspection in a highly unique way that has never before been introduced to the field of endocrine surgery.

The work I accomplished will greatly lower the barrier of bringing parathyroid NIR fluorescence detection technology into the clinic by demonstrating efficacy, utility over diverse patient factors, safety, and easy integration into the clinic. I showed NIR fluorescence spectroscopy can detect all parathyroid glands with 97% accuracy, which improves upon the current standards of care for parathyroid detection. Demonstration of the viability of the technique over diverse patient factors was necessary to ensure surgeons that the technique is useful across their patient population. The development of OTIS as a novel overlay imaging

approach sets the stage for imaging systems that deliver more intuitive direct information at the surgical incision. Finally, I obtained an improved understanding of the parathyroid fluorophore mechanism. Though exact fluorophore identity was not uncovered, I believe our new understanding of the behavior and location of the fluorophore will allow the device to move forward into clinical use.

We have already received overwhelming enthusiasm about this parathyroid detection tool from patients and surgeons both in the United States and abroad. The standard of care for parathyroid detection has not been altered in many years, and it seems as though endocrine surgeons desire new breakthroughs to meet the clinical need. In 2015, I presented this work at the American Association for Endocrine Surgeons Annual Meeting, which gathered approximately 300 leading endocrine surgeons. The presentation won “Best Basic Science Presentation”. I believe this is one reflection of the excitement for the technology and is an indicator for its quick adoption.

9.4.2 Impact on Biophotonics

Optical methods have been studied for many years as a non-intrusive, real-time automated tool for tissue detection. However, these methods have typically been applied to the detection of disease. In contrast, this dissertation provides a tool for anatomical detection of the parathyroid gland using NIR autofluorescence.

9.4.2.1 Characterization of a new endogenous fluorophore

I am the first to characterize an endogenous near-infrared fluorophore present in the parathyroid glands. Unlike ultraviolet and visible wavelengths, endogenous fluorophores are not common in the NIR region. The endogenous NIR parathyroid fluorophore discovered by our lab and evaluated in this dissertation is highly unique because of its long emission wavelength. Imaging of the NIR parathyroid fluorophore takes advantage of the minimal tissue absorbance and autofluorescence in the “optical window” between 650 and 1450 nm without requiring exogenous dyes. This dissertation is a crucial step towards identifying the precise mechanism of the fluorescence. I believe this work will lead many surgical guidance, diagnostic, and basic science applications beyond parathyroid gland imaging. Similar fluorescence signals observed in adrenal pheochromocytoma and pancreatic islet tissue suggests it can be used as a marker for

surgical guidance in other types of endocrine surgeries. Once the identity of the fluorophore is established, it could be used as a diagnostic indicator for disease progression. I believe the robust, degradation-resistant, heat-resistant, detergent-resistant nature of the NIR fluorophore makes it a very attractive biomarker that will be widely useful in the biophotonics field.

This discovery could change the course of action for NIR dye developers. They will need to be aware of this endogenous NIR fluorophore to avoid its contributions to background autofluorescence. As previously mentioned, NIR wavelengths are commonly taken advantage of in dye applications because it has few known endogenous fluorophores. Dye developers will need to adjust their concept of the optical window to avoid mistaking fluorescence from this NIR endogenous fluorophore for fluorescence emitted from their NIR dyes. In fact, it is possible that researchers reporting high levels of background NIR autofluorescence in tissue measurements of, for example, soft-tissue sarcomas (19) and colon (20) are detecting the same NIR fluorophore. Overall, researchers must be consider the best applications to utilize the fluorophore and when to avoid it.

This work could lead to new applications in diagnostics, therapeutics and basic science. The field of endocrinology could benefit from studying this fluorophore as a way to achieve better understanding of normal and diseased processes. For example, metastasized tumor cells expressing the fluorophore could easily be tracked in animal models to understand the process by which cancer spreads. The observation of high autofluorescence in pancreatic beta cells could lead to expanded diabetes related studies using the fluorophore as a marker. In the future, the fully isolated fluorophore could be used in many applications outside of endocrine research. If the isolated fluorophore is determined not to be toxic or affect protein activity or mobility after fusion, the isolated fluorophore could be used as a fluorescent tag for live-cell fluorescence microscopy systems. Most small fluorescent molecules such as FITC (fluorescein isothiocyanate) is strongly phototoxic when used in live cells. This fluorophore, like green fluorescent protein, could be used to observe cells over time that express this fluorescent protein (21). I predict the uses for this fluorophore are vast due to its resistance to heat, photobleaching, detergents, and degradation, much like green fluorescent protein.

Finally, it is possible that the fluorophore observed is a protein or protein co-factor that has never been discovered. This dissertation has focused on identifying the fluorophore from libraries of pre-established proteins or co-factors. Future work may establish the fluorophore as a

novel component, which would bring new understanding to endocrinology and mark a significant advancement in the scientific field.

9.4.2.2 Novel imaging approach

The overlay imaging approach developed in this dissertation is fundamentally unlike any standard of care imaging modality. Projecting the fluorescence images directly on the patient provides easily interpreted information directly on the patient. Display monitors, which have been a staple in surgical imaging, could be replaced by overlay imaging in the future. The OTIS imaging system is the first of its kind to achieve direct image overlay of autofluorescence on human patients during surgery.

OTIS is a platform technology. Although we have applied OTIS imaging to NIR fluorescence imaging of the parathyroid gland, I believe it can be extended to many optical imaging modalities and disease states. With changes to the detector, filters, processing algorithm, or light source, OTIS can detect and overlay laser speckle perfusion information, drug responses, cancer margins, etc. With further refinement of the technology (i.e. decreasing the footprint), I believe we will see the overlay technique widely applied in the future.

9.4.3 Commercialization

This dissertation work extends beyond academic boundaries. The commercialization pathway is underway as a result of our close collaboration with Anasys Biomedical Instruments who have licensed this technology from Vanderbilt University. During the course of this PhD, I was able to assist the company in taking the device from the drawing board, to a benchtop prototype, to its current commercial design. I gave significant input on the scientific development such as choice of light source, type of detector, design of the probe, functionality of the display monitor, and configuration of the parathyroid detection algorithm. I led the clinical tests of the device across multiple stages of its development while facilitating conversations between our surgeon collaborators and commercial partners to identify appropriate design constraints. Patent protection of the probe-based device has just been approved in Europe, which is likely where the device will first go on the market. PTEye is currently undergoing safety testing. It is also in the approval process with the FDA for class determination (513g) as well as a presubmission for going De Novo. There is no predicate to the parathyroid detection technology

we have developed. In many ways this is highly favorable because it means the device has little competition in the market. On the flip side, however, the FDA approval process is much lengthier. A majority of the development to date has been done on the probe-based parathyroid detection system (PTEye), though the overlay imaging system is also under development. A non-provisional patent has recently been submitted for the overlay imaging technology similar to the design described in Chapter 8.

Navigating this process alongside Anita Mahadevan-Jansen (the primary inventor), the Vanderbilt technology transfer office, and Anasys Biomedical Instruments was one of the most invaluable components of my PhD training. Through this experience, I learned the effort required to commercialize a medical device. I observed and directly contributed to the translation of our laboratory grade spectroscopy system into a commercial design. At the guidance of the engineers working for Anasys, I learned the considerations that commercial medical device makers must have and that they often contrast with the considerations of researchers in academic environments. I learned one basic pathway towards regulatory approval of a medical device and the importance of constant communication with the Food and Drug Administration (FDA) throughout. I worked with lawyers to draft a patent for the protection of our intellectual property, which taught me the nuances of legal language. The commercialization of this technology is a biomedical engineering success story. Many biomedical technologies fall into the “valley of death”, a term for the place new technologies go to die if the divide between basic research discovery and marketable product development is not navigated (22). I believe improved parathyroid detection through the commercial availability of this technology is imminent.

9.5 Protection of Research Subjects

As stated in the materials and methods sections of each chapter, all patient samples were de-identified and collected with approval from the Vanderbilt University Institutional Review Board (#070795). Prior to clinical measurements during parathyroidectomy and thyroidectomy surgeries, informed written consent was obtained by the surgeon in a manner approved by the Vanderbilt IRB (#070795).

9.6 References

1. Paras C, Keller M, White L, Phay J, Mahadevan-Jansen A. Near-infrared autofluorescence for the detection of parathyroid glands. *J Biomed Opt.* 2011 Jun;16(6). PubMed PMID: WOS:000293086800038. English.
2. McWade MA, Paras C, White LM, Phay JE, Mahadevan-Jansen A, Broome JT. A novel optical approach to intraoperative detection of parathyroid glands. *Surgery.* 2013 Dec;154(6):1371-7. PubMed PMID: WOS:000327571200059. English.
3. Kannan S, Milas M, Neumann D, Parikh RT, Siperstein A, Licata A. Parathyroid nuclear scan. A focused review on the technical and biological factors affecting its outcome. *Clinical cases in mineral and bone metabolism : the official journal of the Italian Society of Osteoporosis, Mineral Metabolism, and Skeletal Diseases.* 2014 Jan;11(1):25-30. PubMed PMID: 25002876. Pubmed Central PMCID: 4064437.
4. Torregrosa JV, Fernandez-Cruz L, Canalejo A, Vidal S, Astudillo E, Almaden Y, et al. (99m)Tc-sestamibi scintigraphy and cell cycle in parathyroid glands of secondary hyperparathyroidism. *World journal of surgery.* 2000 Nov;24(11):1386-90. PubMed PMID: 11038211.
5. Butte PV, Mamelak A, Parrish-Novak J, Drazin D, Shweikeh F, Gangalum PR, et al. Near-infrared imaging of brain tumors using the Tumor Paint BLZ-100 to achieve near-complete resection of brain tumors. *Neurosurgical focus.* 2014 Feb;36(2):E1. PubMed PMID: 24484247.
6. Tartaglia F, Blasi S, Giuliani A, Merola R, Livadoti G, Krizzuk D, et al. Parathyroid autotransplantation during total thyroidectomy. Results of a retrospective study. *International journal of surgery.* 2015 Dec 18. PubMed PMID: 26708849.
7. Dunn AK. Laser speckle contrast imaging of cerebral blood flow. *Annals of biomedical engineering.* 2012 Feb;40(2):367-77. PubMed PMID: 22109805. Pubmed Central PMCID: 3288249.
8. Boas DA, Dunn AK. Laser speckle contrast imaging in biomedical optics. *J Biomed Opt.* 2010 Jan-Feb;15(1):011109. PubMed PMID: 20210435. Pubmed Central PMCID: 2816990.
9. Durduran T, Burnett MG, Yu G, Zhou C, Furuya D, Yodh AG, et al. Spatiotemporal quantification of cerebral blood flow during functional activation in rat somatosensory cortex using laser-speckle flowmetry. *Journal of cerebral blood flow and metabolism : official journal of the International Society of Cerebral Blood Flow and Metabolism.* 2004 May;24(5):518-25. PubMed PMID: 15129183.
10. Melanson J. Living with Hypoparathyroidism 2015 [cited 2016]. Available from: <http://running4rare.org/2015/02/09/living-with-hypoparathyroidism/>.

11. Ernandes-Neto M, Tagliarini JV, Lopez BE, Padovani CR, Marques Mde A, Castilho EC, et al. Factors influencing thyroidectomy complications. *Brazilian journal of otorhinolaryngology*. 2012 Jun;78(3):63-9. PubMed PMID: 22714849.
12. Pahon E. FDA approves Natpara to control low blood calcium levels in patients with hypoparathyroidism 2015 [cited 2016]. Available from: <http://www.fda.gov/NewsEvents/Newsroom/PressAnnouncements/ucm431358.htm>.
13. Recombinant human parathyroid hormone (Natpara). *The Medical letter on drugs and therapeutics*. 2015 Jun 8;57(1470):87-8. PubMed PMID: 26035748.
14. Mohebati A, Shaha AR. Imaging techniques in parathyroid surgery for primary hyperparathyroidism. *American journal of otolaryngology*. 2012 Jul-Aug;33(4):457-68. PubMed PMID: 22154018. Pubmed Central PMCID: 3311773.
15. Fraker DL, Harsono H, Lewis R. Minimally invasive parathyroidectomy: benefits and requirements of localization, diagnosis, and intraoperative PTH monitoring. long-term results. *World journal of surgery*. 2009 Nov;33(11):2256-65. PubMed PMID: 19763685.
16. van der Vorst JR, Schaafsma BE, Verbeek FP, Swijnenburg RJ, Tummers QR, Hutteman M, et al. Intraoperative near-infrared fluorescence imaging of parathyroid adenomas with use of low-dose methylene blue. *Head & neck*. 2014 Jun;36(6):853-8. PubMed PMID: 23720199. Pubmed Central PMCID: 3779489.
17. Asher SA, Peters GE, Pehler SF, Zinn K, Newman JR, Rosenthal EL. Fluorescent Detection of Rat Parathyroid Glands via 5-Aminolevulinic Acid. *Laryngoscope*. 2008 Jun;118(6):1014-8. PubMed PMID: WOS:000260662200011. English.
18. Hyun H, Park MH, Owens EA, Wada H, Henary M, Handgraaf HJ, et al. Structure-inherent targeting of near-infrared fluorophores for parathyroid and thyroid gland imaging. *Nature medicine*. 2015 Feb;21(2):192-7. PubMed PMID: 25559343. Pubmed Central PMCID: 4319985.
19. Nguyen JQ, Gowani Z, O'Connor M, Pence I, Nguyen TQ, Holt G, et al. Near-infrared autofluorescence spectroscopy of in vivo soft tissue sarcomas. *Optics letters*. 2015 Dec 1;40(23):5498-501. PubMed PMID: 26625035.
20. Shao X, Zheng W, Huang Z. In vivo diagnosis of colonic precancer and cancer using near-infrared autofluorescence spectroscopy and biochemical modeling. *J Biomed Opt*. 2011 Jun;16(6):067005. PubMed PMID: 21721826.
21. Zimmer M. Green fluorescent protein (GFP): applications, structure, and related photophysical behavior. *Chemical reviews*. 2002 Mar;102(3):759-81. PubMed PMID: 11890756.
22. Frederickson RM. Escaping the valley of death. *Molecular therapy : the journal of the American Society of Gene Therapy*. 2012 Mar;20(3):476-8. PubMed PMID: 22378029. Pubmed Central PMCID: 3293617.

APPENDIX A

**ALTERNATIVE APPROACHES TO INVESTIGATE THE SOURCE OF NIR
AUTOFLUORESCENCE IN THE PARATHYROID GLAND:
UNPUBLISHED RESULTS**

A1.1 Abstract

The following work consists of unpublished results to alternate approaches towards understanding the biological basis of parathyroid NIR autofluorescence (Specific Aim 2). It outlines the positive and negative findings of experiments not included in the submitted manuscript, which is Chapter 5 of this dissertation.

A1.2 Background and Motivation

At the beginning of this project, there was very little known about the nature of the NIR fluorophore in the parathyroid gland. We approached this problem through simultaneous “top-down” and “bottom-up” approaches. In the top-down approach, we tested specific hypotheses formed through our clinical data and experimental results. The initial fluorescence spectroscopy results showing high levels of NIR autofluorescence in the parathyroid gland, lower levels in the thyroid, and no autofluorescence in the muscle, fat and surrounding tissue led us to form the preliminary hypothesis that calcium-sensing receptors (CaSR) were responsible for the fluorescence signal. We tested this hypothesis along with several others as part of our top-down approach to understanding the NIR endogenous fluorophore.

The bottom-up approach was more open-ended and exploratory in nature. We evaluated the endogenous fluorophore through multiple avenues by probing biochemical properties, structure and morphology, optical properties, or clinical correlates of the fluorophore. The combination of the bottom-up and top-down approaches was an efficient way to eliminate potential fluorophore candidates while gaining broad understanding of the fluorophore behavior. Ultimately, the experiments led to the hypothesis that the NIR parathyroid fluorophore is localized in the secretory granules of endocrine tissues. Section A1.3 describes the experiments assessing the calcium-sensing receptor hypothesis. The majority of bottom-up studies were described in Chapter 5. However, Sections A1.4-A1.9 describe alternative approaches.

A1.3 Testing the Calcium-sensing receptor hypothesis

The calcium-sensing receptor is a G- protein-coupled, seven-transmembrane receptor that is also a key mediator of direct effects of extracellular calcium ions on the parathyroid gland and several other tissues (1). It plays an important role in the extracellular calcium ion regulated parathyroid hormone (PTH) secretion. The release of PTH is inhibited in response to elevations

in plasma calcium concentrations and activation of the calcium receptor. Inactivating CaSR mutations are shown to cause mild and severe increases in PTH secretion, resulting in several hypercalcemic disorders such as familial hypocalciuric hypercalcemia and neonatal severe hyperparathyroidism. Studies have also shown parathyroid adenomas from patients with severe secondary hyperparathyroidism have reduced CaSR expression compared to that of normal parathyroid glands (2).

CaSR are found in many cells and have especially high concentrations in parathyroid cells (3). The CaSR is also present in smaller concentrations almost exclusively in the C-cells of the thyroid (which comprise roughly 5% of the gland) but nowhere else in the muscle, fat or lymph of the neck region. The calcium-sensing receptor can also be found in most of the renal tubule and is present at the highest levels in the cortical thick ascending limb of the nephron, brain, bone and epithelial lining of the colon. Our probe-based fluorescence spectroscopy measurement showed decreased fluorescence signal in the hypersecreting parathyroid glands of patients with hyperparathyroidism (4). This led to the initial hypothesis that CaSR could be responsible for the signal. Many studies were performed to assess the validity of this hypothesis.

A1.3.1 Parathyroid homogenization with varying detergents

In order to determine whether CaSR are the source of the parathyroid autofluorescence, our first goal was to isolate the protein for fluorescence measurements. Protein isolation and purification requires the use of detergents for tissue disruption and homogenization. Parathyroid tissue was homogenized using five different detergents ranging in

stringency: 2X Laemmli buffer (10% SDS, 1M Tris-Cl, 5% Beta-mercaptoethanol, glycerol, pH 6.8), NP-40 (1% NP-40, 150 mM NaCl, 50 mM Tris-Cl, pH 8), Triton X-100 (1% Triton X-100, 150 mM NaCl, 50 mM Tris-Cl, pH 8), Urea/Thiourea Buffer (7M Urea, 2M thiourea, 4% Chaps, 30 mM Tris-HCl, pH 8.5), and RIPA buffer (50 mM Tris-HCl, 150 mM NaCl, 0.1% SDS, 1%

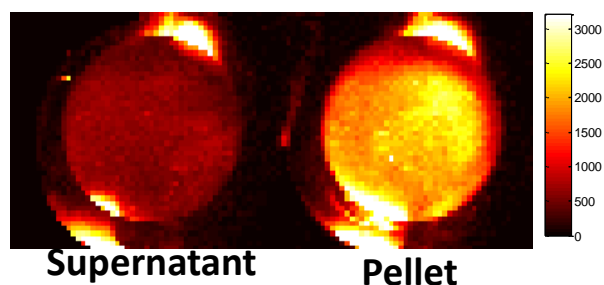


Figure A.1: Near-infrared autofluorescence of parathyroid pellet and supernatant homogenized in RIPA buffer

IGEPAL CA-630, 0.5% sodium deoxycholate, pH 8) (Sigma). Ionic buffers such as Laemmli buffer and RIPA buffer are highly denaturing due to their ability to disrupt hydrophobic and polar bonds. This allows ionic detergents to solubilize membrane proteins which have large hydrophobic domains. Laemmli buffer has a higher stringency than RIPA buffer. Non-ionic buffers such as NP-40 and Triton X-100 are less denaturing than ionic buffers because they are only able to disrupt non-covalent bonds which cause protein-to-protein interactions. Furthermore, urea-based buffers denature proteins by breaking hydrogen bonds and reducing disulfide bonds (5).

To test each buffer, frozen human parathyroid adenoma tissue samples were pulverized to a fine powder using a mortar and pestle precooled in liquid nitrogen. Ground tissue was homogenized with 20 strokes of a Potter-Elvehjem tissue grinder (Wheaton Industries, Inc.) in ice cold detergent with the addition of protease inhibitors (Sigma). Parathyroid homogenate was centrifuged at 10,000 x g for 10 min at 4C. After centrifugation, the parathyroid supernatant was aspirated and set aside. The remaining pellet was diluted with the lysis buffer it was brought up in such that it was suspended in a volume equivalent to the supernatant. Equal volumes of the parathyroid pellet and supernatant were placed in a 96-well plate and imaged using a NIR fluorescence scanner with 785-nm excitation (LI-COR Biosciences).

Parathyroid homogenization with each lysis buffer revealed the autofluorescence was higher in the parathyroid pellet than in the supernatant. The pellet contains the tissue material that is not solubilized with the detergent such as cell debris, nuclei, and insoluble proteins. Figure A.1 shows an example result of parathyroid fluorescence in the parathyroid pellet compared to supernatant when brought up in RIPA buffer. While there is no detergent that can solubilize all proteins, the high fluorescence in parathyroid pellet indicated the parathyroid fluorophore is not easily solubilized with typical broad-spectrum lysis buffers. Another approach for fluorophore isolation is needed. Furthermore, these results indicated that the parathyroid fluorophore is not easily solubilized using Laemmli buffer, RIPA buffer, and Urea/thiourea buffer using published protocols, despite the fact that these buffers are highly denaturing. This further validates the point made in Chapter 5 that the parathyroid fluorophore is highly robust.

A1.3.2 A Detergent-free method for isolation of caveolar membranes

Previous studies to isolate the CaSR from parathyroid tissue have shown these proteins reside within the caveolar membranes, caveolin-rich membrane domains in the parathyroid cells (6). Research has shown that the caveolar membranes are insoluble to detergents such as Triton X-100 (7). Our hypothesis that the CaSR is the parathyroid fluorophore, along with the observance of the detergent resistance of the NIR fluorophore led to the investigation of alternative methods to isolate the caveolar membranes in parathyroid tissue. The goal of the study was to isolate caveolar membranes and determine if these membranes emitted higher levels of fluorescence due to the high concentration of CaSR.

All steps were carried out at 4°C. The following buffers were prepared: buffer A (0.25 M sucrose/1 mM EDTA/20 mM Tricine, pH 7.8); buffer B (0.25 M sucrose/6 mM EDTA/120 mM Tricine, pH 7.8); buffer C (50% OptiPrep in buffer B); buffer D (20 mM Tris, pH 7.6/137 mM NaCl/0.5% Tween 20). A plasma membrane fraction was prepared from 8 mg of human parathyroid adenoma tissue. Frozen tissue samples were homogenized, suspended in 1 mL of buffer A, and homogenized further with 30 strokes of a Teflon homogenizer. Tissue homogenates were transferred to a centrifuge tube and spun at 1000 x g for 10 minutes. The post-nuclear supernatant fraction (PNS) was removed and stored on ice. The pellet from each tube was resuspended in 1.0 ml of buffer A, homogenized, and centrifuged at 1000 x g for 10 min again. The two PNSs were combined, layered on the top of 23 ml of 30% Percoll in buffer A, and centrifuged at 84,000 x g for 30 min in a Ti 70 rotor (Beckman). The plasma membrane fraction was a visible band approximately 6 cm from the bottom of the centrifuge bottle. The membrane fraction, which contained, was collected with a Pasteur pipette, adjusted to 2.0 ml with buffer A, and placed in a Sorvall TH641 centrifuge tube on ice. We placed a sonication probe equidistant from the bottom of the tube and the top of the solution and sonicated the sample two successive times (total power, 50 J/W per sec each time). The sample was then incubated on ice 2 min to maintain the sample at 4°C before a second round of two sonications. An aliquot of the sonicate was saved before mixing the remainder with 1.84 ml of buffer C and 0.16 ml of buffer A (final OptiPrep concentration, 23%) in the bottom of the same TH641 tube. A linear 20% to 10% OptiPrep gradient (prepared by diluting buffer C with buffer A) was poured on top of the sample and then centrifuged at 52,000 x g for 90 min in a Sorvall TH641 swinging bucket rotor. The top 5 ml of the gradient (fractions 1-7) was collected, placed in a fresh TH641

centrifuge tube, and mixed with 4 ml of buffer C. The sample was overlaid with 2 ml of 5% OptiPrep (prepared by diluting buffer C with buffer A) and centrifuged at 52,000 x g for 90 min at 4°C. A distinct opaque band was present in the 5% OptiPrep overlay about 4-5 mm above the interface. This band was determined by Smart et al to be the caveolar membrane.

This experiment was performed in triplicate with three different parathyroid adenoma samples. Results showed no significant NIR autofluorescence emitted from the caveolar membrane fraction. The majority of the fluorescence signal was found in the pellet separated from the parathyroid tissue after centrifugation at 1000 x g. Slight amounts of NIR autofluorescence was observed in the plasma membrane fraction, which was isolated as an intermediate step in the isolation of the caveolar membranes. These plasma membrane fractions were run through SDS-PAGE using the protocol described in Chapter 5. Results of the gel did not show an autofluorescent band. This low fluorescence signal observed prior to SDS-PAGE could be background autofluorescence due to the high amount of tissue isolated in the plasma membrane fraction. These results did not support the hypothesis that CaSR is responsible for the parathyroid autofluorescence.

A1.3.3 NIR autofluorescence of medullary thyroid xenografts

The NIR fluorescence spectroscopy results described in Chapter 3 and 4 reveal low yet consistent autofluorescence signal emitted from the thyroid gland in patients undergoing parathyroidectomy and thyroidectomy. The parafollicular cells (C-cells) of the thyroid are known to express CaSR at lower levels than parathyroid cells. To harness this information and further test our hypothesis of CaSR, Dr. John Phay, our collaborator at The Ohio State University, donated two different medullary thyroid xenografts grown with either TT (with CaSR expression) or MZ-CRC-1 (without CaSR expression) cell lines (8). Bulk frozen samples of these two tumor types and control mouse tissue (i.e. heart, liver, and lung) were measured using probe-based NIR fluorescence spectroscopy. Results showed no significant difference in the autofluorescence signal emitted from xenograft tissues with CaSR expression and medullary thyroid xenograft tissues without CaSR expression. Each tissue type had very low fluorescence. The results of this experiment were not conclusive as to whether CaSR were contributing to the NIR autofluorescence because no fluorescence signal was seen from either tissue type. This

could be due to the cell lines, animal model, or freshness of the tissue measured. These results could neither be used to validate or invalidate the CaSR fluorophore hypothesis.

A1.3.4 Immunoprecipitation with anti-CaSR

An immunoprecipitation protocol was performed using anti-CaSR antibodies to directly isolate CaSR from parathyroid tissue homogenates. Parathyroid tissue was homogenized in a liquid nitrogen cooled mortar and pestle. Tissue was lysed with immunoprecipitation buffer containing 150 mM NaCl, 10 mM Tris, pH 7.4, 1 mM EDTA, 1 mM EGTA, 0.2 mM sodium vanadate, protease inhibitors, and the following detergents: 60 mM octyl glucoside, 1% Triton X-100, 0.5% sodium deoxycholate, and 0.1% SDS. The tissue lysate was centrifuged at 10,000 x g for 10 min and precleared with protein A-Sepharose CL-4B beads (Pharmacia) for 30 min at 4 °C. For immunoprecipitation, equal amounts of protein were incubated with 5–10 mg of rabbit polyclonal antibodies for 1 h. Protein A-Sepharose beads were then added for a further 1 h at 4°C. Bound immune complexes were washed three times with immunoprecipitation buffer containing protease inhibitors and detergents. The pellet was eluted by boiling for 5 min with 2x Laemmli sample buffer. The supernatant and beads were measured with the NIR fluorescence scanner and compared to the NIR fluorescence signal of remaining parathyroid homogenate.

The results showed no significant NIR autofluorescence present in CaSR component compared to the remaining parathyroid homogenate. The beads and buffers were measured for NIR autofluorescence to ensure no obstruction of the NIR autofluorescence. If CaSR was the fluorophore, we expected high NIR autofluorescence in the CaSR isolated tissue component. These results did not support the hypothesis that CaSR was responsible for the NIR fluorescence in parathyroid tissue.

A1.3.5 CaSR overexpression lysates

The final experiment performed to determine whether CaSR are responsible for the NIR autofluorescence in the parathyroid gland was to compare the fluorescence signals between cells with high CaSR expression compared to cells with no CaSR expression. To do this, CaSR transfected human embryonic kidney cells (HEK-293) and wild-type HEK-293 cells were

obtained (Origene). CaSR-HEK cell lysates and wild-type HEK cell lysates were placed in a 96-well plate and imaged with a NIR fluorescence scanner with 785 nm excitation (Figure A.2A). Results showed no NIR autofluorescence emitted from either cell type. Probe based NIR fluorescence spectroscopy revealed no fluorescence peak above 800 nm (Figure A.2B).

The results of the experiments aimed at determining the fluorescence of CaSR revealed no autofluorescence emitted from this protein. From these studies, we concluded that the NIR fluorophore in the parathyroid gland is not likely to be the calcium-sensing receptors.

A1.4 Photobleaching

Photobleaching is a phenomenon that occurs when a fluorophore loses its ability to fluoresce due to photon-induced chemical damage and covalent modification. The average number of excitation and emission cycles that occur for a fluorophore before photobleaching is dependent upon its molecular structure and the local environment. Some fluorophores bleach quickly after emitting few photons, and others that are more robust can undergo millions of cycles prior to bleaching. As a way to uncover information on the parathyroid fluorophore behavior, we conducting a photobleaching study to determine the manner in which the parathyroid and thyroid fluorophore photobleaches.

Bulk, snap-frozen samples of human thyroid tissue were thawed to room temperature and placed in a petri dish with phosphate buffered saline. An optical probe was mounted over the tissue such that the tip came in direct contact with the sample. Near-infrared fluorescence spectra were collected continuously for 30 seconds with 80 mW excitation and 300 ms integration time per spectra. After 30 seconds, the laser was turned off for 1 min to allow for fluorophore recovery. This was repeated for 7 minutes. This experiment was conducting for samples that had been thawed for 10 minutes and samples thawed for 40 minutes in order to measure the effects of thaw time and temperature on fluorescence and photobleaching. Figure A.3 plots the peak

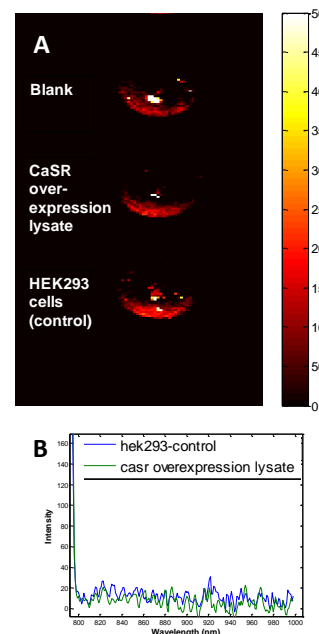


Figure A.2: NIR autofluorescence of HEK-CaSR overexpression lysate compared to wild-type HEK cells measured with A) NIR fluorescence imaging and B) probe-based NIR fluorescence spectroscopy

fluorescence for each spectra in two samples with 10 and 40 minute thaw time. The alteration between gray and black or red and light red indicate where there were 1 minute breaks for fluorescence recovery. Results from Figure A.3 show the permanent photobleaching of the thyroid tissue as was indicated by ~80% decrease in fluorescence signal in the 40 min thawed thyroid and ~70% decrease in fluorescence signal in the 10 min. thawed thyroid sample. Temperature is known to play a role in peak emission of fluorescence, which could account for the greater decrease in fluorescence intensity in the 10 minute thawed thyroid sample.

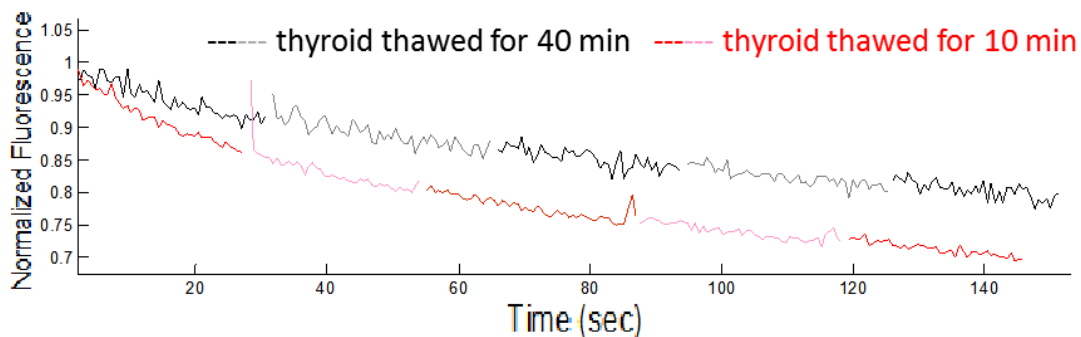


Figure A.3: Thyroid tissue fluorescence signal decreases over time as a result of photobleaching

This qualitative study demonstrates the photobleaching behavior of the NIR fluorophore observed in parathyroid and thyroid tissue. The results identify the NIR fluorophore as being relatively resilient to photobleaching with high levels of irradiance and lengthy time courses of stimulation. This information was also useful for future *in vitro* studies because it demonstrated the relative robustness of thyroid and parathyroid autofluorescence under constant stimulation. Future quantitative studies could be done using fluorescence lifetime imaging (FLIM), fluorescence recovery after photobleaching (FRAP) and fluorescence loss in photobleaching (FLIP). FLIP is a microscopy technique that has been used to reveal the connectivity between different compartments in the cell or the mobility of a fluorophore within the whole compartment. FRAP involves the study of a cell's ability to recover after a single photobleaching event by studying how well fluorophores move back into a bleached site. FLIM maps the spatial distribution of the lifetimes within microscopic images (9). In future studies, these three methods could yield valuable information on the fluorophore behavior in parathyroid and thyroid tissue.

A1.5 Troubleshooting Gel Electrophoresis Studies

The molecular weight of the NIR fluorophore was determined to be 15 kDa as described in Chapter 5. A limited description of the process used to determine the parathyroid fluorophore molecular weight was described in Chapter 5, but a series of informative troubleshooting steps were required before that information was obtained. The main roadblocks to performing sodium dodecyl sulfate polyacrylamide gel electrophoresis (SDS-PAGE) were solubilizing the fluorophore and ensuring that the NIR autofluorescence could withstand the SDS-PAGE processing steps. Here, I address the steps taken to bypass these obstacles.

The detergent-resistance of the NIR fluorophore to a variety of lysis buffers was described in A1.3.1. Solubilization efforts using Triton X-100, NP-40, RIPA, and Laemmli buffers were performed in accordance with protocols established in either the detergent distributor manuals (if the detergent was bought off the shelf) or closely related studies in the scientific literature. Parameters such as volume of buffer per gram of tissue, incubation time of tissue in solution and centrifugation speed and duration are reported in a range of values across studies. Because the parathyroid fluorophore has never been reported, the protocols for its solubilization and isolation are not clearly delineated. Therefore, the optimal parameters for solubilization were estimated based on numerous previously published protocols. As a result, initial studies revealed a large majority of the NIR autofluorescence in parathyroid homogenates was present in the insoluble tissue portion and a much smaller portion of the NIR autofluorescence was present in the solubilized supernatant.

Typically, parathyroid homogenates were incubated in lysis buffer on ice for 30-60 minutes before a clearing spin was performed to separate soluble and insoluble material. However, in preparation for SDS-PAGE studies, we eventually discovered that incubating the parathyroid tissue in RIPA buffer or 2X Laemmli buffer for approximately 24 hours was much more effective in solubilizing the NIR fluorophore. After 24 hours of tissue incubation, a majority of the NIR fluorescence was found in the solubilized tissue supernatant compared to the insoluble tissue pellet. This result is consistent with the findings from Chapter 5 showing the robust nature of the parathyroid NIR fluorophore. Increasing incubation time of tissue in detergent to accomplish more complete solubilization may be necessary due to the resistance of this fluorophore to chemical disruption.

The processing steps prior to loading a sample for SDS-PAGE are highly denaturing (10). The sample is mixed with lithium dodecyl sulfate (LDS) sample buffer that denatures proteins under slightly alkaline pH conditions. Dithiothreitol (DTT) is added as a reducing agent that prevents intramolecular and intermolecular bonds from forming between cysteine residues of proteins. The sample is then boiled for 10 minutes to further denature the proteins and breakup the tertiary and quaternary structures. Solubilized parathyroid homogenates in RIPA and Laemmli buffer were prepared for SDS-PAGE. The NIR autofluorescence signal was measured before processing and after the addition of LDS, DTT and heating to ensure the denaturing steps did not remove the fluorescence signal and confound the results. For example, if autofluorescence was maintained after all processing steps and no fluorescent bands were visualized after the gel was run, this could be due to the fact that the fluorophore is either caught in the well of the gel or transported to the bottom of the gel along with the dye front. Results showed the NIR autofluorescence signal persisted even after highly denaturing conditions. This indicated that SDS-PAGE would be a suitable approach for determining the molecular weight of the fluorophore. This result also indicates that the fluorescence of the parathyroid fluorophore is not affected by protein unfolding, a result which was also confirmed in the heating study in Chapter 5. Green fluorescent protein (GFP), for example, has fluorescence that is highly dependent on the protein structure. Protein unfolding causes loss of fluorescence for GFP (11). The NIR parathyroid fluorophore again reveals robust fluorescence activity.

Report of autofluorescence in the 15kDa band in Chapter 5 was a result of multiple SDS-PAGE experiments performed on parathyroid tissue solubilized in Laemmli buffer. Studies were also done using Triton X-100 for tissue solubilization prior to SDS-PAGE. Homogenization of parathyroid samples in 2x Laemmli buffer yielded high NIR autofluorescence in only the low molecular weight 15 kDa band. Homogenization of parathyroid tissue in 1% TritonX-100 revealed more intense NIR

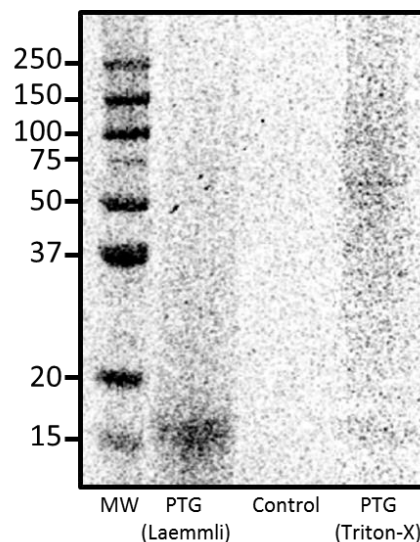


Figure A.4: SDS-PAGE showing fluorescence in parathyroid homogenates solubilized in Laemmli and Triton X detergents

autofluorescence centered at 57-kDa with a faint band at 15-kDa (Figure A.4). Because only 25 µg protein could be loaded onto the gel, a low signal-to-noise ratio of autofluorescence was observed. Laemmli buffer, which is ionic and highly denaturing due to high concentration of sodium dodecyl sulfate, appeared to homogenize all of the fluorescent material into the 15-kDa form. Triton X-100 buffer, which is a relatively more mild non-ionic, does not fully denature proteins or break protein-protein interactions like Laemmli buffer. This may be the reason a higher molecular weight fluorescent component at 57-kDa is observed in samples homogenized with Triton X-100. Incubation times of approximately 24 hours was necessary to solubilize the fluorophore further confirming the robust nature of the fluorophore in parathyroid tissue. Although the addition of Lithium Dodecyl Sulfate (LDS) sample immediately prior to running the samples through the gel introduced ionic denaturing detergents into the samples prepared with Triton X-100, the incubation time may not have been long enough to see total cleavage of the fluorescent material. Future studies can be focused on characterizing the difference in behavior of parathyroid autofluorescence in SDS-PAGE in ionic and non-ionic solutions. Furthermore, mass spectroscopy can be characterized in depth to understand contents of each fluorescent band.

A1.6 Multidimensional Protein Identification Technology Analysis

Multidimensional Protein Identification Technology (MudPIT) is a robust and widely accepted chromatography-based method for protein identification. MudPIT allows for qualitative and quantitative proteomic analysis through two-dimensional high performance liquid chromatography (HPLC). Complex peptide and protein mixtures are loaded onto a triphasic microcapillary column packed with reversed phase, strong cation exchange, and reversed phase HPLC grade material, which is directly in line with a tandem mass spectrometer. The mass spectrometer data is then searched to generate the protein content in the sample. With this technique, protein levels of whole proteomes and differential protein expression can be measured (12).

Bulk human parathyroid and thyroid tissue was homogenized in RIPA buffer. Differential centrifugations was performed to isolate the fluorescent fraction in a manner similar to what was described in Chapter 5. The homogenates were centrifuged at 600 x g for 3 minutes and the supernatant was aspirated. The supernatant was centrifuged at 6,000 x g for 8 minutes and the

remaining pellet was retrieved and re-suspended in RIPA buffer. A bicinchoninic acid assay (BCA Assay) was performed to determine the total concentration of protein in each solution. The NIR fluorescence intensity of equal amounts of parathyroid and thyroid protein was measured. The parathyroid sample had 2.8 times greater NIR autofluorescence than the thyroid sample. Parathyroid and thyroid samples were submitted to the Vanderbilt Mass Spectrometry Research Center Proteomics Laboratory for MudPIT analysis. After processing, a report of the protein counts for approximately 1,050 proteins was generated for both parathyroid and thyroid samples. The protein report was assessed to determine which proteins had relative expression at the same proportion as the differential fluorescence intensities observed in parathyroid and thyroid tissue. Specifically, proteins were identified that had approximately 2 to 4 times greater expression in parathyroid than thyroid tissue, because this was the relative proportion of fluorescence observed. Over 200 proteins were identified that fit this criteria. Because of the large number of proteins, this experiment could not serve to narrow the pool of potential fluorophore candidates. Though it did not yield conclusive results, the report generated with MudPIT analysis served as a reference for evaluating hypothesized fluorophore candidates. Future studies could be done to run this experiment with a more refined parathyroid and thyroid tissue sample so that the number of proteins reported is fewer.

A1.7 Building a custom microscope for NIR autofluorescence microscopy

NIR autofluorescence microscopy images of unstained parathyroid cross sections revealed location of the fluorescence signal in the cytoplasmic regions of parathyroid tissue in Chapter 5. These microscopy images were collected on a customized NIR fluorescence microscope that was built specifically for the purpose of parathyroid autofluorescence imaging with excitation at 785 nm and emission above 800 nm.

Six microscopes were tested to determine whether they were optimized for parathyroid fluorescence imaging based on excitation wavelength, emission wavelength, and detector sensitivity. Several issues arose with the microscopes tested. In some cases, microscopes utilized a broad spectrum white light source that could be filtered to excite over a range of wavelengths based on the narrow band-pass filter used. However, the white light sources commonly used were designed for excitation wavelengths below 700 nm. The light intensity at 785 nm was not sufficient to generate detectable autofluorescence emission from parathyroid tissue. In other

cases, the microscope did not have a detector with enough sensitivity to detect the parathyroid autofluorescence. Although the NIR fluorescence signal in the parathyroid is relatively strong for an endogenous fluorophore, many cameras did not have sufficient quantum yield above 800 nm. For example, microscopes equipped with 785 nm light sources are often used for two-photon fluorescence. Because two-photon fluorescence with NIR excitation requires detection at visible wavelengths, these systems would not suffice. No microscopes readily available on Vanderbilt's campus could detect parathyroid autofluorescence and provide information on location of the parathyroid fluorescence.

A customized NIR fluorescence microscope solution was constructed to achieve autofluorescence microscopy of parathyroid tissue cross sections. A Zeiss Axiovert 135 (Carl Zeiss) fluorescence microscope equipped with a PhotonMax 512B (Princeton Instruments) cooled CCD camera cooled to -70°C . Fluorescence excitation was achieved with a NIR 785-nm diode laser (Innovative Photonic Solutions), which provided sample trans-illumination via an optical fiber delivering an average 4.7 mW to sample. A 785-nm edge long-pass filter (Semrock) was placed in the optical path to filter excitation light. Images were acquired with WinView/32 software (Roper Scientific) with 3 accumulations and 15 s exposure times. Low magnification images were collected using a $2.5 \times / 0.075$ objective (Carl Zeiss). High magnification images were collected using a $40 \times / 0.60$ objective (Carl Zeiss). This customized microscope allowed clear fluorescence images to visualize fluorophore location in tissue cross sections (microscopy images shown in Chapter 5).

A1.8 Protein Over-expression Lysates

Clinical and laboratory results outlined in this Appendix and Chapter 5 generated evolving hypotheses on the parathyroid fluorophore identity. To test each hypothesis, overexpression lysates were obtained to compare the NIR autofluorescence intensity of HEK-293 cell lysates transfected with the protein of interest and wild-type HEK-293 cell lysates without the protein of interest. Three proteins were hypothesized to be contributors to the parathyroid fluorescence: Vitamin D receptor (VDR), Caveolin-1, and Chromogranin A.

Vitamin D receptors were hypothesized to contribute to parathyroid fluorescence due to their high concentration in parathyroid tissue. These receptors are known to be down-regulated in patients with hyperparathyroidism (13). Because the NIR fluorescence signal observed in

patients with hyperparathyroidism was lower than the signal in parathyroid glands of patients with thyroid disease, VDR was postulated as a likely fluorophore candidate. Transient overexpression lysate of vitamin D (1,25- dihydroxyvitamin D₃) receptors in human HEK-293 cell lines were obtained (Origene). One-hundred μ L of VDR overexpression lysate and one-hundred μ L of wild-type HEK-293 cells were placed in a 96-well plate and imaged under a NIR fluorescence scanner. Probe-based fluorescence spectra were also collected from each sample. With both imaging and spectroscopy, no NIR autofluorescence peak was detected in the 800 – 1000 nm range. Purified laboratory grade 1-alpha-25- dihydroxyvitamin D (Sigma) was also measured for NIR autofluorescence. A total of 0.1 mg of 1-alpha-25- dihydroxyvitamin D was diluted in 100 microliters of ethanol and measured with NIR fluorescence spectroscopy. No fluorescence was observed.

Caveolin-1 was also hypothesized to contribute to parathyroid fluorescence. Caveolin-1 is a scaffolding protein found in the caveolae membranes of parathyroid gland tissue. Because of the difficulty solubilizing the parathyroid fluorophore, other insoluble proteins that are co-localized with calcium-sensing receptors were postulated. Caveolin-1 immunoprecipitates with calcium-sensing receptors and is located in both parathyroid chief cells and thyroid epithelial cells (6). Transient overexpression lysate of caveolin-1 in human HEK-293 cell lines were obtained (Origene). One-hundred μ L of Caveolin-1 overexpression lysate and one-hundred μ L of wild-type HEK-293 cells were measured with probe-based fluorescence spectroscopy and imaging. No NIR autofluorescence peak was detected.

Finally, overexpression lysates of chromogranin A (Origene) were measured to determine if it contributed to the NIR autofluorescence in the parathyroid gland (14). Chromogranin A was postulated as a hypothesis for the NIR fluorophore in the parathyroid gland because of the high amount of secretory granules present in parathyroid gland tissue. Results described in Chapter 5 show transmission electron microscopy images of fluorescent components of parathyroid tissue contain granular, electron dense structures with a similar size to secretory granules. In addition, the heat resistance of the parathyroid fluorophore is consistent with proteins such as Chromogranin A in the granin family (15). NIR fluorescence imaging and spectroscopy revealed no NIR autofluorescence in chromogranin A overexpression lysates compared to control lysates.

The use of over-expression lysates to validate or invalidate a fluorophore candidate requires the assumption that the fluorescence of a given protein is independent of its interactions within

the context of parathyroid tissue. It is possible that one of the proteins measured in this study emits NIR autofluorescence when it is in the parathyroid chief cells and that environmental conditions are a factor in fluorescence emission. The potential for this phenomenon contributes to the difficulty of determining the exact identity of the parathyroid fluorophore.

A1.9 Pancreatic Islet Cell Autofluorescence

Multiple types of endocrine tissues aside from parathyroid gland tissue emitted NIR autofluorescence signal, including normal pancreas, thyroid gland, and adrenal pheochromocytoma (Chapter 5). As a result of this finding as well as imaging and purification studies in Chapter 5, the leading hypothesis for the NIR fluorophore is a protein co-localized in the endocrine secretory granules. The pancreatic islets or islets of Langerhans are the regions of the pancreas that contain its endocrine cells. Studies have shown that the beta cells, one of the cell types in the islets of Langerhans, contains more than 10,000 secretory granules (16). This presents a method for testing the hypothesis that the NIR fluorophore is localized in the secretory granules of endocrine tissues.

Isolated human pancreatic beta cells were acquired from Dr. Nathaniel Hart at Vanderbilt University. Beta cells were placed on a quartz slide and imaged at 10X using the fluorescence microscope described in section A1.7. The fluorescence images in Figure A.5 revealed robust fluorescence emitted from pancreatic beta cells. This result supports the hypothesis that the NIR fluorophore is present in multiple endocrine tissue types and may be associated with endocrine secretory granules.

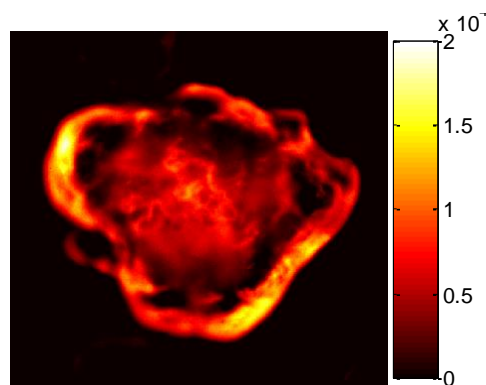


Figure A.5: NIR auto-fluorescence microscopy image of human pancreatic beta cell at 10x magnification

A1.10 Conclusions

The intent of this Appendix is to provide supplementary information on experiments aimed at uncovering the NIR fluorophore. It serves as supporting material to Chapter 5. A wide variety of approaches were tested including SDS-PAGE, fluorescence microscopy, direct measurements of overexpression lysates, and photobleaching studies. This study explores several fluorophore hypotheses including calcium-sensing receptors, caveolin-1, vitamin D, vitamin D receptors, and chromogranin A. None of the results supported these proteins as fluorophores. Results do suggest that a component of the parathyroid tissue related to its endocrine function, such as secretory granules, may contribute to the NIR autofluorescence observed. This appendix provides a more in-depth description of the fluorophore evaluation studies that can be built upon in the future to identify the precise biological basis of the NIR fluorescence signal in the parathyroid gland and other endocrine tissues.

A1.11 References

1. Brown EM. The calcium-sensing receptor: physiology, pathophysiology and CaR-based therapeutics. *Sub-cellular biochemistry*. 2007;45:139-67. PubMed PMID: 18193637.
2. Brown EM. The calcium-sensing receptor (CaR) and its disorders. *Hormones*. 2002 Jan-Mar;1(1):10-21. PubMed PMID: 17018434.
3. Kifor O, Kifor I, Moore FD, Butters RR, Brown EM. m-Calpain colocalizes with the calcium-sensing receptor (CaR) in caveolae in parathyroid cells and participates in degradation of the CaR. *J Biol Chem*. 2003 Aug 15;278(33):31167-76. PubMed PMID: WOS:000184658800094. English.
4. McWade MA, Sanders ME, Broome JT, Solorzano CC, Mahadevan-Jansen A. Establishing the clinical utility of autofluorescence spectroscopy for parathyroid detection. *Surgery*. 2015 Oct 7. PubMed PMID: 26454675.
5. Helenius A, Simons K. Solubilization of membranes by detergents. *Biochimica et biophysica acta*. 1975 Mar 25;415(1):29-79. PubMed PMID: 1091302.
6. Kifor O, Diaz R, Butters R, Kifor I, Brown EM. The calcium-sensing receptor is localized in caveolin-rich plasma membrane domains of bovine parathyroid cells. *J Biol Chem*. 1998 Aug 21;273(34):21708-13. PubMed PMID: 9705306.
7. Smart EJ, Ying YS, Mineo C, Anderson RGW. A Detergent-Free Method for Purifying Caveolae Membrane from Tissue-Culture Cells. *P Natl Acad Sci USA*. 1995 Oct 24;92(22):10104-8. PubMed PMID: WOS:A1995TB46700035. English.

8. Ding H, Yusof AM, Kothandaraman S, Saji M, Wang C, Kumar K, et al. Localization of CaSR antagonists in CaSR-expressing medullary thyroid cancer. *The Journal of clinical endocrinology and metabolism*. 2013 Nov;98(11):E1722-9. PubMed PMID: 24030941. Pubmed Central PMCID: 4326510.
9. Ishikawa-Ankerhold HC, Ankerhold R, Drummen GP. Advanced fluorescence microscopy techniques--FRAP, FLIP, FLAP, FRET and FLIM. *Molecules*. 2012;17(4):4047-132. PubMed PMID: 22469598.
10. One-Dimensional SDS Gel Electrophoresis of Proteins with NuPAGE® Novex® Pre-Cast Gels: ThermoFisher; [cited 2016]. Available from: <http://www.thermofisher.com/us/en/home/references/protocols/proteins-expression-isolation-and-analysis/sds-page-protocol/one-dimensional-sds-gel-electrophoresis-of-proteins-pre-cast-gels-.html#troubles>.
11. Khan F, Kuprov I, Craggs TD, Hore PJ, Jackson SE. 19F NMR studies of the native and denatured states of green fluorescent protein. *Journal of the American Chemical Society*. 2006 Aug 23;128(33):10729-37. PubMed PMID: 16910667.
12. Florens L, Washburn MP. Proteomic analysis by multidimensional protein identification technology. *Methods in molecular biology*. 2006;328:159-75. PubMed PMID: 16785648.
13. Yano S, Sugimoto T, Tsukamoto T, Chihara K, Kobayashi A, Kitazawa S, et al. Decrease in vitamin D receptor and calcium-sensing receptor in highly proliferative parathyroid adenomas. *European journal of endocrinology / European Federation of Endocrine Societies*. 2003 Apr;148(4):403-11. PubMed PMID: 12656660.
14. Mouland AJ, Hendy GN. Regulation of synthesis and secretion of chromogranin-A by calcium and 1,25-dihydroxycholecalciferol in cultured bovine parathyroid cells. *Endocrinology*. 1991 Jan;128(1):441-9. PubMed PMID: 1986936.
15. Rosa P, Gerdes HH. The granin protein family: markers for neuroendocrine cells and tools for the diagnosis of neuroendocrine tumors. *Journal of endocrinological investigation*. 1994 Mar;17(3):207-25. PubMed PMID: 8051343.
16. Rorsman P, Renstrom E. Insulin granule dynamics in pancreatic beta cells. *Diabetologia*. 2003 Aug;46(8):1029-45. PubMed PMID: 12879249.